Space and Time Occurrence of Algal Blooms in the Mediterranean: their Significance for the Trophic Regime of the Basin

Thesis

UNRESTRICTED

Space and Time Occurrence of Algal Blooms in the Mediterranean: their Significance for the Trophic Regime of the Basin

Fabrizio D'Ortenzio
Laurea in Fisica
Università di Roma "La Sapienza"
Italia

Doctor of Philosophy

Sponsoring Establishment
Stazione Zoologica Anton Dohrn
Napoli, Italia

September 2003

Submission date: 23 September 2003
Award date: 14 January 2004

ProQuest LLC.
789 East Eisenhower Parkway
P.O. Box 1346
Ann Arbor, MI 48106 – 1346

Table of contents

List of Figures

List of Tables

CHAPTER 1

Introduction

1.1 THE MEDITERRANEAN SEA

In spite of its limited size (~ 0.6% of the global ocean in surface, 0.3% in volume), the Mediterranean Sea is considered one of the most complex marine environments on the Earth, because of the variety of physical processes that occur there (Williams, 1998). These processes span from the mesoscale to the basin-scale , and include also deep-water formation.

Consequently, the basin has often been considered a "miniature ocean" or a "laboratory basin" (Lacombe, et al., 1981; Robinson and Golnaraghi, 1995) because most of the processes controlling the global ocean general circulation are present there, though in reduced temporal and spatial scales.

1.1.1 Basin topography

The Mediterranean Sea is an elongated semi enclosed basin (see Figure 1-1) that spans between 6°E and 37°W, and 30°N and 46°N approximately and is connected to the Atlantic Ocean through the Gibraltar Strait and to the Black Sea through the Dardanelles Strait. The basin owns its name to the roman word *Mediterraneus*, which translates *within lands*. Thus, the main feature of this sea, i.e. the fact of being semi-enclosed, is embedded in its name since ancient times.

It is divided in two main subbasins, Eastern and Western Mediterranean (EMED and WMED hereafter) by the system of the straits of Sicily, which have narrow and shallow

sills hardly reaching 500 m depth. The two main subbasins are in turn divided in smaller subbasins with complex coastlines and different sized islands (see Figure 1-1). Most of the names have historical origin and demonstrate the strong links between the Mediterranean and its surrounding areas.

The Alboran Sea (from the name of a little island located between Spanish an African coasts) is the region near the Gibraltar Strait, and therefore is the only Mediterranean subbasin directly connected with the Atlantic Ocean.

The region bound by the three WMED main islands (Corsica, Sardinia, and Sicily) and by the Italian Peninsula is named Tyrrhenian Sea (from the name of the ancient pre-roman population living in the central part of Italy, the *Tirreni*). The Ligurian Sea (whose name derives from another pre-roman population, the *Liguri*) and the Balearic Sea are located in the northern part of the Western Mediterranean, facing the Italian and Spanish-French coast, respectively.

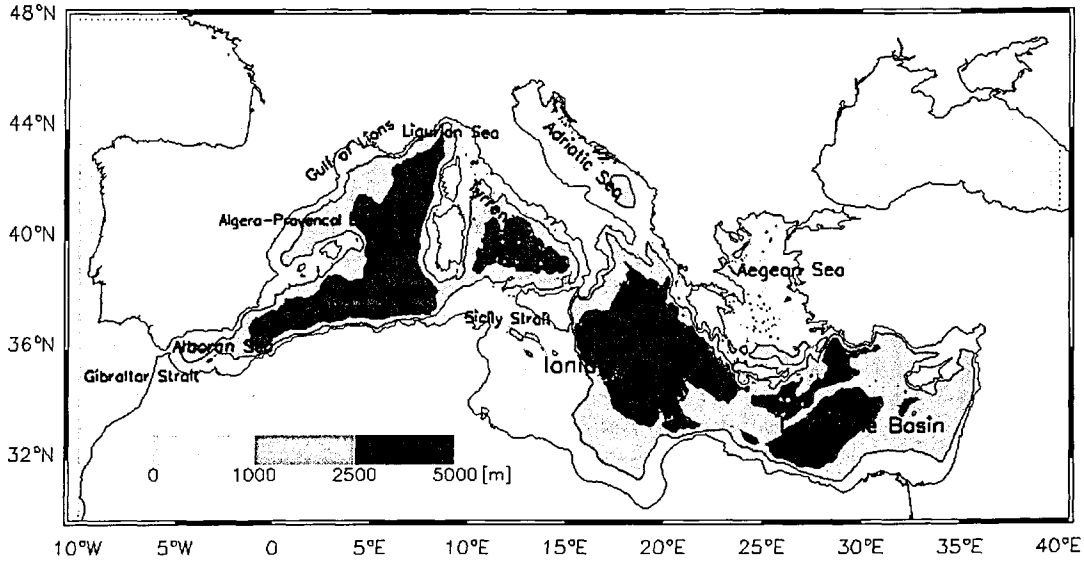

Figure 1-1. Mediterranean regions and their bathymetry.

Also the EMED is divided in two main subbasins: the Ionian sea (from the name of an Indo-European population, the *Ionians*, who conquered part of the Mediterranean area during the VIII-VI centuries BC) spans from 15°E to 25°E , while the Levantine basin (literally the *sea of rising sun*) is located from 25°E to 36°E.

In the northern part of the EMED (between 40°N and 45°N), is located the Adriatic Sea (deriving its name by the Etruscan city *Adria*), which divides the Italy from the Balkans, and is connected with the Ionian Sea at the Otranto Strait. Between the Hellenic and the Anatolia peninsulas, is located the Aegean Sea, which is bound to the south by the Cretan island and to the north by the continental southern European margin.

The depth of the WMED is quite constant (about 2500 m), with the exception of the Alboran and the North Tyrrhenian seas, which are significantly shallower (~ 300 m). The deepest pits of Mediterranean are located in the Ionian Sea at Capo Matapan (more than 5000 m), even though the average depth is around 2000-2500 meters. By contrast, the Aegean and the Adriatic are two shelf seas, even if the latter is more than 1100 meters depth in its southern part.

In summary, the Mediterranean can be considered as a series of deep basins interconnected among them and with the Atlantic Ocean by shallow sills, entirely surrounded by land and with a complex topography and coastlines.

1.1.2 The physical framework

The functioning of the seas is strongly affected by the surface meteorological processes, which drive the oceanic deep convection, the vertical mixing, and the Ekman transport, and play a key role in the heat and salt budgets (Gill, 1982).

In particular, the wind field drives the ocean surface circulation, transferring mechanical energy to the sea and inducing the motion of the fluid, which in turn modifies the upper ocean circulation.

Superimposed on the wind driven circulation, and interacting with it, the seasonal dynamics of the air-sea fluxes, with the local and regional anomalies, produce variations in the depth of the mixed-layer, *via* the winter convective overturning and the summer heating processes (Follows and Dutkiewicz, 2002; Williams, et al., 2000). In the first

case, it causes a cooling of the surface waters, which results in the deepening of the layer of well-mixed waters. In the second, it produces a thermal stratification in the upper layer, which prevents further vertical mixing.

At particular sites, the winter convection mixes the whole water column, and the newly formed water reaches the intermediate depth or the sea bottom. The deep water formation is a multi-cause process: a preconditioned hydrodynamic situation and an intense cooling due to meteorological extreme events are considered the main responsible of the formation of dense water masses (Marshall and Schott, 1999 and references therein), which in fact occurs only in polar regions and in the Mediterranean. Such process is critical for the ocean dynamics. In fact, convection in polar region drives the global thermoaline circulation, and it is responsible for half of pole-ward transport required by the atmosphere-ocean system (Macdonald, 1998; Macdonald and Wunsch, 1996).

The equator-ward spreading of the dense waters and the opposite pole-ward surface flow of warm and salty waters, produce a thermohaline cell encompassing all the main Earth's oceans. The subsequent global conveyor belt, which extends through the Southern Ocean to the Indian and Pacific Oceans, induces the ventilation of the bottom water masses and is responsible of the heat exchange between polar and tropical regions (Emery and Pickard, 1990).

Most of the above takes place also in the Mediterranean Sea. The basin is then suitable for a better understanding of the mechanisms playing a role in the functioning of the marine system and of their interactions at different spatial and temporal scales. In addition, the basin should display faster responses to the climate change (Bethoux and Gentili, 1999; Duarte, et al., 1999), being its temporal scales shortest than the global ocean ones. Therefore, the Mediterranean is considered a unique site to verify the intensity and the consequences of the changes due to climate variability.

The Mediterranean is a condensation basin, where the evaporation exceeds the sum of precipitations and of the inputs from river runoff (Gill, 1982). The freshwater budget has been estimated in different ways (Bethoux and Gentili, 1999; Bryden and Kinder, 1991; Gilmann and Garrett, 1994; Hopkins, 1999) resulting in a net negative value ranging between 0.56 and 1 m yr^{-1}.

The precipitation annual rate is estimated between 0.31 and 0.70 m yr^{-1} (Bethoux, 1979; Legates and Wilmott, 1990), while the river runoff has been recently re-estimated by Margat (1992) who gave a value of 0.21 m yr^{-1} updating the previous estimates of 0.25 m yr^{-1} (Cruzado, 1979), that did not account for the damming of the Nile River. The resulting negative freshwater budget is partially compensated for by the Atlantic inflow at Gibraltar Strait, where a complex two layer system is at work. The long-term equilibrium of both water and salt budgets brings about an outflow across the strait of Gibraltar ranging from 0.8 to 1.6 Sv (Bethoux, 1979; Hopkins, 1999), which, because of the shallow sills at Gibraltar strait (284 m), involves mostly the intermediate layers. A similar depth constraint works at the Straits of Sicily. In other words the main connecting sills inhibit significant exchanges of deep waters (Astraldi, et al., 2001).

The winds drive the Mediterranean surface circulation (Robinson and Golnaraghi, 1995), which is mainly characterized by the spreading and modifications of the Atlantic Water (AW). In its eastward flow, AW produces meanders and jets, which in fact alter the density structure of upper layer water column. In addition, it interacts with sub-surface and intermediate layers waters with a progressive increase of both temperature and salinity. Because of this, the AW is currently referred to as the Modified Atlantic Water (MAW) (Millot, 1987; Millot, 1999).

Seasonal thermocline develops around April-May, depending on the year and on the latitude, and a strong thermocline persists for 4–5 months until it is eroded by storms between mid-September through late October (Duarte, et al., 1999).

The winds blow stronger in winter, with larger effects in the West than in the East (Myers, et al., 1998), and show a regime characterized by two main permanent features, the Mistral wind over the western basin and the Etesian ones over the eastern. In addition, a strong catabatic wind, the Bora, is present in the Adriatic Sea during the winter season.

On the other hand, the irradiance over the Mediterranean area is about 20% greater than the mean irradiance incident at similar latitudes (Bishop and Rossow, 1991). However, the latitudinal shift of the EMED respect to the WMED, results in a different insolation regime, which in turn provokes significant differences in the heat fluxes and on the seasonal dynamics of the mixed layer.

As mentioned above, the Mediterranean is the only temperate sea where dense water formation processes take place during exceptional convective events that occur approximately once a year (Marshall and Schott, 1999; MEDOC Group, 1970). The physical process is generally described in three phases that have different time and space scales (for a review see Marshall and Schott, 1999)). During the "pre-conditioning" phase from fall to early winter, seasonal cooling occurs on a large horizontal scale (order of 100 km). If pre-conditioning is sufficient, wind events in winter can trigger the "deep convection" or "violent mixing" phase, i.e., the formation of localized deep mixing "plumes" that are embedded within a "mixed patch", characterized by a horizontal scale of ~ 1 km and ~50 km, respectively. In the "sinking and spreading" or, more accurately, "lateral exchange" phase, the predominantly vertical heat transfer eventually gives way to horizontal transfer involving geostrophic eddies (order of 10 km), ultimately leading to the disintegration of the mixed patch. This entire process can be intermittent, and the last two phases are not necessarily sequential and can occur concurrently (Marshall and Schott, 1999). The extent of deep water formation typically shows considerable inter-annual variability and is driven by meteorological conditions; thus, the convective penetration depth is principally

determined by the year-to-year variability in local heat fluxes (e.g. Lascaratos, et al., 1993; Mertens and Schott, 1998; Visbeck, et al., 1995).

The circulation and the spreading of the Mediterranean water masses show a complex phenomenology, complicated by the multiple driving forces, strong topographic and coastal influences, and internal dynamic processes.

As for the general circulation, it is possible, following Robinson (1995), to define three main spatial scales describing the physical dynamics of the basin.

1.1.2.1 The basin scale

A large thermohaline cell encompasses the whole Mediterranean and is mainly driven by the water deficit and by the heat fluxes, compensated by the exchanges through the Gibraltar Strait (Bryden and Kinder, 1991; Gilmann and Garrett, 1994; Hopkins, 1999). Due to the above mentioned shallow depth of the Sicilian Straits, the main cell is driven by the intermediate water. Its formation and subsequent spreading, together with the inflow of the AW through the Gibraltar strait, generates the thermoaline cell of the Mediterranean.

Deep circulations in the two main sub-basins are decoupled and are composed by two minor thermoaline cells forced by events of dense water formation occurring in the Gulf of Lions for the WMED (Hopkins, 1999; Robinson and Golnaraghi, 1995) and in the South Adriatic and in the Rhodes Gyre regions for the EMED. More recently, events of deep water formation have been observed also in the Aegean Sea in the EMED.

Extreme climatological events and favorable hydrographic conditions cause bottom and intermediate waters formation, which in Mediterranean occurs where strong breezes and cyclonic structures are recurrently observed. The different dense water masses formed in the basin include the Western Mediterranean Deep Water (WMDW) in the WMED and Eastern Mediterranean Deep Water (EMDW), Cretan Deep Water (CDW),

Cretan Intermediate Water (CIW), Levantine Deep Water (LDW) and Levantine Intermediate (LIW) in the EMED.

The Etesian winds and the Rhodes Gyre cyclonic structure induce the formation of the LDW and of the LIW (Lascaratos, et al., 1999); (Ozsoy, et al., 1993); (Sur, et al., 1993). The latter, characterized by maximum in salinity and in temperature, represents the most important actor of the Mediterranean thermoaline circulation and is in fact the principal component of the eastern-originated waters flowing in the Western basin through Sicilian Channel (Astraldi, et al., 2001). In addition, it represents the main component of the Mediterranean outflow at Gibraltar (Bryden and Kinder, 1991).

The EMDW forms in the Southern Adriatic Sea, where intense winter Bora bursts act on a permanent cyclonic structure. Similar mechanisms (Mistrals burst and cyclonic permanent circulation) force the formation of the WMDW, which takes place in the Gulf of Lions during the winter season.

Mediterranean dense water is warm if compared with the rest of ocean and salty, and it is not dense enough to sink to the bottom, after exiting the Strait of Gibraltar. It flows then at an intermediate depth in the Atlantic (*circa* 800 meters), and it is supposed to play a key role in the maintenance of the global thermohaline cell. It has been demonstrated that without the inflow of salty Mediterranean water, the formation of dense water would probably not occur continuously in the North Atlantic (Dickson, et al., 1996).

As anticipated before, basin-scale hydrological surveys conducted in the EMED in the 80's and 90's have recently evidenced the role of the south Aegean Sea as an additional source of dense water (Malanotte-Rizzoli, et al., 1999; Roether and al., 1996), affecting the deep and intermediate EMED thermohaline circulation. The change in the source of deep-water masses was named Eastern Mediterranean Transient (EMT), because the phenomenon lasted only 5-7 years. The new observations indicated that the Cretan/Aegean Sea had become an additional driving engine of the intermediate and

deep circulation of the EMED, with the CIW and the CDW spreading out from the Aegean Straits region into the basin interior. Due to the high density of the CDW (> 29.1) the bottom layer of a vast area of the EMED was occupied by this new water mass, which displaced the older EMDW, thus rising the isopycnal surfaces and the nutricline by several hundred meters (Klein, et al., 1999).

1.1.2.2 Subbasins scales

Superimposed on the main thermoaline circulation, several features characterize the Mediterranean circulation, such as gyres, fronts and jets.

The MAW, with its sub-basin instabilities, bifurcations and multiple pathways, which enters from Gibraltar to the Levantine, is present almost everywhere in the basin. It forms two large (100-200 km) anticyclonic gyres in the Alboran Sea, and then bifurcates around the Sardinia Island in two different branches (Millot, 1999). One branch flows into the Tyrrhenian Sea and enters in the large-scale cyclonic circulation occurring in the North Western Mediterranean; the other crosses the Sicilian Channel and penetrates in the Ionian Sea (Font, et al., 1998), feeding the Mid-Mediterranean Jet (MMJ), which, meandering through the Levantine basin, reaches the Cyprus Island (Malanotte-Rizzoli, et al., 1999).

The recirculation of the MAW from the Tyrrhenian produces a large cyclonic circulation in the WMED, encompassing the entire region between the Balearic Islands and the Sardinia. The center of the gyre corresponds to the region of deep water convection in the WMED. Principal features of the cyclonic circulation (Millot, 1987; Millot, 1999) are the strong current (the Liguro-Provencal Current, LPC), which leaves the Italian coast and moves southwestward along the continental margins, and an intense front spanning from the Balearic Islands to the Sardinia (Font, et al., 1988).

The North-western cyclonic circulation has been intensively investigated in the last years (Astraldi and Gasparini, 1992; Conan and Millot, 1995; Sammari, et al., 1995) and

the emerging picture suggests that the main forcing is very likely the geostrophic adjustment to the dense water formation occurring in the Gulf of Lions.

In the Adriatic Sea the surface circulation is cyclonic in all seasons, with the Ionian surface water entering the basin through the Straits of Otranto (Artegiani, et al., 1997a; Artegiani, et al., 1997b). Part of that water flows northward along the Balkans side and returns as a southward flow along the Italian coast. Most of the water does not penetrate north of the 43°N, but instead turns immediately west and recirculates along the Italian coast, thus forming the Southern Adriatic Gyre. The Southern Adriatic Gyre is the principal site of Adriatic Deep Water formation (Artegiani, et al., 1997a), which together with the CDW from the Aegean Sea, are the principal sources of EMDW (Roether and al., 1996). Recent data suggests that Adriatic and Aegean deep waters alternatively prevail (Klein, et al., 2000), underlining the importance of inter-annual variability.

Regarding the EMED, the basin has been recently the subject of a very intensive research coordinated by the international programs POEM (Physical Oceanography of the Eastern Mediterranean) and POEM-BC (Biological and Chemical component of the POEM program). The results (summarized in Malanotte-Rizzoli and al., 1997; Malanotte-Rizzoli, et al., 1999) provided a detailed picture of the basin circulation, and revealed the important changes occurred during the EMT.

The elements of the EMED surface circulation are sub-basin scale gyres and permanent or quasi-permanent cyclonic and anticyclonic structures interconnected by intense jets and meanders. The flow of the MAW in the Ionian is divided in two main branches; the first turning southward enclosing an anticyclonic area with multiple centers, the second moving northward up to 39°N and then turning southward becoming the MMJ. The position of this second branch displays a strong interannual and seasonal variability (Malanotte-Rizzoli, et al., 1999).

In the Levantine basin, several permanent features are recurrently observed, mostly of those with anticyclonic regime (i.e. Pelops gyre, Marsa Matrhu gyre, Iera Petra gyre, Shikmona gyre). An important exception is represented by the Rhodes gyre (Lascaratos, et al., 1999), where in the cyclonic permanent structure, events of atmosphere cooling lead to the formation of dense waters. It was demonstrated (Nittis and Lascaratos, 1998) that the variability of the mean buoyancy loss and the characteristics of the synoptic scale atmospheric events modulate the LIW formation process. In addition, (Sur, et al., 1993) during the cold winter 1992, LIW formation had been found in other areas of the Levantine basin, with concurrent bottom water formation in the center of Rhodes gyre. After its formation the LIW moves westward (Malanotte-Rizzoli, et al., 1999) at the average depth of 250 meters, overlying the EMDW, which in fact occupies the entire layer below 1000 meters.

1.1.2.3 Mesoscale

An intense mesoscale activity has been frequently observed in different regions of the basin, mainly produced by the interactions of the sub-basin structures with the surrounding waters. The mesoscale dynamics are important in Mediterranean since the structures not only affect the circulation at local and sub-basin scale but also influence the exchanges between the different sub-basins and the basin-scale flow.

The typical scale of Mediterranean mesoscale (i.e. the Rossby radius of deformation) is around 10-20 km (Robinson, et al., 1987), because of the peculiar T-S properties of the Mediterranean waters. It comprises structures (eddies and filaments mostly) found usually in shelf/slope areas (Send, et al., 1999) and characterized by strong density gradients resulting in velocities of up to 100 cm/s, on a mean slope current of the order of 20-30 cm/s.

The impact of the mesoscale activity on the general and sub-basin dynamics of the basin as well on the biota was intensively studied in the last years. Among the others, in

the framework of the EU-funded Observations and Modelling of Eddy scale Geostrophic and Ageostrophic motions (OMEGA) project (Allen, et al., 2001; Fielding, et al., 2001), a detailed study was conducted on the mesoscale frontal instability of the Almeria–Oran frontal jet (Alboran Sea). By using high-resolution modern sampling techniques, it has been possible to characterize the mesoscale activity of the area, inferring also the effects of such structures on the biological compartment.

Similar studies were conducted in the Algerian basin (Taupier-Letage, et al., 2003). Exploiting both *in situ* and remote observations, some mesoscale structures associated with the Algerian current were observed and characterized by a long lifetime and by a strong impact on the density field of the area. In addition, it resulted that such features provoked an intense biomass increase, due to the increased vertical velocities and enhanced nutrient refueling of the upper layers. The results confirmed the picture emerged by the studies conducted in the area in the 80's (EUROMODEL Group, 1995). Analyzing the data collected off Algeria, the mesoscale eddies in the area (30-120 km large) were characterized, observing that in some cases such features developed in more consistent structures extending up to 100 km from the coast. Regarding the North Western Mediterranean, Levy et al. (1999), using a high-resolution eddy resolving numerical model, discussed the role of mesoscale in redistributing matter and energy after a deep water convection event and hypothesized that it had a primary impact on the on-set and development of the observed phytoplankton bloom.

Similar findings were reported for the EMED (Robinson, et al., 1991) where the interactions between the large structures of the subbasin circulation induce an intense mesoscale activity in the area. In addition, the mesoscale features seem to play a role in the spreading and transferring the LIW across the basin. Hecht (1988) showed that the spatial distribution of the LIW in the eastern basin was highly correlated with the small-scale spatial variability. Similarly, in the WMED, Millot (1987) observed transport of

LIW from Sardinia into the interior of the central basin by small-scale, mostly anticyclonic, mesoscale eddies.

1.1.3 Biogeochemical processes

The Mediterranean Sea is considered an oligotrophic basin (Antoine, et al., 1995; Azov, 1991; Duarte, et al., 1999; Sur, et al., 1993; Williams, 1998). Oligotrophic, mesotrophic, eutrophic are definitions borrowed from limnologists and are not very suited for the marine environment (for a thorough comment about this issue see Platt, 1985). In this context, it is considered oligotrophic any marine region with an annual primary production smaller than 40 gCm^2y^{-1} (Longhurst, 1995).

Various studies have quantified the total Primary Production (PP) of the basin, utilizing different methods and data (see Table 1-1).

In the table, the values in parenthesis are calculated assuming measured or estimated *f* ratios (the ratio between new and total production), proposed by Marty (2002) for the WMED and by Boldrin (2002) for the EMED. In the second case, the so called *e* ratio, which give the percentage of exported carbon as measured with sediment traps, was used in place of the *f* ratio; however in a steady state situation the *e* and the *f* ratios can be considered equal (see Eppley and Peterson, 1979)).

The budget-derived values suppose a steady state system, which is probably not true, and are based on some assumptions that are still controversial (i.e. the precipitation rate or the river runoff).

The in-situ-derived values, calculated on a basis of few points distributed on the basin, suffer of the classical problem of the extrapolation and then can be considered representative for only the particular conditions of the sampled area.

MED

Total	New	Method	Source
156		Satellite (1979-1983)	(Antoine, et al., 1995)#
190		Satellite (1998)	(Bricaud, et al., 1995)
	8.2	Phosphorus Budget	(Bethoux, et al., 1998)
80-90			(Sournia, 1973)

EMED

Total	New	Method	Source
137	(5.5)	Satellite (1979-1983)	(Antoine, et al., 1995)#
183	(7.32)	Satellite (1998)	(Bricaud, et al., 1995)
(137-150)	5.5-6.0	Phosphorus Budget	(Bethoux, et al., 1998)
	12.0	Oxygen utilization	(Bethoux, 1989)
20.3	11.0	*In situ* data and *f* ratio	(Dugdale and Wilkerson, 1988)
61.8-97.3		*In situ* ^{14}Cdata†	(Boldrin, et al., 2002)†
<11.5	<4.7	Coupled 3D model*	(Civitarese, et al., 1996)*

WMED

Total	New	Method	Source
197	(53.2)	Satellite (1979-1983)	(Antoine, et al., 1995)#
198	(53.5)	Satellite (1998)	(Bricaud, et al., 1995)
(30.4)	8.2	Phosphorus Budget	(Bethoux, et al., 1998)
120	52	Oxygen utilization	(Bethoux, 1989)
83-235	19-71	*In situ* ^{14}Cdata‡	(Marty and Chiaverini, 2002)‡

Table 1-1. Estimates of annual primary production in the MED pelagic system and of its two main subbasin. Units are in g C m^{-2} y^{-1}. † data relative to Ionian and Adriatic station only. *data relative to Ionian Sea only. ‡data relative to DYFAMED station (Northwestern MED) only. #(Antoine, et al., 1995) corrected by a value of 1.25. This correction assumes that the ratio of active-to-total pigments is 1 instead of 0.8 (see Morel, et al., 1996).

The satellite estimates are based on the chlorophyll-*a* values in the upper layer extrapolated to depth and depend on strong assumptions on the vertical biomass distribution. Finally, the model-derived values are subject to the simplifications obviously embedded in a model-like parameterization. In addition, the *f* ratio estimations adopted to compute some of the values in the table, represent in fact an unresolved issue: evidences of the main role of the microbes and bacteria in supporting the Mediterranean PP has been recently analyzed by both experimental data and conceptual models (see Thingstad and Rassoulzadegan, 1999, and references therein).

The uncertainties increase when the seasonality and the interannual variability of the Mediterranean PP are accounted for.

Time series of PP and biomass in the JGOFS-French station DYFAMED (Dynamique des Flux de mAtière en MEDiterranée) located in the Ligurian Sea offshore the French coast have been recently observed by Marty (2002; 2002). During the seven years (1993-1999) of monthly sampling (with important gaps, mainly during winter), the DYFAMED PP displayed a strong interannual variability, with values ranging between 85 to 235 $gCm^{-2}\ y^{-1}$. However, the typical seasonality of the temperate sea, with high values in late winter-early spring and very low values in summer, is clearly evident (see figure 4 in Marty and Chiaverini, 2002). The observed seasonality seems to be an intrinsic characteristic of ecosystem functioning of the basin (Duarte, et al., 1999). The presence of high atmospheric pressure conditions and of a stable water column has been considered the main responsible of the observed early spring bloom. The relatively high irradiance and the high nutrient concentrations due to winter mixing, result in a fast phytoplankton growth.

Duarte et al. (1999), reviewing data from some Mediterranean time series, conclude: "*The development of a late-winter (February to March) phytoplankton bloom is one of the most coherent seasonal features of Mediterranean phytoplankton communities*".

The circumstances leading to the spring bloom appears also in autumn ("Estate di San Martino"), even if the more instable atmospheric conditions prevent a long lasting of the bloom events (Zingone, et al., 1995).

1.1.3.1 WMED and EMED

Despite of the differences between the diverse PP estimates, Table 1-1 underlies an important characteristic of the Mediterranean Sea: the differences between the two subbasins.

Such differences are not only related to the PP.

Crise et al. (1999), for example, showed, on the basis of *in situ* data, a decrease of the Deep Chlorophyll Maximum (DCM) depth moving eastward from the Alboran Sea to Levantine basin. The same authors, using a 3D physical-biological coupled general circulation models of the Mediterranean, reproduced the observed east-west variability in the nutrient and biomass fields, emphasizing the effects of the thermoaline circulation on the ecological zonation of the basin.

Por (1978) demonstrated that the biodiversity is high in the WMED, but relatively impoverished in the EMED. Differences are found also in the biochemical budgets (Bethoux, et al., 1992) and in the nutrient distributions (Moutin and Raimbault, 2002; Sournia, 1973). The observed differences are generally explained invoking the latitudinally shift between the two main sub-basins (Crise, et al., 1999). In fact, the different insolation regimes lead to diverse environmental conditions and in turn to different ecosystem responses. In addition, the prevailing cyclonic circulation of the WMED (see before) permits a more effective uptake of nutrient in the illuminated layer, which is less efficient in the prevalent anti-cyclonic regime of the EMED (Crispi, et al., 2001).

The resulting picture describes then different ecological behaviours for the two Mediterranean sub-basins.

In the EMED, the prevalent anti-cyclonic regime of the surface circulation and the increased thermal stratification are supposed to prevent an effective and diffuse vertical uptake of nutrient. This should produce a deepening of the DCM and a relative increase of the regenerated production (Crispi, et al., 1999; Thingstad and Rassoulzadegan, 1999).

On the other hand, in the WMED, the more energetic air-sea exchanges are believed to induce a more effective nutrient refuel of the euphotic zone, which is also improved by the presence of permanent cyclonic structure in the surface circulation (Crise, et al., 1999; Send, et al., 1999).

In addition, the two straits of Gibraltar and Sicily, which separate and regulate the hydrological dynamics, increase the ecological differences between the occidental and oriental Mediterranean regions.

At Gibraltar the deep layer exports more nutrients than are received from the Atlantic via the surface layer; the net loss of nitrate has been estimated to vary from 490 Mmol/year (Gómez, et al., 2000) to 600 Mmol/year (Coste, et al., 1988).

In the Sicily channel, the situation is quite similar. Commonly, the Strait is described as a two-layer system: the fresher MAW enters the EMED in the surface layer while the more saline LIW flows in the opposite direction in the lower layer (Manzella, et al., 1988). The LIW flows into the WMED through two deep passages, although the major part of the outflow takes place through the eastern passage with a sill depth of 430 m (Bethoux, 1979; Hopkins, 1999). The export of nutrient has been estimated in 294 - 470 Mmol mol/year (Bethoux, 1979; Bethoux, et al., 1998), and similar to the Gibraltar situation, occurs mainly in the intermediate layers.

1.2 THE KEY QUESTIONS OF THIS STUDY

Budget analysis revealed a strong difference in the bio-geochemical processes of the EMED and of WMED, mostly explained by the strait constraints and by the diverse interactions between external forcing (i.e. air-sea fluxes, wind regime) and nutrient dynamics. In addition, mesoscale dynamics and high frequency atmospheric events add variability to the system, inducing a response in the plankton dynamics that could be limited in both temporal and spatial extensions.

The Mediterranean has been investigated intensively in the last decades in the framework of several national and international research programs (among the others: POEM-BC, PROSOPE, ADIOS, SINAPSI etc) and most of the issues concerning its biogeochemical and physical dynamics were addressed and partially solved.

However, as already pointed out, there are still several open questions.

1.2.1 What are the patterns of the Spatial and Temporal biomass distributions in the Mediterranean and what do they reveal on the functioning of the basin?

Several signals suggest the presence of a wide range of "biological processes" that might strongly affect the general behavior of the basin, as the ones retrieved, for example, from the budget analysis. In addition, the knowledge on the spatial and temporal variability of the biomass distribution is far from being complete. In fact, even if the basin has a relatively small size, the classical sampling *via* oceanographic cruises alone is not able to determine with the accuracy needed the events occurring at basin-scale. This is particularly true for the biotic processes, which are more subject than the physical ones, on the changes in the amplitude and timing of the events. In addition, due to the biogeochemical dynamics of the basin, events of large accumulation of phytoplankton biomass are less frequent in the Mediterranean than in other similar seas, making the detection of the areas and of the periods for the sampling difficult. All the above (and the discussions in the chapter 1.1.3) ***highlights that the temporal and spatial distribution of the phytoplankton in Mediterranean Sea is still poorly defined.*** In fact, due to the nature of the hydrographic dynamics (with strong mesoscale activities and complex sub-basin circulation), the nutrient field could be subject to local changes caused by particular environmental conditions that in turn can modify the productivity of the region (see for example Anderson and Prieur, 2000; Krom, et al., 1992; Lohrenz, et al., 1988; Moran, et al., 2001; Send, et al., 1999).

The remote sensing is therefore a basic source of information to improve our knowledge on the basin.

The advantages of the satellites in the study of the ocean are quite evident: high quality of data, synopticity of the measurements; the possibility to investigate phenomena from basin scale to mesoscale; simple procedures for data exploitation; high resolution in temporal sampling.

The CZCS sensor was the first instrument specifically devoted to the study of the biological dynamics of the ocean (see later chapter 2.2.3), but being an explorative mission, some of the described advantages were missed. In particular, the quality of the data rapidly decreased after the 1983, because of decay in the instrument performance, while the temporal resolution was subject of several changes, making in fact impossible the creation of a consistent time series. However, the mission was considered a success, and several other missions became operative in the recent years or are planned for the next future.

Using the data obtained by the CZCS sensors, Morel and co-workers described and analyzed the biological patterns of the Mediterranean surface waters in two papers (Antoine, et al., 1995; Morel and André, 1991) [AMA95, MA91]. The results obtained by MA91 and AMA95 became, for the years following, the "truth" for everything regarding the Mediterranean surface chlorophyll-*a* field and PP. From their results, the Mediterranean appeared as an oligotrophic basin where accumulation of biomass occurred only in particular regions (Alboran Sea, Balearic Sea, South Adriatic and Rhodes Gyre region), partially relaxing the axiom of "*a sea desert* " (Azov, 1991).

However, because of the cited problems of the CZCS, the MA91 and AMA95 analysis was limited to a description of the climatological dynamics of the basin, because of the inconsistency of the CZCS time-series.

The recent development and launch of the SeaStar satellite (October 1997) with the ocean color SeaWiFS sensor onboard, offers the possibility to address some of the unresolved questions.

The main aim of my research was then ***to define the temporal and spatial distributions of the chlorophyll field of the Mediterranean***, making an intensive use of the SeaWiFS data available for the basin.

A full exploitation of ocean color satellite data has as a prerequisite the truthfulness of the remote sensing information; i.e. the quantification of the "error bar" on the

SeaWiFS data (and on the other similar sensors), in a particular region as the Mediterranean.

Therefore, an intense and accurate effort of calibration and validation of the SeaWiFS data was performed, including both the atmospheric and marine terms. The CAL/VAL activities resulted in an improvement of the accuracy of the Mediterranean ocean color data, but helped also to infer on specific aspects of the ecological dynamics of the basin, which, with its trophic regime (i.e. strong oligotrophy with local/subbasin blooms), can be considered a case study for the oligotrophic seas.

The *in situ* data used for the CAL/VAL exercise were composed mainly of the data set collected by the Stazione Zoologica groups during the last years, together with data provided by cruises specifically carried on during the period of my research, which include most of the bio-optical data I used for the calibration. In addition, data deriving from public databases were utilized (i.e. most of the atmospheric ground truth data).

Finally, the corrected and validated Mediterranean SeaWiFS data were averaged to obtain the ***"climatological"*** behavior of the biomass surface field of the basin, highlighting the changes, if any, respect to the AMA95 and MA91 results. ***Time series of the chlorophyll concentration*** were reconstructed from satellite data, to define the seasonal and interannual patterns of the Mediterranean biomass field. Available ***climatological information***, comprising nutrient distributions and mixed layer depths, sea surface temperature and meteorological forcing, was used to verify ***any correlations*** with the observed plankton dynamics.

1.2.2 What is the relevance of phytoplankton blooms in the Mediterranean and to what extent are they regulated by the local physical forcing?

Several studies (see before) highlighted the presence of a strong interannual variability in the plankton dynamics of the MED. The variability is supposed to be

mostly related to the complex interactions between the factors necessary to the plankton growth, i.e. the water column stability and the nutrient and light availability.

The relationships between the external physical forcing and the biological response are, however, still poorly defined in the Mediterranean Sea.

Up to now, the questions was mainly addressed with the wide use of physical-biological models. Several coupled physical-biological modellistic approaches were used for the Mediterranean: the one dimensional approach (Napolitano et al. (2000) for the Rhodes Gyre and Ionian sea; Levy et al. (1998) for the Ligurian Sea), the box-model (Crispi, et al., 2001), the 3-dimensional one (Crise, et al., 1999, Levy et al., 1999; Crispi, et al., 1999; Levy, et al., 2000, for the influence of the atmospheric forcing on the dynamics of the whole basin and of the NW Mediterranean respectively); Stratford and Haines (2002), focused on the effect of the EMT on the nutrient field in the East Med; Zavatarelli et al. (2000), for the Adriatic Sea).

The main finding of the modeling approach was the definition of a clear relationship between the atmospheric forcing and the biomass growth.

Therefore, in my research, a more detailed study was devoted to the ***regions displaying the strongest signal*** in biomass climatological distribution (i.e. the Mediterranean blooms), to better constrain the ***role played by the physical forcing in the regulation of the phytoplanktonic blooms***.

The spatial and interannual variability of the major phytoplanktonic events were analyzed, exploiting the fine temporal and spatial resolution of satellite data. Correlations with the physical forcing supposed to cause the algal variability were studied, addressing in particular the role of the atmospheric forcing.

The areas of the main Mediterranean Blooms have been investigated with a multi disciplinary approach attempting ***to define the scales of the events and the main factors driving the dynamics***. The main approach was based on satellite data, using in turn *in situ* and model derived data.

The model data were obtained by simulation exercises performed in collaboration with other Italian research group; however a part of the simulations were developed at the SZN during my study.

Finally, data by public databases have been collected and used for the purpose of the research. They consist mainly in the atmospheric data, which were obtained from European Center of Medium Weather Forecast (ECMWF) and from National Center Environmental Prediction (NCEP).

1.2.3 Is it possible to obtain a more robust estimate of Mediterranean primary production from remote sensing observations?

Table 1-1 clearly underlies the strong differences between the various assessments of Mediterranean PP. The most obvious problem arises by the diverse methodologies used to retrieve the estimates. In fact, the values in the tables were derived by four different methodologies:

- *In situ* incubations with ^{14}C.
- Budget analysis based on the estimates of the different terms of the nutrient cycling.
- Outputs of general circulation models coupled with bio-geochemical processes.
- Satellite based assessments.

The ***in situ estimates of PP*** were based on the ^{14}C method (JGOFS, 1988), and are in general available for short time intervals and for particular areas, where oceanographic cruises were conducted. In addition, the extrapolation of the point measurements to the whole basin and throughout the year is in general affected by errors, due to the spatial and temporal variability of the system. Moreover, the data obtained before 1988 (i.e. after the JGOFS protocols for the measurements of PP) tended to be lower than the recent ones (JGOFS, 1988). These could be the case of the Mediterranean estimates of Dugdale et al. (1988), which were based on measurements obtained in the seventies.

However, the *in situ* data obtained following the JGOFS protocols are considered the most reliable, and are taken as the "reference".

Budget analysis of total Mediterranean PP was firstly developed by Bethoux and his group (Bethoux, 1979; Bethoux, 1981; Bethoux, 1989; Bethoux and Copin-Montégut, 1986; Bethoux and Gentili, 1996; Bethoux and Gentili, 1999; Bethoux, et al., 1998). It was devoted to the explanation of the relative contribution of the single terms of the nutrient cycling, exploiting the topography of the basin, which permits exchange only through narrow straits. From the nutrient budget, estimates of PP were computed, using the standard C:N ratio. The budget estimates are considered truthful and can be used as a reference for the production of the whole basin (or of the two subbasins). However, they do not resolve the seasonal and interannual variability of the basin, which are the most interesting terms in the biological response to the environmental changes.

Coupled physical bio-geochemical models of the basin have been recently used to give estimates of the general functioning of the Mediterranean (see before). PP is one of the derived products of those models, which are generally based on a GCM, coupled with a multi-compartment (the exact number depending of the complexity of the analysis) chemical-biological model.

The use of models to estimates PP is stimulating, because it permits the analysis of the processes leading to the development of a particular observed condition. In addition, the estimates are available throughout the entire basin and for all the time periods, permitting the determination of the spatial and interannual variability of the PP. However, the modellistic approach is still approximate, mainly in the biological terms, where the simplifying assumptions intrinsic in using models are cruder.

Satellite derived PP estimates are considered the unique way to obtain reliable information on the ocean aerially integrated productivity at basin scale and on its temporal variability. However, "*the extrapolation of surface estimates of chlorophyll to estimates of aerially integrated primary production has been difficult; the variations in*

estimates of production derived from models of satellite images are as great as the variations between shipboard observations" (Falkowski, 1988).

The only ***satellite-derived estimate of Mediterranean PP*** was performed by Morel and his group in MA91 and AMA95 (see before). The method was based on a light-photosynthesis model (Morel, 1988; Morel and Berthon, 1989) initialized by the profile of biomass, obtained by statistical relationships correlating the pigments concentration of the euphotic layer with the upper layer biomass concentration as derived by the CZCS satellite time series (Morel and Berthon, 1989). External information on cloud cover and on sea surface temperature (SST) allowed the assessment of the incoming radiation and the estimate of the quantum yield of photosynthesis. Both were derived from public data sets. As already highlighted in the section on biomass distribution, the AMA95 and MA91 results were considered for long time the "truth" for the evaluation of total PP in the Mediterranean. However, some features described by AM91 and AMA95, do not match with the picture of the Mediterranean ecosystem as emerged by the previous and current literature (see Mediterranean bio-geochemical section). The AMA95 evaluations of annual PP for the whole MED and for the two subbasins were definitely among the highest of the values summarized in the Table 1-1, even if the corresponding chlorophyll values were not biased as compared to the previously obtained ones. Further discrepancies arose by the examination of the PP time series. An intense late-spring PP peak was evidenced by MA91 in the WMED, while in the EMED the maximum of PP was in summer. Those two features disagree with the picture derived from other methods.

Recently, Bricaud et al. (2002) exploited the new available ocean color-sensors (SeaWiFS, OCTS, POLDER) and a series of improved ancillary data set as input for the model of AMA95 for the Mediterranean. The PP estimates obtained were considerably higher than the previous ones and the summer maximum was still present.

However, the Bricaud et al. (2002) approach seems to be the most promising in the definition of a good algorithm for the assessment of the Mediterranean PP. They showed that most of the problems of the Morel and Berthon (1988) model in the PP prediction arise from the ancillary information and by the initial guess of the satellite chlorophyll. They used new ocean-color sensors to increase the quality of the chlorophyll data and weekly Reynolds SST (instead of the monthly mean used by AMA95) to upgrade the final estimates. The high values obtained probably derived by the supposed bias in the Mediterranean satellite-derived chlorophyll (see before), while the "strange" temporal behavior is still unresolved.

I made an effort to ***update the AMA95 method to estimate Primary Production in the Mediterranean***, considering the results of Bricaud et al. (2002) and improving, whenever it is possible, the other possible ancillary information.

The updated PP has been used to compute PP maps of the Mediterranean. ***Estimates of yearly PP at basin and sub-basins scales were carried out*** and compared with the previous values summarized in Table 1-1. Finally, the maps of PP were used to address ***the variability of the plankton activity on a spatial and temporal basis***.

1.2.4 How does the Mediterranean respond to climate variability and transients?

A special analysis has been devoted to the effect of the dramatic change in the thermoaline circulation affecting the EMED in the years 1991-1996 (the EMT) resulting in a rise of the isopycnal surfaces and of the nutricline by several hundred meters (Klein, et al., 1999).

The effects of this evident uplift of the nutricline on the biological activity of the basin are still weakly known.

Civitarese (2001) analyzed the impact of the EMT in the Southern Adriatic, but could not give a definitive answer. As a matter of fact, they showed, through the comparison of nitrate concentrations in the intermediate layer, that during the years

1987-1999 new production had not increased significantly. In general, *in situ* data collected both in the years preceding (Rabitti, et al., 1994) and following the EMT (Boldrin, et al., 2002) confirmed the oligotrophic nature of the area, with surface values of chlorophyll concentration ranging from 0.01 to 0.1 mg m^{-3}. However, ***the measurements conducted after the onset of the EMT were limited in time and space*** and, therefore, ***preclude an assessment of whether an enhancement in chlorophyll concentration and primary production occurred because of the EMT.*** Stratford and Haines (2002) analyzed the results of a coupled physical-biogeochemical GCM for the Mediterranean, and suggested that the EMT might have changed the biological production of the basin by no more than 20-30%. According to their analysis, even if the depth of the nutricline had changed, only anomalously deep winter mixing events would have allowed significant nutrient transport from the uplifted nutricline to the photic zone.

It is worth noting that the effect of the EMT may not have been visible macroscopically. The rising of the nutricline may not have resulted in a temporally and spatially diffuse increase in phytoplankton concentration, but merely in episodic and locally relevant phenomena of chlorophyll enhancement, which could have been detected only with systematic, highly temporally resolved observations of the whole basin.

In fact, as pointed out by Stratford and Haines (2002), an increase in the vertical transport of nutrient could occur anywhere in the basin, because of the subsurface circulation. For this reason, the EMT impact might have altered just the spatial distribution of biomass peaks.

Due to the relatively restricted time span between pre-EMT and the present phase, a comparative analysis of remotely sensed properties becomes a very useful tool to assess any significant changes caused by the EMT, although only in the surface layer of the water column.

The EMT was reasonably circumscribed in time. Thus, a comparison between pre-EMT status and the present condition should permit a first order quantitative assessment of any hypothesized changes in the trophic dynamics of the basin.

The pre-EMT satellite observations were thoroughly analyzed by AMA95. As for the post-EMT period the SeaWiFS data available since 1998 are used. The biomass fields retrieved by satellite were then compared at basin and local scale and the time series of different regions of interest were analyzed to detect any patterns in the spatial and temporal distributions of autotrophic biomass to be compared with the pre-EMT CZCS existing information.

It is worth remembering that the satellite data represents a very powerful tool in the assessment of the sea surface chlorophyll-*a* spatial and interannual variability, though limited by the specific coverage of the sensors and by the cloud coverage. Therefore ***the comparison between two time series of ocean color, twenty years apart, should allow verifying or falsifying the hypothesis that the EMT produced, because of the uplift of the nutricline by several hundred meters, a detectable biological response in the epipelagic layer***. The implicit assumption is that, due to the demonstrated exceptionality of the EMT on the multi-decadal time scale, the CZCS years were representative of the prior to EMT stationary functioning of the basin.

The observed differences between the two periods were also investigated by means of ancillary in-situ data and model derived reconstruction of the hydrographic dynamics and the trophic regime of the basin. A hypothesis of the effect of the EMT on the biological dynamics of the basin was then discussed, especially for the region where the main differences are observed.

CHAPTER 2

Remote Sensing of Ocean Color: a synthetic overview

2.1 OVERVIEW

The presence and activity of the phytoplankton, the microscopic organisms that represent the first step of the marine food web, modify the optical properties of the water in the visible range (the "color" of the water), which changes from blue (absence or low concentrations of phytoplankton) to green (high concentrations). Clarke et al. (1970) in the end of sixties suggested that a satellite-mounted sensor, able to measure the upwelling light in the visible range, could infer the concentrations of phytoplankton in the ocean. Based on the 8 years of life of the first ocean color sensor (the Coastal Zone Color Scanner (CZCS) mounted on the NIMBUS-7 satellite) "*it can be demonstrated that this is not only true, but that the sensitivity of the methodology is surprisingly good*" (Lewis, 1995).

The dynamics of the marine biota exhibits such strong variations in both time and space that shipboard observational programs very often fail to build a large-scale view of their variations. Satellites represent then an unique way to increase the knowledge of the dynamics of marine biota.

In these two chapters, the physical and biological bases of the ocean color remote sensing are succinctly illustrated, and the applications of the described theory to the two most important operational satellites in the visible spectrum (CZCS and SeaWiFS) are

discussed. Finally, the applications and the validation of these data on the Mediterranean Sea, as part of my PhD work, are described.

2.2 OCEAN COLOR DATA

2.2.1 Theoretical background

2.2.1.1 Inherent optical properties

Following Preisendorfer (1961) it is possible to define some properties of water body, which are independent by the relative geometry of the light field within it. Because they depend only on the substances present in the medium, they are defined *inherent optical properties.*

When a photon hits the water, it can be *scattered* or *absorbed.* Accordingly, it is possible to define the *absorption coefficient* (a) and the *scattering coefficient* (b) of a medium, which are, respectively, the absorbed and scattered fractions of incident flux, divided by the infinitesimal thin layer of the medium. It is usual, for the remote sensing purposes, to decompose the scattering coefficient in two components depending on the direction of the scattered flux.

The *forward scattering coefficient* (b_f), indicating the flux scattered from the beam in the forward direction, and the *backscattering coefficient* (b_b), relating to light scattered from the beam in the backward direction. The absorption and the scattering coefficients are considered inherent optical properties, because they depend only on the optical characteristics of the substances and their absolute concentrations.

Preisendorfer (1961) demonstrated that the total absorption coefficient a of the water and the total backscattering coefficient b_b are the sum of the individual coefficients due to all the different absorbers and scatterers present.

Three main optically active components are generally considered in the natural waters, beside the water itself; the phytoplankton, the suspended matter and the chromophotic dissolved organic matter (CDOM - *yellow substance*).

Therefore:

Eq. (2-1) $$a_{tot} = a_{ph} + a_d + a_y + a_w$$

Eq. (2-2) $$b_{btot} = b_{bph} + b_{bd} + b_{by} + b_{bw}$$

where the subscripts *ph*, *d*, *y* and *w* are for phytoplankton, detritus, yellow substance and water respectively.

The spectral variation of a and b_b in pure seawater was measured by Morel and Prieur (1977) and is shown in Figure 2-1.

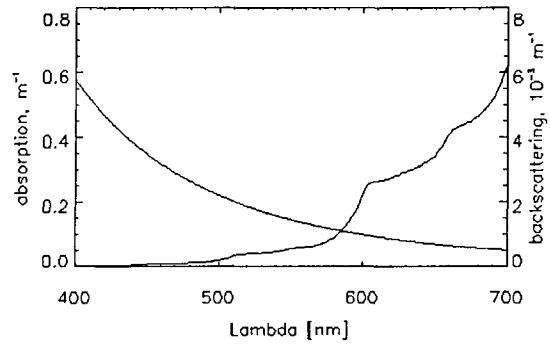

Figure 2-1. Absorption and scattering of pure seawater.

Phytoplankton absorption is strictly related to the photocapturing pigments, which may vary among different algal groups. However, some general characteristics in the spectral behavior are present. On average, the phytoplankton absorption coefficient shows two peaks around 440nm and 675nm (with the first being the higher), while in the remaining part of the spectrum the absorption generally decreases with the wavelength (see Figure 2-2). Backscattering indeed is quite uniform except slight minima in correspondence of the absorption peaks.

As for the so-called *yellow substance*, which is a complex group of compounds deriving from the decomposition of the organic matter present prevalently in coastal waters, its absorption displays a continuos increase from the green part of the spectrum to the blue (Figure 2-2).

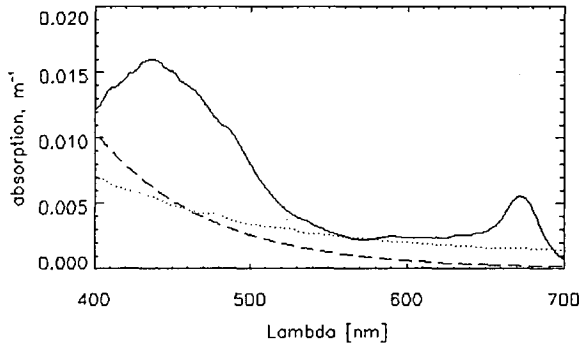

Figure 2-2. Example of absorption of phytoplankton (solid line), detritus (dotted line), yellow substance (dashed line)

Finally, the *suspended particulate matter*, which consists of all particulate not included in phytoplankton. It shows an absorption behavior similar to the yellow substance, though with finite values in the red part of the spectrum (Figure 2-2)

2.2.1.2 Bio-optical algorithms for chlorophyll retrieval

The relationship between the inherent optical properties and the upwelling radiance field has been intensively investigated (Aiken, et al., 1995; Carder, et al., 1999; Jerlov, 1976; Morel, 1980; Morel and Gentili, 1996) because of its relevance in the use of ocean color remote sensing.

Based on data obtained by several *in situ* observations, Morel and Prieur (1977) proposed to divide the natural waters in two main categories, classified in terms of their optical nature. For most of the open ocean waters, variations in the optical properties can be parameterized to a good approximation considering only the chlorophyll (or chlorophyll + active pigments) concentration. They defined those Case I waters. On the other hand, when the concentrations of the yellow substance and detritus do not covary

with the chlorophyll (i.e. mainly in coastal and inland waters), they defined those Case II waters.

Simplified approaches of the radiative transfer theory (Gordon, et al., 1988; Gordon and Morel, 1983; Morel, 1988) led to simple relationships, which were also derived analytically (Zaneveld, 1995), relating the water emerging radiative flux in the visible range of the spectrum to the inherent optical properties. An important one is:

Eq. (2-3)
$$R(\lambda) \propto \frac{b_b(\lambda)}{b_b(\lambda)+a(\lambda)}$$

Where R is the irradiance reflectance (defined as the ratio between total radiant flux incident on surface coming from below and above the surface plane – see Appendix 9.1 for the definitions hereafter) and a and b_b are the total absorption and backscattering coefficient, respectively.

The relationship 2-3 was firstly derived by Preisendorfer (1961), who developed an equation relating the radiant flux to the inherent optical properties:

Eq. (2-4)
$$\frac{R(\lambda)}{Q(\lambda)} = \sum_{i=1}^{2} l_i \left(\frac{b_b(\lambda)}{a(\lambda)+b_b(\lambda)} \right)^i$$

where l_1 = 0.0949 and l_2 = 0.0794, and Q represents the bi-directional reflectance ratio, which should be equal to π in case of perfect Lambertian surface, but it is in general assumed to be equal to 5.0 for near-nadir (i.e. remote sensing) observations (Austin, 1980, but see also Morel and Gentili, 1996).

Afterward, Morel and Prieur (1977) derived a simpler relationship:

Eq. (2-5)
$$R(\lambda) = 0.33 \frac{b_b(\lambda)}{a(\lambda)}$$

The complex spectral dependencies of b_b and a in natural waters, however, prevents a retrieval of information directly from the above expressions.

Therefore, the problem was bypassed analyzing the spectral behavior of *R's*.

In Case I waters (see Figure 2-3) along with the increase in the phytoplankton concentration, *R* decreases in the blue (400-515 nm) and increases in the green (510-600nm).

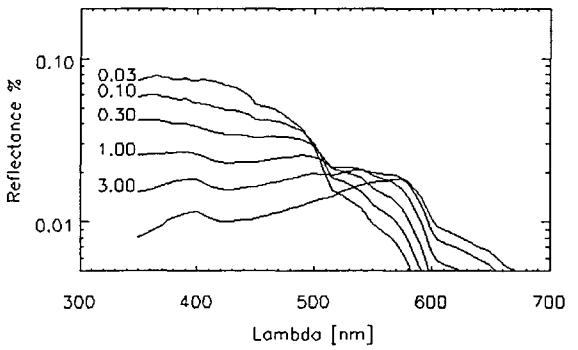

Figure 2-3. Typical reflectance spectra for case 1 water for various chlorophyll concentrations (mg m^{-3}) as indicated.

The variation of *R* with phytoplankton concentration permitted to define an operational method (Clarke, et al., 1970; Morel and Prieur, 1977) to retrieve the concentration of chlorophyll (or chlorophyll + active pigments). In fact, the most widely used approach to retrieve the chlorophyll concentrations from satellite data was based on an empirical relationship between the *R* ratios in the two wavebands and the chlorophyll concentration. The operational algorithm for the CZCS (Gordon, et al., 1980) was derived from a series of simultaneous measurements of *R* at 443,520 and 560 nm and chlorophyll concentrations, and the empirically derived relationship was:

Eq. (2-6)
$$C = 1.15\left(\frac{L_{wn}(443)}{L_{wn}(560)}\right)^{-1.42} \quad ; C < 1\ mg\ m^{-3}$$

Eq. (2-7)
$$C = 3.64\left(\frac{L_{wn}(520)}{L_{wn}(560)}\right)^{-2.62} \quad ; C > 1\ mg\ m^{-3}$$

where C is the chlorophyll-a plus phaeopigments concentration (in mg m^{-3}). Note that in the au-dessus equations, instead of R, it was used the normalized water leaving radiances, which are related to R by simple relationships (see Appendix 9.1).

The case II waters exhibit a complex optical dynamic, making in fact a very difficult task the development of general algorithms able to retrieve information from the R.

2.2.2 Atmospheric correction

To obtain the information coming from below the surface from measurements at the Top-Of-Atmosphere (TOA), as obtained by a space sensor, the optical process occurring in the atmosphere have to be taken into account.

If $L_t(i)$ is the radiance (see appendix 9.1 for the definitions hereafter) measured at the TOA at the wavelength i, the resulting signal will be the sum of the diverse terms acting on the radiation path from sea surface to sensors (see Figure 2-4). Excluding second order terms:

$$\text{Eq. (2-8)} \qquad L_t(i) \cong L_{path}(i) + T(i)L_g(i) + t(i)L_f(i) + t(i)L_w(i)$$

where $L_{path}(i)$ is the radiance due to the scattering along the path and to the specular reflection of skylight from the sea surface; $L_g(i)$ is the radiance arising from reflection of direct sunlight from the sea surface (sun glitter); $L_f(i)$ is the radiance derived from the reflection of sunlight and skylight on the individual whitecaps on the sea surface; and $L_w(i)$ is the water leaving radiance. $T(i)$ and $t(i)$ are respectively the diffuse and direct transmittance of the atmosphere at wavelength i.

The atmospheric correction of the TOA signal is based on theoretical relationships and practical procedures, which permit to obtain, from the measured satellite TOA radiances, the correspondent above water signal.

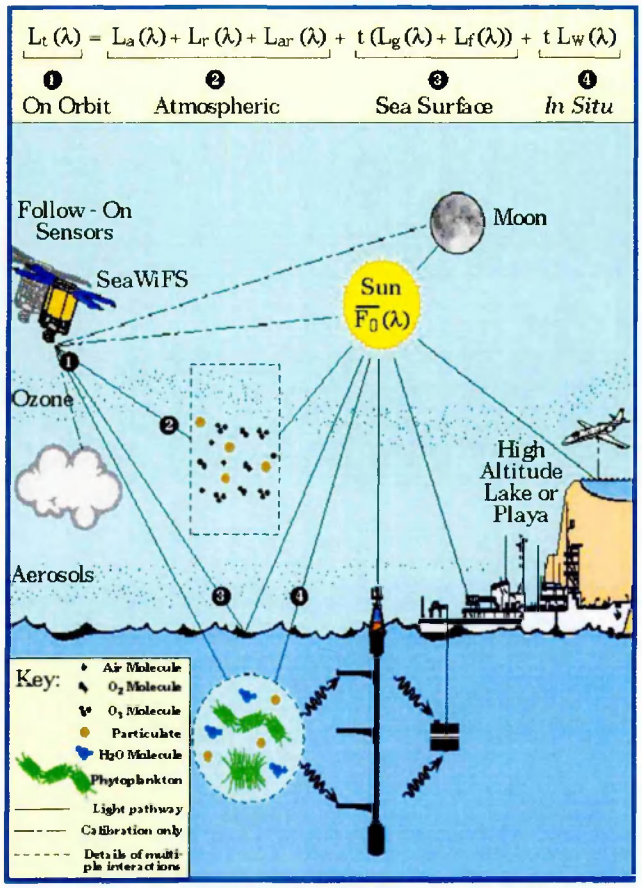

Figure 2-4. Schematic diagram of the terms measured by an ocean color sensor (from NASA-SeaWiFS web-site).

The procedure is achieved estimating or calculating all the terms in equation 2-8, which do not derive from the water.

The water leaving radiance may then be obtained subtracting those terms from the TOA measurements.

Table 2-1 (from Robinson, 1985) reports the different contributions to the TOA signal of the terms in equation 2-8 (the term L_r denotes all the contributions from surface reflection, i.e. the sum of L_f and L_g), at selected wavelengths in the blue, green and near infrared region of the spectrum.

It can be seen that about 80-90% of the radiance received by a satellite sensor derives from the atmosphere.

Wavelength (nm)	Contribution to the signal %					
	Clear water			Turbid water		
	TL_w	L_{path}	TL_r	TL_w	L_{path}	TL_r
440	14.4	84.4	1.2	18.1	80.8	1.1
520	17.5	81.2	1.3	32.3	66.6	1.1
670	2.2	96.3	1.5	16.4	82.4	1.2

Table 2-1. Relative contribution to the TOA radiance from the different terms in the equation 2.8.

L_{path} and T depend on the scattering and absorption properties of the atmosphere, which are described by the dimensionless quantity called *optical thickness* τ (see appendix 9.1 for a definition).

The atmospheric signal originates in the interactions of photons with air molecules and with aerosols. The latter are small solid or liquid particles, which may have been lifted by wind from the earth's surface, or sublimated and condensed gases from atmosphere. The molecular composition of the atmosphere is generally uniform and well known, then it is suitable to consider the molecular and the aerosols effects separately.

Eq. (2-9) $$L_{path}(i) = L_r(i) + L_a(i) + L_{ra}$$

and similarly

Eq. (2-10) $$\tau_{path} = \tau_r + \tau_a + \tau_{ra}$$

The term $L_{ra}(i)$ and τ_{ra} account for the photons that experienced a scattering with both molecules and aerosols particles.

The optical thickness of molecular effects τ_r depends very little on absorption (except for ozone effect, which absorbs around 600nm) and derives largely on the scattering by air molecules. The latter, being the air molecules small compared with the visible wavelengths, can be expressed through the Rayleigh scattering theory. Under these

assumptions it is possible to compute τ_r knowing the sea level atmospheric pressure (Hansen and Tracid, 1977):

$$\text{Eq. (2-11)} \qquad \tau_r(\lambda) = \frac{P}{P_0}(0.008569\lambda^{-4}(1+0.0113\lambda^{-2}+0.00013\lambda^{-4})$$

with P_0 equal 1013.25 mbar.

More complex is the derivation of the aerosols scattering terms τ_a and τ_{ra}. Since aerosols particle are much larger than molecular sizes, the Mie theory has to be invoked, though it requires the knowledge of the aerosol properties of the atmosphere.

To perform an appropriate atmospheric correction procedure to obtain satellite estimates of L_w then some assumptions on the aerosols distributions of the atmosphere and on its interactions with light are required. In general, those are not available at the temporal and spatial resolutions required for the exploitation of the remote sensing advantages.

The problem was solved by Gordon (1978), who derived a method to achieve a moderately accurate atmospheric correction for ocean color images. This finally allowed the development and the exploitation of the first space sensor devoted to the remote observations of ocean color, the CZCS (Hovis, et al., 1980), which was mounted on the Nimbus-7 satellite, and launched in October 1978.

2.2.3 The CZCS sensor

The Coastal Zone Color Scanner was a multi spectral radiometer with four bands in the visible region, each 20 nm wide, centered on 443,520,550 and 670 nm, respectively, one band in the near infrared (700-800 nm) and another band in the infrared (10.5-12.5 μm) for temperature measurement. The satellite was positioned on a polar orbit, which should have produced a daily satellite time pass over the same Earth area (but see below Limits and problems of the CZCS sensor). The sensor had an instantaneous field of

view of 0.05°, corresponding, at a nominal satellite altitude of 995 km, to a unit element of area 1 km square at the surface (Hovis, et al., 1980). In addition, to avoid the signal from Sun glitter, the sensor had the possibility to be tilted, scanning then up to 20° from the nadir.

During its lifetime (it remained operative until 1986), the CZCS produced approximately 66.000 images of the world ocean, thus resulting in one of the most successful missions, in terms of improvements in both marine biota understanding and remote sensing ocean color methodologies.

2.2.3.1 The CZCS atmospheric correction

The CZCS atmospheric correction algorithm was mainly developed by the University of Miami group. Here, we briefly describe its main parts, whereas for additional information it possible to refer to Gordon (1978), Gordon et al (1988), Gordon and Morel (1983), Evans and Gordon (1994).

The first approximations adopted were in the equations 2-8 and 2-9. It was assumed that the photons collected by the instrument experienced only a single scattering event in the atmosphere (single scattering assumption). In addition, a flat sea surface was presumed, considering then the absence of wind. In these cases, the terms $L_{ra}(i)$ and $L_f(i)$ in the equations 2-8 and 2-9 can be considered equal zero, while $L_r(i)$ and $L_a(i)$ can be replaced by their single scattering values ($L_{rs}(i)$ and $L_{as}(i)$) and expressed (Gordon and Morel, 1983) as:

Eq. (2-12) $$L_x = \omega_x(i)\tau_x(i)F_0'(i)p_x(\theta_v,\theta_0,i)/4\pi\cos\theta_v$$

with

$$p_x(\theta_v,\theta_0,i) = P_x(\theta_-,i) + (\rho(\theta_v)+\rho(\theta_o))P_x(\theta_+,i)$$

and

$$\cos\theta_{\pm} = \pm\cos\theta_0\cos\theta_v - \sin\theta_0\sin\theta_v\cos(\phi_v - \phi_0)$$

with x equal to *rs* or *as*.

In the above equation, θ_0 and ϕ_0 are the zenith and azimuth angles of the vector from the observed point on the sea surface to the sun (*solar zenith angle* and *solar azimuth angle*), and, θ_v and ϕ_v are the zenith and azimuth angles of the vector from the point on the sea surface to sensor (*satellite zenith angle* and *satellite azimuth angle*). $\rho(\theta)$ is the *Fresnel reflectance* at surface for an incident angle θ, $P_x(\theta, i)$ is the *scattering phase function* for the x term (x=*as* or *rs*), $\omega_x(i)$ is the *single scattering albedo* of x ($\omega_{rs}(i)=1$), and $\tau_x(i)$ is the *optical thickness* of x.

The term $F'_0(i)$ is the *extraterrestrial solar irradiance* (i.e. the irradiance emitted by the sun at the TOA) which can be written as a function of the Julian day D and of the *ozone optical thickness* $\tau_{oz}(i)$:

Eq. (2-13)
$$F'_0 = F_0(D,i)\exp\left[-\tau_{oz}(i)\left(\frac{1}{\cos\theta_v}+\frac{1}{\cos\theta_0}\right)\right]$$

In the CZCS standard procedure, the ozone optical thickness was determined from measurements carried out by the Total Ozone Mapping Spectrometer (TOMS) instrument, which was mounted on board of the same satellite (Nimbus-7) of the CZCS.

The term L_{rs} was calculated deriving the Rayleigh optical depth $\tau_r(i)$ from the atmospheric pressure (see below). In the CZCS global processing the $\tau_r(i)$ values were kept constant (i.e. without taking in account the pressure correction) with an estimated error of the 1.5 %.

In addition, the presence of a tilting mirror permitted to direct the sensor far from the specular image of the sun, which allowed to neglect the L_g term.

The only unknown was than the aerosol optical thickness $\tau_{as}(i)$, required to estimate L_{as} *via* equation Eq. (2-12).

The operational procedure to retrieve $\tau_{as}(i)$, was based on the assumption (but see later) that in the near infrared region (i.e. in the 670nm CZCS band) the $L_w(670)$ is close to zero (see Table 2-1). Equations 2-8 and 2-9 permitted then to retrieve L_a in the near infrared band (i.e. 670 nm).

To estimate the aerosol radiance in the shortest wavelengths (i.e. 440, 520 ad 550) the method introduced the *atmospheric correction parameter* $\varepsilon(i,670)$, defined as:

$$\text{Eq. (2-14)} \qquad \varepsilon(i,670) = \frac{\omega_a(i)\tau_a(i)p_a(\theta_v,\theta_0,i)}{\omega_a(670)\tau_a(670)p_a(\theta_v,\theta_0,670)} = \left(\frac{670}{i}\right)^{\alpha}$$

where the term α is the Ångstrom coefficient.

The atmospheric correction parameter was independent from the aerosol concentration and become the key to perform the atmospheric correction procedure.

Knowing $\varepsilon(i,670)$, it was possible to estimate the aerosol term L_{as} in the other CZCS bands, and then, applying the equations 2-8 and 2-9, to retrieve L_w for all the bands. Unfortunately, the determination of $\varepsilon(i,670)$ was very difficult to be performed, mainly because the number of bands of CZCS was insufficient to determine its spectral behaviour. "*Simply, there was not enough information to estimate the values of* $\varepsilon(i,670)$ *required to execute the procedure*" (Evans and Gordon, 1994).

The method to overcome this lack of information was finally developed by Gordon and Clarke (1981). They observed that at low chlorophyll concentrations ($C < 0.25$ mg m^{-3}) the L_w at the bands 520, 550 and 670 were quite constant, and therefore could be considered known. Thus, to estimate the atmospheric correction parameters, a region of the image for which C was less than 0.25 was selected, and, in that area, the $\varepsilon(520,670)$, $\varepsilon(550,670)$ and $\varepsilon(670,670)$ were supposed known. Finally, $\varepsilon(440,670)$ was retrieved by extrapolation and the resulting values of ε were used throughout the whole image to derive L_w for all the bands.

2.2.3.2 *Applications of CZCS derived phytoplankton concentration*

After the atmospheric correction, the satellites L_ws were used to retrieve the pigments (chlorophyll a + phaeopigments) concentrations *via* the empirical relationships 2-6 and 2-7.

The analysis conducted since then on the CZCS data cover many oceanographic fields from global scale to mesoscale phytoplankton dynamics, up to commercial applications like fishery researches. In addition, algorithms were developed to estimate oceanic primary production at regional and global scales.

In the following paragraph, a brief list of some of the most relevant studies is reported.

Several papers were devoted to the description and the analysis of the spatial and temporal dynamic of the phytoplankton biomass (Aiken, et al., 1992, Mitchell, 1994 #34; Feldman and al., 1989; Sullivan, et al., 1993; Yoder, et al., 1988). Moreover, the combination of CZCS data with shipboard data and other satellite measurements, such as SST or scatterometer derived winds, provided insights into physical and biological interactions. Relevant contributions are, among the others: multi-platform satellite analysis (Afanasyev, et al., 2001, in the North Atlantic; Denman and Abbott, 1988, in the California current; McGillicuddy, et al., 2001, in the Sargasso Sea); climatological studies combining in-situ and satellite data-sets (Arrigo and McClain, 1994, in the Southern Ocean; Ryan, et al., 1999, in the Middle-Atlantic Bight) and primary production estimates at global or local scales (Antoine and Morel, 1996; Behrenfeld and Falkowski, 1997; Longhurst, 1995).

2.2.3.3 *Limits and problems of the CZCS sensor*

The performances of the CZCS sensor were quite surprising, also considering that it was built with the early 1970s vintage technologies and that it was designed to have a nominal life of one year. In addition, it was the first time that the scientific community

approached the issues of a specifically devoted ocean color mission, and then most of the problems affecting the sensor and the post-processing procedures were practically unknown. Two main groups of problems were identified during and after the CZCS lifetime: the first comprised the "hardware" systems and was mainly related to the malfunctioning and degradation of the sensor apparatus; in the second group were included the algorithms uncertainty (the "software" problems) in both the atmospheric and bio-optical terms.

Hardware problems: the most important problem occurring in the hardware of the CZCS instrument was the strong degradation of the sensor sensitivity (Evans and Gordon, 1994). The system was equipped with an incandescent lamp providing a rough internal calibration; unfortunately, the lamp was not used for that function, since its light did not pass through the entire optical apparatus and the intensity in the blue band was too low. The lamp was then used only to monitor the long-term stability of the detectors.

However, to obtain the needed accuracy in the L_w, a further calibration effort was conducted. Using the (few) available *in situ* data of L_w and C concentrations collected at the same time of a satellite overpass, a so-called "*vicarious calibration*" was performed. This was accomplished by adjusting the calibration to force the sensor plus algorithms outputs to yield ship-based measurements of available L_w and C.

Nevertheless, Evans and Gordon (1994) demonstrated that the sensor experienced both long and short terms degradation, mainly in the blue bands. In fact, even if the calibration lamp worked quite well during the whole CZCS lifetime (Evans and Gordon, 1994), the frequency of its applications decreased constantly in time, leading to a decline in the CZCS performance. In addition the vicarious calibration procedure suffered for the paucity and for the irregular distribution of *in situ* data.

The consequences of the hardware problems were that after an initial period (1979-1981), when all the passes were considered corrected and calibrated, the CZCS data started exhibiting strong inaccuracy.

In addition, due to the power demand of the various on-board experiments, the CZCS operated on an intermittent schedule, resulting then in several gaps in the data time series.

Software problems: the atmospheric correction procedure was definitively limited by the presence of only one band in the infrared region. The method adopted to skip the problem (see before) could not be applied when the examined imagery did not contain pixels with chlorophyll values less then 0.25 mg m^{-3}. Furthermore, even if a clear water ($C < 0.25$ mg m^{-3}) pixel was found, the retrieved ε values varied over the image because of variations in the aerosol type (André and Morel, 1991; Bricaud and Morel, 1987). In addition, even for an invariable aerosol type, there is a weak dependence of the aerosol phase function on the wavelength, which results in a dependence of the ε on the position in the image (Gordon and Morel, 1983). Finally, the assumptions of Rayleigh single scatter, absence of foam and nil signal of L_{wn} in the infrared were often not accomplished, making the outputs of the algorithm incorrect.

Regarding the bio-optical CZCS algorithm several studies were devoted to the validation of the CZCS chlorophyll concentration. Gordon et al. (1980) showed that the pigments concentrations retrieved from CZCS match the concurrent ship measurements within 0.5 log C in the Gulf of Mexico region. Balch et al. (1992) using 731 coincident satellite and *in situ* chlorophyll measurements, demonstrated that the CZCS data underestimated the true pigment concentration in mesotrophic and oligotrophic water ($C < 1$ mg m^{-3}) and overestimated it in eutrophic waters ($C > 1$ mg m^{-3}).

Summarizing, both the atmospheric correction and the bio-optical CZCS algorithms exhibit errors and inaccuracies when the estimated parameters are compared with sea truth data. Furthermore, it is important to note, that the quality and quantity of *in situ*

data was often at low level and irregularly distributed on the globe. In particular, the very scarce number of simultaneous atmospheric and in-water measurements (radiances and chlorophyll concentration) did not permit to verify the relative impact of the different processing procedures (vicarious calibration, atmospheric correction and bio-optical algorithm) on the error of the final satellite chlorophyll concentration.

2.2.4 The SeaWiFS sensor

The Sea-viewing Wide Field-of-view Sensor (SeaWiFS) is the successor of the CZCS. It was launched in the August 1997 on board the OrbView-2 satellite, which, unlike Nimbus-7, was totally devoted to the ocean color mission. The satellite was positioned on a 705 km sun-synchronous polar orbit, with an equator crossing time at noon+20 minutes. The spatial resolution at ground is of 1.1 km for the full resolution data, and 4.5 km for the low-resolution ones. The revisiting time is approximately one day on a routine basis, which produces global daily geo-physical fields in near-real time. The instrument is equipped with a tilting mirror to avoid the direct Sun glint and provides radiance measurements at five bands in the visible range (410, 443, 490, 510, 555 nm) and three in the red and near infrared (670, 765, 865 nm).

The main aim of the SeaWiFS mission was to obtain valid ocean color data of the world ocean with an uncertainty of 5% in determination of the water-leaving radiances in clear-water regions, and within ±35% in the estimation of the chlorophyll concentrations over the range 0.05-50 mg m^{-3} (Hooker and McClain, 2000). To achieve these goals, several dedicated research activities were planned, involving all the steps of the data stream system (satellite imagery, spacecraft engineering, derived products and ancillary fields). Most of the novel features of the SeaWiFS sensor were a heritage of the success (and failures!) of the CZCS mission, which provided an important lesson on the exploitation of the ocean color data.

2.2.4.1 The lessons of the CZCS

Conceptually, the SeaWiFS calibration and processing system is similar to the CZCS one. The main differences arise from the increased number of ancillary information available, both *in situ* (which in most of the cases are specifically collected for SeaWiFS processing purpose) and from space, and in the improvement in the accuracy of the processing methods. Most of the activities related to the SeaWiFS mission are funded and carried out in a framework of several national and international research projects. They are specifically devoted to particular tasks of the SeaWiFS Project, which in fact includes and manages the research activities.

Both atmospheric correction and bio-optical algorithms follow the methodologies already described (see before), even if most of the assumptions and the simplifications of the CZCS are solved.

In the following sections, the main improvements of the SeaWiFS procedures respect to the CZCS ones are briefly listed and explained, highlighting in particular the new methodologies applied to the SeaWiFS.

New bands in the near-IR. Undoubtedly, the main difficulties in the achievement of the CZCS atmospheric correction procedure arose from the presence of only one band in the NIR region. In the SeaWiFS sensor two additional bands were added (765 and 865 nm), permitting a strong increase in the accuracy of the atmospheric correction procedure (see later).

Vicarious and on-board calibrations. The CZCS vicarious calibration depended on occasional and sparse *in situ* data. For the SeaWiFS mission, since the beginning of the data collection, a specifically devoted vicarious calibration program was developed and made operative. A Marine Optical BuoY (MOBY) located near the Hawaii (Clark, et al., 1997) was equipped with an array of marine radiometers, capable to produce a time series of water-leaving radiances usable for the vicarious calibration exercise. In the

framework of MOBY program, measurements of chlorophyll concentrations are also carried out, which are necessary to finalize the vicarious calibration procedure.

In addition to the MOBY time series, the satellite system is set to monitor the sensor calibration over periods of a few orbits, to several months or years, using solar and lunar calibrations performed directly on board, on a daily and monthly basis, respectively (Barnes, et al., 1999).

Pressure effect. Atmospheric sea level pressure is used to modelise the τ_r term (see equation 2-11), but its effect was not accounted for in the CZCS procedure. For the SeaWiFS processing, ancillary information on the surface air pressure deriving from weather numerical models, are used to exactly determine the τ_r term.

Foam and white caps. In the CZCS atmospheric correction procedure, the term in the equation 2-8 due to the foam and white caps (L_f) was considered negligible. However, Gordon and Wang (1994) demonstrated that in particular conditions it might be relevant. In the SeaWiFS processing, the L_f term is taken in account following the suggestions of Moore and al. (2000), who estimated it using the following relationship:

Eq. (2-15) $$L_f = 6.49 \times 10^{-7} W^{3.52}$$

where W is the wind speed in meters per second measured 10 m above the surface.

Black pixel assumptions. Another assumption in the CZCS atmospheric correction scheme was the so-called "*black pixel assumption*". To estimate the term L_a in the equation 2-9 the contribution of the water to total radiance in the NIR band was considered negligible. However Siegel et al. (2000), following the evidences and the methodologies of Ruddick et al. (2000), demonstrated that the black pixel assumption could induce a not negligible error on the estimations of the L_w. This error may be considered significant when the chlorophyll concentrations are high ($C > 2$ mg m^{-3}) but can be relevant even at lower concentrations. They proposed a new method to replace the black pixel assumption, based on a preliminary assessment of the chlorophyll

concentration and on an iterative method to calculate the near infrared water radiance. The Siegel's procedure results in a correction factor, which permits to evaluate, and then to consider, the contribution of the water in the NIR ("*dark pixel*" Siegel assumption).

New atmospheric correction scheme. The new characteristics of the SeaWiFS sensor and the improved analysis on the CZCS atmospheric correction resulted in the definition of a new procedure for the SeaWiFS atmospheric correction (Gordon, 1997; Gordon and Wang, 1994). The SeaWiFS atmospheric procedure includes the Siegel's methodology and accounts for the whitecaps contribution. In addition, it settles the unsolved issues of multiple scattering and of the spectral behavior of the ε, using the new bands in the NIR region. See later for a brief description of the SeaWiFS atmospheric correction procedure.

Bio-optical algorithm. The CZCS standard bio-optical algorithm was derived from the Nimbus Experiment Team radiance-chlorophyll data set (Acker, 1994), which contains less than 60 stations. To improve the accuracy of the ocean color chlorophyll product, the SeaWiFS project convened a working group (SeaWiFS Bio-optical Algorithm Mini-Workshop, SeaBAM) specifically devoted to identify and test algorithms suitable for operational use. A large, globally representative *in situ* data set (Werdell and Bailey, 1999) of water leaving radiances and chlorophyll concentrations were developed (The SeaWiFS Bio-optical Archive and Storage System (SeaBASS), containing more than 600 stations. More then 20 algorithms were tested and validated on the SeaBASS data set (O'Reilly, et al., 1998). Finally, an empirically derived two bands ratio algorithm (OC2) was considered appropriate to achieve the main goal of SeaWiFS project of an error of ±35% in the estimation of the chlorophyll concentrations over the range 0.05-50 mg m^{-3}. The OC2 algorithm had the following functional form:

Eq. (2-16) $$C = 10^{(a_0+a_1R+a_2R^2+a_3R^3)} + a_4$$

where R is the log10 of the ratio of two remote sensing reflectances R_{rs} measured at two different wavelengths (490 and 555 nm), while the coefficients are derived by a statistical fit with SeaBAM archive. In the 2000, the increment of *in situ* data led to a slight modification of the OC2 algorithm and to the development of the OC4 algorithm (O'Reilly, et al., 2000). The OC4 algorithm maintains the same functional form of the OC2, but the ratio R can be either between 443 and 555 nm, or 490 and 555 nm, or 510 and 555 nm, depending on the value of this ratio (the maximum is chosen).

Processing the data. To easy the processing of the data, the SeaWiFS project developed an auto-consistent IDL-based free software (SEADAS) capable to carry out the entire data stream (Baith, et al., 2001). A number of flags and masks are calculated on the processed passage, permitting to define the degree of error in the treatment of the images. In addition, several options regarding all the steps of the data processing are available, permitting to decide the degree of accuracy of the final data.

The software needs the ancillary information required to perform the atmospheric correction procedure (ozone total amount, atmospheric pressure, wind velocity, total precipitable water vapor, and relative humidity), which are provided in near real time by concurrent satellite measurements (i.e. TOMS for the ozone) or by outputs of numerical weather models (i.e. the National Meteorological Center NCEP).

From the beginning of the SeaWiFS project, the number of products provided by the SEADAS is constantly increased. At the moment (May 2003) 21 products for each SeaWiFS wavelengths and 43 miscellaneous products are available

The detailed description of the SEADAS processing and products used hereafter, together the description of flags and mask, is given in appendix 9.2.

2.2.4.2 The scheme for the SeaWiFS atmospheric correction

As already highlighted, the SeaWiFS atmospheric correction procedure is based on the same concepts of the CZCS one. The improvements in the methodologies, needed to

achieve the SeaWiFS Project goal of 5% error in the L_{wn} retrieval, are mainly focused on the solution of the several assumptions in the CZCS procedure.

Firstly, the single scattering assumption was considered one of the main sources of error in the CZCS method (Gordon and Wang, 1994), and then was believed one of the issues to be solved first and foremost, recovering in the equation 2-9 the multiple scattering terms. When multiple photons scattering is included in the system, the term $L_a(i)$ cannot be expressed using the equation 2-12, while the term $L_{ra}(i)$ cannot be neglected.

To solve the issue, the $\varepsilon(765,865)$, which already contains the required spectral information, is calculated from the measured radiance in the same way of the CZCS procedure (see above). The $\varepsilon(765,865)$ value is then used to select two most appropriate aerosol models from a suite of 12 candidate aerosol models (Gordon and Wang, 1994). The selection is operatively performed using $\varepsilon(i,865)$s look-up tables generated with an atmospheric radiative transfer model, which use as input the 12 aerosol models (Shettle and Fenn, 1979). The described comparison permits then to select two aerosol models, which better matches the atmospheric condition of the considered region/pixel. It was also supposed that if $\varepsilon(765,865)$ falls between two aerosol models, the reflectance $L_a(i)$-$L_{ra}(i)$ will fall between the same two models in the same proportion of $\varepsilon(765,865)$. The radiative transfer model is then used to create a set of look-up tables in which $L_t(i)$-$L_r(i)$-$tL_w(i)$ is provided as a function of $L_{as}(i)$. The use of LUT makes easier and faster the application on a pixel basis of the methodology. From the obtained $L_t(i)$-$L_r(i)$-$tL_w(i)$ term, the computed $L_r(i)$ and the measured $L_t(i)$ are subtracted, making then possible to calculate $L_w(i)$. In addition, the selected model give information on the characteristics of the aerosols present in the air column (i.e. $P_a(\theta, i)$, the scattering phase function and $\omega_a(i)$, the single scattering albedo), which, used in conjunction with equation 2-12, permits to estimate the aerosol optical thickness $\tau_a(i)$.

The use of 765 nm band however adds an ulterior term of uncertainness to the atmospheric correction procedure. The SeaWiFS 765nm channel response in fact includes the O_2 absorption band at 750 nm, so its influence on $L_t(765)$ needs to be assessed. Following the method of Ding et al. (1995) the error induced on the radiance can be expressed as:

Eq. (2-17)
$$\frac{L_a(765)}{L'_a(765)} = \left[1 + 10^{P_{r,a}(M)}\right]$$

where $L_a(765)$ and $L'_a(765)$ indicate respectively the aerosol reflectances without and with the O_2 *A*-band absorption present. The term $P_{r,a}(M)$ is a fitting function of air mass M for the Rayleigh and aerosol components and is dependent only of air mass. The correction is then performed using pre-calculated values of $P_{r,a}(M)$ for various M values and then retrieving the corrected $L'_a(765)$ values. It is however important to note that in the computation of the $P_{r,a}$ values, it is implicitly assumed a constant pressure value (i.e. 1015 mbar).

The Gordon and Wang procedure represents a significant improvement respect to the CZCS atmospheric correction method: it can be applied on a pixel basis, works out most of the unsolved issues and permits also to retrieve information on the aerosol characteristics of the observed region.

2.2.4.3 SeaWiFS data and their applications

Since 1997 the SeaWiFS sensor produced global daily maps of chlorophyll concentration, water leaving radiance and aerosol optical thickness at the available visible wavelengths. The archives set up by the NASA, in the framework of the SeaWiFS project, process, manage and make available for the scientific community all the acquired passes at any level of processing. The SeaWiFS data pass throughout several steps, which are briefly explained in the appendix 9.2. Here, it is important to

highlight that using the SEADAS software and the NASA archive, it is possible to obtain all the available information derived from SeaWiFS.

The number of research papers, which directly or indirectly are related to the SeaWiFS data, is incredibly high, even though its relatively short life-time. The good performances of the sensor hardware, the high accuracy of the procedures and of their validation and the organization and management of the SeaWiFS data, permitted to suddenly utilize it in the earth studies.

The most intensively studied topic were undoubtedly the dynamics of the marine biota on the various spatial scales obtainable from SeaWiFS data.

The analysis of chlorophyll field variability on global or regional scale span from purely SeaWiFS-derived studies (Afanasyev, et al., 2001, in the New Foundland region; Chaturvedi and Narain, 2003, in the Arabian Sea; Garçon, et al., 2001; Kudela and Chavez, 2002, in the Pacific; Longhurst, 2001, in the Madagascar Basin; Smyth, et al., 2001, in the Iberian Margin) to multi-platform approaches with both other remote sensed (Alvarez-Salgado, et al., 2003; McClain, et al., 2002) and *in situ* data (Follows and Dutkiewicz, 2002; Wiggert, et al., 2002).

Regarding the bio-optical algorithm, validation efforts are carried out to define the errors in the satellite chlorophyll retrievals (Kahru and Mitchell, 1999; Sasaoka, et al., 2002; Sathyendranath, et al., 2001; Siegel, et al., 2001; Westbrook, et al., 2001), while new algorithms exploiting the large spectral information of the SeaWiFS are developed to estimate other parameters than the chlorophyll-*a* (Gordon, et al., 2001; Iida, et al., 2002, for the coccolithophore concentration estimates; Siegel, et al., 2002b, and ; Stramski, et al., 1999, for the Particulate Organic Carbon –POC; Subramaniam, et al., 2002, for *Tricodesmium* detection).

2.2.5 Ocean Color data in the Mediterranean

From point of view of satellite ocean color data, the Mediterranean can be considered a favorable area. The relatively low cloudiness at these latitudes increases the number of observations from space and the moderately small size of the basin make easiest to deal with satellite data (i.e. the files dimensions are not "impossible", even in the case of the full resolution imageries).

2.2.5.1 Mediterranean CZCS data

Two fundamental papers (Antoine et al., 1995, for the EMED, Morel and André, 1991, for the WMED) were published by Morel and coworkers, with the specific aim of investigate the biological dynamic of the basin using the CZCS remote sensed ocean color data. They used a specific processing methodology (Bricaud and Morel, 1987) permitting to increase the accuracy of the CZCS data in a region such as the Mediterranean. Indeed, the presence of the Saharan desert and of high density of human population, respectively, along the south and north boundaries, make the atmospheric conditions of the area extremely variable and complex. In these situations, the CZCS atmospheric correction, assuming constant aerosol conditions, was doomed to failure. The application of the Bricaud and Morel (1987) method however permitted to overcome the problem processing the image on a "pixel by pixel" basis, which allowed accounting for the local change in the aerosol characteristics. The procedure also allows turbid case II waters to be identified.

In addition, due to the known variations in the sensor sensitivity, two *a posteriori* recalibrations were performed (see MA91 and AMA95). Briefly, for the WMED, they tuned the 443nm bands (the most affected by variations in the sensitivity), in such a way that the minimal estimate of the pigment concentration equals the value measured in the deep convection zone of the Gulf of Lions (*circa* 0.04 mg m^{-3} in winter, the lowest value measured in the West Mediterranean, see MA91 for details). For the EMED,

where similar information was not available, they tuned the calibration of the 443nm bands in such a way that the histogram of pigment concentration matched that derived from a 1979 image of the same period (i.e. when the sensor sensitivity was stable).

However, the irregular temporal sampling of the CZCS data set did not allow performing an interannual analysis on the basin that, in fact, was limited to a single climatological study.

In AMA95 a first validation of the satellite chlorophyll estimates on the Mediterranean was also carried out. Unfortunately, the number of *in situ* data was very low and no concurrent satellite and *in situ* data (match-up stations) was available. That is, only the seasonal and sub basin trends of the Mediterranean pigments fields were compared. The analysis, however, demonstrated the general good performances of the CZCS sensor and of the Morel's group processing.

The biomass observations and the related primary production estimates (see later) produced by the Morel's group are considered fundamental in the understanding of the Mediterranean marine biota dynamic. Their analyses are still relevant, even though the intrinsic limitations of the CZCS data.

A parallel effort in the Mediterranean exploitations of the CZCS data was performed by the Joint Research Center (JRC) at Ispra, Italy, in the framework of the OCEAN project (Sturm, et al., 1999). The whole CZCS data set was re-calibrated and a complex atmospheric correction algorithm was applied on it, starting from the Level-1 satellite data. In addition, the OCEAN data are easily recovered from the JRC web site (http://me-www.jrc.it/OCEAN/ocean.html), which make available all the single re-processed passes.

The available CZCS data on the Mediterranean are summarized in Table 2-2.

	# Passages	Time period	Temporal Resolution	Comments
PO-DACC NASA	6588	1978-1985	Single satellite passage	The data are available at the PODACC in the DSP format
Antoine and Morel (1995)	298 for EMED 114 for WMED	1978-1983 1979-1981	Climatological Monthly Mean	The data are available at the Laboratoire Oceanographie de Villefranche web site (http://www.obs-vlfr.fr/jgofs2/modelisation/mediterr.htm). The averages are computed selecting 298 and 114 images on a total of 2000. See AMA95 and MA91 for details.
JRC	1110	1978-1985	Daily composite	The data are available at the JRC web-site (http://mewww.jrc.it/OCEAN/ocean.html)

Table 2-2. Summary of the CZCS data available on the Mediterranean.

From point of view of CZCS bio-optical algorithm, very few studies were carried out on the Mediterranean, excluding the cited ones by Morel's group. The only relevant analysis on the behavior of the CZCS standard algorithm on the Mediterranean was published by Gitelson et al. (1996). The results of Gitelson, together with the analyses of the Morel's group, will be discussed in the chapter 3.1, where the bio-optical characteristics of the Mediterranean are discussed.

2.2.5.2 Mediterranean SeaWiFS data

The efforts of the SeaWiFS project regarding the availability and the management of the SeaWiFS data results in a huge data set, which include all the level of the satellite data processing. In fact, from the PODAAC web site is possible to obtain all the global area coverage (GAC see appendix 9.2) low-resolution data and all the available local area coverage high-resolution (LAC see appendix 9.2) data, for all the standard SeaWiFS products. In addition, the Level 1B data (i.e. the basic level of satellite data) are also accessible, permitting, using the SEADAS software, to re-process the images with a series of user-defined parameters and options different from the standard ones.

Two HRPT (High Resolution Picture Transmission) stations are located in sites (HROM in Rome and HDUN in Dundee) permitting to collect SeaWiFS high-resolution

data of the basin in real-time. In particular the HROM station is able to provide a daily picture of the whole Mediterranean area (from Black Sea to the Atlantic Ocean) two hours after the end of the western passage. The details of the acquisition system of the HROM station are explained in the appendix 9.2; here, it is only significant to highlight the importance for the thesis work of the availability of a real time acquisition station in the area. In fact, due to the Mediterranean relatively small dimensions, only the high-resolution data are able to catch the small-scale phenomena, which could be relevant for the dynamic of the basin. In addition, the real time processing permits to identify quickly the area of maximum signal, which could be crucial in the periods of research cruises, permitting to point properly the *in situ* sampling. Finally, the opportunity to access to all the segments of the processing task permits to modify easily the data stream processing, whenever this is considered compulsory. All the above resulted in a great advantage for my research, for both the real time availability of high quality data and the opportunity to change the processing system, permitting to optimize the exploitation of SeaWiFS data.

When the LAC passage from Rome or Dundee are unavailable (for example for lack of electrical power supply or for error in the acquisition), it is possible to obtain the missing data from a series of not real time Mediterranean covering stations (i.e. Saclantc Undersea Research Centre (NATO), HSPZ). This kind of stations can process the data only after 15 days from acquisition, but are very useful for completing the time series in presence of gaps.

Summarizing, the SeaWiFS data set used in the thesis spans the period from 1998 to 2002 for both LAC and GAC data. Table 2-3, shows the statistics of the data set with some comments related to the stations.

	Total # of passes	Mean # of Mediterranean daily passes	Station type	Location (Lat.- Lon.)
HROM	3419	2-3	RT	56.46–2.98
HDUN	260	1	RT	41.84 -12.64
HSPZ	59	2-3	NRT	44.09 -9.86
GAC	3564	2		

Table 2-3. Summary of the SeaWiFS data available on the Mediterranean. In the station type column RT means real-time station, NRT not real time station.

After the production of Level2 data (see appendix 9.2), the passes are remapped on the area of interest. Furthermore the passes of the same day are composed in a single image of the basin, producing than a single Mediterranean map for each selected product. The described operations are performed with the Display Software Package (DSP) from the University of Miami (see appendix 9.2 for details).

Due to the various approaches adopted in the thesis work, not a standard processing operation has been performed, but a series of different procedures have been used. In accordance with the planned analyses, different processing options are applied to the raw data and they will be indicated when further explanations are needed. However, most of the differences arise from the application or not of the standard masks and flags, which in fact does not modify the geophysical data. Only in few cases the processing options have concerned the principles of the algorithms (for example in the validation exercise, see later): in those cases a detailed description of the processing will be done.

CHAPTER 3

Validation of the SeaWiFS products over the Mediterranean

Most of the adopted algorithms for color remote sensing are based on empirically derived equations, and therefore depend strongly on the data used to generate them. This applies both to the atmospheric term, which assumes a specific aerosol composition, and to the marine term, which considers a univocal relationship between radiance ratios and, ultimately, chlorophyll concentration. In fact, regional algorithms, fitted to local characteristics, generally perform better than the global algorithms, and appear to be very promising to reach the needed requirements in particular areas. This evidence led Platt and Sathyendranath (1988) to introduce the concept of bio-optical provinces (i.e. oceanic regions with similar bio-optical properties), which might have been related to the widely demonstrated evidence of physical-biological provinces (Hooker, et al., 2000; Longhurst, 1995).

Differences in the performance of regional and global algorithms often depend on the peculiarities of the atmospheric term, which does indeed affect radiances and then result important in a misfit of the algorithm. Before SeaWiFS, the atmospheric correction procedure preceded the retrieval of marine parameters and was substantially independent. Now, with the adoption of the Siegel's (2000) method, the two processes (the atmospheric correction and the bio-optical algorithms) are linked. This results in a more difficult assessment of their relative contribution on the final error on the chlorophyll estimate. The improved scheme for the SeaWiFS however, comprises several intermediate products, which contain information on the atmosphere

characteristics (i.e. the aerosols distribution). Therefore every passage of the SeaWiFS produces a simultaneous picture of both the marine and atmospheric terms.

The perspectives of that are very promising, also because of the role that atmospheric composition and deposition can play in the nutrient and micro-nutrient budget (Martin and al., 1994).

The SeaWiFS sensor offers the possibility to increase the knowledge on some of the atmospheric processes, which affect the plankton dynamics in the ocean, with a sufficient temporal and spatial resolution.

All the above leads to the conclusion that an intense effort to validate the satellite derived products have to be carried out.

The SeaWiFS Project, together with other NASA working groups (i.e. SIMBIOS), areintensively involved in several calibration/validation (CAL/VAL) programs for both the marine (i.e. chlorophyll concentrations) and atmospheric (i.e. aerosol optical thickness) satellite products. However, the final aim of these activities is the definition of algorithms and procedures working everywhere in the global ocean with a given error bar (35% error on the chlorophyll estimate and 5% on the water-leaving radiance). This implies that they ignore the small variability of some specific regions, to reach the needed accuracy for most of the global ocean.

The Mediterranean, which, as anticipated before, is definitively peculiar for its atmospheric and marine bio-optical properties, is then a good site to test the accuracy of the satellite data.

In the next paragraphs, the results of a CAL/VAL exercise carried out on the Mediterranean will be presented. SeaWiFS satellite data were compared with concurrent in situ measurements for both the atmospheric and marine products. The first aim of this exercise was the assessment of the errors in using remote sensing data. The second one was indeed related to highlight the differences of the area, considered as a unique physical-biological province, respect to the global ocean. In other words, the CAL/VAL

activity was also aimed at assessing how much a relatively small ocean as the Mediterranean is "different" from other similar oceanic provinces, and explaining, when possible, the observed dissimilarities.

3.1 VALIDATION OF SEAWIFS CHLOROPHYLL-*a* RETRIEVAL OVER THE MEDITERRANEAN

The first ocean color algorithm specifically developed for the SeaWiFS was the OC2 (O'Reilly, et al., 1998), which represented an important improvement with respect to the CZCS global algorithm (see before).

Subsequent analysis indicated that OC2 could be biased when applied to specific regions. Kahru and Mitchell (1999) showed that OC2 overestimates chlorophyll-*a* at high concentrations in the California Current area. For this reason, they proposed a regional version of the algorithm based on a fit with CalCOFI (California Cooperative Oceanic Fisheries Investigation) data. In a review paper, describing the main results of calibration and validation activity performed in the framework of SeaWiFS Project, Hooker and McClain (2000) showed that chlorophyll-*a* retrievals were within the accuracy targets stated above for most of the data in Case 1 waters . Nevertheless, the same authors found that for very low (< 0.3 mg m^{-3}) and high (> 3 mg m^{-3}) chlorophyll-*a* concentrations, the satellite overestimated the in situ measured values.

Recently, in the framework of several research programs (ENVISAT, 2000; Fargion and McClain, 2000) specifically devoted to the calibration and validation of ocean color sensors, a large amount of in situ measurements have been collected. Using this larger data set, O'Reilly et al. (2000) proposed an updated version of the ocean chlorophyll-*a* two- (OC2v4) and four-band (OC4v4) algorithms. They stated that the OC4v4 is expected to perform better than OC2v4 when applied to satellite-derived water leaving radiances both in oligotrophic and eutrophic conditions. Subsequently, NASA adopted OC4v4 algorithm for the global SeaWiFS processing.

As already mentioned, very few studies have been focused on the accuracy of the satellite *chlorophyll-a* algorithms in the Mediterranean.

The previous study on CZCS data in this basin (Antoine, et al., 1995; Morel and André, 1991) showed that the global CZCS ocean-color bio-optical algorithm worked reasonably well, but often resulted in a poor estimate of the chlorophyll-*a*.

By contrast, Gitelson et al. (1996) showed that the CZCS global algorithm (Gordon and Morel, 1983) overestimated the observed pigment concentrations in the EMED. They proposed a region-specific empirical algorithm to derive pigment concentrations from CZCS images on the basis of a limited number of measurements (21 stations), collected off the Israeli coast (Eastern Mediterranean) in June 1992. Even if this algorithm can be considered a regional algorithm, its general applicability to the Mediterranean Sea is limited by the small number of data used for the regression and the limited area and period (only one day) of the *in situ* measurements.

Recently, Bricaud et al. (2002) performed a quantitative analysis of ocean color data on the Mediterranean Sea from CZCS, SeaWiFS, Ocean Color and Temperature Scanner (OCTS) and Polarization and Directionality for the Earth's Reflectances (POLDER). They divided the basin in 13 regions and calculated the temporal averages of chlorophyll-*a* concentration for each region. In general the retrieved parameters from the different sensors were similar, even if some discrepancies were evident. In particular, SeaWiFS-derived chlorophyll-*a* concentrations displayed an overestimate in the oligotrophic regions of the basin.

In view of the SeaWiFS ocean color algorithms validation in the Mediterranean Sea, a specific data set of bio-optical and pigment concentration measurements has been built during the period 1998-2001. For bio-optical data, the radiance and irradiance measurements in or above water at the same bands of the satellite are considered. The use of these data to test the performance of the chlorophyll-*a* algorithms, removes the problems due to the atmospheric correction procedure. This will in turn allow a tuning

of the retrieval algorithm based only on in-situ data, which will be compared with concurrent SeaWiFS estimates afterwards (match-up analysis).

3.1.1 In situ chlorophyll-a data

In situ chlorophyll-*a* measurements were performed during three cruises carried out in the Mediterranean Sea through the years 1998-2001 on board the R/V Urania of the National Research Council (CNR). The locations of the stations are reported in Figure 3-1. Coastal stations were excluded from the data set in order to avoid Case 2 water properties.

During each cruise, water samples were taken from Niskin bottles mounted on a General Oceanics Rosette equipped with a SBE 911 CTD profiler and a SeaTech Flurometer. Sub-samples to measure chlorophyll-*a* (C) and phaeophytin-*a* (P) were filtered on board on GF/F filters (low *vacuum*) and immediately deep-frozen. Pigment concentrations were subsequently determined at the SZN on 90% acetone extracts within few weeks of the sampling using a SPEX Fluorolog spectrofluorometer with an estimated coefficient of variation for chlorophyll-*a* concentration of ~ 10% (Neveux and Panouse, 1987).

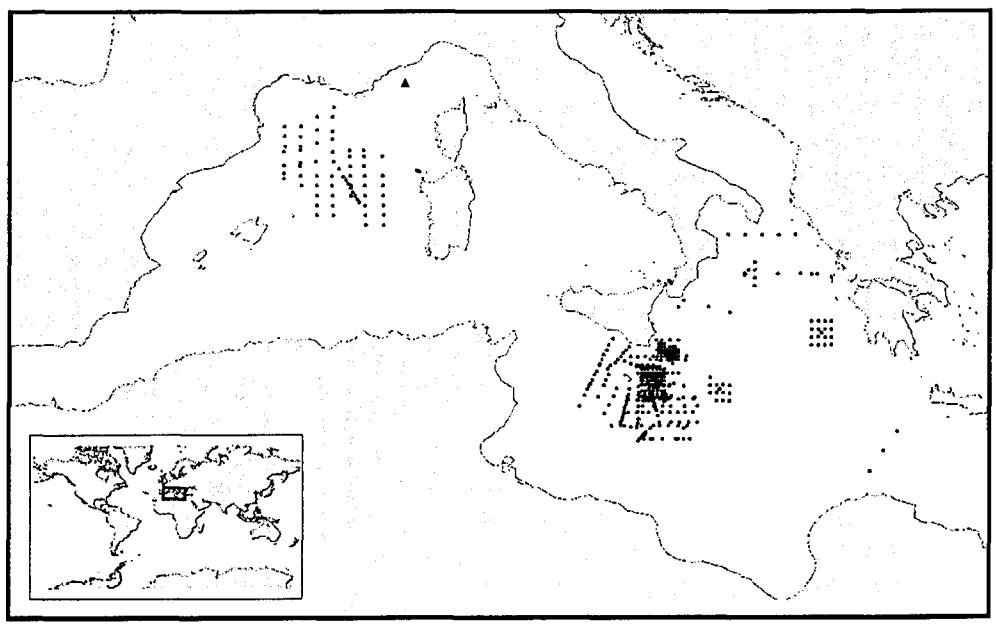

Figure 3-1. The locations of *in situ* chlorophyll-a profiles are reported.
Dots refer to cruises. Triangle indicates the DYFAMED location.

For each cruise, a merging and a linear fitting of the spectrofluorometrically derived chlorophyll-*a* concentrations with data acquired by the SeaTech *in situ* fluorometer was performed. Therefore, the data set consists of 582 chlorophyll-*a* profiles derived from the calibrated fluorescence profiles. Additional data were extracted from the data set of the Dynamique des Flux de mAtière en MEDiterranée (DYFAMED) station located in the Ligurian basin (Marty and Chiaverini, 2002, and Figure 3-1). The data are available on the World Wide Web (http://www.obs-vlfr.fr/jgofs2/sodyf/home.htm).

For the stations where phaeophytin-*a* concentrations were not available (e.g. DYFAMED), an estimation of the total concentration of chlorophyll-*a* + phaeopigments (*C+P*) has been performed, using a linear fit of *C versus C+P*, following an approach very similar to O'Reilly et al. (1998). This fit was based on 798 data points derived from the reported cruises and seven additional ones conducted in the Mediterranean during the years 1995-2000 by the SZN group, and gave the following equation:

Eq. (3-1) $$C + P = 1.1635 \cdot C + 0.0072$$

with a correlation coefficient of $R^2 = 0.997$.

This equation was then used to obtain total pigment concentration profiles in those stations where only chlorophyll-*a* was available.

The final data set covers a relatively wide range of conditions in Case I waters of the Mediterranean Sea, spanning from oligotrophic (Sicily Channel and Ionian Sea) to moderately eutrophic regimes (North-Western Mediterranean). Chlorophyll-*a* concentrations vary between 0.03 and 2.75 mg m^{-3}, though low values (< 0.1 mg m^{-3}) are definitely more numerous (≈ 70%). Most of them were sampled during the stratified season at sites exhibiting one, or seldom two, Deep Chlorophyll Maxima (DCM) located in the 55-85 m depth interval.

The validation procedure requires a comparison of algorithm chlorophyll-*a* estimates with concurrent *in situ* chlorophyll-*a* concentrations (C_M). Following Gordon and Clarke (1980) C_M was computed as:

Eq. (3-2)
$$C_M = \frac{\int_0^{Z_{pd}} C(z)\exp(-2kz)dz}{\int_0^{Z_{pd}} \exp(-2kz)dz}$$

where k is the attenuation coefficient for the downwelling PAR irradiance, $Zpd = 1/k$ is the penetration depth and $C(z)$ can be either the chlorophyll-*a* or total pigment profile. Z_{pd} has been estimated as $Z_{pd} = Z_e/4.6$, with Z_e being the euphotic depth or the depth where PAR irradiance is reduced at 1% of its surface value. Z_e in turn has been determined for each station by the recursive method proposed by Morel and Berthon (1989) using calibrated fluorescence profiles as input. C_M refers to either C or $C+P$, according to the algorithm used.

C_M is very similar to the Optically Weighted Pigment (*OWP*) concentration which "should be an accurate representation of the pigment concentration measured by a remote sensor viewing a stratified ocean" as reported by Clark (1997). The difference resides in the way of computing it and, in particular, in the definition of the lower limit for the integral computation. Clark's approach is based on the knowledge of diffuse attenuation coefficients of downwelling irradiance at various wavelengths ($K_{d,\lambda}$), while the C_M requires the knowledge of Z_e.

The presence of only above water bio-optical measurements in some of the dataset stations, prevents the application of Clark's approach to the entire bio-optical data set. When optical in water profiles were available (i.e. K_d's were available), a comparison between the two approaches has been performed, which confirmed the validity of using C_M instead of OWP (Figure 3-2).

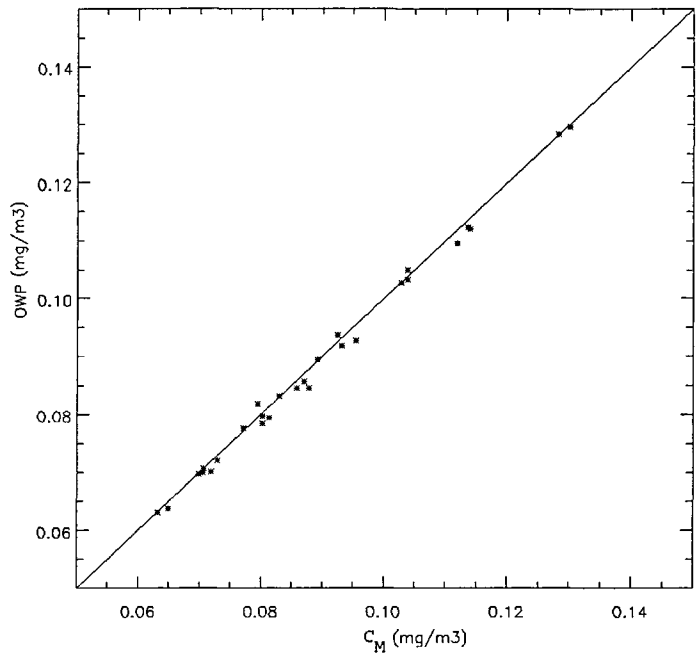

Figure 3-2 Scatter plot of optical weighted pigment (OWP) concentration versus C_M. OWP is computed applying formula (6) in Clark (1997) to the chlorophyll-a profiles and using as $K_d(k,z)$ as the measure obtained by concurrent SPMR Satlantic profiles at 490 nm. C_M is computed using equation 3.2 (see text).

The C_M chlorophyll-*a* concentration collected in stations where bio-optical data are available, range from 0.063 to 1.92 mg/m^3, covering the wide range of conditions of Case I waters of the Mediterranean Sea. Even if the number of stations is not very large, the bio-optical dataset can be used to give indication of algorithm performances for most of the optical/biochemical provinces of the basin.

3.1.2 Optical measurements

A series of optical measurements at selected sites has been also conducted during each cruise, totally 45 stations (see Figure 3-3).

In water downwelling irradiance (E_d) and upwelling radiance (L_u) profiles were taken in 32 stations using a Satlantic SPMR (SeaWiFS Profiling Multichannel Radiometer), which operates in 13 channels of the visible range (400, 412, 443, 470, 490, 510, 532, 555, 590, 620, 665, 683, 700 nm).

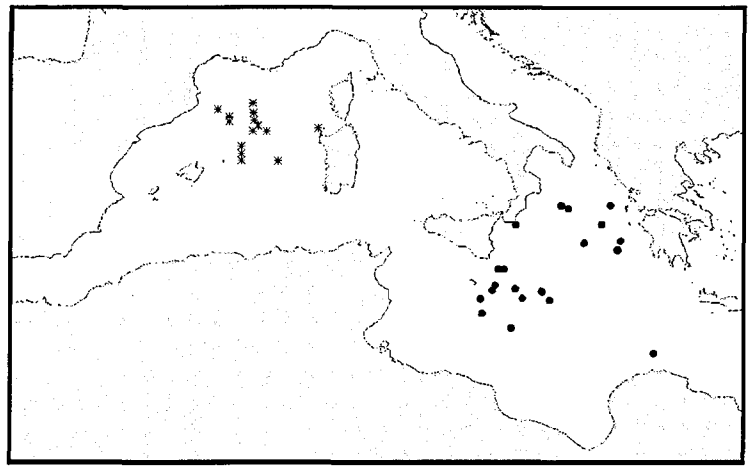

Figure 3-3. Location of concurrent bio-optical measurements and chlorophyll-a profiles. Stars indicate the SIMBAD measurements, dots the SPMR Satlantic measurements.

The data were acquired following the standard SeaWiFS protocols (Mueller and Austin, 1995). The instrument had been calibrated at Satlantic Inc. just prior to each cruise. The above water measurements were made in the remaining 13 stations (when SPMR were not available) using the SIMBAD radiometer operating at 443, 490, 560, 670, 870 nm. SIMBAD data were then processed at LOA (Laboratoire d'Optique Atmospherique) of the University of Lille (Fougnie, et al., 1998). All optical measurements are hereafter used to derive the Remote Sensing Reflectance (R_{rs}) and Water Leaving Radiance (L_{wn}) for algorithm validation.

Spectral in water measurements of E_d and L_u have been propagated up to the surface ($z0^-$ level) using attenuation coefficients K_d and K_u, as estimated from the profiles. The corresponding above water E_d and L_u ($z0^+$ level) were calculated according to the following equations:

Eq. (3-3) $$L_u(0^+) = 0.54 \cdot L_u(0^-)$$

Eq. (3-4) $$E_d(0^+) = 1/0.96 \cdot E_d(0^-)$$

where 0.54 is a mean coefficient summarizing the effect of internal reflection of the upwelling flux during transmission through the interface, and 0.96 accounts for the loss

of downwelling flux by reflection at the air-sea interface (Austin, 1974; Gordon, et al., 1988; O'Reilly, et al., 1998). Both coefficients assume low solar zenith angle and calm sea-surface, which were the experimental conditions of our measurements.

Finally, R_{rs} has been computed at each wavelength λ, available as $R_{rs}(\lambda) = L_u(0^+,\lambda)/E_d(0^+,\lambda)$ and $L_{wn}(\lambda)$ multiplying R_{rs} by the mean extraterrestrial solar irradiance (Neckel and Labs, 1984) weighted by the spectral response of the relevant sensor bands, as proposed by O'Reilly et al. (1998).

Some algorithms may require data at wavelengths different from those available from *in situ* optical measurements. In those cases, R_{rs} estimates have been generated using the interpolation procedure suggested by O'Reilly et al. (2000). The reliability of the interpolation procedure has been also verified by selecting R_{rs} values at 4 of the 13 bands available from SPMR measurements, and then computing the remaining 9 R_{rs} via interpolation.

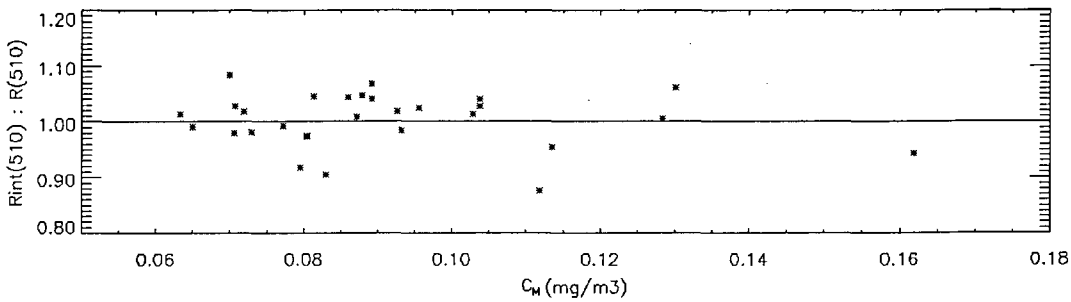

Figure 3-4. The ratio of Rrs at 510 nm based on interpolated Rrs (R_{int}) to measured R_{rs} (R) versus chlorophyll-*a* concentration (C_M).

The comparison between R_{rs}'s obtained by interpolation and those measured by SPMR is quite good and the error introduced by the interpolation appears to be less than 10%. Figure 3-4 shows as an example the results obtained for the 510 nm band.

3.1.3 Validation of the algorithms

To evaluate the performance of some representative empirical algorithms, the OC2v4 and OC4v4 (O'Reilly, et al., 2000; O'Reilly, et al., 1998) as NASA-SeaWiFS

operational algorithms, and the regional algorithm proposed by Gitelson et al. (1996) (hereafter GIT), as an example of a local Mediterranean algorithm, are selected. The functional forms of these algorithms are:

Eq. (3-5) $$C = 10^{(a_0+a_1R+a_2R^2+a_3R^3)} + a_4$$

for the OC2v4

Eq. (3-6) $$C = 10^{(a_0+a_1R+a_2R^2+a_3R^3+a_4R^4)}$$

for the OC4v4 and

Eq. (3-7) $$C = a_0(10^R)^{a_1}$$

for GIT.

In the equation 3-5 R is the $\log_{10}$ of the ratio between Remote Sensing Reflectances measured at 490 and 555 nm. For the OC4v4, (equation 3-6) R is the $\log_{10}$ of ratio of R_{rs} measured either at 443 and 555 nm, or 490 and 555 nm, or 510 and 555 nm, depending on its value (the maximum is chosen). In the case of GIT, R is the $\log_{10}$ of ratio of the water leaving radiance L_w at 440 and 550 nm, and C is the total pigment concentration (chlorophyll-a + phaeopigments). The numerical value of the coefficients can be found in Table 3-1.

Algorithm	a0	a1	A2	a3	a4	R
OC2v4	0.319	-2.336	0.879	-0.135	-0.071	$\log_{10}$(Rrs490/Rrs555)
OC4v4	0.366	-3.067	1.930	0.649	-1.532	$\log_{10}$(Rrs443 > Rrs490 > Rrs510)/Rrs555))
GIT	0.914	-1.86				$\log_{10}$(Lwn440/Lwn550)

Table 3-1 Algorithm coefficients of OC2v4 (O'Reilly, et al., 1998), OC4v4 (O'Reilly, et al., 2000) and GIT (Gitelson, et al., 1996) used in equations 3-5, 3-6,and 3-7.

Bio-optical estimates of chlorophyll-*a* (C_{mod}) were obtained by introducing the *in situ* R_{rs} measurements in the three selected algorithms.

The results of the validation of the chlorophyll-*a* estimates by the three selected algorithms are shown in Figure 3-5.

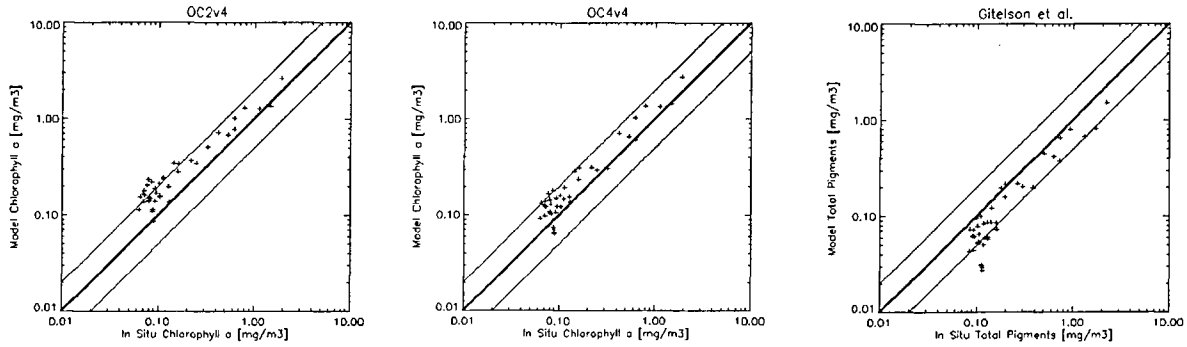

Figure 3-5. Algorithm validation using *in situ* bio-optical measurements and concurrent *in situ* chlorophyll-*a* data C_M : (right plot) scatter plot of OC2v4 model values versus C_M; (central plot) scatter plot OC4v4 model values versus C_M; (left plot) scatter plot of GIT model values versus C_M. The 1:1 (center thick line) 1:2 (bottom thin line) and the 2:1 (top thin line) lines are also plotted.

The scatter plots clearly show that both NASA algorithms overestimate *in situ* chlorophyll-*a* measurements, while GIT algorithm underestimates C_M. To quantify errors, statistical parameters are summarized in Table 3-2 where percent error is defined as:

Eq. (3-8)
$$\%E = 100 \cdot [\frac{C_M - C_{mod}}{C_M}]$$

C_{mod} and C_M being the modelled and measured chlorophyll-*a*, respectively.

Algorithm	$\%E_{min}$	$<\%E>$	$\%E_{max}$	$\%S$	r^2
OC2v4	-192	-73	8	49	0.945
OC4v4	-128	-40	28	41	0.944
GIT	-9	39	76	22	0.930

Table 3-2. Application of the algorithm selected to the bio-optical in situ measurements versus in situ chlorophyll-a measurements (C_M): statistical analysis. The $\%E$ is obtained using equation 3-8. $\%E_{min}$, $\%E_{max}$ and $<\%E>$ are the $\%E$ minimum, maximum and average. $\%S$ is the standard deviation of $\%E$. r^2 is the correlation coefficient

The squared correlation coefficient (r^2) of the modelled *versus* the *in situ* chlorophyll-*a* is nearly identical for OC4v4 (0.944) and OC2v4 (0.945), while GIT exhibits slightly lower r^2 (0.930).

Both OC2v4 and OC4v4 overestimate *in situ* observations by 73% and 40% respectively. On the other hand, the GIT algorithm underestimates *in situ* observations by 39%. Other parameters have been calculated: the maximum and minimum percent deviation of the data from the model's estimates ($\%E_{min}$ and $\%E_{max}$ in Table 3-2), as well as the Standard Deviation of the percent error (% *S* in Table 3-2). The $\%E_{max}$ - $\%E_{min}$ range and $\%S$ give an idea of the spreading of the data around the expected value (modelled chlorophyll-*a*). The $\%S$ values for the three algorithms range from 22% to 49% (Table 3-2). Moreover it is noteworthy that in the case of NASA standard algorithms (more evidently for OC2v4) $\%E$ exhibits a correlation with C_M. Figure 3-6 shows that the $\%E$ increases for low chlorophyll-*a* values with larger error at C_M lower than 0.15 mg m^{-3} for both OC4v4 and OC2v4. On the contrary the GIT's $\%E$ is quite constant in the whole range of sampled C_M (Figure 3-6).

Even if the application of OC4v4 improves the OC2v4 chlorophyll-*a* estimates in the Mediterranean Sea, the results are still very poor. The GIT algorithm exhibits the best statistical performance between the three tested algorithms.

However, the adoption of this algorithm as the standard Mediterranean regional algorithm is limited by three basic considerations. First, the 39% mean error found is still greater than the 35% required by NASA; second, the 440 and 550nm bands used by GIT are no longer available in SeaWiFS or in the next generation ocean colour sensors (e.g. MODIS MERIS); last, the limited range of temporal and spatial coverage of the optical measurements used to develop the GIT algorithm ("21 locations were sampled on 22nd July 1992, in the Southeastern Mediterranean", Gitelson, et al., 1996) might prevent the applicability of this algorithm when applied to a different season or sea region.

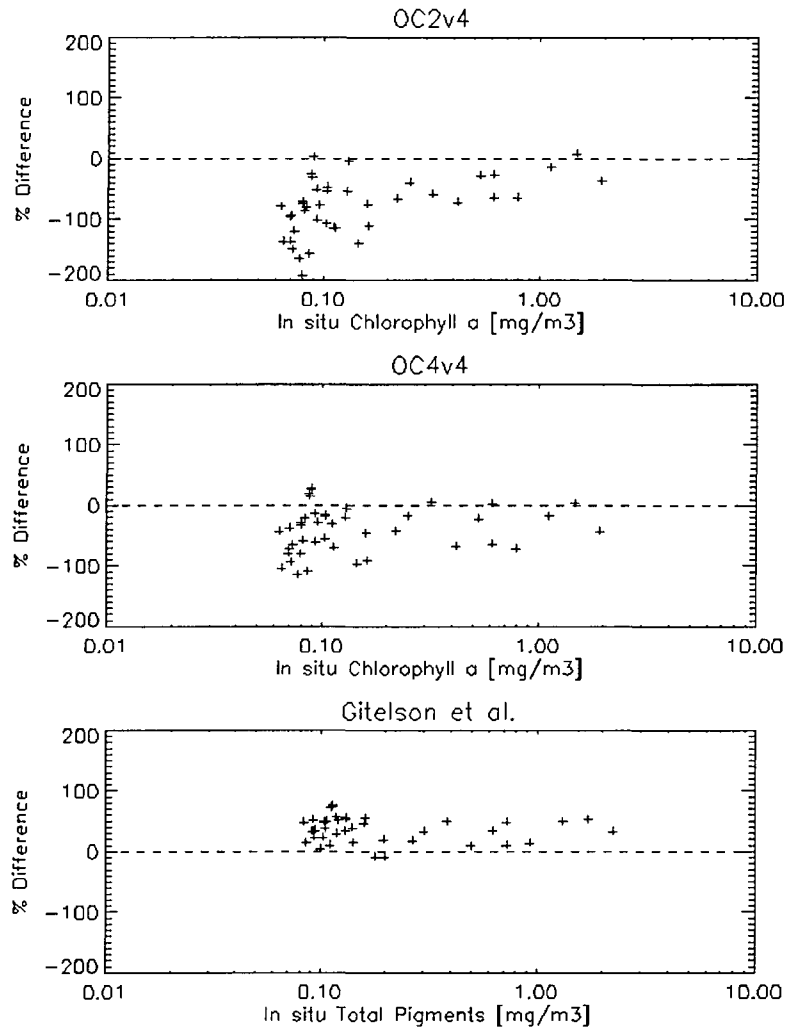

Figure 3-6. Percentage differences between *in situ* chlorophyll-*a* data C_M and model values applied to bio-optical measurements in function of C_M: (a) C_M – OC2v4 versus C_M; (b) C_M –OC2v4 versus C_M;(c) C_M - GIT versus C_M.

3.1.4 A preliminary Mediterranean SeaWiFS chlorophyll-a algorithms

The algorithms validation suggested that a regional algorithm is needed for the Mediterranean Sea.

Even if the bio-optical data set presented above consists of a limited number of data (45 stations), they represent most of the Mediterranean conditions ranging from oligotrophic to moderately eutrophic regimes. It is then possible to use this dataset to develop a preliminary version of a Mediterranean ocean color algorithm. The

distribution of the chlorophyll-*a* data *versus* band ratio suggests that both linear and polynomial function can be used to develop an *ad hoc* algorithm.

The limited size of our dataset suggests the use of a simpler algorithm than OC4v4. In fact, to compute new coefficients for an OC4-like algorithm it is required that, after the selection criterion, all the three possible band ratios should be represented by a significant number of data points in the data set used. Moreover, the application of the OC4v4 selection band ratio criterion to our data set results in a net predominance of the R_{555}^{443} band ratio selection, while the R_{555}^{510} is practically never selected.

Thus, two new sets of coefficients for both the linear and OC2 functional forms are derived from regressions on the available 45 data points.

The new polynomial equation NL-DORMA (NonLinear-D'ORtenzio MArullo) is:

Eq. (3-9) $$C = 10^{(0.217-2.728R+0.704R^2+0.297R^3)} - 0.035$$

while the new linear equation L-DORMA (Linear- D'ORtenzio MArullo) is

Eq. (3-10) $$C = 1.49 \cdot 10^{(-2.51R)}$$

where $R=\log_{10}(Rrs490/Rrs555)$

In the polynomial fit case, the regression was constrained to reproduce OC2v4 derived values for high chlorophyll-*a* concentrations. The statistical results of the new regressions are summarized in Table 3-3.

Algorithm	$\%E_{min}$	$<\%E>$	$\%E_{max}$	$\%S$	r^2
L-DORMA	-64	0.8	49	27	0.948
NL-DORMA	-62	1.8	52	27	0.941

Table 3-3. Statistical results of the new Mediterranean algorithm to the bio-optical in situ measurements versus in situ chlorophyll-a measurements (C_M). The %E is obtained using equation 3-8. $\%E_{min}$, $\%E_{max}$ and $<\%E>$ are the $\%E$ minimum, maximum and average. $\%S$ is the standard deviation of $\%E$. r^2 is the correlation coefficient.

It is evident that the application of linear or polynomial forms gives similar results once the coefficients are optimized with respect to the data.

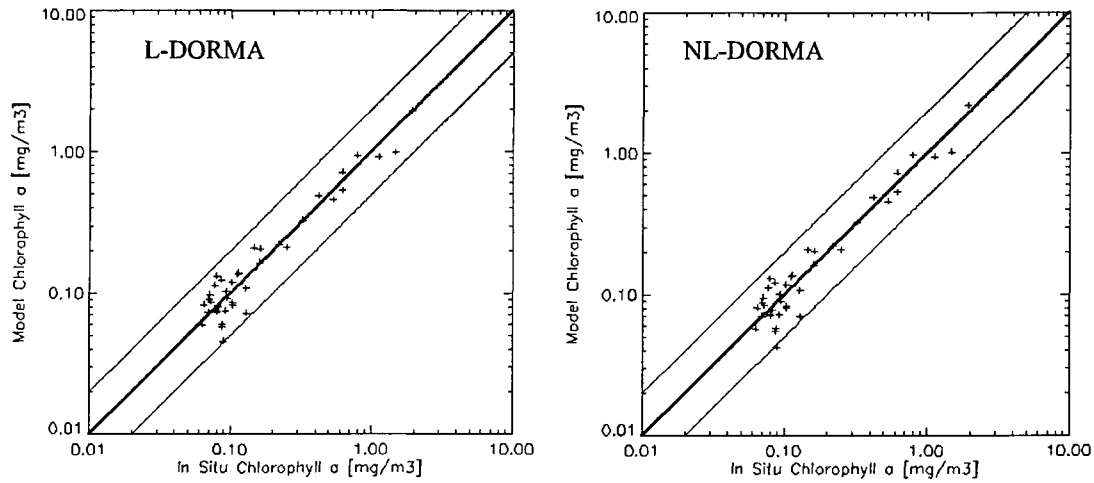

Figure 3-7. Algorithm validation of DORMA algorithms using *in situ* bio-optical measurements and concurrent *in situ* chlorophyll-*a*: (left panel) Scatter plot between L-DORMA model values versus C_M (right panel) scatter plot between NL-DORMA model values versus C_M. The 1:1 (center thick line) 1:2 (bottom thin line) and the 2:1 (top thin line) lines are also plotted.

In Figure 3-7, the comparison between the two new models and the *in situ* chlorophyll-*a* data shows that the points are now distributed around the line of best agreement with a percent error that rarely exceeds 35%.

3.1.5 Satellite match-up analysis

The algorithm validation presented before, however, supplies only partial information about the performance of the algorithms when applied to satellite-derived Water Leaving Radiances. For this reason a validation of the algorithms by comparing satellite estimates with concurrent in situ chlorophyll-*a* observations has been performed. The validation procedure was applied to the algorithm presented before, as well as to the new algorithms developed for the Mediterranean. Moreover, Neural Network Algorithm (NNA) has also been considered, to complete the list of the algorithms provided by NASA's standard processing system (Gross, et al., 2000).

The chlorophyll-*a* profiles that match in time and space with concurrent satellite passes constitute the match-up data set (C_{situ}). Note that C_{situ} and C_M datasets only partially overlap, because C_M includes all those stations where chlorophyll-*a* profiles and optical measurements were present at the same time, while C_{situ} includes the stations where chlorophyll-*a* measurements match in time and location with a valid satellite pixel (match-up analysis). C_{situ} has been calculated using the same formulation 3-2 used for C_M.

High-resolution picture transmission (HRPT) SeaWiFS data have been acquired by the receiving station HROM, and transformed in Level 1A (L1A) standard NASA format. All the SeaWiFS passes relative to the period of *in situ* measurements were extracted from the HROM archive and processed up to Level 2 (L2) standard NASA format to obtain normalized water leaving radiance (L_{wn}) and remote sensing reflectance (R_{rs}) maps for the five available visible bands (412, 443, 490, 510 and 555 nm) using the SeaDAS software v.4.0B (Baith, et al., 2001). Siegel's atmospheric correction algorithm has been applied to L1A raw data (Siegel, et al., 2000), which need a first estimate of chlorophyll-*a* concentration to compute Water Leaving Radiances. Consequently, the L1A SeaWiFS dataset were processed up to L2 for each selected algorithm. The SeaDAS code has been opportunely modified (see Appendix 9.2) to allow the application of the tested bio-optical algorithms, which are not present in the standard SeaDAS software version (i.e. the DORMA algorithms).

Data have been remapped on a 1-km resolution equirectangular projection in the regions of interest, using the University of Miami Display Software Package (DSP). Final maps have been flagged by applying all of the 24 masks provided by SeaDAS (Baith, et al., 2001).

The match-up file has been produced using a time window of 8 hours centered on the satellite pass time. Each satellite-derived parameter has been averaged on 3x3 pixels centered at the location of each station where chlorophyll-*a* profiles were available,

using only those pixels that passed all the above cited exclusion criteria. A threshold of 8 valid pixels was set to include the data points in the match-up file.

After the selection procedure outlined above, 46 match-up points (including the 6 points acquired by the DYFAMED, station) are included in the C_{sat} data base (the location of the match-up points is shown in Figure 3-8).

These data cover a range of C_{situ} values from 0.05 to 1.14 mg m^{-3} of chlorophyll-*a* concentration (0.06 to 1.34 mg m^{-3} of pigment concentration) with a significant prevalence of values typical of the Mediterranean oligotrophic regime (C_{situ}<0.1 mg m^{-3}). All the data exceeding 1 mg m^{-3} (7 %) have been collected in the NW Mediterranean, during the intense bloom occurring at the end of winter 2000. This area is among the few where the Mediterranean Sea does not display its characteristic oligotrophic regime.

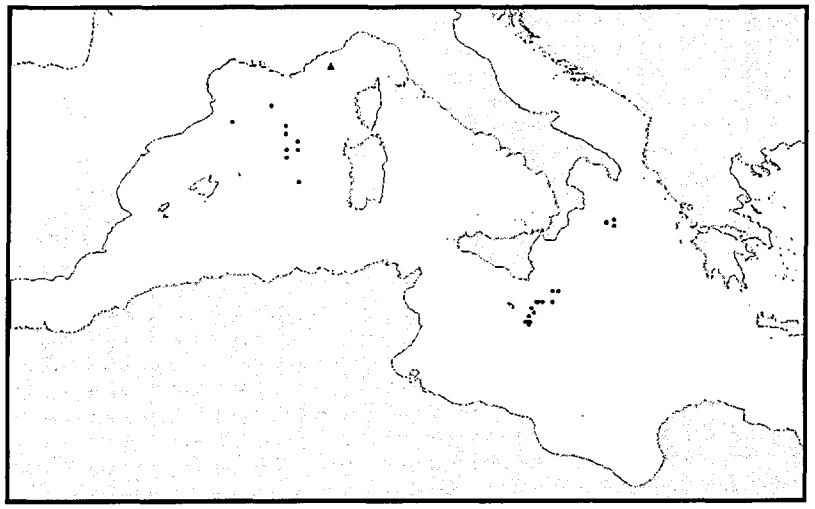

Figure 3-8. Geographical distribution of the satellite and *in situ* chlorophyll-*a* match-up data.

It is noteworthy that the numbers of locations where C_{situ} and C_M overlap are only 5. In these 5 stations optical measurements, chlorophyll-*a* profiles and satellite estimates are present at the same time.

The results of the match up analysis for the different algorithms are summarized in Table 3-4, Table 3-5,and in Figure 3-9, essentially confirming the picture revealed by the analysis of the in situ bio-optical data (see Figure 3-9).

Algorithm	$\langle \%E_{sat} \rangle$	$\langle \%E_{sat}^{-} \rangle$	$\langle \%E_{sat}^{+} \rangle$	$\%S_{sat}$	$\%S_{sat}^{-}$	$\%S_{sat}^{+}$	r^2
OC2v4	-84.9	-96.2	-9.8	69.4	66.9	25.0	0.932
OC4v4	-116.2	-131.3	-15.6	81.4	75.8	29.0	0.928
N. Network	-143.6	-162.3	-18.8	93.0	84.3	32.3	0.869.
GIT	9.7	5.1	40.3	40.4	41.0	16.5	0.932
NL-DORMA	-28.1	-31.7	-4.3	50.0	51.9	26.4	0.916
L DORMA	-9.5	-14.7	25.2	37.0	36.2	20.6	0.927

Table 3-4. Application of the tested algorithm to satellite data versus in situ chlorophyll-a measurements (C_{situ}): statistical analysis. The $\%E_{sat}$ is obtained using equation 3-8. $<\%E_{sat}>$ and $\%S_{sat}$ are the average and the standard deviation of $\%E_{sat}$. $\langle \%E_{sat}^{-} \rangle$ and $\%S_{sat}^{-}$ are the average and the standard deviation of $\%E_{sat}$ for values of $C_{situ} < 0.15$ mg m^{-3}. $\langle \%E_{sat}^{+} \rangle$ and $\%S_{sat}^{+}$ are the average and the standard deviation of $\%E_{sat}$ for values of $C_{situ} > 0.15$ mg m^{-3}. r^2 is the correlation coefficient.

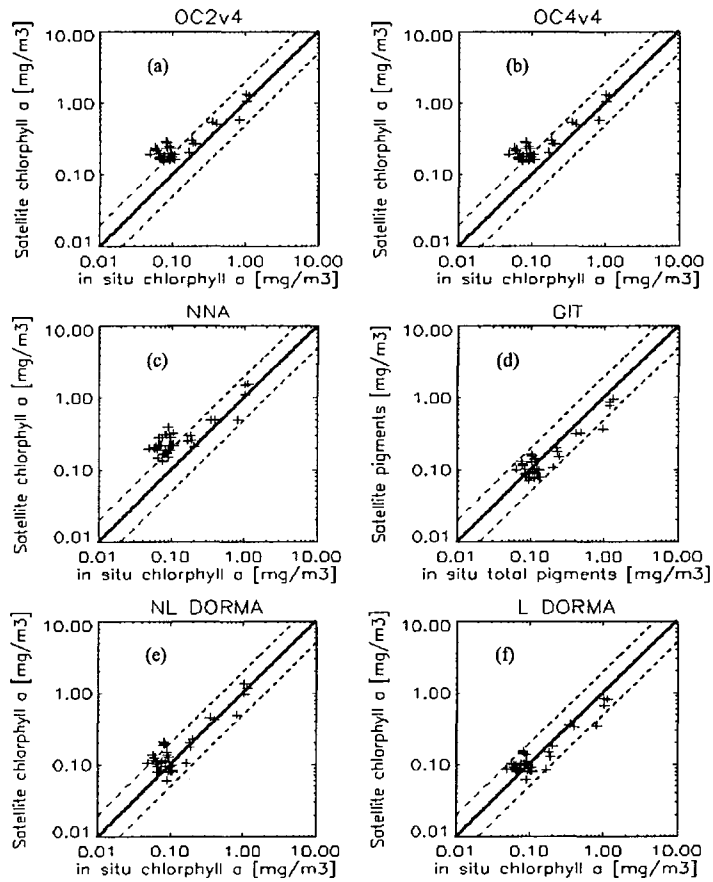

Figure 3-9. SeaWiFS chlorophyll-*a* estimates (C_{sat}) validation against concurrent in situ chlorophyll-*a* data C_{situ}: (a) SeaWiFS estimate using OC2v4 model values versus C_M; (b) SeaWiFS estimate using OC4v4 model values versus C_M; (c) SeaWiFS estimate using Neural Network model values versus C_M; (d) SeaWiFS estimate using GIT model values versus C_M; (e) SeaWiFS estimate using NL-DORMA model values versus C_M. (f) SeaWiFS estimate using L-DORMA model values versus C_M. The 1:1 (center thick line) 1:2 (bottom thin line) and the 2:1 (top thin line) lines are also plotted.

In brief, the standard NASA algorithms (OC2v2, OC4v4 and NNA), overestimate C_{situ}, while the algorithms tuned over the Mediterranean Sea (GIT, NL-DORMA and L-DORMA) are definitively closer to the in situ data.

The parameters have been estimated separately for low ($\%E_{sat}^{-}$) and high ($\%E_{sat}^{+}$) C_{situ} concentrations ($C_{situ} < 0.15$ and $C_{situ} > 0.15$ mg m^{-3}) to evidence the performance of selected algorithms in the oligotrophic regime predominant in most Mediterranean basins.

Algorithm	$<\Delta C>$	$<\Delta C>$	$<\Delta C^{+}>$	S	S-	S+	r^2
OC2v4	-0.074	-0.077	-0.054	0.071	0.044	0.172	0.932
OC4v4	-0.101	-0.105	-0.081	0.072	0.041	0.183	0.928
N. Network	-0.134	-0.133	-0.143	0.110	0.058	0.287	0.869
GIT	0.053	0.012	0.326	0.128	0.037	0.183	0.932
NL DORMA	-0.021	-0.021	-0.019	0.080	0.041	0.212	0.916
L DORMA	0.025	-0.006	0.233	0.107	0.033	0.185	0.927

Table 3-5. Application of the tested algorithm to satellite data versus in situ chlorophyll-a measurements (C_{situ}): statistical analysis. The ΔC is defined as: $\Delta C = C_{situ} - C_{sat}$. and are expressed in mg m^{-3}. $<\Delta C>$ and S are the arithmetic mean and the standard deviation of ΔC. $<\Delta C^{-}>$ and S^{-} are the arithmetic mean and the standard deviation of ΔC for value of C_{situ}<0.15 mg m^{-3}. $<\Delta C^{+}>$ and S^{+} are the arithmetic Mean and the Standard Deviation of ΔC for value of C_{situ}>0.15 mg m^{-3}. r^2 is the correlation coefficient.

The high values of the mean $\%E_{sat}$ ($<\%E_{sat}>$) for the three global scale algorithms is essentially due to the strong overestimation in the low chlorophyll-*a* range. Nevertheless the performances in the high chlorophyll-*a* range are still acceptable. Contrarily to what was observed in the analysis of the in situ bio-optical data, the OC2v4 chlorophyll-*a* estimates agree better than the other two global algorithms, when applied to the satellite data. The NNA estimates are definitely the worst.

The Mediterranean algorithms generally exhibit better results: the $<\%E_{sat}>$ is definitively within 35% value defined as one of the requirements of the SeaWiFS

project (Hooker and McClain, 2000). More in details, the Mediterranean linear algorithms (GIT and L-DORMA) show a mean $\%E_{sat}^{-}$ ($\langle \%E_{sat}^{-} \rangle$) lower than the mean $\%E_{sat}^{+}$ ($\langle \%E_{sat}^{+} \rangle$), signifying that a better estimate occurs in the low chlorophyll-*a* range. The GIT algorithm, in particular, exhibits an unacceptable $\langle \%E_{sat}^{+} \rangle$ of 40.3%. On the other hand, the mean values of the absolute error ($\Delta C = C_{situ} - C_{sat}$) (Table 3-5), relative to the two DORMA algorithms, are very close in the low C_{situ} range, but are definitively better for the NL-DORMA in the high C_{situ} region (see Table 3-5 column mean ΔC^{+}). The difference in the sign of $<\Delta C>$ and $< \%E_{sat} >$ for the L-DORMA algorithm (Table 3-4 and Table 3-5) is due to the different relative weight of the errors in the chlorophyll-*a* estimates. The negative sign of the $< \%E_{sat} >$ demonstrates that most of the percent error is due to the general underestimation of the algorithm, while the positive sign of $<\Delta C>$ account for a higher weight of the overestimated values on the mean error.

3.1.6 Validation of the NL-DORMA algorithm

The NL-DORMA was developed during the first year of my PhD period, and was considered preliminary because a validation with an independent data set was not performed. The reason was that the number of optical data was not sufficient to develop the algorithm and to validate it at the same time. In other words, an independent validation with data not used for the calibration, was precluded. In the following years (2001-2002), the experimental activity carried out in the Mediterranean by the SZN biological oceanography laboratory permitted to increase the total number of bio-optical measurements in the Mediterranean, and then to reconsider the CAL/VAL results.

In situ optical data were collected in the Mediterranean Sea in two different cruises in the year 2001-2002. They were obtained by SIMBAD-A above-water radiometers and by the SATLANTIC-SPMR in-water profiler. At the location of the optical

measurements, water samples were collected at different depths to retrieve chlorophyll-*a* concentration with fluorometric method. The methods used for the data treatment and the criteria adopted to build the data set were exactly the same as already described before (see paragraph 3.1.2).

In addition to the data collected by the SZN, 16 bio-optical stations were obtained by the SEABASS archive (Hooker, et al., 1994) and included data collected in the Mediterranean Sea during the PROductivity of PElagic Oceanic Systems (PROSOPE) cruise (Claustre, et al., 2002). The PROSOPE data have permitted to validate the NL-DORMA algorithm using "truly" independent measurements, and then to verify the accuracy of the algorithm when applied on data collected by different sources.

Summarizing, 41 couples of chlorophyll-*a* concentration and R_{rs} at the SeaWiFS wavelengths (412,443,490,512,555 nn) were obtained and used for the algorithm validation. The number of the new stations is comparable to that used in the NL-DORMA development (45 stations), making us confident on the validity of analysis.

The new data collected are plotted in Figure 3-10, together with the NL-DORMA and OC2v4 algorithms and with the data used in DORMA development.

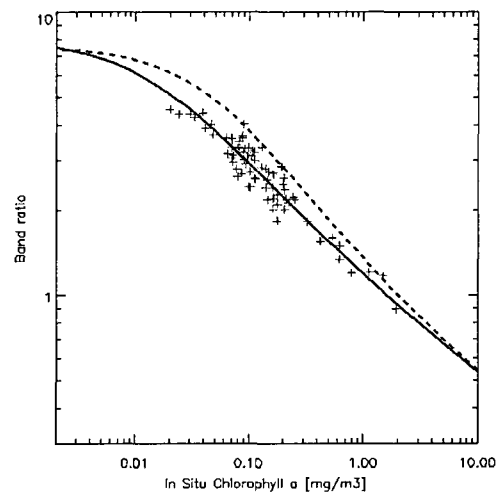

Figure 3-10 Relationship between *in situ* chlorophyll concentration and the Remote Sensing Reflectances band ratios. Red crosses are the data used in the algorithms development. Blue crosses are the new data collected in the Mediterranean. Lines indicate the remote sensing algorithms (OC2-V4 dotted line, NL-DORMA solid line)

Even if the dataset does not cover all the basin areas and all the seasons, it is now possible to test the performance of the algorithms in chlorophyll-*a* ranges not available before. The new data agree very well with the NL-DORMA algorithm estimates, mainly at the very low chlorophyll-*a* values. This is a very important result, principally because the data in this range were collected by other researchers and with different instruments from those used in the NL-DORMA development.

The general agreement of the NL-DORMA algorithm with the in situ data is also confirmed in the chlorophyll-*a* range 0.1-0.3 mg m^{-3}, even if the spreading of the points seems to be slightly large.

The statistical analysis performed on the data is summarized in Table 3-6, where the percentage error (*%E*) is calculated using the equation 3-2.

The equation 3-2 was applied on the C_{mod} obtained with both the NL-DORMA and OC2-V4 algorithms, and on the C_M used in the development of the DORMA algorithm (OLD) and derived by the new data set (NEW). Finally the statistical analysis was performed on the whole data set (ALL; sum of NEW and OLD).

As already pointed out commenting Figure 3-10, the new data confirm the general good performances of the NL-DORMA algorithm on the Mediterranean water leaving radiances.

In particular, comparing the OLD data with the ALL ones, the $<\%E>$ decreases in the absolute value while the squared correlation coefficient (r^2) increases, becoming higher than the OC2v4 corresponding value.

It is noteworthy that the new data, and more precisely the PROSOPE data, ranging in the ultra-oligotrophic region (chlorophyll-*a* concentration less than 0.04 mg m^{-3}), improve the validity of the NL-DORMA and at the same time decrease the performance of the OC2v4 ($\%E_{min}$ from -192.383 to -251.028).

Algorithm	$\%E_{min}$	$<\%E>$	$\%E_{max}$	$\%S$	r^2
NL-DORMA ALL	-115.340	-1.43120	57.3719	33.4608	0.925679
NL-DORMA OLD	-62.8240	1.89644	52.6237	27.3597	0.941107
NL-DORMA NEW	115.340	-5.08349	57.3719	39.1109	0.426165
OC2V4 ALL	-251.028	-81.8524	25.6799	57.7333	0.924371
OC2V4 OLD	-192.383	-73.2649	7.82847	48.9231	0.945595
OC2V4 NEW	-251.028	-91.2778	25.6799	65.3917	0.453040

Table 3-6. Application of the NL-DORMA and OC2-V4 algorithms to the bio-optical in situ measurements versus in situ chlorophyll-a measurements (C_M); statistical analysis. The *%E* is obtained using equation 2-25 *%Emin, %Emax* and $<\%E>$ are the *%E* minimum, maximum and average of *%E*, respectively. *%S* is the standard deviation of *%E*. r^2 is the correlation coefficient.

In addition the percentage differences between the modeled chlorophyll-*a* values and the measured ones (Figure 3-11) do not show a significant trend, demonstrating the applicability of the algorithm to a large range of Mediterranean chlorophyll-*a* values.

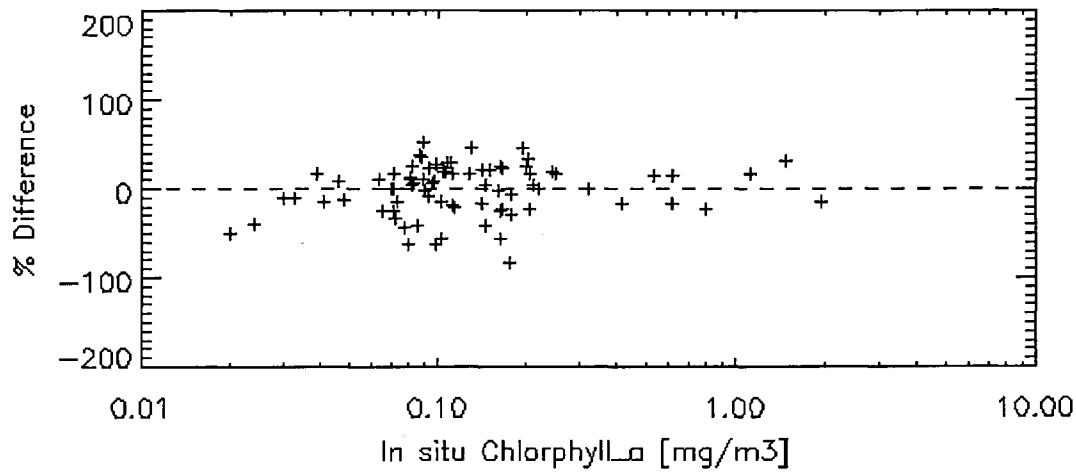

Figure 3-11. Percentage differences between in situ chlorophyll-a data C_M and NL-DORMA model values applied to bio-optical measurements, in function of C_M.

The statistical analysis confirms that the DORMA algorithm works very well on Mediterranean waters, reducing the errors by a factor of 2 respect to the estimates computed with the OC2v4 NASA algorithm. The final performances of the NL-

DORMA are summarized in Figure 3-12, where a scatter plot of modeled and measured chlorophyll-*a* values is showed.

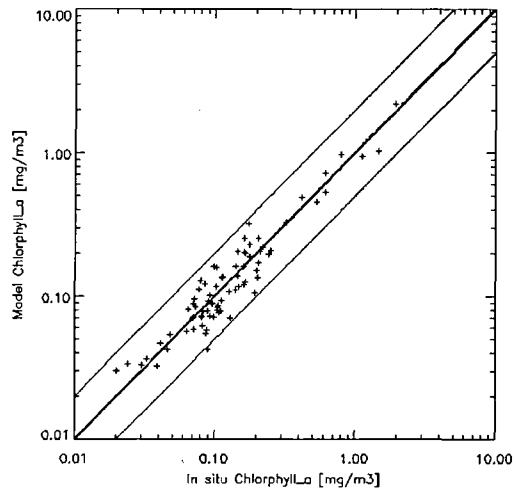

Figure 3-12. Scatter plot of NL-DORMA model values versus C_M. The 1:1 (center thick line), 1:2 (bottom thin line), and the 2:1 (top thin line) lines are also plotted.

3.2 VALIDATION OF SEAWIFS ATMOSPHERIC PRODUCTS OVER THE MEDITERRANEAN

The SeaWiFS atmospheric correction procedure has been designed to retrieve water-leaving radiances with an error within the 5% (Hooker and McClain, 2000). The algorithm derives the atmospheric characteristics of the observed pixel in the near infrared region of the spectrum and then extrapolates it in the visible bands (see chapter 2.2.4). The aerosols optical behavior is then estimated by the SeaWiFS atmospheric correction (see chapter 2.2.4), which permits to retrieve the aerosol optical thickness for each pixel. The extrapolation in the visible range is obtained *via* the definition and calculation of the atmospheric correction parameters ε and of the Ångstrom coefficients α obtained using a set of aerosols models (see chapter 2.2.4). The aerosol optical thickness and the Ångstrom coefficients are related each other by:

Eq. (3-11)
$$\frac{\tau_a(\lambda_1)}{\tau_a(\lambda_2)} = \left(\frac{\lambda_1}{\lambda_2}\right)^{-\alpha(\lambda_1,\lambda_2)}$$

To evaluate the satellite products, an intense effort has been carried out (and it is still in act) by the SeaWiFS project and by the other related projects (i.e. SIMBIOS) to build a global scale ground-truth database of aerosol measurements.

Principal source of in situ aerosol observations was the Aerosol Robotic Network (AERONET). It is a network of ground based automated sun photometers (Holben and al., 1998), which provides globally distributed, near real-time observations of aerosol spectral optical thickness, aerosol size distributions and precipitable water. In addition, in the framework of the SIMBIOS project, a number of hand-held sun photometers were made available for measurements from ships, increasing then the amount of open ocean data (Fargion, et al., 2001).

The development of hand-held instruments, as well as the set up of AERONET sites in coastal region or in islands, is a key factor to validate the SeaWiFS products over the ocean, being the characteristics of land aerosols strongly different by the marine ones.

The results of the validation effort of the SeaWiFS/SIMBIOS projects have been published in a specifically devoted NASA technical report (Wang, et al., 2000). The validation exercise was mainly focused on the comparison between satellite and in situ aerosol optical thickness(AOT) at 870 ($\tau(870)$) and Ångstrom (ANG) coefficient between the bands at 765 and 870 nm ($\alpha(765,870)$) on some selected sites. Particular attention was dedicated to the preparation and analysis of the in situ data set, increasing the tests and the quality controls, which are in general more relaxed in the standard AERONET processing. In fact, even if the AERONET system assures a good quality in the retrieved parameters, the demands of the satellite validation exercises requires an improvements of the requirements for the in situ data (see Fargion, et al., 2001, for details). The results of the validation demonstrated that the SeaWiFS retrieval of the $\tau(870)$ accomplished the requested accuracy, while the performances of the satellite $\alpha(765,870)$ estimates were still weak (Wang, et al., 2000).

More recently, Ainsworth et al. (2001) compared SeaWiFS AOT and Ångstrom coefficient estimaties with *in situ* measurements obtained from four AERONET stations located in islands. They confirmed the Wang et al. (2000) results and showed that ANG(765/870) was significantly underestimated by SeaWiFS. They conclude that the SeaWiFS aerosols models have a flat spectral distribution, typical of large particles as sea salt, which is insufficient to correctly extrapolate the AOT measurements from the red-near infrared toward the visible spectra.

For its peculiar geographic location, the Mediterranean Basin is strongly affected by industrial emissions from the northern border and desert dust from the south (Guerzoni, et al., 1997; Moulin, et al., 1997). In addition, the relatively weak winds should reduce the emission of sea salt particles. Aerosols transported to the Mediterranean Sea consists of anthropogenic-rich "background" materials supplied continuously from North-Central Europe, upon which sporadic pulses of Saharan crust-rich dust are superimposed. Schematically, the latter represents more than 90% of the mass of particulate atmospheric deposition, but is present only 10% of the time in the Mediterranean atmosphere, whereas the inverse figures apply to anthropogenic aerosols (Guerzoni, et al., 1997; Prospero, 1996).

In addition, SeaWiFS aerosols models do not take into account urban and absorbing aerosols that play a fundamental role in this area, surrounded by high density human population.

Consequently, a validation of the SeaWiFS aerosols products in the Mediterranean is mandatory and is the subject of this section.

The ground truth data derived mainly from the AERONET database, which are collected with uniform protocols and are processed with unique software framework. AERONET stations located in the Mediterranean area were selected and processed using a particular approach aimed to improve the results of the match-up comparisons.

The validation activities have been carried out with a multi approach strategy:

- a subjective analyses based on SeaWiFS data analysis only
- a "pseudo-climatological" evaluation, with comparison of the statistical behaviour of the two data-set (satellite and ground-truth data)
- a "classical" point-point exercise (match-up)
- an evaluation of the end-user impact, which is mainly focused on the satellite estimation of chlorophyll concentration.

3.2.1 SeaWiFS satellite data

The SeaWiFS atmospheric correction parameter ε was obtained (see chapter 2.2.4) weighted averaging over two possible ε candidates, derived from the set of aerosols models, summarized in Table 3-7 (Wang, et al., 2000).

The SeaWiFS aerosol optical thickness was calculated by the atmospheric correction parameter (as obtained from the model) and by the measured L_{as} in the selected NIR bands.

The standard atmospheric correction (consisting in the described Gordon and Wang, 1994, multi-scattering atmospheric corrections with the Siegel dark pixel method) was applied then to the available Mediterranean satellite data.

Name	Type	α(440/870)	RH%	Description
T50	Tropospheric	1.4105	50	Back-ground aerosol: water soluble substances + Dust like aerosols
T90	Tropospheric	1.2819	90	
T99	Tropospheric	1.0946	99	
M50	Maritime	0.4951	50	Tropospheric model + Sea-salt aerosols
M70	Maritime	0.4000	70	
M90	Maritime	0.2154	90	
M99	Maritime	0.0992	99	
C50	Coastal	0.7391	50	As Maritime with half fraction of sea-salt
C70	Coastal	0.6353	70	
C90	Coastal	0.4109	90	
C99	Coastal	0.2311	99	
O99	Oceanic	0.0805	99	As Maritime with larger salt particles

Table 3-7. Atmospheric correction models (from Wang, et al., 2000).
α values are obtained by the SEADAS FORTRAN procedure *get_angstrom.f.*

The choice of the models was based on the $\varepsilon(765,865)$, which is considered the best option for the atmospheric correction procedure, and in fact is the default one in SeaDAS software.

For the validation exercise, the 1-km resolution SeaWiFS data for the period January 1 to December 31, 2000 were processed up to Level 2 (L2) standard NASA format to obtain aerosol optical thickness and Ångstrom coefficients using SEADAS software version 4.4 (Baith, et al., 2001). Only land, clouds and stray light SEADAS flags were applied (see appendix 9.2) in order to maintain the maximum number of available satellite data. L2 data have been remapped on a 4-km resolution equirectangular projection in the region of interest (10°W - 43°E and 27°N - 48°N), using the University of Miami Display Software Package (DSP).

3.2.2 AERONET data set

The ground-based measurements, used as ground truth data set, have been obtained mainly from the automated CIMEL sun-sky scanning radiometer, managed as part of the AERONET network (Holben and al., 1998).

AERONET sites at a distance of less than 100 km from the Mediterranean coastline (Figure 3-13) have been selected.

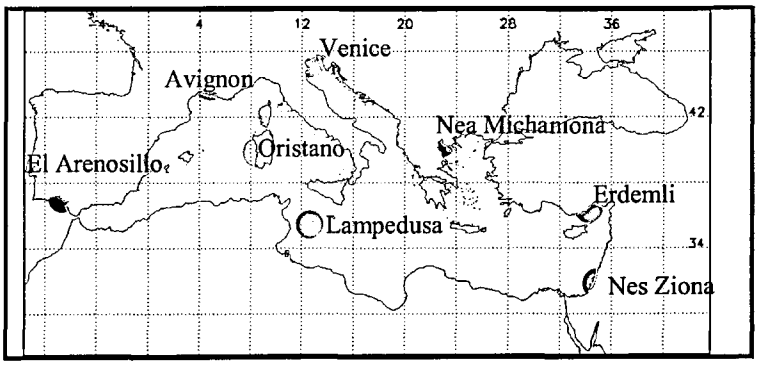

Figure 3-13. Location of the considered AERONET stations

Although the site of El Arenosillo is not exactly in the Mediterranean Sea, it has been retained because it can be assumed as representative of the aerosol condition of the Mediterranean in the southern Spanish coastal region. The decision to maintain also

station 100 km far from coast (i.e. Avignon) in the ground-truth database was based on the possibility to explore the behavior of this kind of stations in the validation exercise. In particular, the rationale to keep these inland stations in the data set was to verify if the information retrieved by stations not directly located on coast or on islands could be useful to verify the limits of satellite data.

In addition to the AERONET, CIMEL data acquired at Nea Michaniona (Greece) during the ADMIRA measurements campaign (Webb, et al., 2002) were also utilized.

The distribution of the selected stations covers the different regions of the Mediterranean and should be representative of the major aerosol condition occurring in the area. Table 3-8 contains some information on the single datasets constituting the ground truth data set.

The ADMIRA dataset was processed mostly using the same approach of the AERONET processing except for the molecular scattering correction that was computed on the basis of measured pressure rather than on an altitude derived pressure and Ozone.

Site Name	Coordinates Lat N Lon E	Elevation (m)	Period	PI	Distance from Coast (km)
Avignon	43°55' - 4°52'	32	1/1-31/12	Verbruge	40
El Arenosillo	37°06' - 6°42'	0	16/2-31/12	Cachorro – Revilla	2-3
Erdemli	36°33' -34°15'	0	1/1 – 29/12	McClain	5
Lampedusa	35°31' - 12°37'	45	27/6 – 17/9	Pugnagli	Island.
Nes Ziona	31°55' - 34°47'	40	24/2-31/12	Holben	8
Oristano	39°54' - 8°30'	10	30/5-31/12	Tanre	1-2
Venezia	45°18' - 12°30'	10	1/1 – 31/12	Zibordi	Island
Nea Michaniona	40°28' - 22°51'	30	3/8 – 13/8	Liberti	5

Table 3-8.Validation ground truth dataset description.

AERONET data are available at three different processing levels (1.0, 1.5 and 2.0). The main differences between levels are the cloud screening (1.5) and the quality control (2.0). The cloud screening produced by AERONET contains a test for low frequency variability and only accept days that are statistically stable. These days are

expected to have cloudless atmospheric conditions, since clouds moving through the sky increase the variability in the CIMEL measurements (Smirnov, et al., 2000). This procedure eliminates entire days of measurements, while for satellite data validation analysis it is sufficient to have cloud-free data in correspondence to the time window selected for the match-up (Ainsworth, et al., 2001). Then all the available levels of AERONET data (level 1.0) have been selected, and a procedure has been built that is general, independently from the AERONET processing levels. The procedure firstly eliminates the records containing in negative value of τ. Then, the procedure identifies periods of measurements in which the data records are acquired with a time sampling less than 1 minute, selecting among the AERONET data records that fall within such period the record in which the time is minimum. Because the CIMEL instrument requires one minute to complete the measurements, data acquired with sampling time <1 minute were suspected to be incorrect.

The adopted procedure eliminates the unreasonable data contained in the AERONET data set, but still retains measurements obtained in presence of clouds. The cloud screening of AERONET data has been performed during the construction of match-up database, in order to take into account also the information on cloud conditions obtainable from SeaWiFS.

CIMEL-AERONET instruments and the SeaWiFS radiometer have only three common wavelengths: (440, 670 and 870 nm), then the aerosol optical thickness at 670 nm and the angstrom coefficient between 440 and 870 nm have been selected for the comparison. The choice of the parameters for the comparison is based on two main considerations: first, the SeaWiFS atmospheric correction procedure is derived entirely from measurements of TOA radiances at two NIR wavelengths only. Because of only two independent parameters could be obtained from only two measurements, the comparison exercise has been limited on just two parameters, being the others derived. Performing the comparison on other wavelengths could lead to a redundancy of the

results. Second, as already showed from Liberti et al. (in preparation), the choice of $\tau(670)$ and of the $\alpha(440,870)$ parameters has been mainly driven by the minimization of the uncertainty in the AERONET data set.

Furthermore, being the final aim of the SeaWiFS mission the estimation of water leaving radiances in the visible range with an error below the 5% (Hooker and McClain, 2000), the analysis of the error on $\alpha(440,870)$ could also give information on the effect of atmospheric correction on the SeaWiFS end-user parameters (water leaving radiances and derived chlorophyll-*a*).

3.2.3 Subjective analysis of climatological maps

The first type of evaluation was based on a subjective analysis of each single orbit product map as well as monthly and seasonal composites ones. From such an analysis it is expected to identify evident algorithm biases such as the occurrence of clearly not-physical features/values, consequence, for example, of calibration, observation geometry and cloud screening. As an example, Figure 3-14 shows the summer (June-July-August 2000: JJA) and winter (December-January-February 2000: DJF) maps of average τ and α.

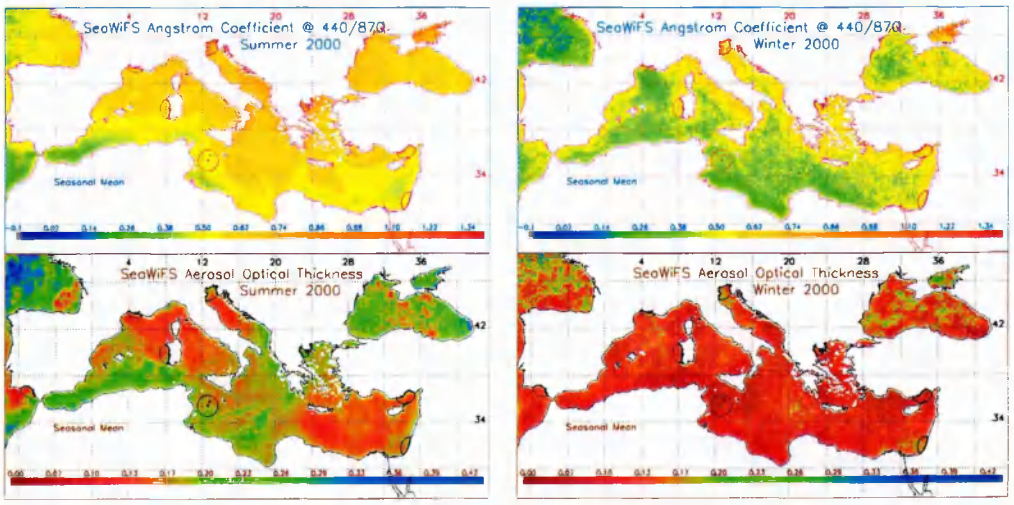

Figure 3-14. Average maps of SeaWiFS Angstrom Coefficient (440/870) and of Aerosol Optical Thickness for the Winter and the Summer 2000.

From these images, and from the analysis of similar products (Figure 3-15), including the maps of occurrence of aerosol models, few interesting features can be observed.

- Lower values of α (i.e. larger particles) occur mostly off the coast of northern Africa. This may be due to desert dust events, which generally spread from Saharan area toward the Mediterranean Basin. Another area of relatively high occurrence of low Ångstrom coefficients is the Gulf of Biscay, where the aerosol model selected most frequently is the oceanic one. It can be physically possible because this area is more representative of a true open sea than the Mediterranean and because of expected larger values of surface wind responsible for the emission of sea salt particles in the atmosphere. On the other hand, I suspect, on the basis of the analysis of the product maps, that part of the measured spectral dependence is due to undetected clouds.

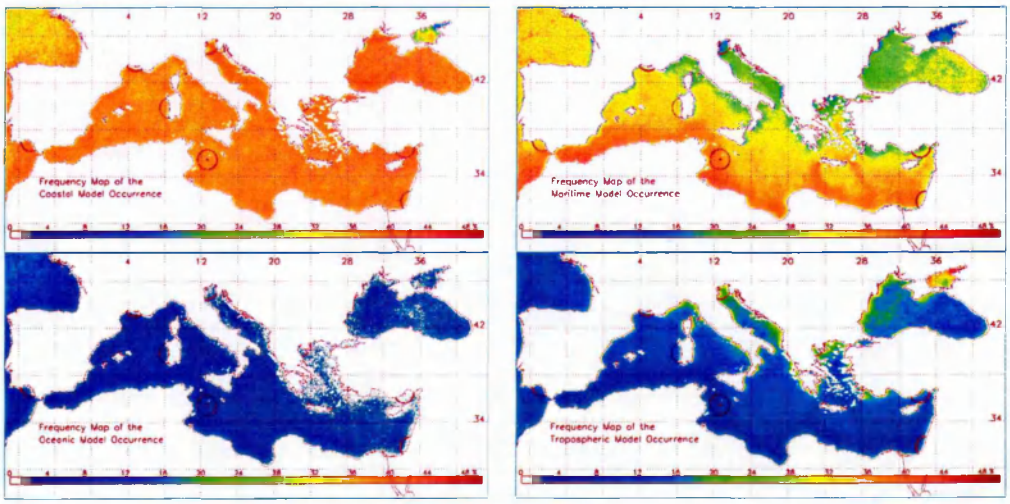

Figure 3-15. Maps of occurrence of SeaWiFS atmospheric correction aerosol models for the Mediterranean area.

- The effect of the coast. This may be partly due to land contamination, but the AOT maps reveal a possible physical feature (i.e. the difference of such an effect between the Northern coasts and Southern ones). This is particularly evident, for example in the western part of the Mediterranean in the winter composite.

Similarly, in the aerosol model occurrence maps, there is a net south-to-north increasing of occurrence of tropospheric model (the smallest one included in the SeaWiFS candidate models). From the surface point of view, assuming a "greener" surface in the north will give larger reflectance at longer wavelengths decreasing the spectral dependence of the supposed atmospheric radiance. This effect firstly would give an opposite distribution of ANG(440/870) close to the coast (smaller values) and second it wouldn't extend off coast as much as observed for example in the winter composite. To support the non-surface nature of such coastal behaviour, it is sufficient to observe the composite of aerosol optical thickness where there is no correspondent off-coast extension of land effects. As a consequence, the hypothesis of direct influence of land surface is rejected, except, of course for the 'very' coastal pixels. From the atmospheric point of view, it is possible to suppose a larger contribution of aerosol from anthropogenic pollution, which exhibits relatively small size. The possible influence of ocean reflectance cannot be rejected, especially when looking at the behaviour of the Azov Sea, that is a particularly shallow and close basin.

- A clear seasonal cycle with lower ANG(440/870) values in the winter and higher in the summer. While, again, part of this signal can be due to the cloudiness seasonal cycle, from the summer maps it is evident a larger influence of continental-like aerosols that extend off coast more than during the other seasons probably because the more active sea-breeze circulation.

3.2.4 Pseudo-climatological comparison

A second kind of validation, relatively more quantitative, was performed by comparing the statistical patterns of SeaWiFS aerosol derived products against the ground truth derived ones. The rationale for this analysis is that climatologies of geophysical parameters for the same areas and periods should match also if areas and

period do not match exactly, but refer to the same climatological regime. Figure 3-16 shows the whole year 2000 cumulative frequency histogram for both τ and α.

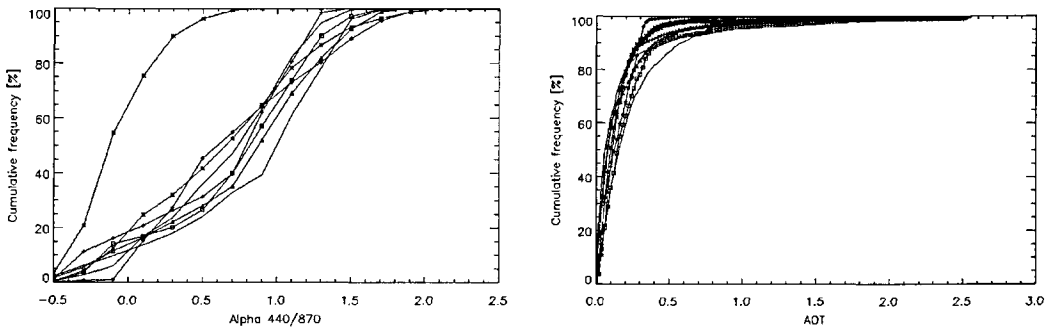

Figure 3-16. Cumulative frequency histogram for the SeaWiFS data and the selected AERONET sites. Left panel, angstrom coefficient, right panel aerosol optical thickness).

In this comparison there is no attempt to co-locate spatially and temporally the two sources of information, therefore the curves of Figure 3-16 have been computed with the whole time series of available ground truth data and with the whole area covered by the SeaWiFS data.

From the analysis of such curves it is evident a first result: while for τ the agreement is relatively good, there is a clear shift of α values derived by SeaWiFS. Most of the α measurements from satellite (90%) are lower than the value of 0.5, while the same percentage for the ground truth data is reached at the value of 1.5. Another evident feature of the α trends is a larger difference within the cumulative histograms compared to τ the ones; this is not only due to different aerosol regimes but is caused probably by different quality of the ground truth data. Finally, it is important to note that even if the stations considered are strongly different in position and time period, the statistical behaviors of the ground-truth data are not so dissimilar. In other words, the "pseudo-climatological" regimes of the AERONET data appear analogous for the whole Mediterranean area. The strong disagreement with the SeaWiFS α curve gives then a first insight of the problem experienced by the satellite procedures in the retrieving the

Mediterranean aerosol characteristics. At this level of analysis, it is impossible to obtain more information: a point-point comparison (a matchup analysis) is needed.

3.2.5 Description of the match-up criteria

The third kind of validation consists in a quantitative comparison of independent estimates of τ and α taking into account the time and spatial co-location.

For each processed orbit, without considering the effective coverage, AERONET data were selected with two different criteria. A first data set was created using the single measurement closest in time within the same day. A second data set was derived from a collection of AERONET measurements within a time window of +/- 0.5 hr from the satellite visiting time, for which statistics as mean, standard deviation, maximum and minimum value were computed.

For both criteria, the SeaWiFS time was assumed as the time of the first acquired data. This may be further North of the Mediterranean, according to the season and the relative position of the satellite respect to the acquiring antenna.

Nevertheless, given the fact that SeaWiFS takes less than 10 minutes to scan the Mediterranean, the error introduced by this approximation is expected to be negligible. Note that the first selection criteria (i.e. the single measurement closest in time) produced a matching point for each day for which at least one measurement was taken.

For this reason, this criterion produced a dataset with a larger number of matching points compared with the one obtained with the maximum +/- 0.5 hr delay from the satellite visiting time. On the other hand, this dataset cannot be considered homogeneous because matching points can be up to about 6 hrs from satellite visiting time. For this reason at each matching point is associated also the information on the time delay.

Unfortunately, except for the site of Venice, the ground truth sites are at the best on the coast.

Therefore, it was necessary to define a spatial autocorrelation of the aerosol products to be able to compare coastal with open sea aerosol products. In absence of such information, in order to take into account of spatial variability of aerosol properties, for each site a mask based on the distance has been produced, grouping the SeaWiFS pixels for classes of increasing distances (0-10 km to 90-100 km).

Once selected ground truth data on a temporal window, the procedure searches for existing satellite products, for each given site. This was done by searching, within a given distance class, processed data in the SeaWiFS products files.

For each of the 10 distance classes described above, basic statistics are reported together with the number of pixels selected. As a result of the above described procedure, a "well-matched" point will be associated with one or two ground-based measurements (and relevant statistics), differing for the temporal matching criteria, and up to 10 satellite derived products (and relevant statistics), according with the different distance matching classes.

As preliminary approach to define the distance and the time windows dependencies of the error in the match-up analysis, bias_α (defined as α_seawifs – α_aereonet), bias_τ (defined as τ_seawifs – τ_aeronet) and the relative RMS errors are computed for the ten distance's classes and for the two temporal windows (see Figure 3-17).

In general, the time-closest data exhibit a larger error then the time-window ones, even for stations with a good temporal resolution. For all the stations, RMS (Bias_α) remains substantially unchanged, with only a slight increase with the distance for some stations (El Arenosillo, Venice, Avignon). On the other hand, RMS (bias_τ) shows a more evident spatial dependency, which permits to define a "best" distance class to perform the match-up exercise.

It is noteworthy that not always the "best" distance class is the nearest to the AERONET station (i.e. Nes Ziona), probably because of the influence of the terrestrial e/o anthropogenic aerosols. In those cases, the "best" distance class is a compromise

between the points "too close" (than more affected by land-derived errors) and the points "too far" (then with information related to a different area respect to the ground-truth station).

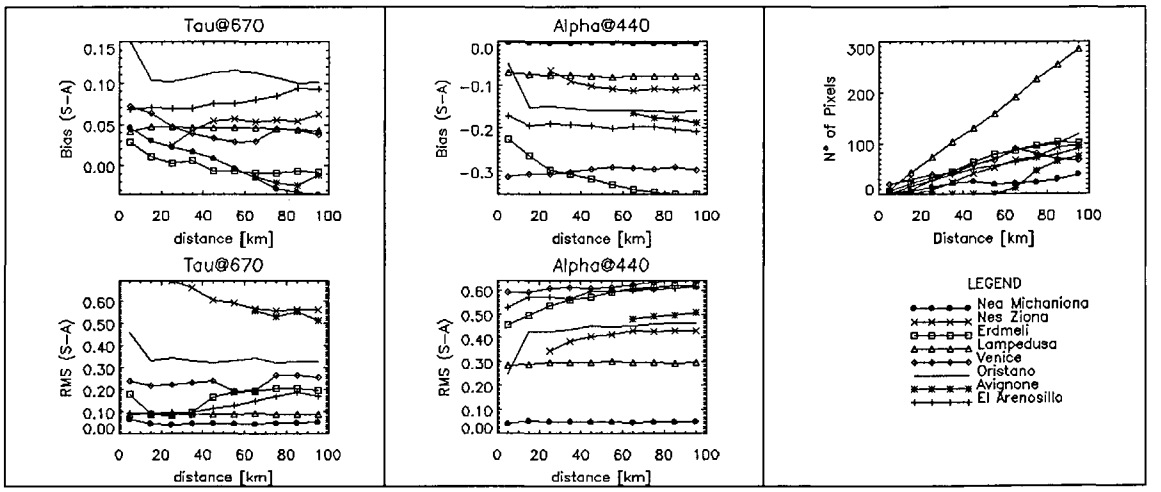

Figure 3-17. RMS errors of the bias between SeaWiFS and AERONET data plotted versus the distance, for the two time windows (see text) and for the considered stations. Left panels refer to AOT(670), central panels to ANG(440/870). On the right panel the number of pixels used in the computations are plotted versus the distance.

Summarizing, satellite data within the distance class with the lowest RMS error, and AERONET data averaged on a time window of +/- 0.5 hr from the satellite pass time have been selected for the point-point comparison.

3.2.6 Results of matchup analysis

Figure 3-18, Figure 3-19 and Table 3-9 show the match up results for the selected ground truth stations and the relative statistics.

A reasonably agreement for the aerosol optical thickness is found, demonstrating the good performance of SeaWiFS procedure in the retrieval of this parameter.

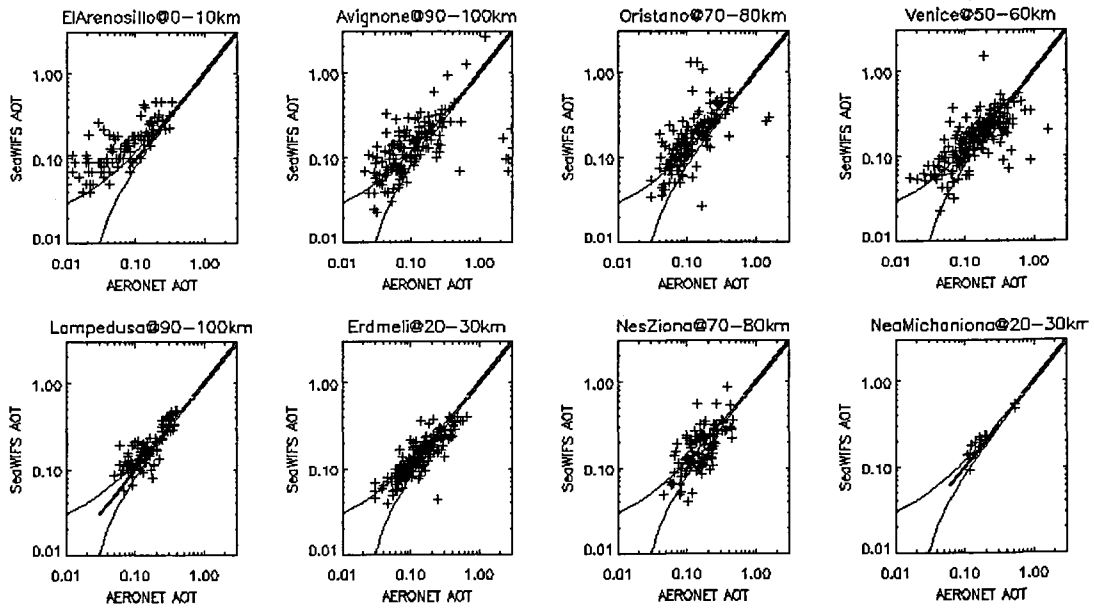

Figure 3-18. Scatter plots of the AERONET versus the SeaWiFS derived AOT's, for the selected AERONET stations and distance classes. Solid lines indicate the 1% deviations from the 1:1 line.

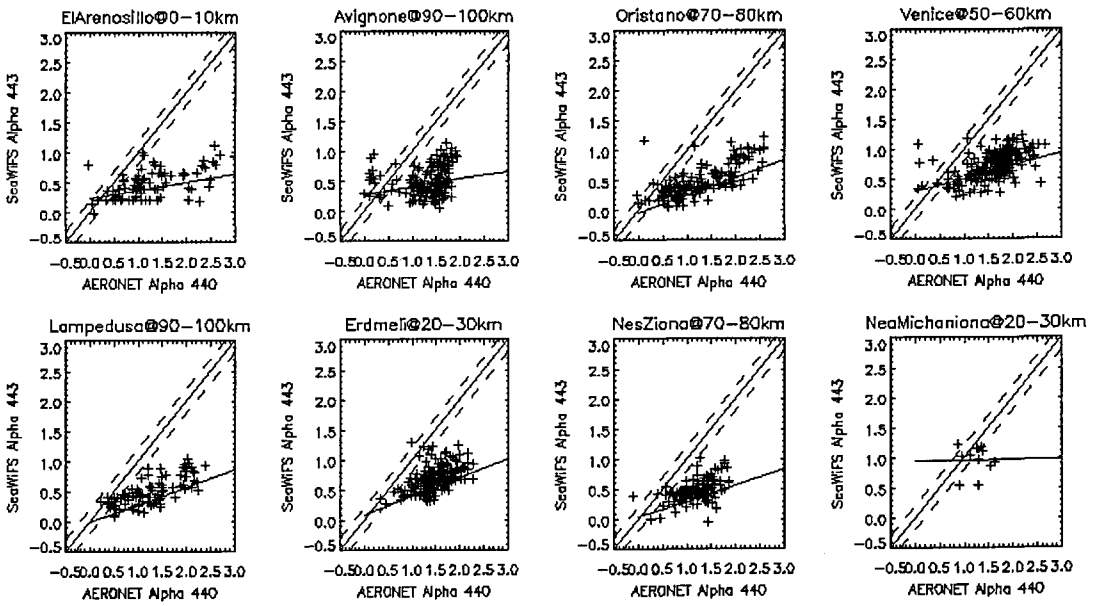

Figure 3-19. Scatter plots of the AERONET versus the SeaWiFS derived ALPHA(440). The 1:1 (center thick line) 1:0.95 (bottom thin line) and the 1.05:1 (top thin line) lines are also plotted. In addition, fitting lines are displayed (see text).

Station	Distance class (km)	Best τ RMS	τr^2	αr^2	# Points
El Arenosillo	10÷20	0.09	0.61	0.24	102
Avignon	90÷100	0,35	0.03	0.06	166
Oristano	70÷80	0,23	0.09	0.51	157
Venice	50÷60	0,13	0.14	0.26	222
Lampedusa	90÷100	0.08	0.78	0.51	93
Erdemli	20÷30	0.08	0.72	0.27	185
Nes Ziona	70÷80	0,38	0.02	0.27	116
Nea Michaniona	20÷30	0.04	0.96	0.00	11

Table 3-9. Statistical results of the matchup comparison.

On the contrary, the comparison of α shows a general underestimation of the SeaWiFS data respect to the AERONET ones for all the considered stations. A simple linear fit of the data was performed (the slopes and bias for the different stations and for the whole data set are summarized in Table 3-10 together with the statistical parameter of the error).

Station	Intercept	Slope
El Arenosillo	0.32	0.14
Avignon	0.35	0.13
Oristano	0.12	0.29
Venice	0.40	0.22
Lampedusa	0.14	0.29
Erdemli	0.24	0.31
Nes Ziona	0.16	0.26

Table 3-10. Coefficients of the linear fit performed on the α values.

The biases showed derive primarily from the lack of aerosol models allowing values larger than 1.7 in the SeaWiFS standard atmospheric correction procedure. In fact, the available models present in the SeaWiFS data processing are not able to retrieve α values greater then 1.7. In addition, the α match-up analysis demonstrated that between the two data sets is present a slope. The lack of adequate aerosols model cannot explain it totally, which seems also to be station-dependent.

3.3 DISCUSSION OF THE VALIDATION EXERCISE

In the previous sections the results of the validation exercise were showed. The main results can be so summarized:

- NASA bio-optical algorithms over-estimate the Mediterranean chlorophyll when applied to both the in situ and satellite R_{rs}. As consequence, a specific algorithm for the Mediterranean. (DORMA) has been developed and then validated with independent data.
- DORMA algorithm applied to satellite R_{rs} over-estimates in situ chlorophyll, even if it has lowest error than the other tested algorithms.
- SeaWiFS optical thickness at 670 and angstrom coefficient at 440, which are intermediate products of the atmospheric correction procedure, exhibit opposite performances. The optical thickness matches the measured values very well, whereas the angstrom coefficient is generally lower then the measured one.

3.3.1 Point 1

The first point raises the question of why the global algorithms overestimate chlorophyll-*a* concentration in the Mediterranean Sea.

A possible cause, which could bias the satellite reflectance ratio as compared to the one expected from in situ pigment concentrations, was discussed by Gitelson et al. (1996). They proposed that a relatively higher abundance of coccolithophores as compared to other groups, which might be typical of oligotrophic open seas, would in fact distort the reflectance ratios. It is noteworthy that this argument holds for relatively low concentrations of coccolithophores, well below the concentrations that make the global algorithms unfit and that are flagged by the routine procedure. This point is quite intriguing, because it is generally assumed that coccolithophore chlorophyll-*a* should be underestimated owing of the peculiar calcareous coverage of the cells (Gordon and

Balch, 1999), with an enhanced reflectance in the visible part of the spectrum (Tyrell, et al., 1999).

The effect of the coccolithophores presence on the blue-green water leaving radiance ratio was already described by Gordon and Balch (1999). They underlined the change in the value of the *lwn*(440)/*lwn*(550) ratio when coccolith concentration ranges between 0 and $200x10^9$ coccoliths/m^3.

Then, to figure out whether the Gitelson hypothesis holds, an analysis similar to that by Gordon and Balch (1999) was performed, but applied to the band ratio used in the NL-DORMA and OC2 (i.e. 490/555 nm). R_{rs} was modelled using the Gordon et al. (1988) assumptions:

Eq. (3-12)
$$R_{rs}(\lambda) = 0.095 \cdot \left(\frac{b_b(\lambda)}{b_b(\lambda) + a(\lambda)}\right) \cdot 0.54$$

where b_b is the total backscattering coefficient and a is the total absorption coefficient.

Absorption coefficient has been calculated according to the bio-optical model of Morel (1991) for case I waters:

Eq. (3-13)
$$a = a_w + a_p + a_{cdom}$$

where the subscripts w, p and *cdom* refer to seawater, particulate and dissolved organic matter contributions to the total absorption coefficient. a_w has been estimated according to Smith (1978), a_{cdom} has been estimated assuming that CDOM concentration covaries with chlorophyll-*a*, and with a spectral dependence described by an exponential function with an exponent of -0.014 (Bricaud, et al., 1981). a_p has been modelled following Morel and André (1991) using chlorophyll-*a* specific absorption coefficients proposed by Sathyendranath and Platt (1988).

Following Tyrell et al. (1999), b_b was expressed as:

Eq. (3-14) $$b_b = b_{bw} + b_{bp} + b_{b,CaCO3}$$

where b_{bw} is the backscattering coefficient of seawater, computed as Morel and Smith (1974), b_{bp} is the backscattering coefficient of particulate and $b_{b,CaCO3}$ is the backscattering coefficient due to the calcite ($CaCO_3$) of coccoliths (for details see equations 5, 6 and 8 in Tyrell, et al., 1999). The values of the optical properties, composition and abundance of coccoliths given by Tyrell et al. (1999) are used and it was also assumed that the coccoliths covering the cells would have the same optical properties of the detached ones. Simulations showed a decrease in reflectance ratio as calcite concentrations increased, confirming the results obtained by Gordon and Balch (1999) for CZCS bands, providing a cue for the overestimation of chlorophyll-*a* at low levels.

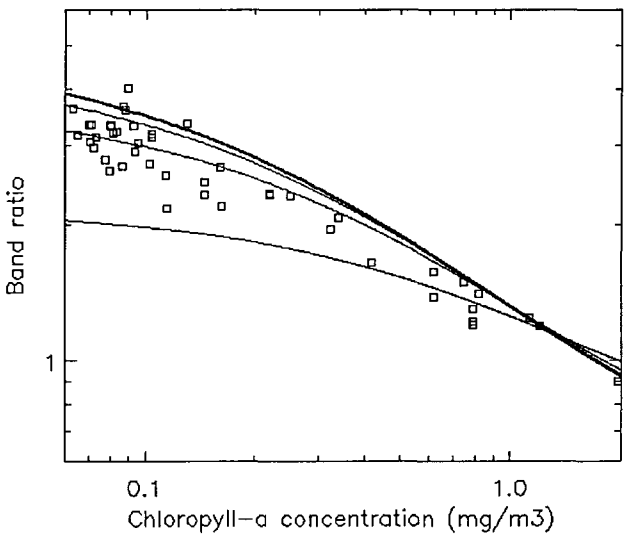

Figure 3-20. Variations in the $R_{rs}(490)/R_{rs}(555)$ band ratio with chlorophyll-a concentration. Squares represent the in situ bio-optical measurements and the concurrent chlorophyll-a presented in section 2.3. The solid line is the semi-analytic radiance model presented in the text. The CaCO3 concentration for the 4 lines are 0,1,5,50 mg m^{-3}. The thick lines represent the lower CaCO3 concentration. The higher CaCO3 concentrations yield the "flatter" curves

However, the derived reflectance ratio fits the experimental bio-optical data (Figure 3-20) for a CaCO3 concentration of about 5 mg m^{-3}.

This amount of calcite would in fact correspond to a coccolithophore concentration in the range between of $3 \cdot 10^4 \div 2.5 \cdot 10^5$ cells/dm^3, which is almost one order of magnitude higher than the concentration found by the SZN group (4000 cells/dm^3) in few stations of the Ionian Sea (Rabitti, et al., 1994) or in the Levantine Sea (Robarts, et al., 1996; Yacobi, et al., 1995).

Thus, the observed systematic overestimate can only partially be explained by the presence of coccolithophores.

A distortion in the reflectance ratio could also originate from a high concentration of CDOM, which might be higher in the Mediterranean Sea, a semi-enclosed basin, than in the open ocean. No CDOM concurrent data and chlorophyll-*a* data were available, but measurements recently carried out in open waters of Mediterranean Sea display very low concentrations of CDOM, always in the range between 50 and 80 μmol/dm^3 (Seritti, et al., 2000).

Therefore, the lower value of the measured band ratio is probably due to a phytoplankton community with optical properties different from the average community on which OC2v4 is based, similarly to what Sathyendranath et al. (2001) observed for the Labrador Sea. This in turn stresses the need for regional algorithms.

3.3.2 Point 2

The performances of the algorithms when applied to satellite data are in general lower, resulting in an increase of the errors and in an overestimate of the chlorophyll-*a* concentration. This effect was particularly evident for OC4v4, which is probably more affected by the error in the atmospheric correction, due to the multiple band ratio option. The poor performance of this algorithm in the satellite chlorophyll-*a* retrieval was evident from the performed study, though it exhibited better results than OC2v4 when

applied to in situ bio-optical data. However, also the DORMA algorithm, which appears to be very promising in the chlorophyll-*a* prediction from the in situ R_{rs}, decreased its performance when applied to the satellite radiances.

The different behavior of the same algorithm when applied to bio-optical measurements or to remotely sensed data, demonstrated that the atmospheric correction is still the main source of error in ocean color data.

To quantify the error related to the atmospheric term, an additional analysis was carried out. Bio-optical data obtained in the 2003, during two Mediterranean particular favorable weather cruises, permitted to increase the number of "total" matchup points (a total matchup points it is a point comprising satellite data and both chlorophyll-*a* and in situ R_{rs}) from the five of the DORMA development to the 24 currently available. The data collection and the matchup procedures were the same as described before. A comparison of the R_{rs} obtained from space and in situ is shown in Figure 3-21.

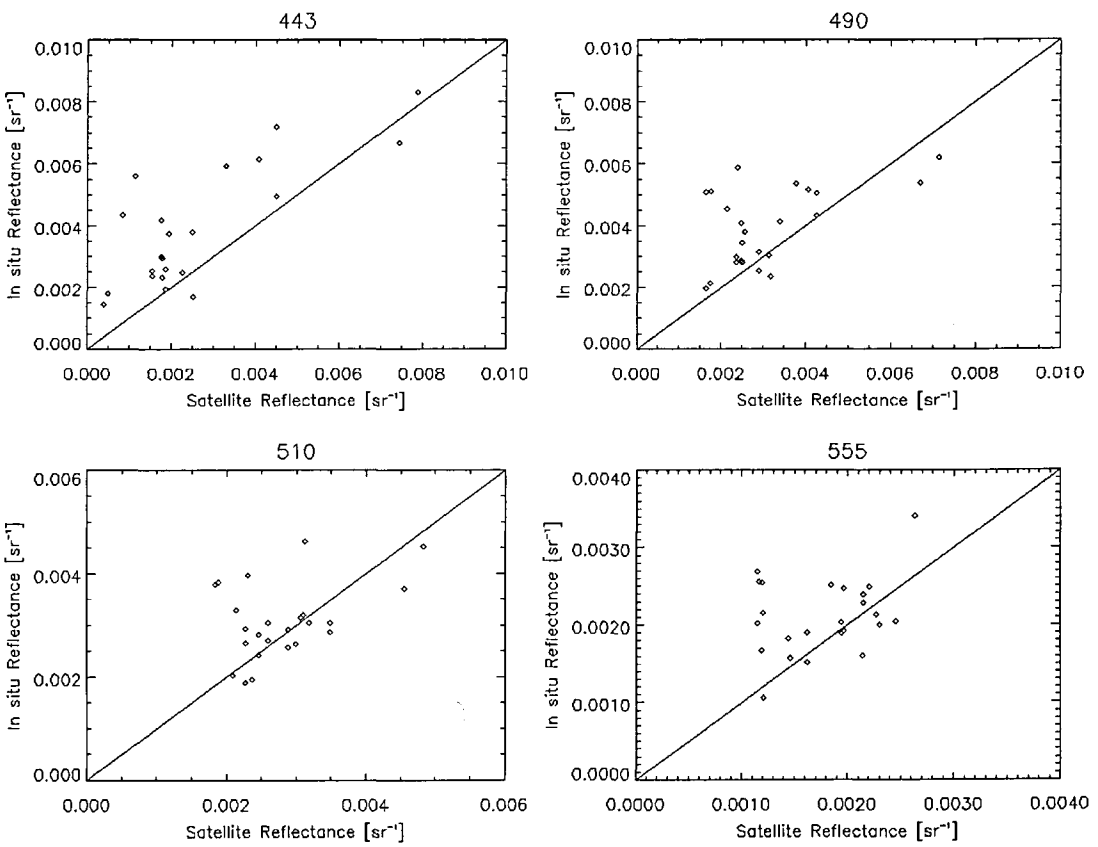

Figure 3-21. Scatter plot of In situ vs Satellite *Rrs* for four SeaWiFS bands.

In general the error showed by the satellite R_{rs} increases with decreasing wavelength (see Table 3-11), even if the $R_{rs}(510)$ exhibits better results than the $R_{rs}(555)$ one.

Band	Mean % error	R^2	Number of points
443	0.39	0.41	24
490	0.18	0.28	24
510	0.06	0.15	24
555	0.13	0.09	24

Table 3-11. Statistical results of the comparisons between satellite and in situ data for the total matchup points.

The satellite $R_{rs}(443)$ display an error larger than the SeaWiFS requirements (i.e. more a 5% in the R_{rs} retrieval), except for the $R_{rs}(510)$.

In fact, the use of algorithms based on radiance ratio, should skip parts of the observed bias on the R_{rs} data, and then, a comparison of the radiance ratio currently used in the satellite algorithms was performed (Figure 3-22 and Table 3-12).

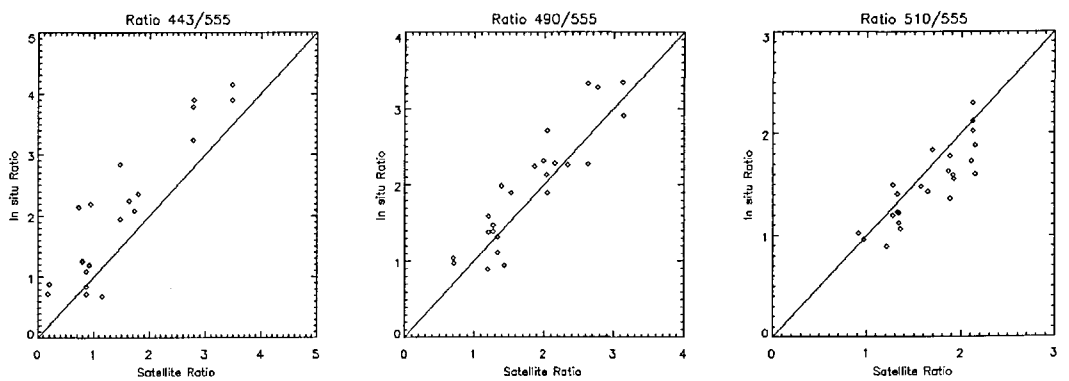

Figure 3-22. Scatter plots between in situ and satellite R_{rs} ratio.

Indeed, compared with the single band evaluation, the percentage error on the bands ratios 490/555 decrease substantially (from 0.13-0.18 of single bands to 0.05 of the ratio), while 510/555 remains substantially unchanged (from 0.06-0.13 to -0.11). Definitely the band ratio 443/555 results in the worst performance (R^2 = 0.35 and 0.35 percentage error).

Band ratio	Mean % error	R^2	Number of points
443/555	0.35	0.65	24
490/555	0.05	0.82	24
510/555	-0.11	0.73	24

Table 3-12. Statistical results of the comparisons between satellite and in situ data for the three tested ratios.

The analysis of the total matchup data explains then the poor performances of the OC4v4 algorithm when applied to the Mediterranean satellite data, as revealed by the marine matchup analysis. That algorithm, working on all the three band ratios available, may become less accurate then the 2 bands ratio algorithms (i.e. DORMA, OC2v2) in the chlorophyll-*a* prediction, because it permits the selection of the ratio 443/555 which exhibits the largest error. The error is more prominent in the oligotrophic range (chl < 0.1 mg m^{-3}) when the ratio 443/555 is most widely used, while the performance of the algorithm improves when applied to high chlorophyll-*a* values (i.e. when the algorithm selects the other ratio).

All the above, even if demonstrated the better accuracy of the OC2V2-like algorithm, does not resolve the question on the decreased performance of the algorithms when applied to space data, only pointing out a general underestimation of the satellite R_{rs}, mainly emphasized on the short wavelengths (i.e.443). Tough, this can be only the consequence of an incorrect atmospheric correction procedure.

3.3.3 Point 3

The atmospheric correction is then claimed as main source of error in the satellite Mediterranean chlorophyll-*a* estimations.

DORMA algorithm was applied to the total matchup radiances obtained from both satellite and in situ measurements, and the results were compared with the simultaneous *in situ* chlorophyll-*a* retrieval (see Table 3-13).

	Mean % error	R^2	# of points
DORMA situ	5.8	0.78	24
DORMA satellite	-20.1	0.52	24

Table 3-13. Statistical summary of the application of the DORMA algorithm to the total matchup points.

The shown values of the errors are in the ranges already discussed and confirm the results obtained with the validation exercise. More interesting, Table 3-13 shows the mean error induced by the atmospheric correction terms on the chlorophyll-*a* estimate. A more rigorous calculation should accounted for the effect of the Siegel assumption on the satellite terms. However, we are here more interested to determine the order of magnitude of the terms involved, rather than evaluate the exact values of the errors, and therefore such effect will not considered. Neglecting the effect of the Siegel assumption, the uncertainty on the satellite chlorophyll-*a* final value can be expressed as the sum of the errors due to the bio-optical algorithm and to the atmospheric correction procedure. Considering the values in the first column of Table 3-13 the error due to the atmospheric procedure was evaluated to be the 14.3% of the real chlorophyll-*a* values, and result in a general overestimation of the biomass contents. Finally, it accounts for almost the 70% of the total error in the final chlorophyll-*a* evaluation.

Is it possible to explain the sources of the observed inaccuracy, with the data available here? Obviously, an accurate analysis should consider all the involved terms, and should be based on a radiative atmosphere-ocean transfer model. Using a semi-quantitatively approach, an effort to evaluate the causes of the problems was attempted. The validation of the atmospheric SeaWiFS parameters, carried out in the previous chapters, demonstrated that the retrieval of the angstrom coefficient 440/870 is affected

by a large inaccuracy, which resulted in general underestimation of this parameter. This should imply an underestimate of the aerosol contribution, which in turn provokes an increase of the water term. This fact contrasts with the total matchup analysis, which demonstrated that the water radiances are on average underestimated.

Other sources of error have to be invoked.

To reconcile the two evidences (low angstrom and low water leaving radiances) the only possibility (excluding an error in the matchup procedure) is that some inaccuracies in the not-aerosol terms provoke an uncorrected increase of the supposed aerosol radiances.

The total matchup data have then been reexamined, to find some relationship between observed error on the radiances and some parameters involved in the atmospheric correction procedure. Attempts to correlate the radiances errors with the viewing geometry (satellite and solar zenith angle) and with angstrom coefficient resulted in no clear evidence. However, an increased error in the absolute radiances with an increase of corrected air mass (see Figure 3-23) was found at the shortest SeaWiFS wavelengths (412, 443 and 490).

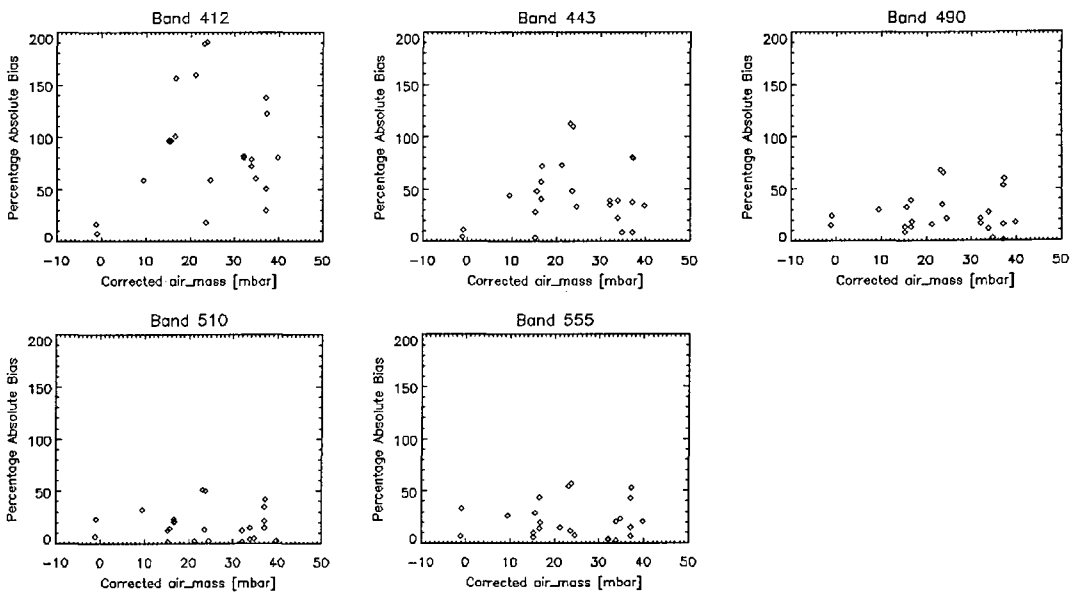

Figure 3-23. Percentage absolute bias between satellite and in situ R_{rs} vs corrected air mass (see text for explanations) for five SeaWiFS bands.

The corrected air mass is the bias on pressure (current pressure minus standard pressure) times the inverse of cosine of satellite zenith angle and of cosine of solar zenith angle (i.e. the air mass), which give an indication of the path length of the photons collected by the space sensor.

SeaWiFS procedure considers the pressure in the evaluation of the molecular optical thickness. In addition, the selected model accounts for the pressure to calculate the multiple scattering processes. Intuitively, at high values of atmospheric pressure and for short wavelengths, a photon experiencing multiple scattering processes should have an increased probability to be backscatter toward the surface and then to be absorbed by the water (which in the blue is quite a "black" surface). In other words, at high-pressure values (as those measured in the Mediterranean area) and for high values of τ, the resulting Rayleigh radiance should decrease. This means that in such a situation, the modeling of the atmospheric term should fail in the assessment of multiple scattering term, giving additional energy to the aerosol one. Then, even if the optical thickness in the near infrared is well retrieved and the angstrom coefficient is underestimated, we suppose an overestimation of the Rayleigh term and of the general multiple scattering contribution in the blue region, which should lead to a too low value of the water radiances.

CHAPTER 4

Climatological dynamics of surface biomass field in the Mediterranean

4.1 INTRODUCTION

The previous chapter was devoted to a synthetic outline of the theoretical background of color remote sensing and to a presentation of the ocean color data available for the Mediterranean. Furthermore, in situ data collected in the basin, were analysed to quantify the uncertainty associated to the data. Two important results emerged from the CAL/VAL exercise described in chapter 3. Firstly, the Mediterranean Basin, assumed as a unique entity, displays a bio-optical response different from other oceanic regions. The relationships relating the blue to green radiance ratio to the upper layer chlorophyll-*a* concentration, which work fairly well for the global ocean (Hooker and McClain, 2000), fails in the Mediterranean Sea. Secondly, it was demonstrated that most of the error on the Mediterranean ocean color data could be ascribed to the atmospheric correction procedure. Errors in the intermediate products, as well as in the final ones (i.e. water leaving radiances), evidenced such problem, in an extreme or quasi-extreme environmental condition. The Mediterranean, with its southern boundary exposed to Saharan dust bursts, which carry tons of optically relevant substances in the atmosphere, and with the very high concentration of anthropic activities on the northern edge, can be regarded critical factors for the atmospheric correction. Results obtained by the CAL/VAL exercise confirmed this hypothesis.

The implementation of the DORMA algorithm solved both problems and permitted to reproduce accurate and confident estimates of the Mediterranean chlorophyll-*a*.

Though, to deal with that intricate problem, the first step is to provide a truthful and highly resolved spatial and temporal description of the autotrophic biomass field.

In this chapter a detailed and accurate description of the surface chlorophyll-*a* field of the Mediterranean will be carried out, based on the SeaWiFS data and the DORMA algorithm. This will give an exhaustive picture of the Mediterranean surface biomass and a first estimate of the temporal and spatial scales of its dynamics. Five years (1998-2002) of daily LAC SeaWiFS data were averaged temporally to build monthly mean climatological maps. The standard processing procedure (see before and appendix 9.2) was applied to produce maps of the water leaving radiances, which were used to obtain chlorophyll-*a* concentration maps *via* the DORMA algorithm. The averages were calculated for each pixel having more than one good (not masked, see before and appendix 9.2) measurement, resulting in 12 monthly and 4 seasonal climatological maps.

The rationale to accomplish this analysis was two-fold.

Firstly, the previous study of AMA95 and MA91 was conducted on a monthly climatological basis (the monthly climatological maps were not presented in the papers by the authors but are available at the Laboratoire Oceanographie de Villefranche web-site, http://www.obs-vlfr.fr/jgofs2/modelisation/mediterr.htm). Their results were compared with the analysis of similar maps derived from the SeaWiFS sensor and a discussion on the main differences, if any, will be conducted. Approximately fifteen years separate the CZCS and the SeaWiFS operational periods and a first assessment of the long-term trends in the Mediterranean can be accomplished.

Furthermore, the climatological analysis will highlight the most prominent features of the biomass fields occurring at basin scale, removing the effect due to the small scale or short term events.

4.2 CLIMATOLOGICAL SURFACE CHLOROPHYLL-*A* FIELDS

SeaWiFS daily maps were generated by compositing passes obtained in the same day, after masking from each single picture the questionable pixels (according to the SEADAS procedure). Arithmetical time averages were used to produce monthly and seasonal climatological maps, which were computed excluding the Black Sea and the Atlantic Ocean. The density of observations used to derive the climatological maps is shown in Figure 4-1.

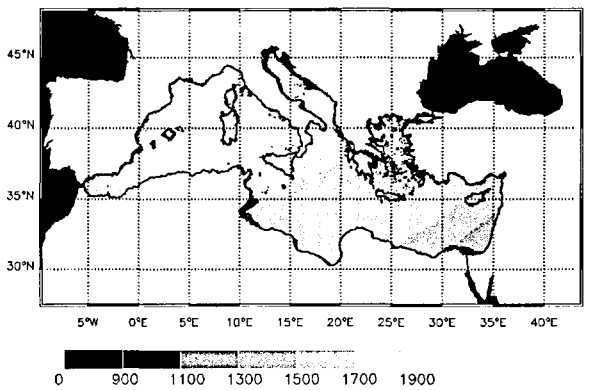

Figure 4-1. Density of SeaWiFS observations.

The climatological map of the basin confirms the oligotrophic regime of the Mediterranean, characterized by strong East-West and South-North gradients and by coastal influences (see Figure 4-2).

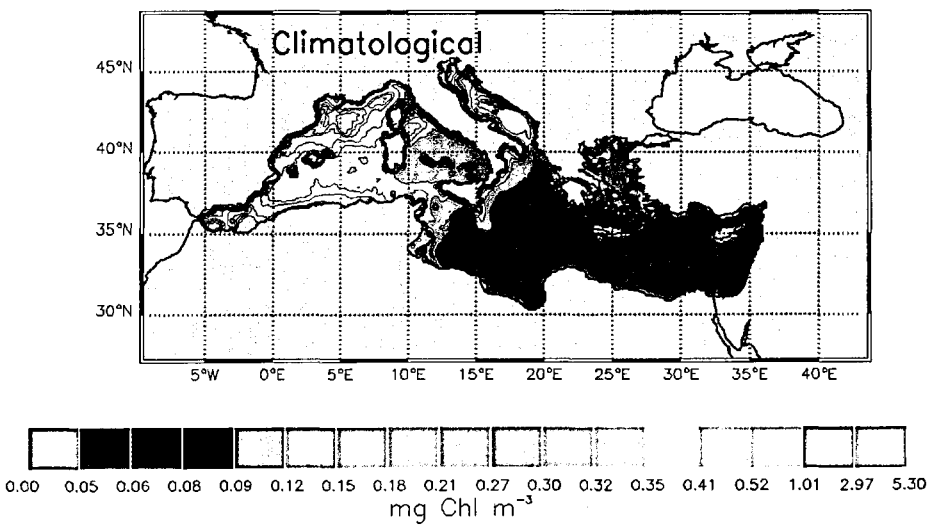

Figure 4-2. Five-years (1998-2002) climatological maps of SeaWiFS derived chlorophyll concentration.

High chlorophyll-*a* values are recurrent in the Northern Adriatic and in the coastal region of the Gulf of Lions, where the influence of the Po and of the Rhone rivers, respectively, induces phytoplankton growth. Note the absence of a strong signal due to the Nile outflow, probably resulting from the application of SEADAS masks and after the damming and a reduction of the river runoff.

Excluding the Adriatic and the Western Ionian, the EMED displays the lowest values, with chlorophyll-*a* concentrations not exceeding 0.12 mg m^{-3}. The Southern Levantine region is definitively the poorest area of the basin in terms of autotrophic biomass.

In the WMED, a relevant feature is present between the Balearic Islands and Corsica Island, with chlorophyll-*a* values spanning between 0.2 and 0.3 mg m^{-3}. Similar estimates are also evident in the North Tyrrhenian, between Sardinia and Corsica islands and the Italian peninsula, while the rest of the Tyrrhenian displays the lowest values for the WMED.

The Alboran region exhibits an important chlorophyll-*a* patch (chl ~ 0.2 mg m^{-3}), which propagates from Gibraltar along the African coast, decreasing in intensity along the path.

4.2.1 Seasonal patterns

4.2.1.1 Summer (June-July-August)

The EMED (Figure 4-3) is characterized by large areas where the chlorophyll-*a* concentrations are at the limit of the sensor sensitivity, in particular at the extreme south of the basin. Western Ionian and Adriatic seas are the less oligotrophic areas of the EMED (chlorophyll-*a* ~ 0.1 mg m^{-3}), while most of the pixels display chlorophyll-*a* values down to 0.06 mg m^{-3}. Biomass slightly increases moving westward and northward, reaching the maximum values in the Gulf of Lions and in the North Adriatic,

where river outflows (from Rhone and Po rivers) maintain high nutrient concentrations and phytoplankton growth. However, the presence of the Rhone outflow, can not explain the significant values (~ 0.15-0.18 mg m^{-3}) in the whole region from Ligurian Sea to Gulf of Lions.

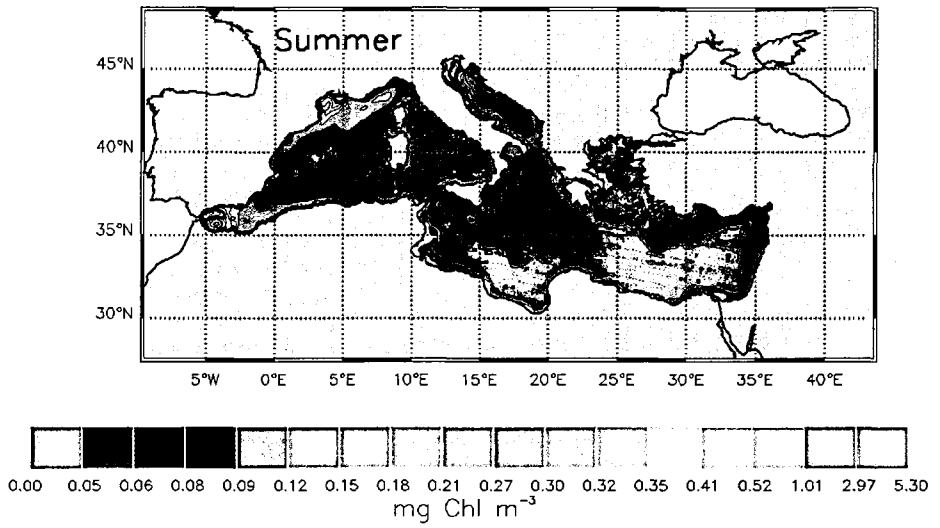

Figure 4-3. Summer (JJA) climatological map of SeaWiFS derived chlorophyll concentration.

Near Gibraltar, higher biomass values are clearly evident (chlorophyll-*a* ~ 0.4 mg m^{-3}), though the signal is limited to a small plume just outside the strait. In the other areas of the WMED, chlorophyll-*a* values are substantially low, with the minimum concentrations observed in the Tyrrhenian Sea.

4.2.1.2 Autumn (September-October-November)

Autumn map (Figure 4-4) is similar to the summer one, showing similar patterns, tough with more pronounced east-west and north-south gradients. However, throughout the basin, the concentrations are slightly higher than in summer, and some patches of higher biomass are observed.

The increase of the precipitation in autumn, leads to an increase of the river run-off, which is revealed in the satellite map in the Adriatic along the Italian coasts and in the Gulf of Lions. In the offshore waters of the latter, biomass reaches 0.3 mg m^{-3}, while a significant event of plankton growth is observed in the North Tyrrhenian Sea (*circa* 0.2

mg m^{-3}). In the southern Adriatic a relative minimum is observed (chlorophyll-*a* ~ 0.07 mg m^{-3}) on a background basin concentration of ~ 0.9-0.12 mg m^{-3}, while, in the Alboran region, the two often observed gyres are clearly evident (values ranging between 0.1 and 0.4 mg m^{-3}).

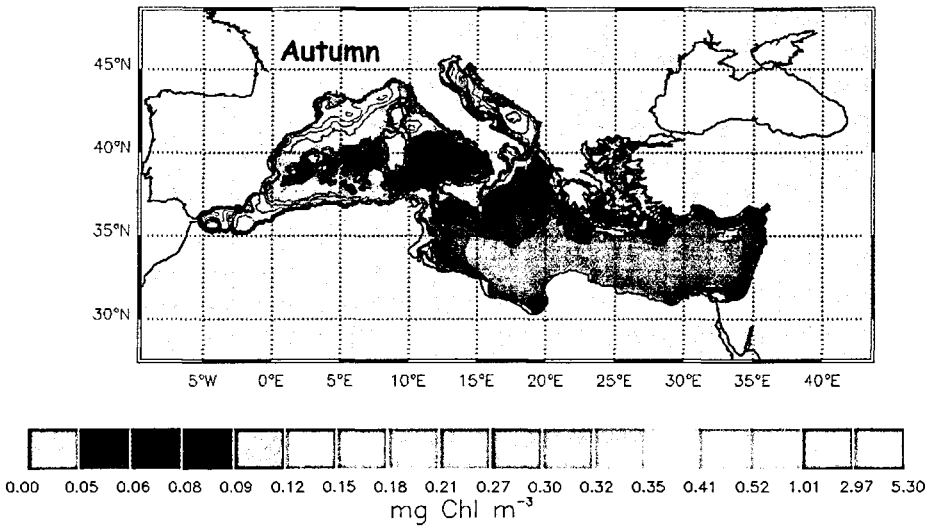

Figure 4-4. Autumn climatological map of SeaWiFS chlorophyll concentration.

In the WMED, apart of the cited regions, the surface chlorophyll-*a* concentration remains quite uniform around values equal to 0.08-0.09 mg m^{-3}. EMED displays a quite uniform field (~ 0.05-0.06 mg m^{-3}), changing only in the Northern Ionian Sea (chlorophyll-*a* ~ 0.08-0.12 mg m^{-3}).

4.2.1.3 Winter (December-January-February)

Winter map (Figure 4-5) displays a diffuse and relevant increase of the surface biomass throughout the entire basin. The typical values span between the 0.09 mg m^{-3} of the EMED to the 0.35 mg m^{-3} of the WMED. The strong latitudinal gradient between the two main sub-basins is still visible, even if in the WMED the biomass displays a more patchy distribution. On average, chlorophyll-*a* in the WMED are about 0.3 mg m^{-3}, with the exceptions of the Alboran Sea, where a high biomass plume (chlorophyll-*a* ~ 0.3-0.5 mg m^{-3}) extends along the African coast, and the Southern Tyrrhenian, which displays the relative WMED minimum (chlorophyll-*a* ~ 0.12-0.15 mg m^{-3}). The low

values observed in fall in the Southern Adriatic are still present and, in someway, more evident, due to the increase chlorophyll-*a* concentrations of the surrounding regions.

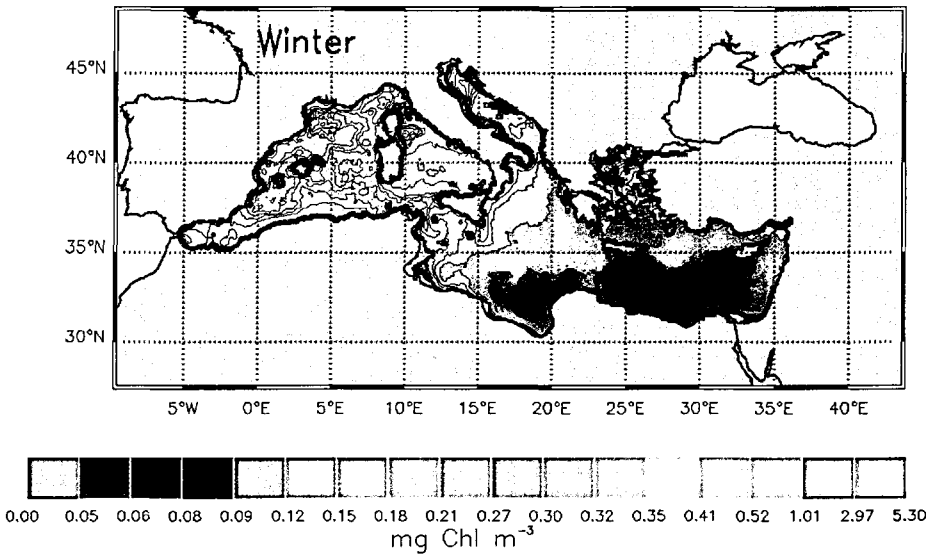

Figure 4-5. Winter climatological map of SeaWiFS derived chlorophyll concentration.

4.2.1.4 Spring (March-April-May)

The climatological spring map shows a diffuse decrease of the chlorophyll-*a* values in the entire basin, where the oligotrophic and ultra-oligotrophic regimes seem to be restored. More in details, average values of ~ 0.05-0.09 mg m^{-3} for the EMED and ~ 0.09-0.12 mg m^{-3} for WMED are retrieved by satellite imagery. Some exceptions, however, modify this picture of low biomass in the basin. In the EMED, the Southern Adriatic and the Western Ionian seas display relatively high values (chlorophyll-*a* ~ 0.15-0.18 mg m^{-3}) respect to the other regions of the basin (Figure 4-6). In addition, a hardly detectable increase in biomass (confirmed however by the analysis of the single images) is present in the Rhodes Gyre region (chlorophyll-*a* ~ 0.09 mg m^{-3}).

The main event, however, appears in the NWMED area. In the Gulf of Lions, and extensively in the whole Northwest Mediterranean basin, a large bloom appears, with values reaching 0.5-1.0 mg m^{-3}. The chlorophyll-*a* concentrations reach the highest

values observed during the year and throughout the basin, permitting to define without doubt that region as the Mediterranean most propitious area for phytoplankton growth.

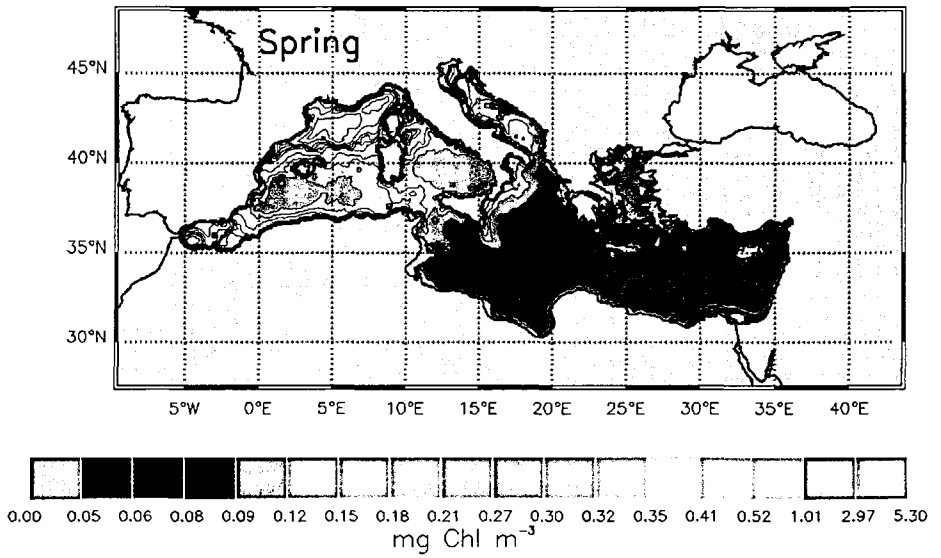

Figure 4-6. Spring climatological map of SeaWiFS derived chlorophyll concentration.

4.2.2 Monthly maps

In Figure 4-7 the 12 monthly climatological maps are reported. The rationale to carry out the analysis on a monthly basis is to expand the seasonal study to verify the timing of the events described before and their monthly variability. The maps substantially confirm the seasonal analysis, but the temporal scales of the events deserve additional comments.

In the EMED, the spatial distribution of biomass exhibits a two-state modality, switching from a general oligotrophic regime in summer and autumn (chlorophyll-*a* ~ 0.06-0.08 mg m^{-3}) to a less oligotrophic state (chlorophyll-*a* ~ 0.06-0.15 mg m^{-3}) in late winter-early spring. The shift between the two modes occurs in October and April, respectively, when biomass distribution and values are very similar. These two months could then be considered as the two nodes in the transition from one trophic state to the other. In the Rhodes Gyre region, where an active cyclonic is present (see chapter 1), SeaWiFS maps reveal maximum value in March, suggesting that the increase in

biomass begins after the winter vertical mixing event and, therefore, at the time of water column stratification (Lascaratos et al., 1999). Similar conditions are present in the Southern Adriatic and are displayed in the satellite maps, though the biomass increase appears in February and lasts until April. More interestingly, the monthly maps show that, embedded in the widespread biomass increase at basin scale in late winter-spring, there are specific areas at sub-basin scale displaying an enhanced response, such as offshore the eastern Calabrian coast (Northern Ionian Sea) in March and April (values up to 0.3-0.35 and 0.18-0.27 mg m^{-3}, respectively).

The WMED chlorophyll-*a* distribution appears more complex. The diffuse winter increase of biomass starts in November and comprises the whole WMED area, with the important exception of the central and southern Tyrrhenian Sea. Phytoplankton concentration increases constantly with the progression of the year; the different areas, however, show different timing in the development of the growth events. In the Alboran Sea, along and northward the Algerian coasts, a strong increase of chlorophyll-*a* concentrations, is detectable in January, to decay in March, when a weak signal is present only near Gibraltar. In the Balearic and Ligurian Seas (NWMED), slight increases of biomass, restricted to the area near the European coastlines, occur starting from October (chlorophyll-*a* ~ 0.2-0.3 mg m^{-3}). In November and December the chlorophyll-*a* concentration increases intensively (chlorophyll-*a* ~ 0.3-0.4 mg m^{-3}) and the high biomass patch expands to the entire NWMED area. In January and February, however, the region of Gulf of Lions experiences an evident decrease of biomass (chlorophyll-*a* ~ 0.15-0.2 mg m^{-3}), while, in the surrounding areas, the chlorophyll-*a* concentration increases (chlorophyll-*a* ~ 0.4-0.5 mg m^{-3}). The region of low biomass concentration is restricted to a specific site, the one where deep water formation events take place (see chapter 1). Finally, in March, a large (chlorophyll-*a* ~ 1.0-3.0 mg m^{-3}) phytoplankton bloom is observed in the Northern Tyrrhenian and in the NWMED regions. The latter disappears only in May, even if evident signals of plankton activity

are visible until July (chlorophyll-*a* ~ 0.15-0.18 mg m^{-3}). The remainder of the WMED returns to oligotrophic values in May and maintains such regime throughout the summer season.

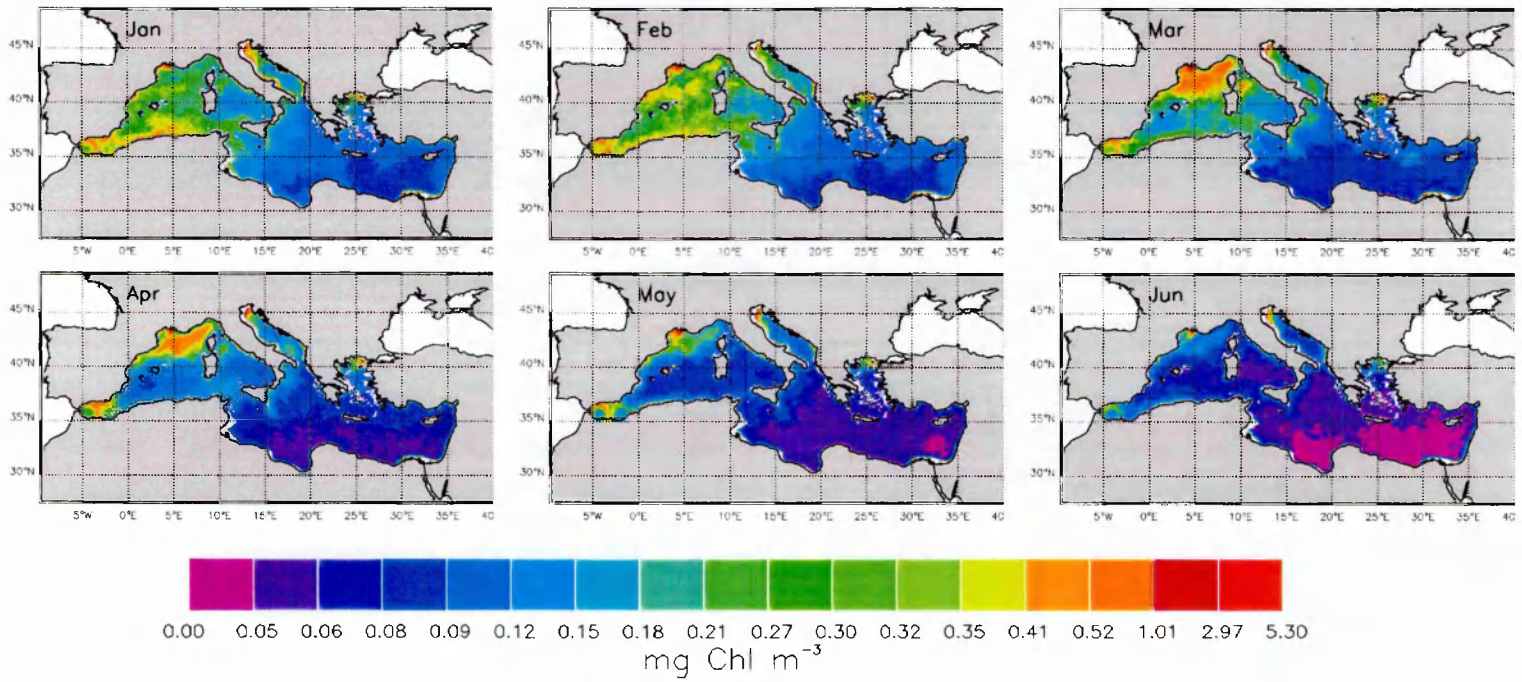

Figure 4-7. (a) Monthly climatological maps of SeaWiFS derived chlorophyll concentration.

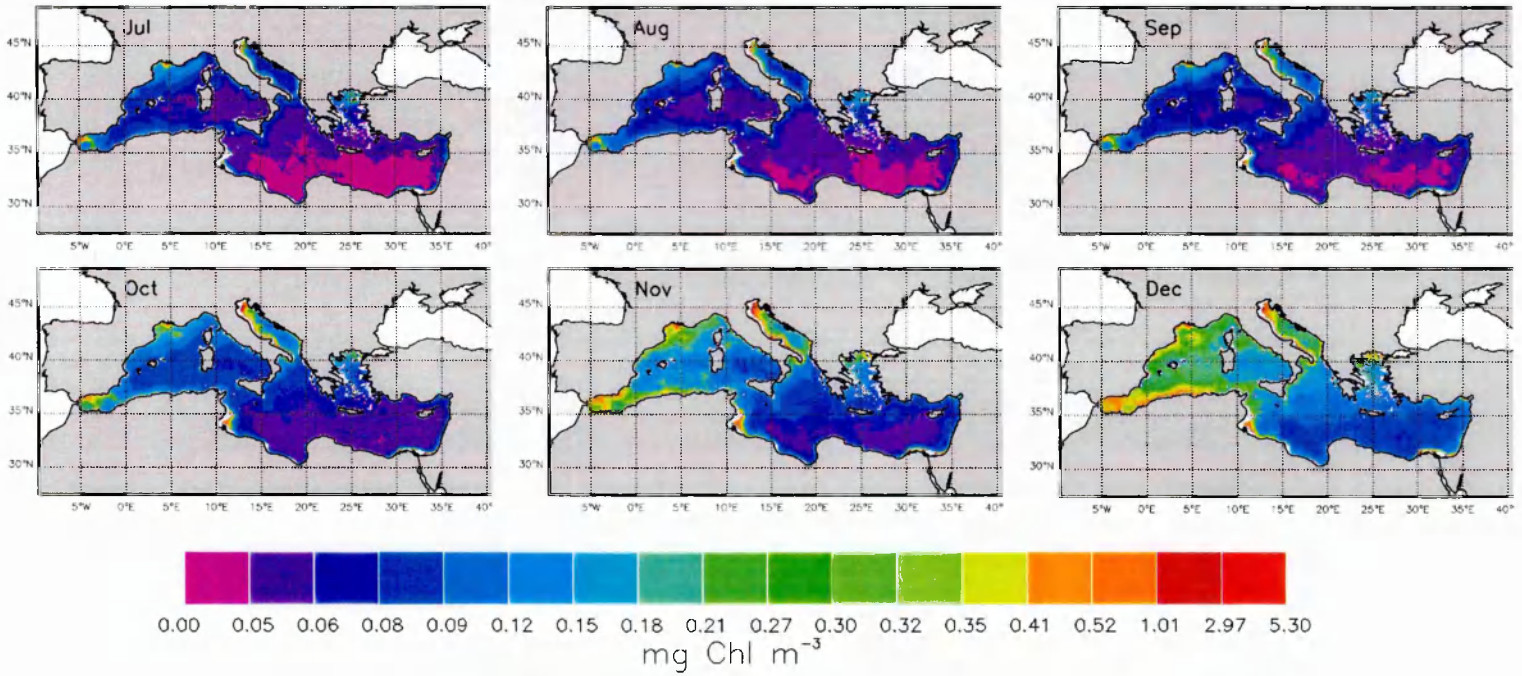

Figure 4-7. (b) Monthly climatological maps of SeaWiFS derived chlorophyll concentration.

4.3 PRELIMINARY SYNTHESIS

The previous analysis confirms that the surface distribution of biomass is typical for the mid latitude seas. The very low (0.05 mg m^{-3} for the EMED) and low (0.07 mg m^{-3} for the WMED) chlorophyll-*a* summer values increase strongly afterwards. In late winter and in spring, a diffuse rise of surface biomass is measured from space and results in averaged values of 0.15 and 0.3 mg m^{-3}, for the EMED and the WMED respectively. In addition, in particular regions, mainly concentrated in the WMED regions but present also in the EMED, large (in both the spatial and temporal extensions) blooms are observed in spring. Such regions, which comprise the Alboran Sea, the NWMED region, the Southern Adriatic Sea and the Rhodes Gyre area, are supposed to be decoupled from the typical behavior of the basin, and are subject to a particular physical-biological dynamics.

As a general comment, the assumption of strong oligotrophy of the Mediterranean basin has to be, at least partially, reappraised.

- High chlorophyll-*a* concentrations are present in the Alboran region throughout the year, with evident peaks in late winter, when the inflow of AW is maximal (Bryden and Kinder, 1991). The high chlorophyll-*a* patch coincides with the anticyclonic structure often observed in the area and appears as a recurrent characteristic of that region. Sometime (i.e. in February), the patch of high chlorophyll-*a* concentration extends to the entire Algerian basin, producing a vast bloom over the area, lasting until March. The Alboran Sea bloom was intensively studied (Garcia-Gorriz and Carr, 1999; Garcia-Gorriz and Carr, 2001) and their analysis is not repeated here. Briefly, the inflow of AW, which is maximum during November and December, produces important vertical motions, which result in a injection of nutrient and in a subsequent bloom in the surface waters (Garcia-Gorriz and Carr, 1999; Garcia-Gorriz and Carr, 2001).

- In the NWMED, in the Southern Adriatic and in the Rhodes Gyres region, increases of biomass are observed in the SeaWiFS images. The blooms in the NWMED and in the South Adriatic are intense and recurrent, being clearly visible in the monthly climatological maps. By contrast, the Rhodes Gyres bloom does not appear as pronounced. However, it displays the highest values of the Levantine basin and the distinctive signal over the low background values of the region. The weak evidence in the climatological maps is very likely linked with the strong interannual variability of the dominant physical processes (see later). In fact, the three blooms are located in areas of strong cyclonic activity, which are also sites of dense water formation. In the next chapter, the dynamics of these blooms will be studied in detail, investigating on the interannual variability of the events and on the main physical forcing that drive the processes.
- Mostly in the WMED, but clearly evident also in the EMED, a late autumn-early winter biomass increase is observed. The phenomenon appears diffuse, and not very intense, even if, mainly in the WMED, the retrieved concentrations can reach relatively high values. It is worth nothing that this phytoplankton accumulation occurs one to two months after the typical fall bloom of temperate regions (see Longhurst, 1995, and references therein). For this reason, a specific analysis was carried out also on this phenomenon.

4.4 THE LATE AUTUMN EARLY WINTER MEDITERRANEAN BLOOM

Seasonal and monthly maps showed a phytoplankton response in the last months of the year (October-November-December) that extended over most of the basin. The pattern was already observed in coastal regions (Duarte, et al., 1999; Zingone, et al.,

1995), or with sediment traps (Boldrin, et al., 2002; Miquel, et al., 1994), but in both the cases data were not sufficient to extend the results to the whole basin.

Following Duarte et al. (1999), the late autumn Mediterranean bloom derives by a stabilization of the water column due to favorable meteorological conditions.

Low cloudiness and absence of strong wind bursts could lead to a momentary stratification of the surface layer, which permits a rapid utilization of the new nutrient injected in the previous periods. In addition, Zohary et al. (1998) observed an increase of autotrophic biomass during winter in a warm-core eddy in the Levantine basin, suggesting that the intermittence of the atmospheric forcing plays a key role in the onset of favorable growth conditions.

Phytoplankton blooms in mixed water (i.e. the typical Mediterranean winter conditions) were analysed also by Huisman et al. (1999) using a 1-d physical-biological model. Their results lead to the definition of a "critical turbulence", considered, together with the Sverdrup "critical depth", another key parameter to establish the onset of a bloom. Smetacek and Passow (1990), in their comments on the Sverdrup model on the initiation of spring bloom, substantially relaxed the concept of critical depth as the fundamental factor to predict a biomass growth, implicitly suggesting a more detailed analysis of the time course of a phytoplankton bloom.

All the above clarifies that for an open ocean bloom to occur, the thermal stratification may be a sufficient but it is not a necessary condition.

To quantify precisely the timing of the blooming events, a median map was generated, calculating for each pixel the median chlorophyll-*a* value in the 5 years of available SeaWiFS data.

Median value was chosen because it is regarded as less affected by spikes in the time series and would represent the mean state of the considered pixel. The data set was then divided into four sub-sets comprising the images of the "enlarged winter", for the four years available (1998/1999; 1999/2000; 2000/2001; 2001/2002). "Enlarged winter" is

here the time period between the first of September (Julian day 244) and the first of April of the following year, encompassing the two transitions in the structure of the water column (stratified – unstratified and *vice versa*). For each ocean pixel and for each sub-set, a comparison with the median map was performed, to identify the day of biomass increase, defined as the first day in the time series with chlorophyll-*a* values 30% higher than the corresponding median value. In addition, the day of bloom initiation, defined as the day displaying a chlorophyll-*a* value 250 % higher than the correspondent median one, was identified and mapped.

The day of bloom initiation, however, was calculated on the whole time series, comprising also summer and spring.

Figure 4-8 and Figure 4-9, show the computed maps for the 4 enlarged-winter sub-sets.

In spite of a large interannual variability, Figure 4-8 demonstrated that the Mediterranean surface chlorophyll-*a* field exhibited a statistical relevant peak in the winter months. Again, differences between the occidental and the oriental basins are evident. Excluding the North Western region and the North Tyrrhenian Sea, the occidental basin shows biomass enhancements occurring prevalently late in the year (November-December).

In the EMED, the enhancement is anticipated to the fall months, September and October, with a clear differentiation between Ionian and Levantine basin. The first, blooming prevalently in September and the second in October (and sometimes in November).

More interesting are the maps of the day of bloom-initiation (Figure 4-9).

In some regions, this condition never occurs throughout the year (white regions in the maps), and this is the case of most part of the EMED basin. As already noted, in particular years (i.e. 2000 and 2002), the Rhodes Gyre region and Ionian Sea display

bloom values in spring, but, in general, the dynamic of the EMED is not characterized by intense chlorophyll-*a* peaks.

More interesting is the WMED regime. Of the four years analyzed, three (1998/1999; 1999/2000; 2001/2002) show evident peaks in November-December, while one (2000-2001) produces bloom values only in late-winter/spring. In the NWMED region, the development of bloom-like values arise always in the spring months, while the other areas are characterized by a more variable dynamics, which lead to a patchy distribution of the "day of bloom".

Following the considerations in the beginning of the paragraph, winter bloom (or bloom in mixed water) could happen if after a period of intense mixing, which provides new nutrient to the surface layer, few days of low or absent wind, and possibly clear sky, prevents the active mixing of the water column, eventually increasing its stability.

This, in turn, could permit the plankton to utilize rapidly the available nutrient.

To verify whether such conditions occur in the Mediterranean basin, atmospheric data from European Center for Medium-range Weather Forecast (ECMWF) were analysed. They consist in the outputs of an atmospheric model, which, forced with in-situ and satellite data, retrieve weather parameters at 1/4° spatial and six hours time resolutions. Data are available only for the years before the 2000, and consist of sea level atmospheric pressure, air temperature at 2m, dew point temperature, cloud cover, zonal and meridional wind components.

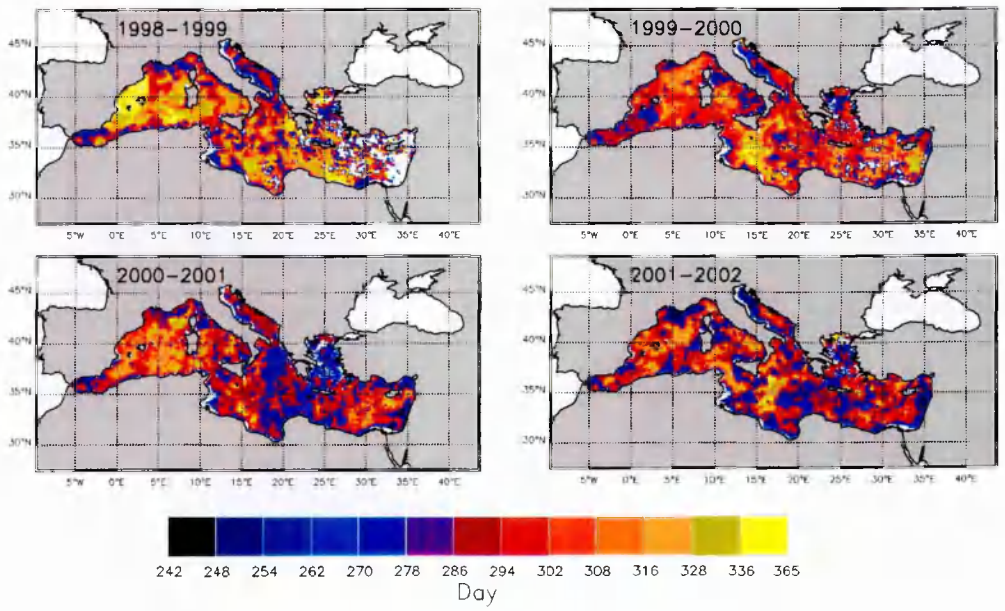

Figure 4-8. Day of enhanced biomass (see text).

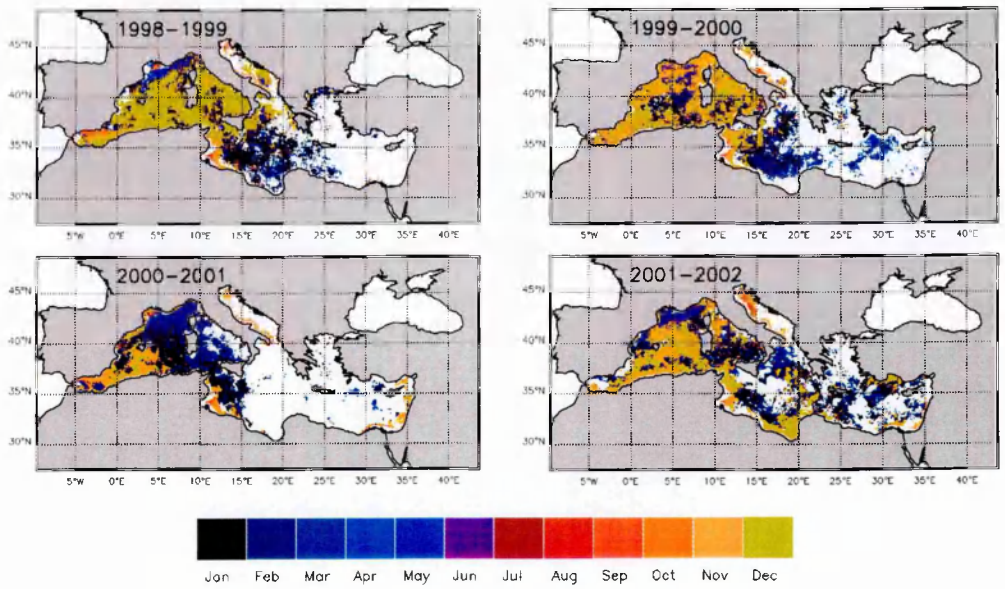

Figure 4-9. Day of bloom (see text).

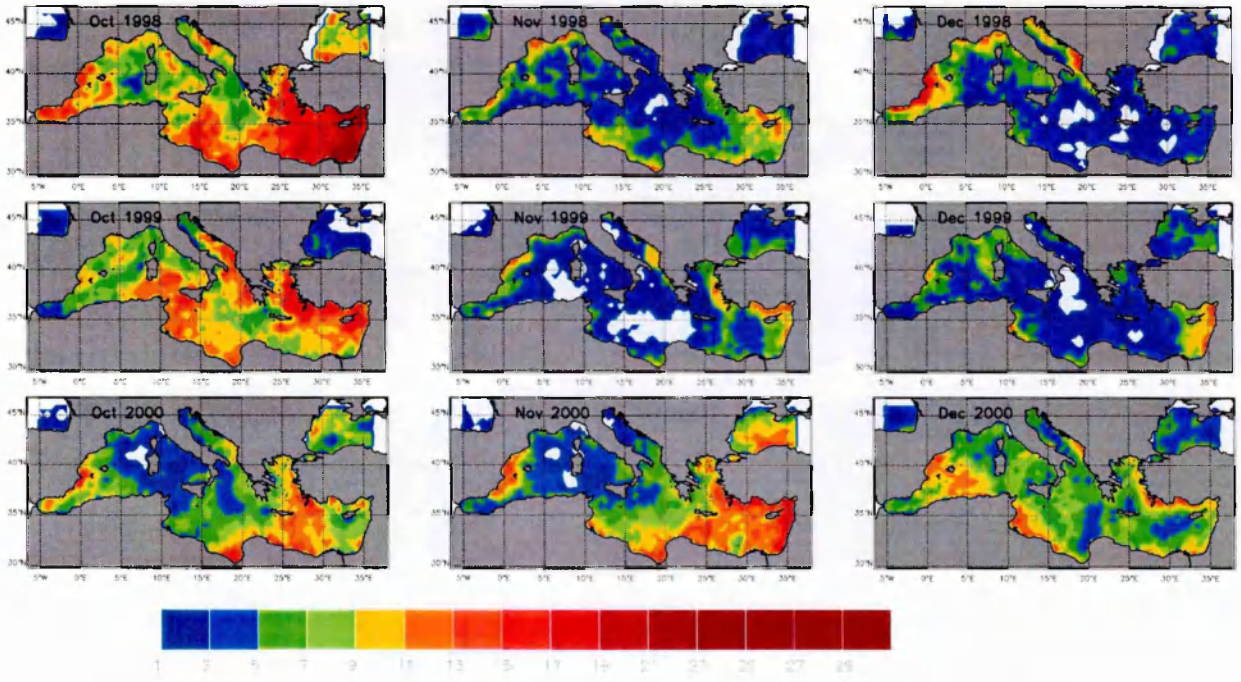

Figure 4-10. Number of days with favorable atmospheric conditions.

From ECMWF data, the number of days exhibiting favorable atmospheric conditions was calculated for October, November and December months and for the years 1998,1999 and 2000. As favorable atmospheric conditions ("good weather" condition), a cloud cover less the 10%, a wind stress less than 0.1 N m^{-2} and a sea level atmospheric pressure 20 % higher than the winter average, were taken as thresholds.

Figure 4-10 shows that favourable atmospheric conditions occur in the basin prevalently in October, explaining the reported biomass increases during the "Estate di S. Martino". However, the most important feature emerging from the Figure 4-10, is the presence of a relevant number of "good weather" days during November and December. More interesting, in December and in the WMED, this number is slightly higher than the correspondent November, and account for the relative biomass maxima in this month shown by Figure 4-9.

Regional and interannual differences deserve further comments. Tyrrhenian Sea displays a first rise in biomass in October 1998 but shows high values in December 1998, explained by 10 days of favourable atmospheric conditions. In the 1999 such conditions occurred only in October leading to a unique event of biomass increase and to the absence of December peaks. Gulf of Lions and Ligurian Sea are always subject to propitious atmospheric conditions in winter, which result in early biomass increases and in December blooms.

Another interesting feature occurs near the Catalan coast, where 25 days of favourable conditions in December 1998 led to an increase in biomass during the same days.

It is important to note that if the number of "good weather" days is too high during the winter, no blooms are observed; on the other hand, to favor phytoplankton growth, such conditions must occur after a mixing event, necessary to bring up the required nutrient. In the EMED, apart of the already described hydrodynamic regime, the atmospheric conditions are "too much" favorable during the early winters (preventing

an efficient nutrients refueling of the surface layers) and "too little" propitious in the late winter (preventing the onset of the steady conditions needed for plankton growth). Diffuse and weak blooms in the EMED occur therefore only in September and October and only rarely in late winter or in spring.

An opposite situation is observed in the WMED. The number of propitious days is more distributed during the autumn and the winter, and rarely exceeds 10.

This intermittent atmospheric regime, which produces events of mixing alternated with brief stabilizations of water column, seems to be crucial in a efficient vertical transport and consumption of the new nutrients, which results in weak phytoplankton blooms, as observed from space. However, the effect of the "good weather" conditions on the Primary Production could be different in the two main-sub-basins. In the discussion section they will be considered and analyzed.

4.5 COMPARISON WITH THE AMA95 RESULTS.

The picture emerging from the five years climatological analysis of SeaWiFS chlorophyll-*a* data substantially confirms the representation of MA91 and AMA95. Averages of surface layer chlorophyll-*a* were computed for the whole basin and for the EMED and WMED respectively, and the retrieved values compared with the assessments by AMA95 (Table 4-1).

	Mediterranean	**EMED**	**WMED**
SeaWiFS 1998-2002	0.16	0.13	0.22
AMA95	0.24	0.18	0.35

Table 4-1. Mean chlorophyll-*a* concentration spatially averaged over the whole basin and the two main-sub-basins Values are in mg m^{-3}.

As a general comment, the values derived from SeaWiFS data are slightly lower than the AMA95 ones. The main differences are in the WMED basin, where the SeaWiFS mean is 50% lower than the correspondent AMA95 estimate. Rather similar values are indeed displayed for the EMED.

Other differences appear from the comparisons of the seasonal maps.

In AMA95, the EMED basin displays a quite constant behaviour, without any dramatic inter-seasonal changes. This trend is reproduced also in the spatial distribution of the biomass, which is fairly invariable throughout the year, with only a slight enlargement of the ultra-oligotrophic patch during winter. Small peaks of chlorophyll-*a* concentration are observed in June-July in the Ionian and Levantine basins (see figure 2 in AMA95), while the lowest values are reported in spring.

On the other hand, SeaWiFS images result in more variable distribution of biomass and in a more pronounced seasonal variability. The seasonal pattern described by AMA95 seems reversed in the SeaWiFS years, when chlorophyll-*a* increase at basin scale is observed in late fall-winter, whereas the lowest values of biomass are detected during summer. In addition, the enhanced biomass concentrations present in the SeaWiFS imageries in the Western Ionian Sea region during spring were not detected by AMA95, which showed only a slight, general and diffuse increment in biomass.

Regarding the Adriatic Sea, which displays strong seasonal signal in the SeaWiFS imageries, the very scarce number of observations available in AMA95 prevented the authors to perform a detailed analysis, which was limited to a brief comment.

For the WMED, no seasonal maps were presented by AMA95 and MA91. However, the data used by the authors are available on the website of the Villefrance Laboratoire d'Oceanographie (http://www.obs-vlfr.fr/jgofs2/modelisation/mediterr.htm) and were then downloaded to produce seasonal and monthly averaged maps to be compared with the SeaWiFS derived ones.

The main structures and features of the WMED are conserved in the two assessments (see Figure 4-11 for the CZCS climatological map). In both the data sets, the Alboran Sea and the NWMED regions are the richest areas, while the Tyrrhenian and the South Western Mediterranean are the most oligotrophic. Moreover, also in the MA91 analysis, the NWMED bloom appears as the most relevant feature of the basin.

However, some discrepancies in the timing of the events between the SeaWiFS and the MA91 time series are found. In particular, MA91 showed that the growth of phytoplankton starts in mid April, one month later the end of dense water formation processes. On the other hand, SeaWiFS data evidence a quite co-occurrence of the two processes (cit. the end of the dense water formation process and the development of the bloom). Discrepancies occur also for the period of maximum extension of the vernal bloom, which occurs in April for MA91 and in March in the SeaWiFS data set.

Similar differences are found regarding the timing of the late Autumn-Winter bloom. In the MA91 and AMA 95 studies, the increase of biomass was observed in October in the WMED (and only limited to the NWMED region) and in November in the EMED. The SeaWiFS data indeed display a diffuse increment from October, which decays only in April, when the general conditions appear again oligotrophic. The characteristics of the two phenomena are distinctly different. As a consequence, the deep-water convection events are still visible in the MA91's January and February maps, but the surrounding areas show only a slight increase of biomass.

I will return to this in the discussion. Anyway, notwithstanding the huge effort carried out by AMA95 and MA91 to improve the estimates, the intrinsic limitations of the CZCS data were sometime insurmountable. In some regions (i.e. the Adriatic but also the Levantine) the CZCS frequency of observations was so scarce that truthful estimates of the surface field were hardly possible. For the same reasons, events retrieved by the five years of SeaWiFS data could have been missed by the CZCS, which had a more random overpass time and then was more subject to the cloud cover problem.

Despite of the described disagreements, the general characteristics of the basin are similarly retrieved by the two data sets. As discussed by Bricaud et al. (2002), the general trends of the Mediterranean are quite analogous for CZCS and SeaWiFS data, and the main differences are principally related to the timing of the events, and not to

the events themselves. This fact, gives more confidence in using both the ocean-color sensors to study the Mediterranean Sea and its long-term trends.

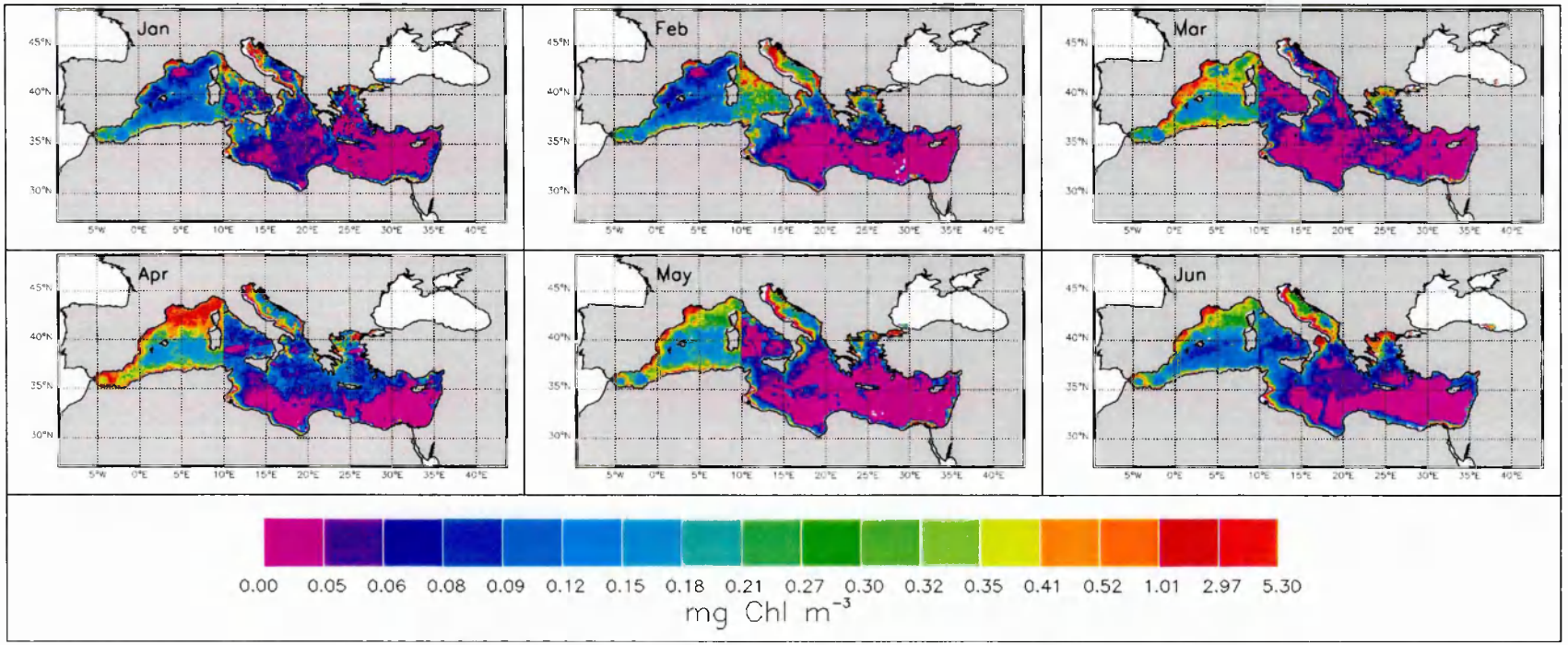

Figure 4-11. (a) Monthly climatological maps of CZCS derived pigment concentration.

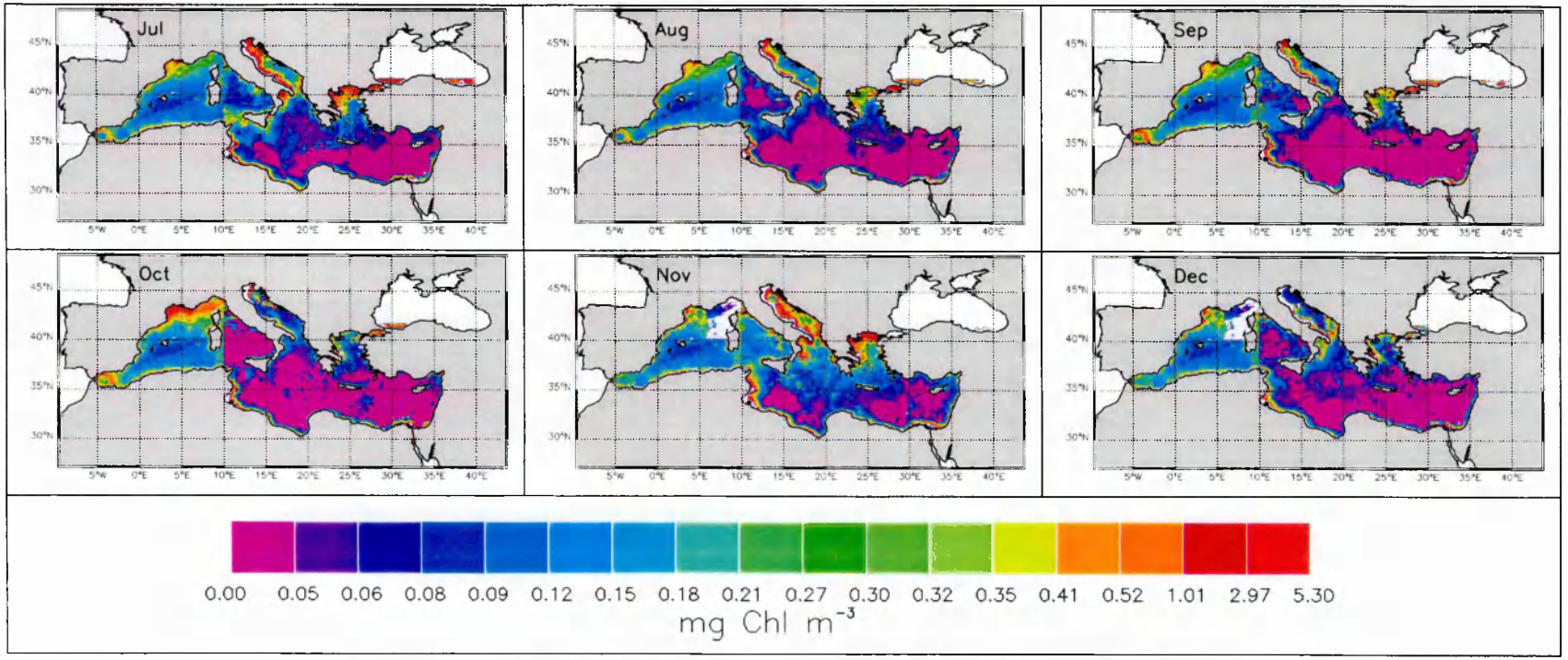

Figure 4-11. (b) Monthly climatological maps of CZCS derived pigment concentration.

CHAPTER 5

Primary Production

5.1 INTRODUCTION

The previous chapter was devoted to an accurate analysis of the climatological aspects of the chlorophyll-*a* field of the Mediterranean and to a comparison with the results obtained in similar studies based on CZCS data (i.e. AMA95 and MA91). Only slight differences were evidenced in the chlorophyll-*a* surface field in the two periods, the most important being related to the timing of the bloom events. In the CZCS years, the EMED basin showed a quite constant dynamics without strong inter-seasonal fluctuations, with only an intense peak in November, mainly located in the Adriatic and in the Aegean. More variable dynamics were indeed present in the SeaWiFS era, when a relevant maximum diffuse throughout the basin resulted in the late-winter/spring period.

Similarly, during the CZCS period, the WMED most relevant features (the NWMED bloom) displayed the maximum intensity in April, i.e. one month later than in the SeaWiFS years. In addition, the evident phytoplankton bloom in late-fall/winter in the SeaWiFS imageries is visible in the CZCS maps only in the WMED and with a different timing.

In summary, even if the regions with favorable conditions for biomass growth were substantially the same (but see later the description of EMT impact), a shift in the timing of the events appears.

To investigate such phenomenon and to assess its relevance on the trophic regime of the basin, primary production (PP) maps were produced from SeaWiFS data and then compared with those computed from the CZCS imageries by AMA95.

The information embedded in the primary production data are more complete, even if less accurate, than those obtained from the chlorophyll-*a* data only, being related also to the "environmental" conditions of the studied marine environment. Giving a certain concentration of chlorophyll-*a* (as a proxy for the phytoplankton abundance), models of PP include the light conditions and the physiological state of the algae, to determine the amount of carbon assimilated by the organisms. To date, the estimates of PP from space are considered still uncertain, also in the most favorable cases (see for example Campbell, et al., 2001, for a review) and thus they have to be considered with care. In addition, the application of available global PP algorithms to the Mediterranean may present additional difficulties, associated with the relatively small size of the basin and to its particular ecological dynamics (see chapter 3).

However, to investigate on the supposed shift of the Mediterranean blooming events between the CZCS and the SeaWiFS periods, it is not necessary to obtain the "exact" values of the basin PP. Even approximate assessments are adequate, provided however that a unique methodology to retrieve the estimates is utilized.

The PP maps were computed from SeaWiFS imageries utilizing the scheme developed by AMA95 (but see also Antoine and Morel, 1996, AM96 hereafter). Two main points were considered in such choice. Firstly, the papers of AMA95 and MA91 represent the sole attempt to estimate PP in Mediterranean from CZCS data. Second, the method was already tested and validated by Bricaud et al, (2002, BRI02 hereafter) for the use with SeaWiFS imageries. Furthermore, their paper was totally devoted to the application of the model on the Mediterranean. The present analysis is then based on the approach of AMA95 and AM96, following the suggestions of BRI02 for its application on the Mediterranean.

A final consideration is however needed as regards the BRI02 paper and our context.

The authors demonstrated that the general patterns of the basin PP did not change respect to the CZCS years, producing similar yearly trends and fairly comparable mean integrated annual production. Their analysis, however, was mainly focused on a validation of the method and of the ancillary data needed to compute the PP estimates. No maps or sub-basin time series of PP were presented, being their analysis limited to a time series of mean PP and to a table with the mean value of annual PP integrated over the EMED, the WMED and the whole basin. In addition, only one year (1998) was considered in their paper, and therefore the interannual variability was not analysed. The analysis of the climatological chlorophyll-*a* surface field obtained in Chapter 4, demonstrated that the mean characteristics of the basin are substantially unchanged, but some modifications however occurred. To explain these phenomena, then, the BRI02 study is not sufficient, and then a reproduction of their work, with a very different aim, is the purpose of this section.

5.2 THEORETICAL BACKGROUND

Primary production maps (in g C m^{-2} day^{-1}) were computed from SeaWiFS data (Chl_{sat}) following the approach of AM96. Briefly (see AM96 for details), the method is based on the following global equation:

Eq. (5-1) $$P = (1/J_c)Chl_{tot}PAR(0^+)\psi^*$$

where Chl_{tot} represents the column integrated chlorophyll-*a* content (g Chl m^{-2}) and $PAR(0^+)$ the incident photosynthetically available radiant energy (spectral range 400–700 nm) at sea level over a given time interval (a day in our case, Jm^{-2}). ψ^* is the "effective" cross-section of algae for photosynthesis per unit areal chlorophyll-*a* (m^2 (g Chl)$^{-1}$) and is a function of both Chl_{tot} and $PAR(0^+)$ as well as of the temperature. J_c is the energetic equivalent of photosynthetic assimilate (equal to 39 kJ (g C)$^{-1}$). To permit

a rapid pixel-by-pixel model application to satellite data, look-up tables (LUT) were produced, permitting to assess ψ^* values for a given set of observable parameters (i.e. latitude, cloudiness index, Julian day, temperature and surface chlorophyll-*a* concentration). The LUTs adopted here, are the ones available at the Villefranche web-site and are the same used by AMA95 and BRI02 to carry out their study.

Chl_{tot} was estimated by Chl_{sat} following the approach of Morel and Berthon (1989), in the case of non-uniform biomass profile, or assuming a uniform chlorophyll-*a* profile with value equal to Chl_{sat} in the case of vertical mixing conditions. The switch between the two conditions was controlled by the retrieved depth of the productive layer (Z_e as obtained from Morel and Berthon approach) and by the estimated depth of the mixed layer as derived by Levitus (1982) climatologies. When the Z_e was shallower of the mixed layer depth, uniform conditions were adopted; otherwise the non-uniform state was assumed.

The other parameters were retrieved following the indications of BRI02. $PAR(0^+)$ derived from SeaWiFS data (Frouin, et al., 2001); Reynolds SST data (Reynolds and Smith, 1995), corrected with LEVITUS data for the Mediterranean conditions (following the approach described by BRI02) were utilized; finally, cloudiness was estimated using cloudiness index, as provided by the International Satellite Cloud Climatological Project (ISCCP) (Rossow, et al., 1996).

Four years (1998-2001) of 8-day SeaWiFS low resolution (GAC) data were used on the Mediterranean, producing then a PP map every 8 days. From such imageries, climatological, seasonal and monthly maps were derived, integrating over the single period and then averaging the maps relative to the different years (for example the climatological summer map was produced integrating the single 8-days maps over the season for each available year. Then a mean summer map was created averaging the summer imageries of the 4 years considered).

5.3 CLIMATOLOGICAL PATTERNS

The map of the climatological PP of the Mediterranean is showed in Figure 5-1. The observed patterns are very similar to those observed in the climatological map of chlorophyll-*a*, displaying a strong difference between the eastern and the western regions of the basin and different areas with high level of production.

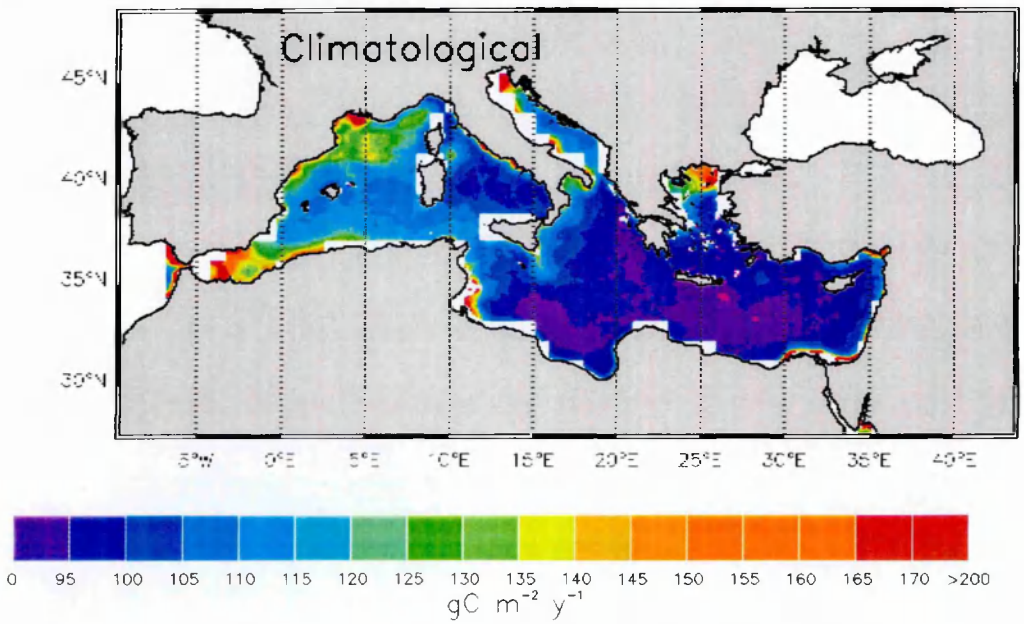

Figure 5-1. Year averaged derived annual primary production.

Respect to the AMA95 results (see their plate 4), the differences in the patterns are surprisingly few and are mainly related to the more uniform distribution of the SeaWiFS PP in the WMED and to the more evident presence of higher biomass events in the Rhodes Gyre region and in the central Tyrrhenian.

On the other hand, the AMA95 estimate displays a large range of variability in the retrieved values, which span from the 65-80 $gCm^{-2}y^{-1}$ of the EMED to the 150-175 $gCm^{-2}y^{-1}$ of the WMED. SeaWiFS map, indeed, displays a more flat variability resulting in values spanning from 100 $gCm^{-2}y^{-1}$ to 165 $gCm^{-2}y^{-1}$. The differences between the two sub-basins are then smoothed in the SeaWiFS map, with an increased value in the EMED and a decreased value in the WMED.

In Table 5-1 the integrated values for the different estimates of the Mediterranean PP are reported, confirming the above analysis. SeaWiFS estimates (BRI02 and the present work) are different in the absolute values, but are close regarding the differences between sub-basins (15 $gCm^{-2}y^{-1}$ for BRI02 and 18 $gCm^{-2}y^{-1}$ for this work, compared with the 48 $gCm^{-2}y^{-1}$ for AMA95).

	CZCS – AMA95	SeaWiFS 1998 - BRI02	SeaWiFS 1998-2001
WMED	158	198	122
EMED	110	183	105
MED	125	190	112

Table 5-1. PP annual estimates (in $gCm^{-2}y^{-1}$) for AMA95, BRI02 and the present study.

The reasons leading to the observed differences will be discussed later. Here, it is important to note that, even considering the diverse absolute values of the estimates obtained by the same sensor, the biases between the two sub-basins are substantially changed in the SeaWiFS and in the CZCS periods. In the first case, small discrepancies are observed (delta = 15-18 $gCm^{-2}y^{-1}$), while in the second, the WMED appear much more productive than the EMED (delta = 48-60 $gCm^{-2}y^{-1}$).

5.4 SEASONAL PATTERNS

Seasonal maps are displayed in Figure 5-2, while time series of the mean PP values, computed for the EMED, WMED and for the whole basin separately are showed in Figure 5-3.

As a general comment, excluding a large and diffuse event occurring in late spring-summer, the basin seems to have a quite constant dynamics, exhibiting PP values not very different between its two sub-basins.

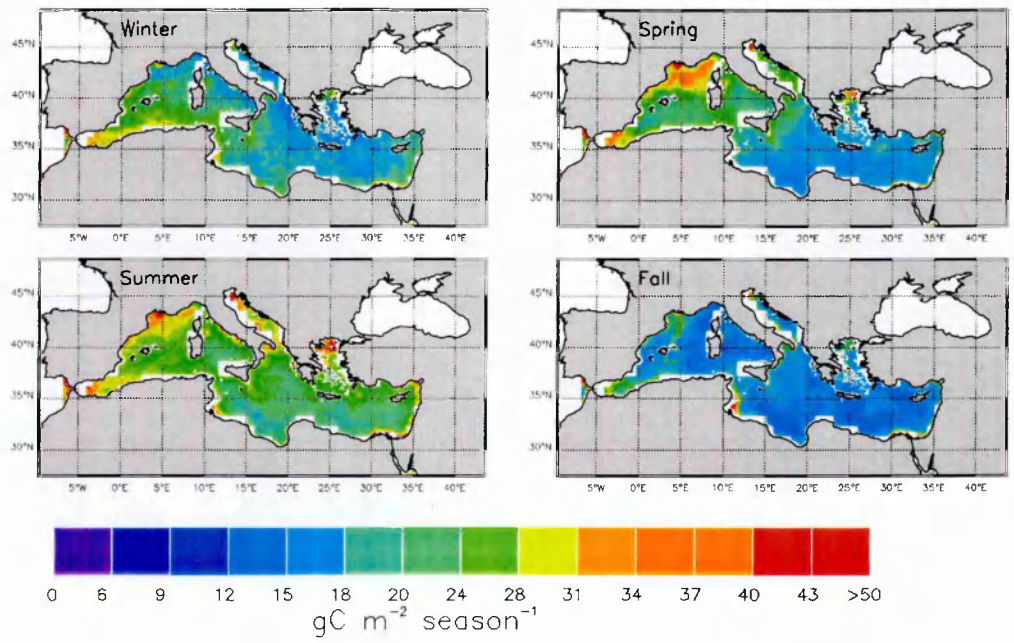

Figure 5-2. Quarterly composites of the primary production over the Mediterranean.

This general picture is modified during the spring season in the bloom areas (Alboran, NWMED, Southern Adriatic, Rhodes Gyre Region and Calabrian). However, such regions appear mainly as "hot spots" embedded in a quite fairly uniform background, which seems to be only slightly different between the two sub-basins.

Excluding such "hot spots", the seasonal signal is evident in the maps only during summer, when a widely diffused increase of PP is observed throughout the basin. In spring, the NWMED area displays high values of PP, which extend also in the central Tyrrhenian, and in general exhibit a north-south gradient. Such gradient is present also in the winter map, even if with opposite sign. In this season, the most productive areas appear the southern ones, while the regions north to 40° parallel display the lowest values of the WMED.

The trends shown in Figure 5-3 confirm the different behavior of the two main sub basins. In the EMED the retrieved PP changes only weekly with seasons, exhibiting peaks in summer and low values in winter, with a low range of variability. This trend appears not far from the results of AMA95 (thin lines in Figure 5-3), though, in their analysis the extremes are more prominent.

In fact the EMED's PP obtained from SeaWiFS display winter values almost twice as by as the AMA95 correspondent ones, whereas the summer ones decrease by a factor of 0.75. The final trend appears then smoothed along the year, though the yearly-integrated values are not very different (see Table 5-1).

By contrast, the WMED displays a stronger seasonal and interannual variability.

In fact, the WMED data for the years 1998 and 2001 show small variations with seasons, and the general annual trends appear close to EMED one. On the other hand, in the 1999 and 2000, the PP peaks in spring were followed by slight decreases during summer. The 1999 appears as the most variable and, definitively, the most productive.

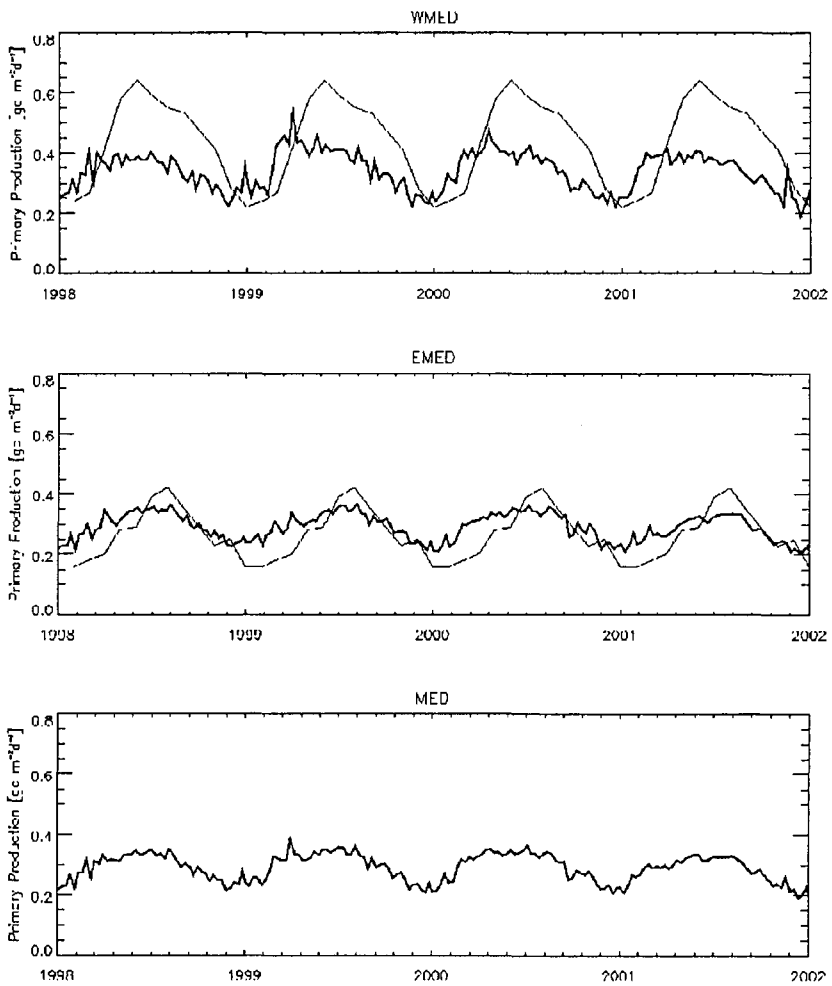

Figure 5-3.Seasonal and interannual courses of the derived integrated primary production for the WMED (upper panel), EMED (central panel) and the MED (lower panel). The thin lines are the climatological values obtained by AMA95.

From all the above results that the PP values in the WMED differ strongly from the AMA95 estimates. Undoubtedly, the already discussed interannual variability explains most of the differences. The AMA95 study was a re-appraisal of the MA91 research, which was performed using WMED-CZCS data relative only to the 1981 (plus some pictures from 1979 and 1982). In other words, the SeaWiFS values for the 1998 and 2002 suggest that two different regimes were probably acting in the two periods. This is confirmed by the comparison between the chlorophyll-*a* monthly averages for the 1998 and 2002 and the relative maps developed by MA91 for the March and April months. In those years, the WMED bloom areas (NWMED, Tyrrhenian and Alboran Seas) are reduced in size and in intensity, whereas, in the MA91-CZCS imageries such bloom areas display larger extensions and high chlorophyll-*a* values. On the other hand, in the 1999 and 2000, the monthly SeaWiFS maps display characteristics closer to the relative MA91 imageries. Focusing on the 1999 and 2000 trends, the dissimilarities between the data set appear then smoothed. Minimum values are close, whereas the peaks are slight lower in the SeaWiFS years (0.55 $gCm^{-2}y^{-1}$ in the 1999 and 0.45 $gCm^{-2}y^{-1}$ in the 2000 respect to the 0.65 $gCm^{-2}y^{-1}$ in the AMA95 data).

The shift in the timing is clearly evident. PP production in the SeaWiFS years starts to increase in December-January until they reach the highest values in March-April. In this period of the year, the CZCS data display still winter conditions (0.2-0.3 $gCm^{-2}y^{-1}$). It is noteworthy that, despite the difference in the interannual trends highlighted before, the shift is observable also in the 1998 and 2002 SeaWiFS data.

5.5 REGIONAL PATTERN

The SeaWiFS derived PP values can be analyzed on a regional basis, following the aerial division introduced in MA91 and AMA95 studies (see Figure 5-4).

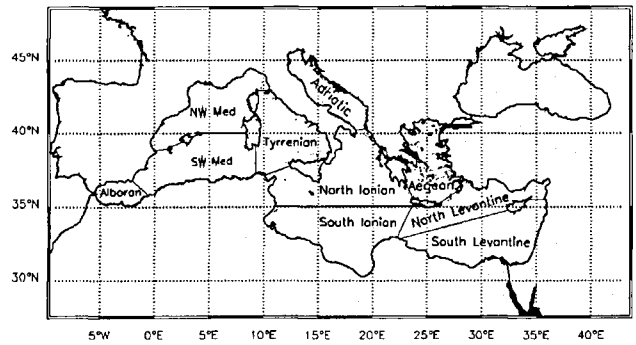

Figure 5-4. Boundaries of the provinces used to calculate the time-series.

Figure 5-5 displays the SeaWiFS derived PP values together with the similar estimates retrieved by AMA95 and MA91. In addition, mean and integrated values of chlorophyll-*a* and PP were calculated in the selected sub-regions and displayed in Table 5-2. For the WMED provinces, the MA91 data are increased by a factor of 1.33, which is due to the improved methodologies applied by AMA95 (see AMA95 for further details). This linear factor, however, considers only partially the modifications of AMA95.

In fact, as reported by the authors, the additional modifications (i.e. the ones not easily parameterized by a linear factor) resulted in an overall increase of the annual mean and in an enhanced production during the warm season. Then, the values showed in Figure 5-5, must be considered as a lower limit of the CZCS-era PP in the WMED.

In the oriental provinces (Adriatic, Aegean, Ionian North and South Levantine) the PP trends are close to the EMED patterns. This confirms the weak variability of the sub-basin, already observed in the maps and in Figure 5-5 and discussed before.

Even in the Adriatic and in the Aegean, where AMA95 data exhibited the highest values, SeaWiFS estimates are close to the time series calculated on the whole EMED, only showing a slight increase in late spring-summer. Except for these areas, the analysis on the provinces revealed the same trends already discussed for the sub-basin time-series and the same differences regard to the AMA95 values. Furthermore, it is important to remember that in AMA95, the authors warned about the reported estimates

for the Aegean and the Adriatic and declared "*while we feel that the trends are real, we cannot confirm the extreme pigment values*" (AMA95).

A different conclusion arises from the analysis of the WMED provinces. Notwithstanding the bias in the AMA95 values (not considered in the plots and in the maps), the CZCS and the SeaWiFS trends in the Alboran and in the Tyrrhenian regions are surprisingly similar.

The few differences are observed again in the timing of the beginning of productivity increase, but in general the two time series are very close. Regarding the SWMED, the situation appears similar to those observed in the EMED provinces, with only a small increase of the peaks values. Where the trends show a strong contrast respect to both the AMA95 data and the other occidental provinces, is in the NWMED region, then in the area that encompasses the large bloom observed in the chlorophyll-*a* maps.

I will consider firstly the impact of the area on the general WMED dynamic, to discuss later the difference with the AMA95 estimates.

Figure 5-5, highlights that the NWMED region mainly drives the observed interannual variability of the PP in the whole WMED. This is not surprising considering the large extension of the bloom in the area and its duration. However, from the above statements, follows that the other regions of the WMED do not influence the general dynamics of the basin.

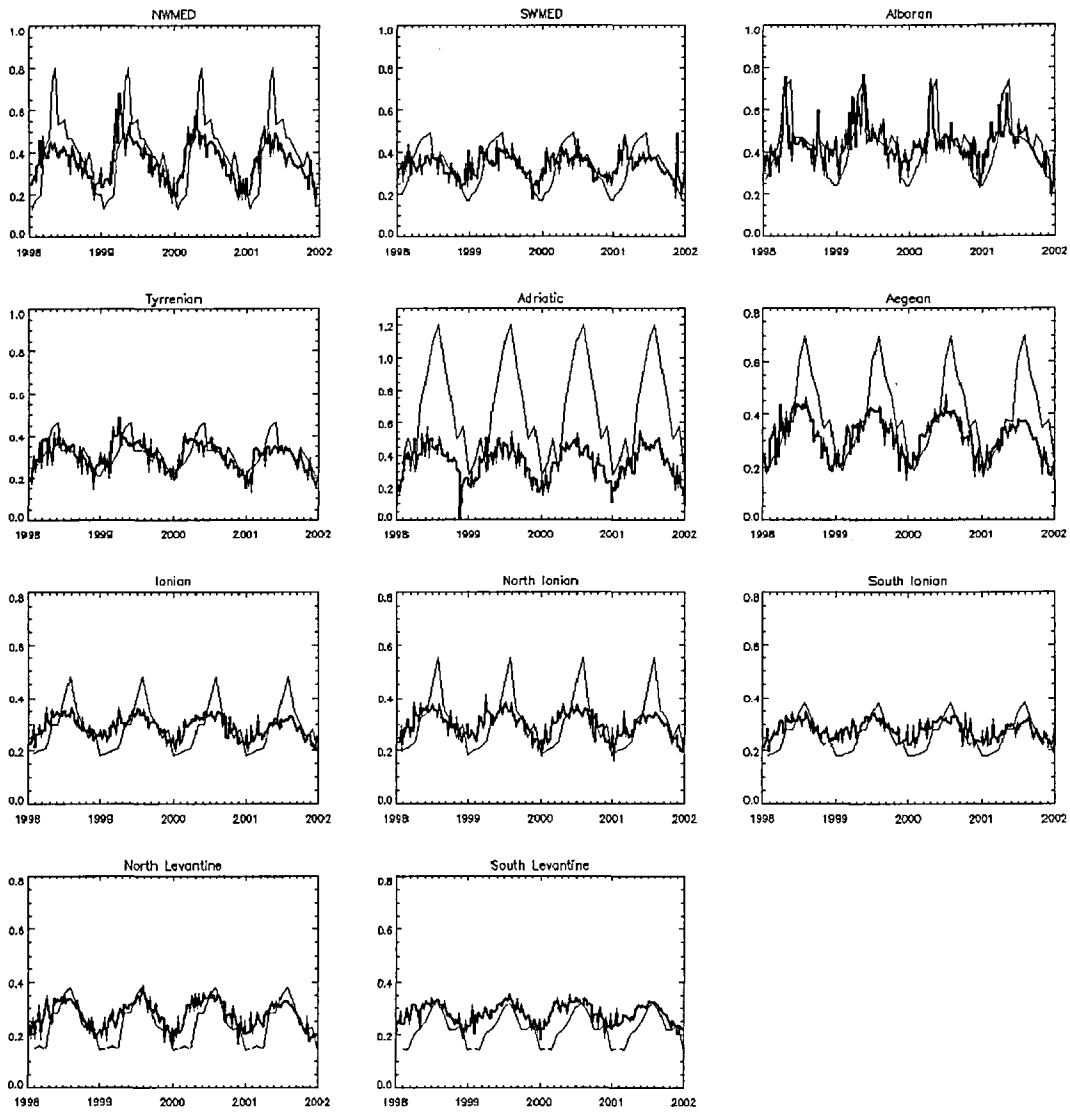

Figure 5-5. Seasonal and interannual courses of the derived primary production inside the defined Mediterranean provinces (see text). Thin lines show the AMA95 and MA91 values (see text).

The trends in Figure 5-5 confirm the above conclusion and show a WMED basin weakly variable but with a strong interannual variability in its NW regions. It is important to note that the PP values for other areas of the WMED are comparable to those derived in the NWMED area (see Table 5-2). However, they display a weak interannual variability, impacting on the PP budget of the whole area as a quite constant factor (see later in the Discussion chapter).

	C_{sat} CZCS	C_{sat} SeaWiFS	PP CZCS	PP SeaWiFS
Adriatic	0.90	0.33	240.8	128.0
Aegean	0.28	0.15	140.6	114.0
Ionian	0.13	0.10	104.0	104.6
N. Levantine	0.08	0.09	86.8	100.2
S. Levantine	0.07	0.08	81.8	101.3
EMED	**0.18**	**0.11**	**109.4**	**105.4**
NW Med	0.50	0.25	177.6	129.7
SW Med	0.23	0.18	143.7	121.0
Tyrrhenian	0.29	0.15	143.8	110.2
Alboran	0.50	0.38	200.0	157.9
WMED	**0.35**	**0.21**	**157.7**	**122.8**
MED	**0.235**	**0.156**	**125.0**	**112.4**

Table 5-2. Mean Values of Csat (in mg m^{-3}) and Integrated values of Primary Production (in $gCm^{-2}y^{-1}$) for the various provinces. The CZCS data were obtained by table 4 in AMA95.

The comparison with the AMA95 results merits further comments.

When the bloom in the NWMED region appears weak or limited in size (i.e. in 1998 or in 2001), the two time series differ strongly. Otherwise, (i.e. in 1999 and 2000) the trends of the PP are closer, with the AMA95 peaks being more pronounced. Even more, the main difference resides in the peaks period, which seems anticipated in the SeaWiFS years. A more careful analysis revealed however that the supposed shift is more pronounced during the "weak" SeaWiFS conditions (i.e. 1998 and 2001).

This fact will be reconsidered in the discussion section, where a detailed analysis of the hypothesized shift will be carried out and discussed.

CHAPTER 6

The Mediterranean Blooms

6.1 INTRODUCTION

The recently available SeaWiFS data were utilized to revisit the climatology of Mediterranean autotrophic biomass as obtained by the AMA95 and MA91 analyses. The general view did not change substantially, though novel features emerged. On the other hand, the better spatial and temporal resolution of the SeaWiFS sensor confirmed the characteristics of the main and of the occasional events of phytoplankton growth in the Mediterranean.

In the previous chapters, five areas of recurrent blooms were identified in the open sea: four had already been observed by AMA95 and MA91 (Alboran Sea, North Western Mediterranean, Southern Adriatic Sea and Rhodes Gyre region) while one (the Calabrian region) could be considered a novel feature of the basin.

In this chapter, a detailed analysis of the first regions will be performed, with the exclusion of the Alboran Sea, which was already extensively studied by other authors. The aim of this study is two fold. Firstly, throughs the intensive use of the ocean color data from SeaWiFS, time and spaces scales of the variability of the blooms events will be determined, extending the analysis also to the interannual differences. Secondly, the observed variability in the biomass surface field will be compared with the external forcing acting on the Mediterranean basin, in particular the atmospheric one, which is supposed to be the primary drive of the phytoplankton response. It is noteworthy that

the three regions mentioned above are all sites of dense water formation (see Introduction).

6.2 THE NORTH WESTERN MEDITERRANEAN BLOOM

The North Western Mediterranean Sea (NWMED) is characterized by an intense phytoplanktonic bloom, which is unequalled in the oligotrophic Mediterranean basin (MA91).

The region is known to be a site of dense water formation (see Introduction), which occurs mostly in winter (at the end of February), when the atmospheric forcing is particularly intense. Winds blowing from North West (Mistral) are the main players in determining the climatological dynamics of the basin and of the ocean response.

The region was the subject of numerous studies concerning physical and biological aspects (Anderson and Prieur, 2000; Gascard, 1978; MEDOC Group, 1970; Millot, 1987; Millot, 1999). However, the coupling between physical and biological dynamics is yet not fully understood. Levy et al. (1999; 2000) used a physical-biological model with realistic forcing to understand the role of atmospheric forcing and of the mesoscale structures on the bloom onset. They concluded that the extent and the duration of the bloom should be limited to the area of dense water formation and to no more than 3-4 weeks. Several papers exploited the data available from the long-term station DYFAMED located in the Gulf of Genova between Corsica and French coastline, which was outside the area of deep water formation but has located at the same latitude. Vidussi et al. (2000) used such data to characterize the phytoplankton pigment variations at the boundary of the bloom, while Marty et al. (2002; 2002) discussed the temporal trends of the phytoplankton and nutrient. The trophic regime of the DYFAMED station, as resulted by their analysis, was characterized by a typical mid latitude dynamics, with oligotrophic and ultra-oligotrophic summers and intense phytoplankton blooms in spring.

From the analysis of NWMED SeaWiFS data, the area appeared as the most prominent in the Mediterranean for what concerns autotrophic biomass concentrations. The largest extension of the bloom area occurred in the climatological March, even if the increase of biomass started in October and experienceed a relative maximum in December. However, the whole bloom area and the Gulf of Lions region appeared decoupled. In the latter, the December bloom appeared as the highest of the area, while in the surrounding regions only a slight biomass increase was observed. As the time goes on, the NWMED chlorophyll-*a* surface concentration started to rise, while in the Gulf of Lions the surface biomass decreased, as consequence of the deep water formation. Only in March, and in the following months, the bloom appeared as a single structure encompassing the whole area.

The influence of the dense water formation on the bloom dynamics was then very clear. However, the time course of the events questions the fact that the physical events following the deep mixing and its development influence the plankton response in the whole area from Balearic to Ligurian Sea. From the analysis of the climatological SeaWiFS maps, it appeared that the supposed influence of the deep water formation acts only in the Gulf of Lions area, while the other regions have different forcing.

Single daily passes of SeaWiFS data were then analysed to describe the plankton dynamics of the area. Only relatively cloud free passage were selected and remapped in NWMED region and DORMA algorithm was applied on the SEADAS water leaving radiances.

The analyses were performed focusing on the two main phenomena of the area: the deep water formation events and the phytoplanktonic blooms.

6.2.1 The NWMED deep water formation

Deep-water formation events can be very well detected in the satellite imageries of chlorophyll-*a* concentration: the vertical mixing due to the deep water formation,

disperses surface plankton, and leads to a local decrease of the surface chlorophyll-*a* concentration. The consequent depletion of phytoplankton results in a "deep blue hole" in the satellite imageries.

This structure (the "mixed-patch") was evident from middle January to the end of February in the years 1999,2000 and 2001, always in the same location (42°N 5°E) and with rather constant shape and dimensions (a circle of ~100 km radius) in agreement with in situ data (Gascard, 1978; MEDOC Group, 1970).

In 1998, the feature was not clearly evident, even if the number of cloud free images was similar to that of the other years. The surface chlorophyll-*a* field in 1998 showed overall low values in the whole basin in January, whereas the very low chlorophyll-*a* zone was not present in the other years. The only image showing the presence of the "deep blue hole" is the one of February 12, although the portion of clouds-free region in the map is very small.

It is noteworthy that "deep blue hole" can be easily detected because the surrounding area displays a slight increase in biomass (0.6-0.7 mg m^{-3}), which in false color shows up as light green. The observations indicated that the area was characterized by a weak bloom, similar in magnitude and in time to the similar event occurring in the rest of the Mediterranean. This phenomenon was the already described winter Mediterranean bloom.

6.2.2 The spring algal bloom

In the five years analysed, the spatial and temporal extension of the algal bloom was greatly different and then a separate discussion for each year was needed (see Figure 6-1).

Figure 6-1. SeaWiFS chlorophyll imagery time series in the NWMED regions (see separate document)

6.2.2.1 1998

In 1998, the bloom did not appear spatially homogenous. It was possible to identify two separate regions of enhanced chlorophyll-*a* concentration: the first one in the southern part of Gulf of Lions, the second one in the Gulf of Genova, between the Italian coast and the Corsica island (see the images: 17 Feb 1998- 26 Feb 1998 – 28 Feb 1998 – 18 Mar 1998 – 20 Apr 1998 – 24 Apr 1998 – 25 Apr 1998). The maximum spatial extension of the bloom was in early March, when the two different patches seem to merge in a unique feature (see 18 Mar 1998 image). From late February, a consistent increase of biomass (chlorophyll-*a* concentration. > 1mg m^{-3}) wass measured (see 26 Feb 1998), but only in March the bloom became evident (chlorophyll-*a* = 1-2 mg m^{-3}, 1 Mar 1998). After March, the bloom rapidly decreased (both spatially and in chlorophyll-*a* concentration), even if two patches last until early May, in the Gulf of Lions and in the Gulf of Genoa (see the sequence 19-24 Apr. 1998). Finally the bloom disappeared in early May, with mean chlorophyll-*a* values falling down to 0.2-0.3 mg m^{-3} in the whole region.

6.2.2.2 1999

In 1999, the bloom started in March and remained substantially active until the end of April, disappearing only in early May. The bloom development was very fast: in few days (from 26 February to 11 March) the chlorophyll-*a* values increased from a value of 0.2-0.3 mg m^{-3} to 2-4 mg m^{-3}. The feature appeared like a single huge structure, including the whole region from 41° N to southern Italian and French coasts and from 4° E to 10 °E (see the image sequence from 31 March to 18 Apr 1999). In late March a dramatic decrease of chlorophyll-*a* (< 0.3 mg m^{-3}) appeared in the region of deep-water formation (29 Mar 1999 –31 Mar 1999), almost certainly due to the vertical mixing. After four days, the region came back to a bloom situation, showing also an intense front (41°N) in chlorophyll-*a* field, separating the "red" region (chlorophyll-*a* > 2.5 mg

m^{-3}) from the "blue" one (chlorophyll-*a* < 0.5 mg m^{-3}) (see images 4 Apr 1999 – 5 Apr 1999). It is well known that along the 41° parallel, between the Spanish coast and Sardinia Island, a stable dynamic front (Font, et al., 1988) was observed in spring, representing the southern physical boundary of the bloom. In fact, in proximity of the front, subduction pushes down phytoplankton cells (Iudicone and NORBAL Team, 2002).

6.2.2.3 2000

The development of the bloom in 2000 was similar to the 1999 situation. The bloom started in early March, and similarly to 1999 situation, the chlorophyll-*a* values increased from 0.2-0.3 mg m^{-3} to 2-4 mg m^{-3} in few days (see images from 2 March to 9 March 2000). In this year, the most intense increase of chlorophyll-*a* occurred in the Gulf of Lions (see images 22 Mar 2000 - 24 Apr 2000). The 41° parallel front was present since to the first days of bloom and remained a constant characteristic of the 2000 event.

6.2.2.4 2001

The region showed a lower phytoplanktonic activity than in 1999 and 2000. The spatial extension of the event was limited to two areas of the 1998 blooms (south of Gulf of Lions and Gulf of Genova), even if the patches appeared reduced in size respect to the previous years. The two blooms remained separated for most of the time, showing also a different history: the bloom in the Gulf of Lions was evident from middle March (14 March 2001 picture) to early May (12 May 2001), while the Gulf of Genova bloom appeared and disappeared earlier (from middle February to middle April). When the bloom area extended to encompassing the two distinct regions (i.e. in middle March), it displayed a different spatial orientation respect to the 1999 and 2000 blooms. In fact, the "red region" did not enlarge to the whole NWMED area but remained limited by an

imaginary line parallel to the continental coastline. As a consequence, the strong separation between bloom and oligotrophic areas along the 41° parallel, clearly visible in the previous years, was slight inclined toward the coasts in 2001.

In conclusion, the 2001 event appeared slight different from to the other years studied.

6.2.2.5 2002

The spring bloom in the 2002 appeared similar to the situation in the 2001. Biomass increase started in the last days of February and reached its maximum extension in March. Similar to the 2001 event, the bloom area extended along the continental coastlines, but the different dynamics observed in 2001 in the Gulf of Lions and Gulf of Genova were not present. The bloom area did not show distinct patches and its temporal evolution followed a uniform dynamics in the onset and development of the biomass growth. However, starting to middle April, the bloom began to decay and only the areas of the Gulf of Lions and of the Gulf of Genova displayed high chlorophyll-*a* values.

6.2.3 Recurrent features

Despite of a large variability, the NWMED bloom exhibited features that remained unchanged throughout the whole period analysed:

- The start of the bloom occured in the first days of March except than for 1998. There was an appreciable correspondence between the end of deep water formation (when it was possible to detect it) and the most active phase of the bloom, in agreement with the numerous models present in literature (Levy, et al., 1999; Levy, et al., 2000; Tusseau-Vuillemin, et al., 1998). By contrast, there were some discrepancies with the analysis performed by MA91, mainly in the timing of the event. Although the general trend of the phenomenon was similar, they indicated mid-March as the end of the convection period and mid-April as

the beginning of the bloom, with an interval of one month between the two events. In the SeaWiFS images, there was no solution of continuity between the end of convection and the increase of biomass, and in some cases (for example in 1999) the two regimes seemed to co-occur.

- The bloom was always bound by the Ligure-Provencal Current (LPC) to the north and by the Balearic front to the south. Previous studies demonstrated that these two dynamic surface features were linked to the main cyclonic regime of the NW Mediterranean Sea (Millot, 1987; Millot, 1999) and were considered as permanent hydrological characteristics of the area.
- The time scale of the bloom was of the order of two months. It is noteworthy that, even though a large interannual variability was observed, this scale was an important peculiarity of the phenomenon. Given the characteristics of the Mediterranean basin, the long duration of the bloom in the region appeared like an anomaly.

6.2.4 Wind impact on phytoplankton dynamics

A strong variability was observed on the NWMED bloom as inferred from SeaWiFS images. It resulted in variations of the bloom spatial extension and in an irregular temporal dynamics, which showed relative peaks (both minimum and maximum) in the surface layer chlorophyll-*a* content. The winter large-scale hydrographic dynamics of the area was well known (Millot, 1987; Millot, 1999) and was mainly driven by the vast cyclonic circulation, which encompasses the whole sub basin (see chapter 1.1.2.2). Such feature could be considered a permanent characteristic of the NWMED area and it was supposed to be the main responsible of the bloom onset.

The patchy distribution and the irregular temporal evolution of the biomass, as observed from SeaWiFS, imply however that a more variable forcing acts on the basin. As already suggested by Levy et al. (2000), superimposed on the general isopycnal

uplift produced by the cyclonic circulation, intermittent events of winds burst generated local and highly variable mixing processes, which could in turn enhance or disturb plankton growth.

To verify how the winds forcing drives the variability of the observed events in the biomass evolution, a comparative analysis between the surface wind fields and the surface chlorophyll-*a* distribution was performed.

Two data sets of winds field were available to date.

One source of data derived from the SeaWinds sensor on QUIKSCAT satellite (Spencer, et al., 1997), which supplied daily surface winds components at 0.25° spatial resolution. Despite of the relative high spatial resolution, the overpass satellite time is about two days. Unfortunately, SeaWinds instrument is operative only since 2000, therefore ECMWF data were used for the comparison, for the 1998 and 1999 years.

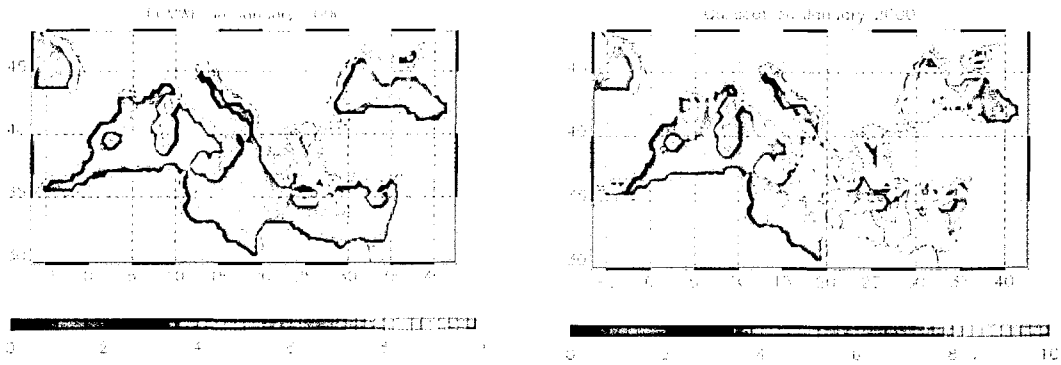

Figure 6-2. Winds module for January 2000. Left panel ECMWF; right panel SeaWinds. Values are in m s^{-2}

Model outputs from the ECMWF data base (see chapter 4.4) provide sea surface *u* and *v* components of the wind field at 0.5° of spatial resolution, every six hours. ECMWF wind retrievals were known to underestimate the in situ data, mainly when extreme situations occur (i.e. extreme events of winds burst). For the sake of comparison, winds module data from both SeaWind and ECMWF, obtained in the period of overlap (i.e. January 2000) are showed in Figure 6-2 for the Mediterranean area. Even if the absolute values are different (the ECMWF the lowest), the retrieved features are in reasonably good agreement and in particular, the gradients are conserved.

Then, for the purpose of this study, which is aimed more at evidencing the spatial and temporal dynamics than at the determining the absolute magnitude of the wind field, the two data sets can be used together.

Sea surface winds stress were then calculated (Gill, 1982) according to the bulk formula:

Eq. (6-1) $$(\tau_x, \tau_y) = \rho_a C_D |W| (w_x, w_y)$$

where τ and w are the wind stress and speed, respectively, and subscripts x and y denote zonal and meridional components. ρ_a = 1.2. kg m^{-3} is the air density and c_d is the drag coefficient, which was estimated according to Smith (1980):

for $|W| \leq$ 6 m s^{-1} $\quad 10^3 c_d = 1$

for 6 m s^{-1} < $|W| \leq$ 6 m s^{-1} $\quad 10^3 c_d = 0.61 + 0.063 |W|$

for $|W|$ > 22 m s^{-1} $\quad 10^3 c_d = 2.$

Finally, ten-days averages of winter-spring wind stress module and chlorophyll-*a* concentrations are displayed on Figure 6-3 for the 5 years considered.

Figure 6-3. Chlorophyll-*a* concentrations and winds field stress (see separate document)

The area shows a highly intermittent regime, characterized by period of scarce or albeit absent wind, interrupted by intense burst events occurring prevalently in the Gulf of Lions, but sometime extending also to Sardinia Island.

Such events produce different consequences on the chlorophyll-*a* distribution, depending on the period of the occurrence and on the trophic state of the surface biomass.

In winter, the high values of wind stress coincide spatially and temporally with the mixed patch area, site of the dense water formation. This fact is evident in 1999, 2000

and 2001 and, less clearly, in 2002, when the mixed patch appeared during scarce wind conditions.

The importance of the wind in switching on the process of mixing was already intensively studied (Marshall and Schott, 1999; Mertens and Schott, 1998), and is confirmed by the SeaWiFS and SeaWinds/ECMWF analysis performed here.

The periods of winds burst leading to the intense mixing process ("mixing wind event") last on average for 10-15 days, and generally decrease the surface biomass in the whole region, even if the strongest signal is observed in the mixed patch area. Chlorophyll-*a* concentrations result generally low during such events, as consequence of the mixing process induced by wind stirring, which prevents nutrient consumption by phytoplankton and biomass growth.

As the season proceeds, phytoplankton concentrations increase. High chlorophyll-*a* concentrations develop after the mixing events, when the winds stress reaches its minimum. The water column stabilizes and permits a rapid (i.e. 5-10 days) plankton growth, as reported by the SeaWiFS imageries. The "true" NWMED bloom starts only after the end of the wind events that produce the deep mixing. The 1998 situation confirms this hypothesis: the relative low atmospheric forcing, which led to a small or almost inexistent mixed patch, results in the lowest values of chlorophyll-*a* concentrations over the 5 years analysed. In the other years the maximum biomass increase is observed within the 20 days period just following the decay of the "mixing winds event" (see Table 6-1).

More interesting is the effect of the wind when the bloom is fully developed. Sometime, the bloom decays without any particular wind influence. This is the case of the 1999 situation, when biomass slowly decreases during April and May, probably after the consumption of all the available nutrients in the upper layer, no more refuelled by de-stratification events, and/or a strong grazing pressure.

	Mixed patch	Mixing wind event	Bloom onset	Secondary wind events
1998	not observed	12 Jan - 21 Jan	2 Mar - 11 Mar	No
1999	12 Jan - 1 Mar	22 Jan - 3 Mar 12 Mar - 21 Mar	12 Mar - 21 Mar	11 Apr – 20 Apr
2000	13 Jan - 2 Mar	13 Jan – 2 Mar	13 Mar - 22 Mar	13 Mar - 22 Mar*
2001	3 Jan - 2 Mar	23 Jan - 1 Feb 22 Feb – 2 Mar	13 Mar - 22 Mar	2 Apr – 21 Apr
2002	3 Jan - Mar	12 Feb - 21 Feb	3 Mar - 12 Mar	25 Mar – 13 Apr

Table 6-1. Summary of the comparison wind stress-chlorophyll-*a* concentration. (* Only in the Gulf of Lions).

Different phytoplankton conditions occur indeed when intense wind events take place during a well developed bloom. In April 2001, for example, in the first half of month, strong winds were blowing in the area, decreasing to almost zero values in the second half. Biomass, which in the period was in full blooming conditions, decreased rapidly (from 0.5-1 mg m^{-3} to 0.2-0.3 mg m^{-3} in ten days), to come back at high chlorophyll-*a* values when the winds decayed (i.e. ten days later). These "secondary wind events" disturb the plankton growth, which is momentarily stopped in the region where wind stress is higher. An example is the period from 2 to 21 April 2001). When the secondary winds event is not extended to the whole region, but interests only a limited area of the bloom region, the decrease of biomass is observed only in that area. (see for example the period from 3 to 12 March 2002, when the winds burst occurs only in the Gulf of Lions region and near the Balearic Island. This event produced a diffuse decrease in biomass in the interested area, but left unaltered the concentrations in the surrounding areas.

6.3 THE SOUTHERN ADRIATIC BLOOM

The Southern Adriatic (SA) Sea is the most productive region in the Eastern Mediterranean (AMA95) and is an important site of open ocean deep convection in the Mediterranean. Satellite imagery has been useful in elucidating oceanographic processes in the Adriatic Sea. CZCS data has been used in the past to investigate seasonality and circulation, as well as the influence of the Po River in the north Adriatic (Barale, et al., 1984; Barale, et al., 1986; Orlic, et al., 1992). Barale et al. (1986) was the firsts to highlight that high CZCS pigment levels co-occurred with meteorological conditions associated with dense water formation. Gacic et al. (1997) used remotely-sensed sea surface temperature field to investigate its spatial and temporal variability on a seasonal to interannual scale in the Adriatic Sea, and found that a temperature minimum associated with the SA Gyre was prominent from late autumn to early winter (corresponding to the preconditioning and deepwater formation phases) and exhibited strong inter-annual variability. Buongiorno Nardelli and Salusti (2000) used thermal imagery to estimate the SA horizontal space scale of the deep convection area, which was then used together with the winter density stratification and the buoyancy fluxes to compute the depth of the convective chimney from theoretical criteria. Variability in the extent of Adriatic dense water formation has been invoked to explain differences between years (1998 and 1999) in satellite-derived monthly temperature and chlorophyll-*a* fields (Banzon, et al., 1999).

Interannual changes in subsurface nutrient availability in the SA area and inflowing Ionian intermediate water within the last decade have been reported by Civitarese and Gacic (2001), who showed that an increased nutrient availability below 200 m occurred from 1987 to 1995 with a subsequent decrease after 1997. They found that this increase of the SA gyre internal nutrient pool did not determine a significant increase in the new production because of the concomitant relaxation of the winter vertical convection, and

concluded that the interannual variability of the surface nutrients and new production in the SA region is strongly controlled by deep convection penetration depth rather than the nutrient content of the intermediate waters. This idea is further developed by Gacic et al. (2002) in their analysis of vertical carbon flux data for 1998 with remotely sensed algal biomass and in situ nutrient data.

This section will report the main results of a study conducted on the interannual variability of the SA area. SeaWiFS daily data, generated using DORMA algorithm, were remapped on the area of interest for the period January 1 to April 30, 1998-2000. A total of 298 remapped chlorophyll-*a* images were produced for the Adriatic Sea using all the available SeaWiFS passes. As usual, chlorophyll-*a* maps were flagged for clouds or other contamination factors using a sequence of mask criteria (McClain, et al., 1995): land, cloud, sun glint, atmospheric correction failure, high total radiance, large solar zenith angle (70°), large spacecraft zenith angle (56°), coccolithophores, negative Lw, and Lwn (555) < 0.15 Wm-2 sr-1. Table 6-2 shows the availability of the images per month and the monthly mean cloud cover in the south Adriatic area based on the SeaWiFS cloud masks.

Month year	**Cloud cover percent**	**Number of images used**
January 1998	80.1	20
February 1998	61.0	22
March 1998	55.6	29
April 1998	63.2	24
January 1999	75.3	23
February 1999	62.3	25
March 1999	65.2	30
April 1999	68.9	26
January 2000	54.1	28
February 2000	64.1	27
March 2000	57.8	24
April 2000	43.2	20
TOTAL		298

Table 6-2. Summary of the SeaWiFS data used in the SA area.

6.3.1 Year-to year variability of SeaWiFS chlorophyll imageries

In this section, the time series of satellite images by year is presented in order to describe the chlorophyll-*a* pattern from the beginning of the year to the end bloom period. Rather than showing images at regular intervals, significant phases of the bloom and its rapid evolution are shown in Figure 6-4, Figure 6-5, and Figure 6-6.

Figure 6-4. Year 1998: SeaWiFS chlorophyll-*a* imagery time series of the SA region

Figure 6-5. Year 1999: SeaWiFS chlorophyll-*a* imagery time series of the SA region

Figure 6-6. Year 2000: SeaWiFS chlorophyll-*a* imagery time series of the SA region

(see separate document)

6.3.1.1 Year 1998

The chlorophyll-*a* concentrations in the SA region were moderate for January (Figure 6-4), i.e., on the order of 0.18-0.21 mg m^{-3}. Advection of chlorophyll-rich Albanian coastal water is observed in Feb 9 –10, which probably contributed to the phytoplankton increase (> 0.4 mg m^{-3}) in the SAG interior by Feb 14. This early bloom disappears in one week (Feb 18), but high-chlorophyll-*a* patches rapidly reform (Feb 21). The southerly patch becomes better-developed with pigment concentrations reaching 1.0 mg m^{-3} (Feb 27-28). Small scale features probably associated with the cyclonic flow of the SA Gyre form (Mar 2-6), after which the bloom weakens. The following days are cloudy (Mar 7-11) but areas visible through cloud gaps suggest that the feature disappears.

In the next sequence of images, an asymmetric low chlorophyll-*a* area (<0.1 mg m^{-3}; referred to as a "hole" hereafter), appears (Mar 17-28). The "hole" is initially not well-defined but becomes highlighted as pigment concentrations increase on the eastern meandering edge (Mar 23-28, see Figure 6-7 for an enlargement). Within 2 days, the "hole" has disappeared (Mar 30), and in few days (by Apr 1), a large central bloom (> 1 mg m^{-3}) covers most of the SA region. It is more spatially extended than the February

bloom, and high pigments are observed until Apr 5. The bloom is no longer visible a week later (Apr 15) and no further increase occurs over the rest of the month.

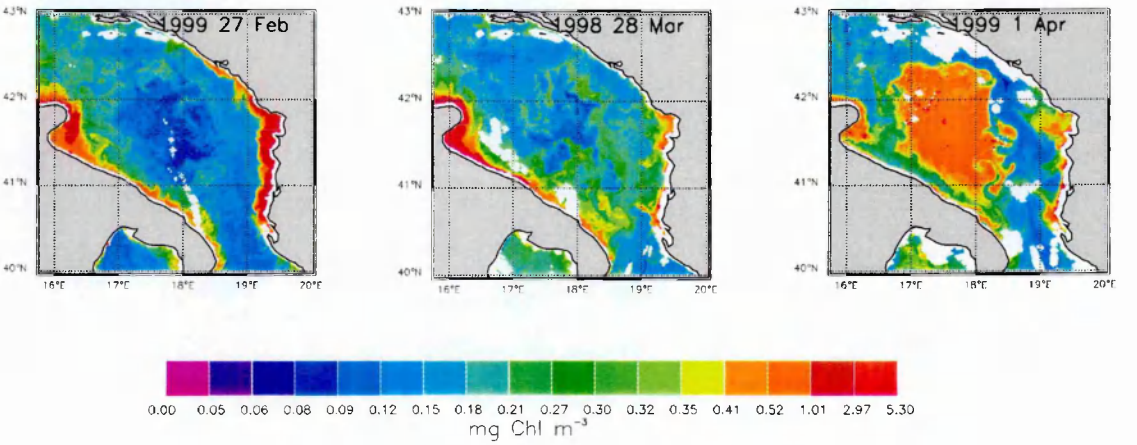

Figure 6-7. Principal phases of the South Adriatic phytoplankton bloom onset following deep convection: a) chlorophyll-*a* minimum feature at the end of the deep convection phase; b) contracted chlorophyll-*a* minimum with enhanced chlorophyll-*a* at the meandering edges; c) final phase of the bloom onset: well developed spring bloom.

6.3.1.2 Year 1999

Unlike the previous year (see Figure 6-5), the low-chlorophyll-*a* "hole" is observed from the beginning of the year and persists for several weeks in the 1999 imagery (Jan 7-27). Minimal chlorophyll-*a* patches discernible on Jan 7 quickly develop into a large "hole" with meandering edges by Jan 16. The shape of the "hole" varies over the next few weeks (Feb 5-27). In February 27 (Figure 6-7) the "hole" is more than 50 km across which is the consistent with the size of a mixed convective patch (Marshall and Schott, 1999). The 2-month persistence of the "hole" resulted in much lower chlorophyll-*a* concentrations compared to that of the previous year for the same dates. Chlorophyll-*a* concentrations above 0.4 mg m^{-3} were not observed in the central area until March 3, when mesoscale patches of high chlorophyll-*a* appear. These patches almost completely disappear in the next few days (Mar 5-10), and then reform but shifting around, to eventually reach a more northerly position (Mar 12-21). The bloom is initially more intense in the northern part of the SA area (Mar 24), and then becomes

more widespread, covering most of the center, highlighted by the contrasting oligotrophic Ionian Sea water inflow (Mar 25-Apr 7). The surface chlorophyll-*a* concentrations reach a maximum around Mar 30, and then slowly decline even though the meandering structure is preserved (Apr 1-7). Although the structure dissipates by Apr 12, traces of elevated chlorophyll-*a* (~0.3 mg m^{-3}) remain (Apr 26).

6.3.1.3 Year 2000

The image time series for 2000 (see Figure 6-6) differs from the previous years in that, except for a few days, pigments levels were below 0.2 mg m^{-3} from January to March. Although a low chlorophyll-*a* area was easily identifiable in the images, the location was neither central nor fixed. Instead, the "hole" shifted around. First, the asymmetric "hole" developed in the SA Gyre center (Jan 20-29). Then, the minimal chlorophyll-*a* area briefly disappeared (Feb 1), re-appearing east along the Croatian coast (Feb 4), then becoming less distinguishable again (Feb 5-25). By Feb 28, the "hole" was centrally located but southward towards the Otranto Straits. The subsequent clear images (Feb 28-Mar 14) show rapid closure of the "hole" and chlorophyll-*a* concentrations increasing towards the center over time. However, the bloom onset, marked by an increase in chlorophyll-*a* concentrations above 0.3 mg m^{-3} (Mar 11-14), was interrupted by the appearance of another "hole" (Mar 19-23). By Mar 29, the bloom resumes but, unlike the previous years, concentrations do not exceed 0.5 mg m^{-3}. The highest chlorophyll-*a* patch was located at a very southerly location and later propagated northwards inside the SA Gyre following its rotation (Mar 30-Apr 23). By April 27, the bloom disappears.

6.3.2 Mixed layer evolution in the SA region

The large variability of the surface chlorophyll-*a* distribution, as observed by SeaWiFS imageries, was investigated using a 1-D physical model, forced with realistic

air-sea heat fluxes data in the centre of the SA Gyre. The rationale to conduct this analysis was to verify how much variability in the plankton distribution could be explained by the atmospheric forcing.

6.3.2.1 Surface fluxes, initial and boundary conditions

The net surface heat flux at the air-sea interface (Q_{tot}), consists of the absorbed solar radiation (Q_s) minus the back radiation (Q_b) , latent (Q_e) and sensible (Q_h) heat flux:

Eq. (6-2) $$Q_{tot} = Q_s - (Q_e + Q_h + Q_b)$$

Each component of the heat budget can be computed using the so-called bulk formulae that are based on knowledge of some meteorological parameters. Here, sea level atmospheric pressure, air temperature at 2m, dew point temperature, cloud cover, zonal and meridional wind components from ECMWF (European Centre for Medium-range Weather Forecasts) were obtained. Sea surface temperature at the same location was extracted from daily AVHRR Pathfinder data (Kilpatrick, et al., 2001). The SST data voids were interpolated in space and time using objective analysis (Marullo, et al., 1999). The low resolution of the ECMWF data (0.5° degree) precludes a bi-dimensional analysis of the atmospheric forcing over the SA region (which is only 100 km in diameter). Therefore, the ECMWF grid point located in the center of the gyre (41.5 ° N, 18.0 °E), which can be considered representative of the meteorological conditions of the gyre, was selected.

The Reed's relation (1977) was used to estimate mean daily insolation including cloud attenuation. The shortwave radiation budget including the effect of the sea surface albedo is:

Eq. (6-3) $$Q_s=Q_0*(1 - 0.637 * C + 0.0019 * h)*(1 – A)$$

where Q_0 is the clear sky radiation, C is the mean daily cloud clover, h is the solar elevation at noon and A is the sea surface albedo.

The latent heat flux was computed using:

Eq. (6-4) $$Q_e = \rho_a * C_e * w * (q - q_s) * L$$

where ρ_a is the air density, $C_e = 1.14 \times 10^{-3}$ is the Dalton number, w is the wind intensity, q is the specific humidity, q_s is the saturation humidity and $L = 2.456 \times 10^6$ J kg $^{-1}$ is latent heat of water (Gilmann and Garrett, 1994). The specific humidity and saturation humidity were computed from water vapor pressure and saturated water vapor pressure (Gill, 1982, pp. 40-41) that in turn were calculated from the ECMWF dew point temperature and AVHRR sea surface temperature, taking into account atmospheric pressure correction and salt correction (Gill, 1982, p. 606).

The sensible heat flux was computed using:

Eq. (6-5) $$Q_h = \rho_a * C_p * C_h * (T_s - T_a) * w$$

where $C_p = 1005$ J $kg^{-1}K^{-1}$ is the specific heat of air, T_s is sea surface temperature and T_a is air temperature. The Stanton number C_h was estimated as a function of the wind intensity:

$$C_h = \{0.720 + (0.0175 * w * (T_s - T_a))\} * 10^{-3} \quad w < 8 \text{ m*s}^{-1}$$

$$C_h = \{1.000 + (0.0015 * w * (T_s - T_a))\} * 10^{-3} \quad w \geq 8 \text{ m*s}^{-1}$$

The infrared radiation budget was computed using the formula of Bignami et al. (1995):

Eq. (6-6) $$Q_b = \varepsilon * \sigma * T_s^4 - \sigma * T_a^4 * (0.653 + 0.00535 * e)] * (1 + 0.1762 * C)$$

where e is the water vapor pressure, ε is surface emissivity and σ is the Stefan-Boltzman constant and C the cloud cover. To drive the model, daily values for each component of the heat flux were computed using the above parameterisations for the October to April of each year. Time series of the surface heat fluxes are showed in Figure 6-8.

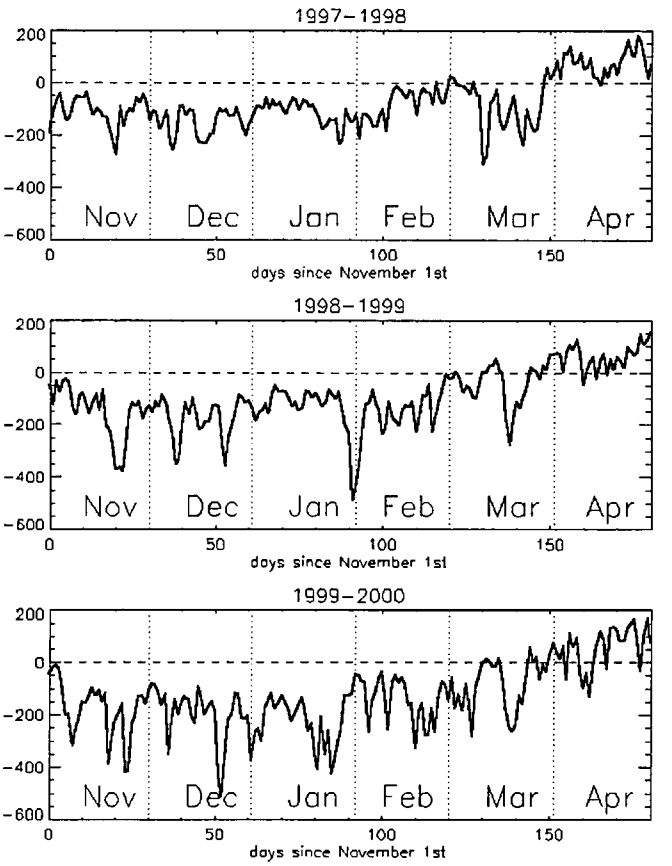

Figure 6-8. Time series of the total heat fluxes in the center (41.7 ° N, 17.9 °E) of the SAG computed from ECMWF data. November 1997 – 30 April 1998 (a); 1 November 1998 – 30 April 1999 (b); 1 November 1999 – 30 April 2000 (c)

Wind stress time series were calculated from ECMWF winds using the expressions described in the paragraph 6.2.4. The October climatological temperature and salinity profiles from MED6-MODB (Brankart and Pinardi, 2001) ware used to initialise the model. Tough, since profiles for each year were not available, all runs were performed using the same initial temperature and salinity profile. Consequently, only the year-to-year variability of the vertical mixing and water properties due to the variability of the local atmospheric forcing have been investigated.

6.3.2.2 Model results and comparison with SeaWiFS data

Density values derived as output of the MXL model are shown in Figure 6-9 for the three considered periods, together with some mixed layer depth in-situ data, plotted to sake of comparison.

Such data for the 1998 and 1999 are obtained from literature (Gacic, et al., 2002), while for the 2000 are provided by an XBT transect performed every two weeks in the framework of the Mediterranean Forecasting System Pilot Project (MFSPP; for the data see http://doga.ogs.trieste.it/mfspp_ogs/index.html).

In general, the model outputs agree well with the in situ assessments of mixed layer depth, both in timing and intensity of the convective overturning process.

This result indicates that in the SA region, the role of the local air-sea fluxes is dominant and can explain most of the year-to-year variability of the depth and time of vertical mixing.

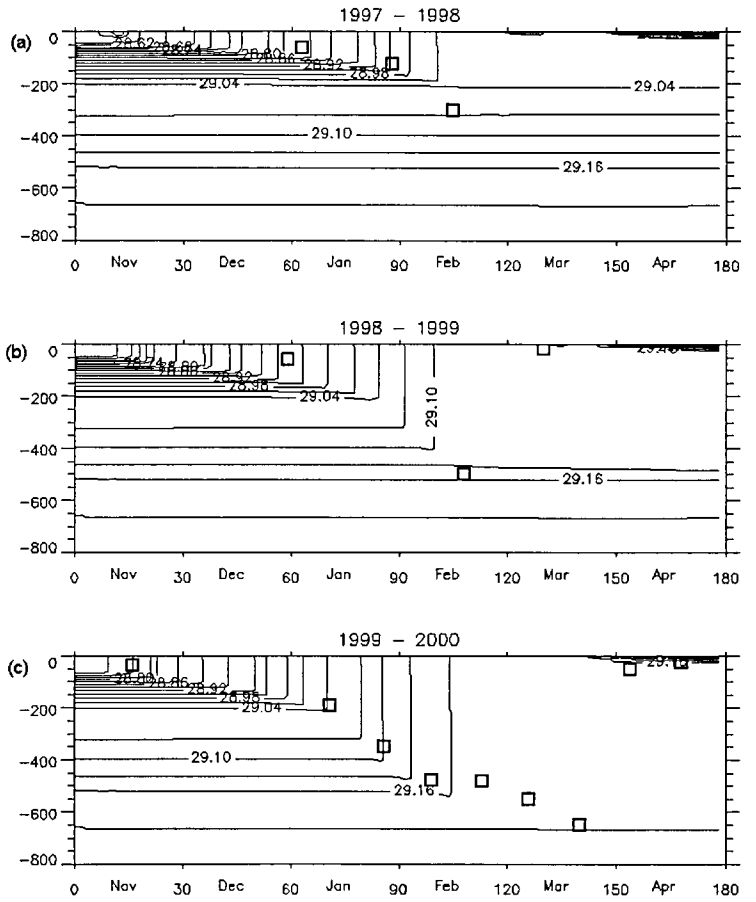

Figure 6-9 The model simulated water column density in the SAG center. Density contour interval is 0.03 σ .1 November 1997 – 30 April 1998 (a); 1 November 1998 – 30 April 1999 (b); 1 November 1999 – 30 April 2000 (c). Squares indicate mixed-layer depths as derived by XBT observations (year 2000) and published CTD measurements (year 1998, 1999 see text).

Model outputs were then compared with SeaWiFS derived chlorophyll-*a* concentrations. To facilitate comparisons and to better visualize the timing of bloom events, chlorophyll-*a* concentrations along a transect (shown in Figure 6-10) were interpolated in time and space using a weighted Gaussian function with e-folding of 3 days in time, and 10 km in space.

The temporal progression of chlorophyll-*a* along the transect is compared with the model evolution of the density structure from January to April of each year to investigate the correspondence in the timing of events (Figure 6-11). The transect summarizes the bloom development for the three years and clearly shows differences in timing, spatial extent and intensity.

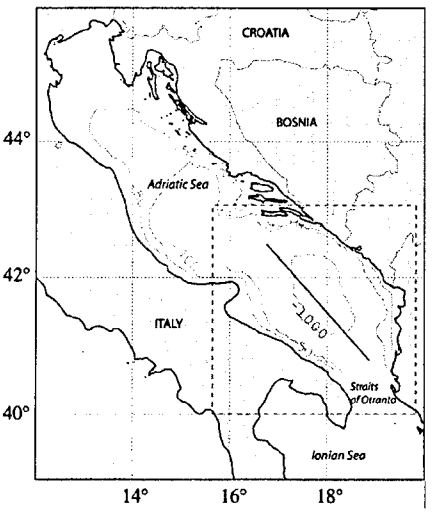

Figure 6-10. Bathymetric map of the Adriatic Sea. Box shows area represented in SeaWiFS images. The thick line shows the transect for extraction of chlorophyll-*a* data from individual passes.

In correspondence of decreased wind stress and the increased solar radiation over the area, the heat fluxes become positive (Figure 6-8) and the simulations show density restratification in the upper layer. The period of low chlorophyll-*a* observed in the SeaWiFS transect corresponds to deepening of the mixed layer up to its maximum extent (see also Figure 6-9).

In the chlorophyll-*a* transect of 1998, the two main bloom events described before, as well as the appearance of the minimal chlorophyll-*a* "hole" in between, are easily recognized. The first well-developed bloom occurs shortly after the progressive mixed layer deepening has ceased at the end-February. In March, a series of intense wind bursts lasting for 20 days interrupts the initial bloom, and destroys the stratified layer, also leading to maximum mixing penetration.

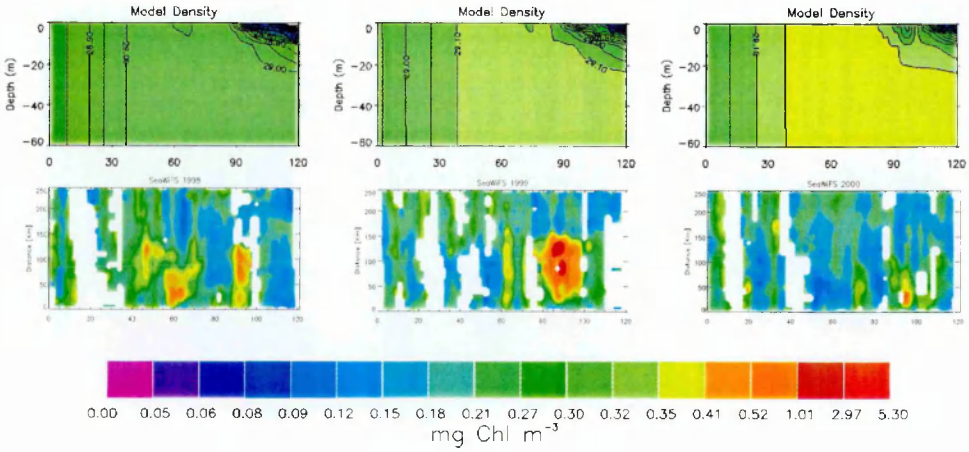

Figure 6-11. Time evolution of the bloom in the three years. (a) Interpolated SeaWiFS chlorophyll-*a* concentrations along transect (shown in Figure 1) for 1998, (b) 1999, (c) 2000. Contour interval is 0.2 mg m^{-3}, white region indicate no-data available. (d) Simulated density distribution within the upper 60 m depth for 1998, (e) 1999, (f) 2000.

This minimum in chlorophyll-*a* concentration, which appears as the "hole" in the image time series, suggests that the minimum area in pigment concentrations correspond to the deep convective patch. By April, a net heat gain in the upper ocean (Figure 6-8) permits the seasonal pycnocline to develop. With the onset of restratification, the second bloom occurs, lasting for about two weeks in the imagery.

The chlorophyll-*a* transect shows that 1999 is characterized by a single significant bloom event, preceded by a prolonged period of minimal chlorophyll-*a*. The period of depressed pigment concentration is associated with continuous penetrative mixing. During these first two months, recurrent wind events and significant heat losses contribute to the absence of restratification and inject nutrients into the euphotic zone. Chlorophyll-*a* reaches its minimum value in mid-February when the penetration depth extends to maximum of 500 m, which is much greater than the previous year. Chlorophyll-*a* values moderately increase in early March and reach a maximum after March 20 when the seasonal thermocline begins to be re-established. The main bloom lasts for over three weeks and is more intense compared to the other years. Experimental evidence of this bloom is provided by Boldrin et al. (2002) who report a surface maximum of 1 mg m^3 in the centre of SA Gyre in early March.

For 2000, Figure 6-6 shows generally low pigment conditions for most of the entire period examined, with two very moderate bloom events. The first chlorophyll-*a* increase occurs around March 10, much later than the previous two years. This bloom delay can be attributed to strong wind events and prolonged mixed layer deepening down to 600 m. The brief chlorophyll-*a* increase corresponds to positive heat fluxes and low winds, but these conditions did not last long and were not sufficient to induce stratification in the model. In mid-March, an intense cooling event results in minimal chlorophyll-*a* values along the transect and the re-appearance of the "hole" in the imagery.

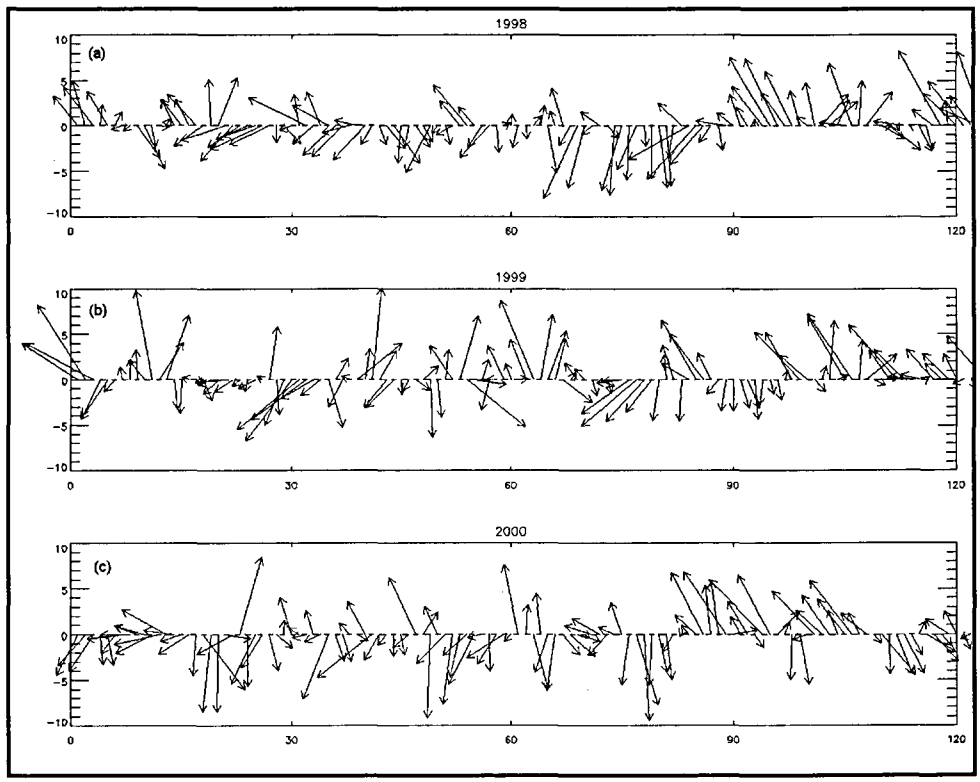

Figure 6-12 Stick diagram of the wind in the center (41.7 ° N, 17.9 °E) of the SA gyre from ECMWF data.

At end of March, seasonal stratification began as heat fluxes became positive. These conditions favored the development of a bloom which was definitely less intense than that 1998 or 1999. The wind regime in early April shows many frequent wind events of moderate intensity mainly from south-east (Figure 6-12).

The combination of wind and cloud cover variability contributed to the negative/positive heat flux oscillations, thereby modulating the restratification process in the model. In the simulation, the onset of the bloom corresponds to the beginning of restratification.

6.3.3 Preliminary Discussion

The use of a mixed layer model, forced with realistic air-sea fluxes and winds, resulted in a good assessment of the timing of the phytoplankton growth events in the SA region. The classical "Sverdrup-like" series of events leading to biomass growth is well described by the evolution of the density field obtained with the numerical exercises and confirmed by satellite data.

However, this simplified picture deserves further comments.

As often observed and reproduced by models (Wiggert, et al., 2002; Williams and Follows, 1998), the response of biomass to the atmospheric forcing, via convective process, is not linear. Even if other factors controlling the growth are disregarded, the simple mechanism "more convection equal more biomass" is not always verified.

The results described in the previous paragraphs, even reliable in the events sequence description, do not explain totally the observed trends of biomass. SeaWiFS data show that for 1999 and 2000 when the convective depths were increasing, the productivity was much lower during the latter year.

In fact, the effect of atmospheric forcing on the plankton growth is not limited to convective penetration depths but also extends to the mixing rates. In the framework of the Sverdrup's critical depth theory, Dutkiewicz et al. (2001) proposed a simple model to examine the interannual variability in springtime chlorophyll-*a* concentration as a response to these factors. They suggested that the plankton production is a function of the mixing rates and identified regimes in which enhanced mixing can either increase or decrease bloom intensity. The extent of these regimes was defined simply throughout

the non-dimensional parameter (h_c/h_m): the ratio of spring critical layer depth and winter mixed layer depth. They found that, in subtropical regime ($0.6<h_c/h_m<\sim1$), the vertical mixing can promote surface productivity through enhanced nutrient supply while in subpolar regime ($h_c/h_m < 0.4$) the vertical mixing can retard the bloom due to transport of phytoplankton below Sverdrup's critical depth.

In Table 6-3, the year-to-year variability of h_c/h_m for the SA area is showed for the studied periods.

YEAR	Winter Mixed Layer Depth hm	Spring Critical Depth hc (March-April)	hc/hm	TKE (March-April)
1998	200 m #	41	0.20	3.7
1999	500 m #	38	0.08	3.7
2000	650 m #	43	0.07	5.5
1997	23-35 m $^{+}$	45	1.9-1.3	nodata
1998	300 m $^{+}$	41	0.14	nodata
Clima	550 m$^{\&}$ - 600 m$^{£}$	46*	0.084-0.077	nodata

Table 6-3. Estimate of spring critical depth (h_c) and Winter mixed layer Depth (h_m) ratio. h_c was computed as the depth at which vertically averaged flux of photosynthetically active radiation (PAR derived from ECMWF shortwave radiation budget) is reduced to 21 W/m^2 and averaged over the bloom period (Follows and Dutkiewicz, 2002). Symbols: (#) – Mixed layer depth estimated from the mixed layer model; (*) – Critical depth derived using shorthwave radiation obtained from Southampton Ocean Centre climatology (Josey, et al., 1999); (+) – mixed layer depth from Gacic et al. (2002) ; (&) – mixed layer depth from MOM – GFDL (Artale, et al., 2002); (£) – Mixed layer depth from MED6-MODB. Model derived Turbulent Kinetic Energy (TKE) integrated both over the mixed layer and in time during the bloom period.

The h_c was calculated as described by Follows and Dutkiewicz (2002) and the winter mixed layer depth and turbulent kinetic energy (TKE) was provided by the model outputs and published in situ observations. During the studied periods, all h_c/h_m fall within the sub-polar regime and show a steady decrease from 1998 to 2000. The ratio for 1999 and 2000 is very similar to the climatological value while that for 1998 is

distinctly greater. Thus, a difference in biological response to physical forcing can be expected. Actually, the SA region exhibits a much greater variation in the critical depth ratio if other years are considered. For example, Gacic et al. (2002) report that in 1997, there was almost no winter convection, and phytoplankton production, as inferred from sediment trap data, was low. The h_c/h_m ratio for this year is well within the sub-tropical regime. The shifting from subtropical to subpolar regimes (as defined by the h_c/h_m ratio) in the SA area implies that this ecosystem's sensitivity to mixing can change dramatically.

This hypothesis was further tested by examining the whole CZCS time series from 1979 to 1985. During these years only very moderate spring blooms (chlorophyll-*a* concentration between 0.3 and 0.5 mg m^{-3}) were observed. The most intense bloom occurred in March 1982 when chlorophyll-*a* concentrations reached 0.7 mg m^{-3}. This agrees with the previous analysis by AMA95 who found that the spring average chlorophyll-*a* in SA is 0.3-0.4 mg m^{-3}. Even if the frequency of the CZCS observations was not as high as that from SeaWiFS, the number of available scenes and the typical duration of the event strongly support the hypothesis that the 1998 and 1999 blooms were "special events" while the weaker 2000 bloom can be considered the normal south Adriatic situation.

6.4 THE RHODES GYRE BLOOM

In the Rhodes Gyre (RG) region, the climatological maps highlighted the presence of chlorophyll-*a* increase during spring. The region appears then as the unique area in the Levantine Basin having events of relevant surface biomass increase, showing chlorophyll-*a* values considerable higher than on the surrounding regions.

As already showed by AMA95, an active cyclonic structure and a particular wind regime (Ozsoy, et al., 1993; Sur, et al., 1993) present in the area provoke a moderately eutrophic regime in spring (AMA95). Several studies were conducted in the region in the past years (Ediger and Yilmaz, 1996; Yilmaz, et al., 1994), showing that the increment in chlorophyll-*a* may be directly related to the strong vertical mixing due to the dense water formation observed in the gyre. Peaks are observed in March, confirming that the increase in biomass begins when the mixing event is already finished and the water column starts to stratify. The structure is present also in the CZCS maps and a detailed study of the bloom is discussed in AMA95. Other studies investigated the interaction between strong cooling events and phytoplankton response (Ediger and Yilmaz, 1996; Napolitano, et al., 2000; Yilmaz and Tugrul, 1998) in the Rhodes Gyre region. In particular, Napolitano et al. (2000), using a five-compartment physical-biological 1-D model forced with realistic heat fluxes, analysed the effect of the cooling event on the biomass field, and reproduced very well the time course of the chlorophyll a increase, though with higher values than those retrieved by AMA95.

Here, a detailed analysis of the phenomena will be performed, using intensively the high-resolution SeaWiFS imageries available for the area. Furthermore, the interannual variability of the bloom events will be examined on a long time period, exploiting the CZCS data and the AMA95 results. Finally, the supposed effect of the atmospheric cooling on the phytoplankton dynamics will be discussed, comparing air-sea fluxes and ocean color data.

6.4.1 Year-to year variability of SeaWiFS chlorophyll images

The climatologically analysis and the previous studies revealed that the occurrence of the blooming events is mainly centered in March, with a variable time period which span from late February to April. The present analysis was then focused on that period even though the whole time series of available data was analysed. Four years (1998-2001) of SeaWiFS LAC-data were processed with the standard procedure (i.e. see before and appendix 9.2) and the chlorophyll-*a* concentrations were derived via DORMA algorithm, after that all the questionable pixels, as resulted by the SEADAS masks, were flagged. The chlorophyll-*a* maps were then re-mapped in the RG area (25°-35° E; 32°-37° N) and the resulting cloud free pictures were displayed for each year in Figure 6-13.

Figure 6-13. SeaWiFS Imageries of the RG region. (see separate document)

6.4.1.1 1998-1999

In these years the RG region appears totally oligotrophic, showing chlorophyll-*a* values generally below 0.1 mg m^{-3} and close to the estimates of the surrounding areas. A slight north-south gradient is observed in the SeaWiFS imageries during the period considered, disappearing only in late April, when the entire region assumes the ultra-oligotrophic values, characteristic of the EMED summer.

The highest chlorophyll-*a* values are retrieved along the Turkish coast, in the Gulf of Antalya, where a long biomass-rich filament is often detected (31 March 1998, 25-28 February 1999).

A weak chlorophyll-*a* increase occurs in 1998 (chlorophyll-*a* values ~ 0.2-0.3 mg m^{-3}) in early April, close to the region of the RG structure. The phenomenon is however clearly visible in only two maps (4-5 April), disappearing in the following pictures and obscured by the cloud cover in the previous period. However, the picture of 31 March,

free from clouds in almost all the area, demonstrates that, if any events occurred, it lasted only 3-4 days.

Similar regime appears in the 1999, even though local and weak biomass enhancements was detected.

6.4.1.2 2000

The conditions described for 1998 and 1999, appear strongly modified in the 2000 maps, which reveal the occurrence of an important event of biomass growth unseen in the other years. The bloom appears in March-April with relatively high values of chlorophyll-*a* (0.4-0.5 mg m^{-3}) and a large spatial extension. It started in mid March, even if an enhanced biomass occurred in the region in early March (chlorophyll-*a* values ~ 0.3 mg m^{-3}), and lasted until early-April. Unfortunately, the cloud cover disturbs the view of the structure and of its progression with time, and then only a partial view of the enriched patch can be obtained. The bloom center is located in the RG area (see 24 March and 2 April), even if in some cases it seems that the enriched patch extends to the surrounding regions (see for example 6-11 and 15 March imageries). The intense cloud cover in late April prevents to examine the decay of the bloom. The small portion of cloud free imageries (not shown) seems however indicate that it disappeared after April 20, when the area reverted to the typical ultra-oligotrophic conditions of summer.

6.4.1.3 2001

Unlike the other considered years, the chlorophyll-*a* dynamics in the RG area for the 2001 appears anticipated in time and with a different evolution. A structure of enhanced biomass (chlorophyll-*a* values ~ 0.2-0.3 mg m^{-3}) is detected in the RG region by early February, and observed throughout the month, for finally decaying in early March. The enhanced patch appears very limited in size during early February (see 8-9-10 February

imageries), though, by March, it weakly enlarges. However, the enriched area does not reach the spatial extension observed in the 2000 bloom, and also the chlorophyll-*a* values are considerably lower. As anticipated, the bloom decays in middle March (i.e. one month before the 2000) when the region displays strong oligotrophic conditions. Similar to the 2000, the cloud coverage is particularly strong in the area, preventing a more detailed analysis. The plume observed in the previous year near the Antalya Gulf, is clearly detached in 2001 (15-17-19 May), with a large extension enlarging to the off-shore waters for hundreds kilometers.

6.4.2 Influence of the atmospheric forcing

As already mentioned, the cyclonic structure and the atmospheric cooling are considered the main causes of the enhancement of biomass in the RG area. Being the cyclonic structure a permanent feature of the local dynamics, the atmospheric forcing could be hypothesised as the factor controlling the interannual variability of the blooming events.

To verify such hypothesis, net heat flux derived by the NCEP data set were extracted and calculated on the area and for the period considered. In addition, from each SeaWiFS ocean color daily scene, a 20x20 pixel box (22 km side) was extracted and the pixels in the box that passed the exclusion criteria were spatially averaged. The time series of NCEP net heat fluxes were produced integrating over each day starting from October 1 to October 1 of the following year, in order to calculate the integrated net heat flux relative to each year. Finally the two parameters (chlorophyll-*a* concentration and integrated net heat flux) were plotted as function of time (Figure 6-14) in order to investigate on the relationship between the atmospheric forcing and the occurrence of the phytoplankton blooms.

The rationale for conducting a simultaneous analysis of the surface chlorophyll-*a* content and the atmospheric forcing resides in the evidence that, as also noted by

Stratford and Haines (2002) along with Sverdrup (1953), the preconditioning mechanism to make the internal nutrient pool available for the autotrophs in the photic zone of the open sea must be the winter convective mixing.

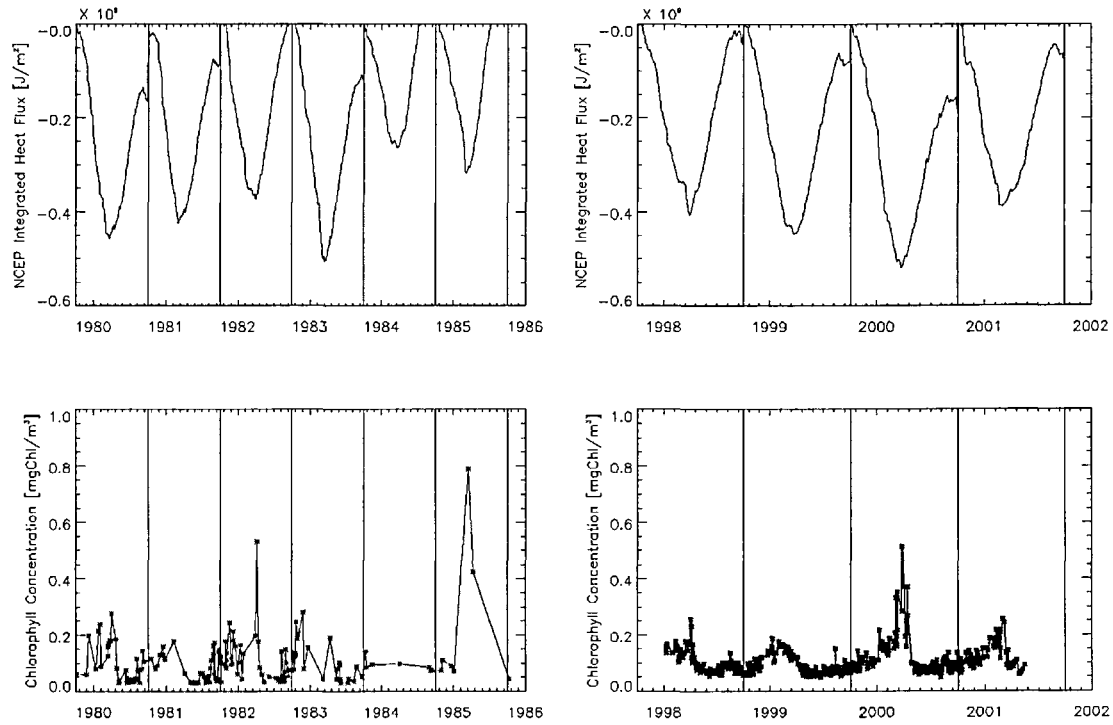

Figure 6-14. Upper panel: NCEP-derived integrated heat fluxes for the selected region. Lower panel: box averaged satellite chlorophyll concentration time series (CZCS-OCEAN left; SeaWiFS right). Vertical lines are the 1st October starting data for the computation of integrated heat fluxes.

Therefore, the analysis of the atmospheric forcing would allow determining to what extent and where any observed variability of the RG biomass field, could be attributed to the enhanced vertical transfer of nutrients due to convection.

In the RGB region, the correspondence between the integrated heat fluxes and the increase in biomass is evident. Only when strong atmospheric events occurred (i.e. winter 1999-2000 with peaks of integrated heat fluxes reaching the value of $-0.5 \cdot 10^9$ J/m^2) a biomass bloom took place.

The correlation between heat fluxes and phytoplankton response is fully confirmed by the combined analysis on the SeaWiFS and NCEP data, showing that the RGB is

directly related to atmospheric forcing. Most of the interannual variability of the biomass field, evident in the time-series, could be explained by the variability in the time series of heat fluxes.

6.4.3 The RG bloom during the CZCS era

The RG structure was present also in the CZCS climatological maps (see Chapter 4) and a detailed study of the bloom is discussed in AM96. It appears as a permanent feature of the basin, since the surface biomass is generally higher than the surrounding area for most of the year. Such characteristic is retrieved in both the data sets (present SeaWiFS and AM95 CZCS) and then the RG region can be considered a first test site to verify the long term trends of the Mediterranean basin, as well as the consistence of the two ocean color data set.

Following AM95, the RG bloom appears in the CZCS data in March and, with a reduced extension and intensity, in July. The chlorophyll-*a* values for the March bloom were around 0.5 mg m^{-3} and then close to the values obtained from SeaWiFS during the 2000 event. In addition, also the spatial extensions of the feature were similar. Despite of the irregular and scarce temporal frequency of the observations, the CZCS analysis displayed a RG dynamics very similar to the one resulting from the more resolved SeaWiFS imageries. In fact the persistence of the structure as a prominent feature of the basin, confirms that the two data sets reproduce quite well the dynamics of the site and thus further confirm that they are comparable.

CHAPTER 7

Impact of the EMT

7.1 INTRODUCTION

The Mediterranean Sea experienced a vast change in the thermoaline circulation during the years 1991-1996 (the Eastern Mediterranean Transient, EMT), which resulted in a rise of the isopycnal surfaces and of the nutricline by several hundred meters (Klein, et al., 1999). Affecting the depth of nutricline, the EMT could have modified the trophic regime of the basin, inducing unseen events of surface biomass growth.

In this section, the results obtained in the previous chapters will be reconsidered and expanded, to define if any alteration in the surface phytoplanktonic dynamics occurred due the EMT.

Some issue related to such question emerged in the previous pages:

- The two data sets of ocean color data available for the Mediterranean (SeaWiFS and CZCS) covers a period which span from 1979 to 2002, with a large gap in the data series between the 1985 and the 1998. The EMT occurred during this gap. However, it is supposed that the response of the system was not so fast to prevent any evidence after the 1998. Though, if any change due to the EMT affected the basin, it should be detectable by SeaWiFS.
- Changes in the atmospheric forcing are considered the main factor inducing the EMT. The proceedings paragraphs highlighted that the bloom events of the basin are strictly controlled by the atmospheric forcing. Though, either an

intensification of the known blooms or a set-up of novel ones could be hypothesized as consequence of the EMT during the SeaWiFS years. Regarding the first possibility, Santoleri et al. (2003) demonstrated, that the Adriatic Bloom enhanced its strength in the years just following the end of the EMT (1998-1999), as compared to pre-EMT conditions. For the second case, the discussion in Chapter 4 anticipated that an evident, even if weak, difference between the CZCS and SeaWiFS surface climatological chlorophyll-*a* fields was detected in the North-Western Ionian Sea. A detailed analysis of the single daily SeaWiFS passes revealed the existence of an intense and large biomass patch offshore the eastern Calabrian coast (North-Western Ionian) in early spring, with values reaching 0.6-0.9 mg m^{-3}. The next paragraph will be focused on this feature and on its connection with the EMT.

- The analysis carried out before, showed that, despite their coarse sampling frequency, the CZCS data were able to retrieve the principal features of the basin, as detected by SeaWiFS. The observed differences in the climatologies arise mainly in the timing of the events, but not in their general description. Furthermore, the study performed on the RG bloom confirmed this result, demonstrating the capacity of the CZCS data to infer also on sporadic and not permanent features.

The CZCS data used in the previous chapters of this study derived primarily from the AMA95 analysis, which were provided as monthly climatologies. To detail the present study, the OCEAN-CZCS data (CZCS-JRC) were used (see chapter 2.2.5.1). The OCEAN project made available single CZCS daily passes remapped on the Mediterranean basin, providing a powerful tools to determine the occurrence, even if sporadic, of a phenomenon.

7.2 CZCS DATA: COMPARISION BETWEEN AMA95 AND OCEAN ARCHIVE

To date, no comparison between CZCS-JRC and CZCS-AMA95 data was ever performed.

Hence, to verify the consistency of the two different procedures the values reported in the table 3 of AMA95 paper and the chlorophyll-*a* values as derived by the CZCS-JRC data set were compared, for the same areas and time intervals.

The consistency of the OCEAN pictures with the former maps was checked, by comparing the chlorophyll-*a* values derived by the two procedures after averaging the OCEAN scenes as in AMA95. The result is reported in Table 7-1, and shows a general agreement; hence CZCS-JRC and CZCS-AMA95 may be taken as interchangeable.

Region	Period	AMA95 (mg m^{-3})	JRC (mg m^{-3})	In situ (mg m^{-3})
South East Lev	July, Dec, Apr	0.00-0.05	0.03-0.07	0.03-0.07
North East Lev	Jun, Jul, Sep	0.05-0.1	0.03-0.04	0.05-0.1
Eastern Lev	Apr	0.00-0.05	0.03-0.07	0.03-0.05
Eastern Lev	Jul	0.00-0.05	0.00-0.03	0.02-0.04
Cyprus eddy	Feb	0.00-0.05	0.10-0.25	0.15-0.25
Cyprus eddy	May	0.00-0.05	0.00-0.03	0.04
Cyprus eddy	Sep, Nov	0.00-0.05	0.00-0.03	0.03
Lev + Ion	Summer	0.1	0.05-0.08	0.09
Along Israel	Year	0.1-0.3	0.1-0.2	0.14
Off the Nile	Jun, Jul	0.05-0.1	0.00-0.06	0.1
Off the Nile	Dec, Jan	0.1-0.3	0.2-0.6	0.5-0.6
Off the Nile	Apr	0.1-0.5	0.1-0.8	0.5-1.0
Off the Nile	Aug	0.00-0.05	0.00-0.05	0.02
Off the Nile	Nov	0.00-0.05	0.00-0.06	0.05-0.1
Aegean Sea	Extrema of year	0.05-0.3	0.06-0.32	0.01-0.18
South East Cyprus	Sep	0.00-0.05	0.00-0.03	0.03-0.04

Table 7-1. Comparison among various chlorophyll determinations in the Eastern Mediterranean Sea from CZCS satellite (AMA95 and JRC data sets) and in situ surface data retrieved from the literature (table 3 in AMA95)

7.3 THE CALABRIAN BLOOM

7.3.1 Description of the ocean color variability in the Calabrian Bloom area

In Figure 7-1, SeaWiFS maps zoomed on the region offshore the Calabrian coasts are displayed, for the years 1998-1999 and 2000. The detected patch of enhanced biomass (the Calabrian Bloom, CB hereafter) shows great time variability in the three years analyzed. However, it was almost always present in March and disappears in mid-April. In 1998 it started in early April, in 1999 during the first days of March, while in 2000 it appeared in mid March. In 1999 it extended from the coast to a distance of at least 150 km, with a fairly uniform chlorophyll-*a* distribution, until its decay a few weeks later, with the exception of a narrow band closer to the coast where the chlorophyll-*a* concentration remained always high. Considering the narrow shelf (see Figure 7-2), the length scale and the absence of large rivers, the structure was clearly related to an open ocean event. This is much more evident in 1998 when the highest chlorophyll-*a* values were centered approximately 100 km offshore.

Figure 7-1. Selected images SeaWiFS chlorophyll-*a* concentration over the CB region (see separated document)

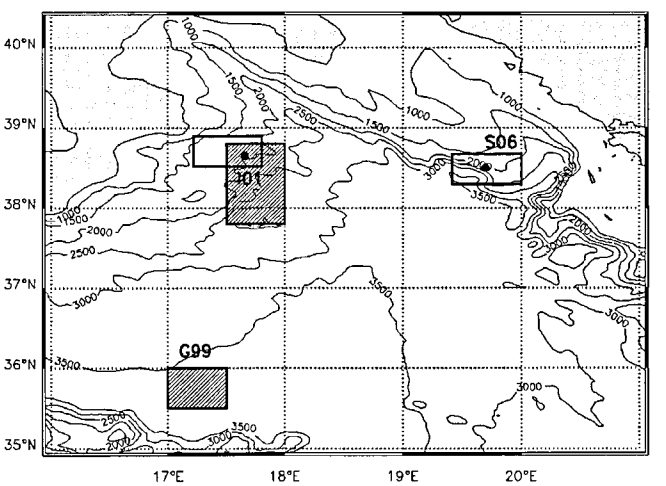

Figure 7-2. Map of the Ionian Sea region with bathymetry. The boxes indicate the locations where the time series of chlorophyll-*a* concentration and NCEP fluxes have been extracted. The dots indicate the locations where the in-situ data used for the 1D model has been collected.

No evidence of this structure exists in the CZCS data, even if the number of the CZCS cloud-free scenes in the period of interest is quite large. A careful visual inspection was performed, displaying all the available single scenes and checking out not only the absolute values of chlorophyll-*a* estimates but also biomass gradients in the region. AMA95 reported a slight, general and diffuse increment in biomass in the Northern Ionian Sea in April (Plate 1 in their paper), but the pattern was definitely different with a clear gradient decreasing offshore.

Similarly to the analysis carried out on the Rhodes Gyre bloom, NCEP integrated heat fluxes were extracted for the CB region and compared with the chlorophyll-*a* concentration as retrieved by SeaWiFS and OCEAN data.

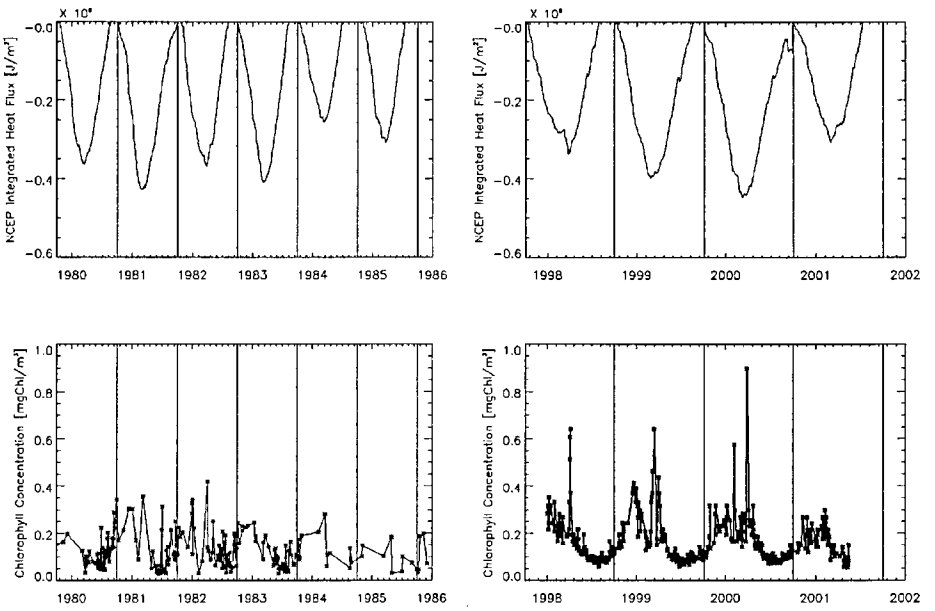

Figure 7-3. Upper panel: NCEP-derived integrated heat fluxes for the selected region. Lower panel: box averaged satellite chlorophyll-*a* concentration time series (CZCS-JRC left; SeaWiFS right). Vertical lines are the 1st October starting data for the computation of integrated heat fluxes.

The analysis (Figure 7-3) reveals that the increase of biomass is related to strong events of heat loss in the period just preceding the bloom, which is a typical pattern for the onset of plankton bloom in late winter-early spring in temperate regions, as already noted also for the RG bloom. The correlation between the two events suggests that the

timing of this ocean-atmosphere coupling determines also the time when the bloom occurs in the three years studied. In addition, the magnitude of the biomass enhancement seems to be directly dependent on the intensity of the atmospheric events: the highest values of chlorophyll-*a* are observed in year 2000 when the heat loss reaches the maximum value observed in the studied years; on the other hand, when the atmospheric forcing is below the value of $-0.3 \cdot 10^9$ J/m^2 (i.e., in 1998) the bloom appears less pronounced. Even if no studies similar to those conducted in the Rhodes region are available, one could argue that the dynamics of the two blooms is similar. Strong atmospheric events force deeper convection in a cyclonic structure such as the one reported for the Northern Ionian Sea since 1998 (Manca, et al., 2002) and produce a larger vertical transport of nutrients in the photic layer, allowing an enhanced plankton growth. The above description is also confirmed by Boldrin et al. (2002) that present data of a sediment trap located in the region of the CB, through the years 1997-1999. The peak of Total Mass Flux in 1998 (figure 8 in their paper) occurs in late April, i.e. about 15 days after the decay of the CB, substantiating the presence of a high biological activity in the surface layer.

The scarce number of observations of the CZCS sensor and the relatively short duration of the phenomenon (the maximum duration was 30 days in 1999) does not permit to absolutely exclude its occurrence in the CZCS period. On the other hand, the evidence of the structure is very clear in all the SeaWiFS years and not in the CZCS years, notwithstanding similar atmospheric forcing in the area.

7.3.2 In situ nutrient profiles

The previous analysis was based on remote sensing observations, which evidenced variations only in a relatively restricted area of the basin. As mentioned above this approach was the only feasible because of the lack of in situ data covering the two decades between the CZCS and SeaWiFS periods. Nevertheless, to investigate whether

the reported uprising of the nutricline (i.e. Klein, et al., 1999) could be considered a consistent feature of the late nineties in the Ionian Sea, the available existing nutrient data for two sites, which had been sampled a few times over the last decades, were compiled and discussed. Both sites are located on the western side of the Ionian basin, with the northern site being the area of the CB. The sampling location areas are reported in Figure 7-2, whereas nitrate profiles for the upper 500 m. are shown in Figure 7-4, which includes also the list of the cruises, which they belong to.

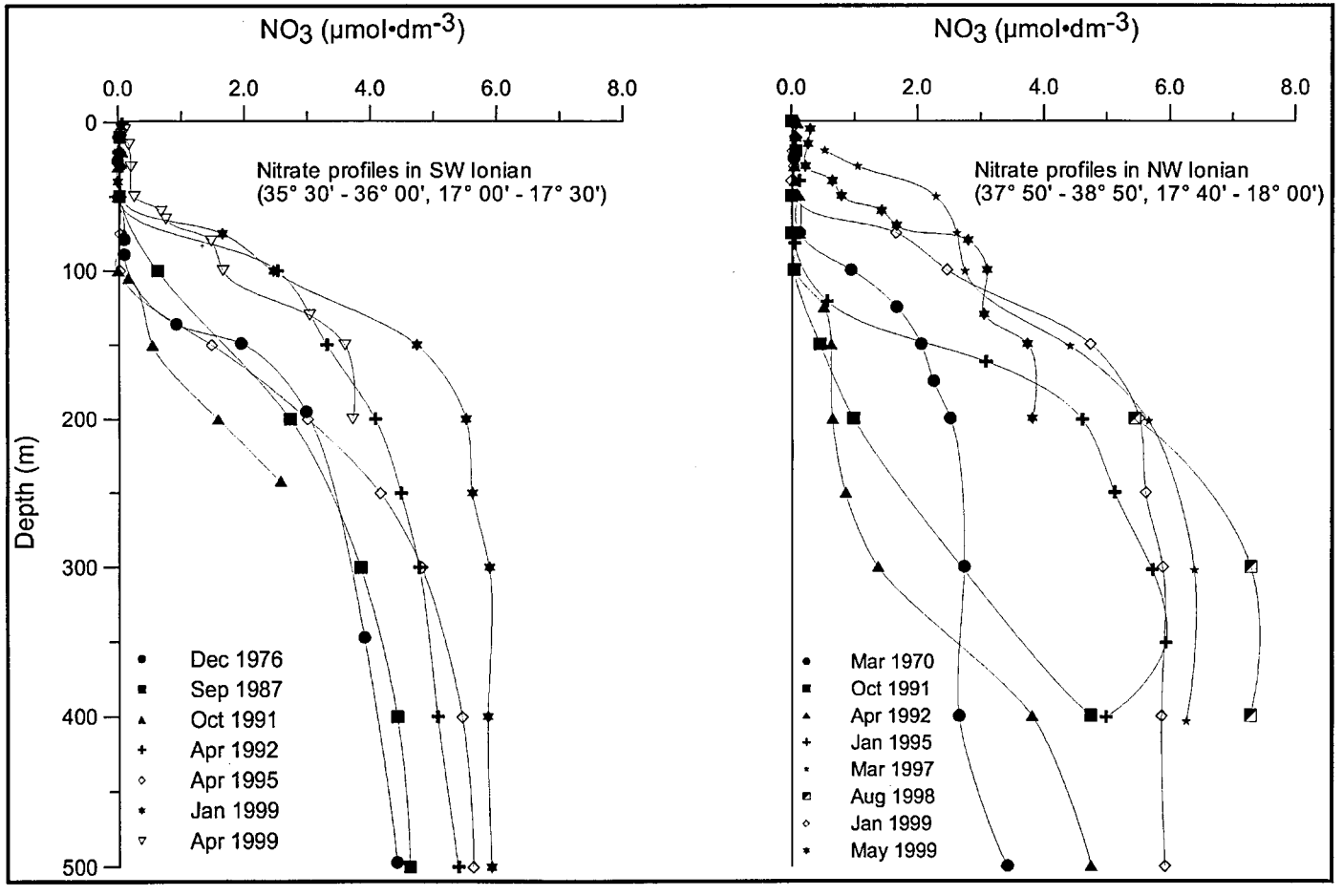

Figure 7-4. Vertical profiles of nitrate for the two Ionian regions selected (left panel South Western Ionian, right panel North Western Ionian). The dates of the sampling are indicated in the legends.

The discrete data were fitted with a spline interpolator to better visualize the profile. At both sites the progressive uplift of the nitracline is evident, especially for what the 150-500 m layer concerns. Even more relevant, is the resulting increase in the subsurface concentrations. At 150 m nitrates are, on average, 3 $\mu mol \cdot dm^{-3}$ higher in the nineties than they were until the end of the eighties. It is also worth noting that the profiles cover similar seasons and that, notwithstanding their very reduced number, they span over most of the western Ionian. The implications of the change in the subsurface concentrations will be discussed in the next paragraph.

7.3.3 Is the EMT the cause of the observed Calabrian Bloom?

One of the expected responses of the system to the EMT is a change in its biogeochemistry, being the uplift of the nitrogen pool towards the surface one of the most important result of the EMT. How much closer to the surface must the nutricline go to drastically change the upward nutrient fluxes into the photic zone?

To investigate on the vertical dynamics, it was adopted the simplified approach already used for the SA bloom, based on a 1-D mixed layer model and realistic forcing conditions. It was adopted the widely used 1-D modulus of the Princeton Ocean Model (Mellor, 1998) forced with the NCEP heat fluxes and wind stress computed in the Ionian region for the year 1999, for which temperature and nutrient in situ profiles are available. Data come from the station I01 and S06 in winter (cruise SINAPSI-3), and S06 in spring (cruise EMTEC); see Figure 7-2 for the location of the station. As initial conditions, vertical climatological profiles of salinity and temperature (Figure 7-5) extracted from the Mediterranean Oceanic Data Base (MODB) are used

The question we asked the model was a simple one. How deep could the winter mixing go and to what extent did the vertical transport alter the surface values of nutrient concentrations?

We were not interested to accurately reproduce the mixed layer evolution in the area, but only to verify the intensity of the winter convection in a "mean" Ionian condition.

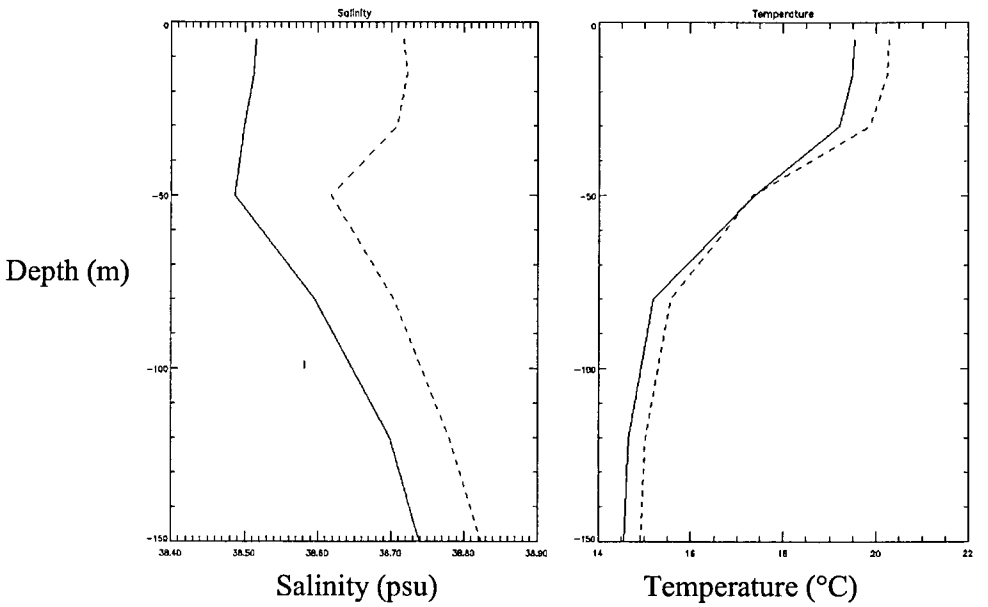

Figure 7-5. Salinity (left) and temperature (right) profiles used for the mixed layer model initialisation. Solid line refers to the I01 station location; dashed line refers to the S06 station location.

The outputs of the model (Figure 7-6) demonstrate that, neglecting the lateral advection and the mesoscale and sub-mesoscale structures, the atmospheric forcing in the area would have allowed a convective mixing down to 100 m, in the mean Ionian water column. Therefore, only in the areas where the nutricline was above 100 m or where a less buoyant water column was present, a significant transport could have occurred.

The available data for 1999 show that the simulations of the mixed layer depth are in good agreement with the in-situ data and that the nutricline was still below that depth, which might suggest that the response in the surface layer might have been absent. Only in the station I01 in winter a difference between in situ and simulated mixed layer depth is observable. In fact the station is located in a region where a cyclonic circulation was observed in the winter 1999 (Manca, 2000), i.e. in a hydrographic regime where the 1D model, initialized with climatological hydrological profiles, does not work properly.

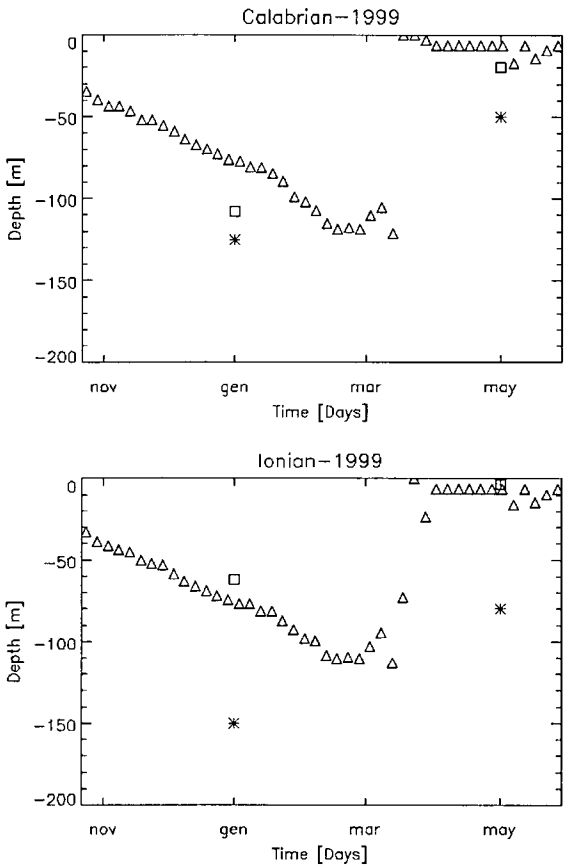

Figure 7-6. Time evolution of the mixed layer depth in the Calabrian Bloom region (upper panel) and in the Eastern Ionian region (lower panel) for the year 1999. Triangles indicate the output of the model. Squares indicate the measured mixed layer depths. Asterisks indicate the depths of the measured nutricline.

It can be also noted (Figure 7-1) that the chlorophyll-*a* patch displays a quite homogeneous concentration and extends over the shelf-break toward the coast. In other words, it is not just centered on the structure described by Manca (2000). Therefore, it is possible to hypothesize the following: buoyancy fluxes during the years 1998, 1999 and 2000 were not strong enough to produce convection down to 120-150 m, i.e., the depth where nitrate concentration was high enough to alter the transport into the photic zone and sustain a greater biomass. The doming produced by the cyclonic circulation released the constraint in the Northwestern area, but we suspect that the W-E asymmetry of the patch in respect to the location of the cyclonic structure is due to the interaction of the haline front that separates the coastal current from offshore waters and

the cyclonic circulation, that very likely generates a strong ageostrophic component on the western rim of the structure, thus making the vertical transport more effective.

In other words, the previous satellite observations confirm what the oceanographic community had already hypothesized and Stratford and Haines (2002) analysis had anticipated: the EMT needed a concourse of different processes, such as the uplift of the nitrate maximum, the buoyancy loss of the upper part of the water column and a dynamic scenario (doming, frontal divergence, etc) to be effective. The two latter events are quite typical of many regions of the global ocean and are, as analyzed, the factors controlling the RG bloom, the SA bloom and partially the NWMED bloom, whereas the former event is the novel contribution due to the EMT and explains, in our view, the absence of the CB during the CZCS years. In addition, modeling studies (Pinardi and Masetti, 2000) suggest that also during the CZCS years the circulation in the North-Western Ionian during winter and spring was cyclonic, thus substantiating the hypothesis that was the pre-EMT location of the nitrate maximum to prevent the occurrence of CB.

Furthermore the observed reversal of the circulation has only recently been reported and its short life is supported by the wind pattern over the basin (Manca, 2000; Manca, et al., 2002). On the other hand, while in the late eighties there is a strong evidence of an anticyclonic circulation in the late summer (Malanotte-Rizzoli and al., 1997) at the beginning of the nineties all the observations converge in assessing that the circulation kept an anticyclonic rotation all year round.

Then the question rises on what happened during the years where the SeaWiFS was not yet active and when the supposed change started.

The question was addressed again relying on remote sensing. Advanced Very High Resolution Radiometer (AVHRR) data can contribute to investigate the interannual variability of the Sea Surface Temperature (SST) distribution in the Ionian Sea in a period of time that goes from pre-EMT to now. Even if SST distribution does not

strictly reproduce the surface circulation it can represent an interesting proxy to discuss some aspects of variability of the general circulation.

An analysis of the interannual variability of the surface temperature field in the Eastern Mediterranean Sea has already been described by Marullo et al. (1999) for the period 1984-1992.

They found that the winter SST distribution in the Ionian Sea was essentially zonal for the period 1984-1990. From their analysis, it results that the years from 1985 to 1990 show an overall zonal pattern of the isotherms, suggesting that the Atlantic Ionian Stream (AIS) jet follows the typical path of the winter climatology, i.e. much closer to the southern boundary of the basin. In 1991 and 1992 they observed a winter SST pattern much more resembling the summer situation, with the warm water of the Gulf of Sirte spreading over the Ionian interior, suggesting the presence of an overall anticyclonic tendency of the Ionian circulation.

Extending the Marullo et al. (1999) SST time series to the entire decade up to 2000, it appears evident that the "anomalous" winters 1991 and 1992 were in effect the first two years of a longer transient period that lasted until 1997.

Figure 7-7 illustrates the Ionian winter SST distribution during the last four years of the decade, from 1997 to 2000. In 1997 the transient anticyclonic SST distribution is still present, but, since 1998, the SST field reverts to the 80's picture described by Marullo et al. (1999).

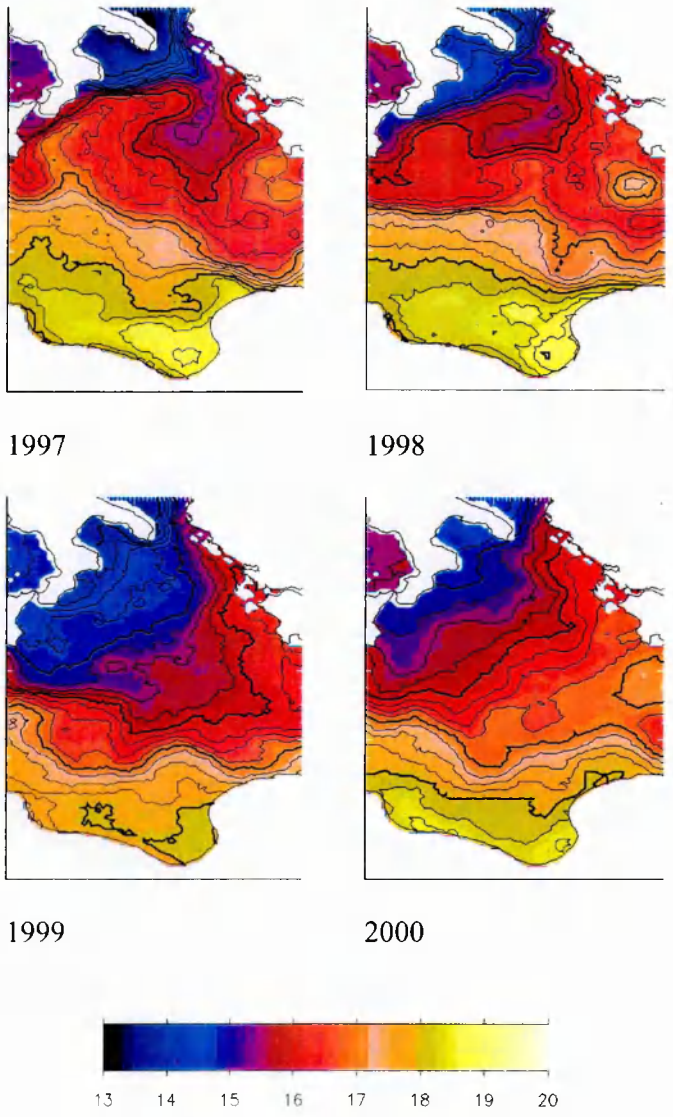

Figure 7-7. Winter averaged maps of the AVHRR-derived Sea Surface Temperature in the Ionian Sea for the years 1997,1998,1999 and 2000

In the years from 1998 to 2000 the SST distribution indicates that the warmer waters of the south Ionian tend to propagate northward in the eastern side of the Ionian Sea while the colder surface waters in northwestern Ionian Sea (probably of Adriatic origin) protrude southward on the western side suggesting the presence of a general cyclonic tendency of the circulation.

This description also agrees with the recent results of Larnicol et al. (2002), which analyzed seven years of altimeter and SST data (from 1993-1999) on the Mediterranean Sea. In particular the Sea Level Anomaly (SLA) seasonal averaged maps in the Ionian

Sea show a cyclonic circulation in the Northern part of the basin developed after the 1997 and not evident before.

In addition, they demonstrated that the structure is strengthened in 1999, when the rest of the basin remains substantially unchanged.

In synthesis, the time series of the winter SST distribution in the Ionian Sea and the results of Larnicol et al (2002) support the hypothesis of the presence of a cyclonic circulation until 1989 that switched to anticyclonic from 1990 to 1997, to return to a cyclonic pattern from 1998 onwards. The intrusion of warm waters in the Northern Ionian region, as a consequence of the winter anticyclonic regime of the surface layer, weakened the winter convective overturning in the years 1990-1997. After the EMT (i.e. after 1997), the reestablishment of the winter cyclonic circulation and the consequent cooling of the sea surface temperature in the area, facilitated a more efficient winter vertical mixing. Therefore, during the EMT, the weakened vertical mixing reduced the entrainment of nutrient to the surface layer, even if an uplifting of the nutricline due to the EMT was observed, while, after 1991, the hydrographic conditions of the basin became favorable to the injection of uplifted nutrients in the upper layer.

7.4 SYNTHESIS

The ocean color data analysed in the previous paragraphs (and in the previous chapters) highlighted that the Levantine basin did not appear to have been affected by the EMT. The statement is consistent with the existing analyses of the water property redistribution after the EMT. The study of the evolution of the RG bloom demonstrated that the pre-EMT and post-EMT dynamics were basically the same, i.e., a dynamics driven by the convective events in a permanent cyclonic structure. Other areas of the EMED showed a very similar dynamics in the two periods considered. As already pointed out, this is probably the most important result of the present analysis. Even in

presence of large and dramatic change in the thermohaline circulation and in the distributions of nutrient, the biological activity of the epipelagos remained substantially unaltered. The hypothesis presented here, in agreement with previous suggestions from other authors, is that the EMT changed the intermediate and deep behavior of the basin, but was not able to affect the upper layer.

By contrast, the pre-EMT and post-EMT patterns of biomass distribution in the Northwestern Ionian Sea and in the South Adriatic were different. Santoleri et al. (2003) demonstrated that the SA bloom increased its amplitude in the period just following the EMT, and related such change to the atmospheric forcing and to the increase of nutrient in the area due to the EMT.

Here, the study was focused on the NorthWestern Ionian region. Prior to the EMT there was an evident, though small, increase in chlorophyll-*a* concentration offshore the Calabrian coast, at the time of the spring bloom, with a consistent onshore-offshore gradient, probably fed by upwelling events and/or land runoff. After the onset of the EMT a recurrent and large bloom was detectable, which encompasses a wide area of the Northwestern Ionian Sea. This bloom did not accumulate large quantities of biomass (chlorophyll-*a* up to 0.8 mg m^{-3}) but was a novel feature of the basin. An in depth analysis of the existing data strongly suggests that the CB was linked to the changes due to the EMT because, without the uplift of nutricline caused by the EMT, the nutrient needed to sustain a bloom would have been unavailable. Furthermore, the analysis suggests that a series of concurrent factors such as doming and convection were present to favor the transport of nutrient to the photic zone and that this occurred only in particular restricted areas.

In conclusion the EMT did not affect the surface biological dynamic of the EMED, principally because the uplifted nutrients remained in layers that cannot be reached with the typical forcing of the area, except for the western Ionian Sea and the SA region.

CHAPTER 8

Discussion

The main scope of my study was to reconstruct the time and space variability of phytoplankton distributions in the Mediterranean surface waters in order to:

- reassess the seasonal patterns of plankton growth, which were previously based on coastal data, modeling studies and the coarse CZCS time series;
- confirm and interpret the zonal and latitudinal gradients observed both in situ and through the CZCS time series;
- determine the biologically most active areas at the level of primary producers, and confirm or improve the existing knowledge on their functioning;
- reassess the total production of the different basins and determine the year-to-year fluctuations related to changes in amplitude and phase of phytoplankton growth so as to infer possible changes in the functioning of the food web;
- analyze the interannual variability in the amplitude and phase of phytoplankton blooms or growth and detect the existence of trends in Mediterranean functioning as well as the response of plankton communities to recent climatic fluctuations that occurred in the nineties in the Eastern Mediterranean.

All the above in order to improve the available tools for a better prediction of the response of marine systems to global climate change.

The results of the study will be discussed focusing on the six themes listed below, which better lead to the conclusions reached on the defined questions.

- Bio-optical response
- Patchy distribution of blooming areas

- Zonal and latitudinal gradients
- Interannual variability
- The diverse role of atmospheric processes
- Long term trends

8.1 BIO-OPTICAL RESPONSE

Two different validation exercises were carried out to validate the SeaWiFS satellite data in the Mediterranean.

The first addressed mainly the performance of the SeaWiFS sensor, and resulted in a new chlorophyll-*a* algorithm, which substantially decreased the error on chlorophyll-*a* retrieval in the Mediterranean from satellite observations.

This also conducted to discuss plausible hypotheses on the reasons of the particular bio-optical characteristics of the basin such as, e.g., the presence of coccolithophores or of a greater than normally reported concentration of yellow substance.

The main aim of the second validation exercise was the definition of the errors due to the atmospheric correction procedure, and the assessment of the induced error on the chlorophyll-*a* estimates. The issue was addressed using AERONET in situ data and few matchup points of concurrent satellite and in situ radiances and chlorophyll-*a* concentrations (the total matchup data set). The analysis revealed that the atmospheric correction procedure is the primary source of error for the retrieval of chlorophyll-*a* in the Mediterranean. The conclusion was that it accounts for approximately 25% of uncertainty in the final chlorophyll-*a* estimates (see Chapter 3). The limited data set and the lack of an appropriate radiative atmospheric-water model (which was out of the aim of the present research) did not permit to clearly define the source of errors. However, a hypothesis on the effect of the high atmospheric pressure events that occur regularly in the Mediterranean area, was proposed after the analysis of the total matchup data set.

In conclusion, the development and the application of DORMA algorithm seems to mitigate the two observed problems.

Even if the reasons leading to the errors in the satellite data are not fully understood, the utilization of the DORMA algorithm should prevent large errors in the chlorophyll-*a* concentration estimates. The sole use of 490/555 ratio should decrease the bias coming from defective atmospheric correction, while the particular Mediterranean bio-optical response should be accounted for in the statistical regression giving the algorithm coefficients.

The analysis on the retrieved algorithm has two additional implications.

Firstly, the bio-optical response of the Mediterranean waters is such that the global ocean color algorithms fail in retrieving chlorophyll-*a*. In other words, the Mediterranean waters, on average, contain optical relevant components, which alter their color. Even if the characteristics of those components are still unknown, they could reflect peculiar aspects of the functioning of the Mediterranean ecosystem. As anticipated above, the anomalous radiance ratios were related in the recent past to the presence of coccolitophores (Gitelson, et al., 1996) or to an unforeseen concentration of yellow substance. Recently, Claustre et al. (2002) supposed that the presence of dust particles in the surface Mediterranean waters could be the main responsible of the anomalous radiance ratios. Whatever the answer is, all the above mentioned putative causes call for further inspections

The second result of the CAL/VAL exercise confirms and enlarges to the physical domain the preceding statements. The failure of the atmospheric correction procedure for the Mediterranean is mainly due to the high variability of the atmospheric and aerosols terms. Both influence the biota as external forcing and as additional carriers of available nutrients (see Guerzoni, et al., 1997, for a detailed review) adding supplementary sources of variability to the biomass field.

In other words, simple models of phytoplankton dynamics applied to the Mediterranean might likely to fail if not all of the physical and biological interactions (simply outlined in the CAL/VAL activities) are not taken into account.

As a final consideration, it is important to remember that in the recent past a series of new ocean color sensors became operational. They represent a further evolution in the visible remote sensing and are considered the new-generation of ocean color sensors. The most relevant are undoubtedly the Moderate Resolution Imaging Spectroradiometer (MODIS) from NASA and the MEdium Resolution Imaging Spectrometer (MERIS) from ESA. The two NASA-MODIS sensors are mounted on the Terra and Aqua satellites and supply data since 2000/2003, whereas the ESA MERIS instrument (onboard of the ENVISAT satellite launched in March 2002) is still in the commitment phase. They doubled the number of bands respect to SeaWiFS, and include also channels in the range 660-720 nm, which measure the Sun-induced *in-vivo* fluorescence (Gower, et al., 1999). In addition, the new sensors benefit from major instrumental improvements, such as an increased radiometric accuracy and sensitivity. However, the theoretical and practical backgrounds of these new sensors are not far from SeaWiFS, and so could be subject to similar inaccuracy, mainly in the atmospheric terms.

More interesting is the recent development of two automatic marine-buoys, equipped with optical sensors and deployed in open ocean environments. The first buoy is already operative and it was deployed not far from the Mediterranean (English Channel, Pinkerton, et al., 2003). The other, which will positioned in the Ligurian Sea, close to the DYFAMED station, experienced some problems in the set-up, but it should become operative during the next months (Report of the International Ocean Color Coordinating Group Meeting, Florence, Italy February 2003)

The impact of their data in the error assessment of the ocean color remote sensing, could be crucial in areas, as the Mediterranean, which challenge the full exploitation of the sensors working in the visible light spectrum. In addition, as already presented by

Pinkerton et al. (2003), they could be also important in the assessment of the errors of SeaWiFS data, in verifying the performance of the NASA vicarious calibration and allowing, if the case, for variations in the calibration factors for the areas where they fail.

However, even with the availability of such new instruments, CAL/VAL studies, as the one carried out in my research, will remain relevant for verifying, and in some cases correcting, the satellite estimates in specific regions.

8.2 PATCHY DISTRIBUTION OF BLOOMING AREAS

Apart from the coastal runoff driven areas, most of the Mediterranean blooming areas are driven by the deep convection. It is worth noting that this mechanism acts also for the Rhodes gyre. It is well known that intermediate convection occurs there every year, but the real bloom seems to be associated only with the deep convection.

Surface convection occurs throughout the ocean (see the review by Marshall and Schott, 1999) in response to a surface buoyancy loss or wind stirring: the combination of solar irradiance and atmospheric forcing induces characteristic diurnal and seasonal cycles in the mixed layer thickness. Convection increases the surface nutrient concentrations whenever the mixed layer thickens and nutrients are entrained from below the underlying pycnocline. The maximum thickness of the mixed layer usually occurs just before the end of winter (defined by the time when the surface buoyancy loss to the atmosphere ceases) and denotes the extent of the seasonal boundary layer. Deep convection occurs when particularly intense surface buoyancy loss and wind stirring act on pre-formed favourable density field, provoking a mixed layer extending down and eventually reaching the bottom. Deep convection involves an overturning of dense water in narrow plumes with horizontal scales of a few kilometers (Marshall and Schott, 1999). In the Mediterranean, the maximum thickness of the mixed layer is on average 100-120 m in the WMED (Pinardi and Korres, 2002) and 80-100 (Krom, et al.,

1992) in the EMED. The main differences between deep convection and seasonal winter overturning reside in the spatial scales of the involved process. The effects of these differences were analyzed during this study utilizing simple approaches based on 1-D mixed layer models combined with realistic forcing. The results can be summarized as follows:

- in Mediterranean, interplay among the intensity of the external forcing, the typical hydrodynamic conditions and the characteristic depth of the nutricline generally prevents an efficient nutrient re-fuelling of the upper layers during the seasonal overturning (see Chapter 7). There are very few sites were the above constraints are relaxed, as for example, in North Western Ionian Sea after the 1998 or in the Alboran Sea.
- only in deep convection regions, where the convective processes are amplified, phytoplankton blooms are observed in surface layers. Furthermore, the pre-conditions needed to trigger the deep convection (i.e. cyclonic regimes), provoke also an uplift of the nutricline, which in turn facilitates a larger nutrient vertical flux and enhances the biomass growth.
- on the other hand the relationship between deep convection and phytoplankton growth is not linear. Even if the observed or modelled mixed layer depth accounts for most of the observed dynamics of the bloom variability, a description of the phytoplankton evolution based only on that single physical process does not, always, account for the observed dynamics, as is the case of South Adriatic gyre.

A more detailed analysis is required for the NWMED area where most of the cited processes are superimposed.

It is noteworthy that the impressive bloom observed from space is not equaled by other blooms occurring in the basin. Furthermore, the bloom experiences a high variability in the spatial extension, though displaying less variability in the duration.

Even when the bloom was not particularly intense (i.e. in 1998 when only a reduced area was affected by the biomass increase), the feature was observed for two months, starting in late February and disappearing only in May.

The bloom extends often up to the Ligurian coast, hundreds of kilometres from the deep-water formation area and the only constant feature exhibited by the bloom is the presence of a southern limit at the North Balearic front.

In their numerical approach, Levy et al. (2000) demonstrated that the small-scale processes (both marine and atmospheric) are essential to describe the variability of the bloom. They claimed that the bloom could be described considering only the physical characteristics of the area (mainly the large cyclonic circulation and the intense cooling of the surface water leading to the deep-water formation and to the nutrients injection in the surface layer) and concluded that the wind bursts and their high frequency variability was modulating the "efficiency" of the nutrient uptake and was the putative determinant in the variability of the chlorophyll-*a* field.

Satellite observations confirm this picture only partially: the deep-water formation event and its driving mechanisms alone cannot explain the particular characteristics of the NWMED bloom. Even if the relative importance of the different physical-biological factors making the region most favourable for a bloom are not easy quantified, it is possible, however, to outline some specific points highlighted by the remote sensing observations.

- The deep-water formation event (defined as an homogenization of the water column down to the bottom) cannot be considered the primary cause of the whole phytoplanktonic bloom. The distance between the mixed patch area and other regions with very high values of biomass (i.e. the Ligurian Sea) suggest that in this site also winter overturning is playing a role. More important, the "blue hole" observed in the SeaWiFS images, indicating the deep-water formation, is surrounded by a "light green" area (0.2-0.3 mg m^{-3} of chlorophyll

concentration), suggesting that the bloom starts before the end of deep convection.

- On the other hand, in all the years studied, the mixed patch area shows very high values of chlorophyll concentration at the end of the deep-water formation event. Even when the bloom appears limited in size (e.g. 2001), the region with the maximum values in chlorophyll concentration is always coincident with the mixed patch area.
- Also, the long duration of the bloom and its extension in some years rule out the recapping of the mixed patch as the main process, keeping the phytoplankton in the photic zone. Similar conditions occur over the whole area, from the Balearic Sea to the Ligurian Sea. Instead, the intense and continuous winds stirring occurring throughout the winter mix, the water column and frequently prevent the utilization of the upwelled nutrient. When the wind weakens, the response of phytoplankton is immediate and the entire stock of nutrients previously accumulated can be consumed. Such effect seems to be crucial to explain the temporal and spatial patterns of the bloom (see also later).
- Finally, the bloom does not always appear as an unique process but is separated in two or three different structures, which follow different life histories.

In general terms, the role of the wind control on phytoplankton dynamics can be summarized as follows:

- The wind induces the upper layer surface circulation ("wind driven circulation"), which controls partially the basin scale dynamics (for example in provoking the pre-conditions for deep water formation). In second order, then, it drives also the surface and sub-surface nutrient distributions;
- It modifies the local effect of the air-sea exchanges (the wind is considered in the computation of both the sensible and latent heat fluxes, via bulk formula).

Though, it is one of the co-causes of the dynamics of the heat-fluxes, which in turn control the seasonal overturning, first engine of the upper layer fertilization;

- Wind effects modulate the mixing rate in surface, stirring the upper layers and breaking, even if partially, the thermal stratification of the water column. This fact, as observed also in the NWMED area, can have a direct effect on the phytoplankton dynamics, and, depending on the bloom condition, could result in an enhancement or in a decreasing of the biomass growth.

An in situ study carried out at DYFAMED (Anderson and Prieur, 2000) showed that even in May (at the end of the bloom period) the nutricline was sufficiently shallow (20-40 m), so that a relatively strong wind burst could easily induce an injection of nutrients in the surface layer. In this situation, the deep-water formation event adds a positive feedback, intensifying the mixing and increasing the vertical advection, but does not act as the bloom's primary engine.

Therefore, the wind field (with its spatial and temporal fine structure), superimposed on the favourable hydrodynamic large-scale cyclonic circulation, rules the observed chlorophyll field and the exceptionally long duration of the phytoplanktonic bloom, as observed by the satellite, in addition to the "classical" sequence: convection, stratification, bloom. This supports, to a certain extent, the analysis of Levy et al. (2000), but also explains why the thermal stratification is not a prerequisite for the bloom initiation.

In summary, the NWMED bloom is quite complex and peculiar as compared with the other Mediterranean blooms. However, I showed how the described multi-platform approach can partially explain the evolution of the Mediterranean blooms, providing tools for predictive analysis.

Finally, one aspect has to be highlighted. Table 8-1 reports the mean values of PP, total Primary Production (TPP calculated multiplying the PP for the area of the selected region) and chlorophyll-*a* concentration, for the whole Mediterranean, the two main

sub-basins and the areas of main blooms, respectively. The total production due to the main blooms (derived from the relative TPP values for each area) amounts to $32.87*10^{12}$ gC $year^{-1}$, then, only the 12% of the TPP of the whole basin. In other words, even if the bloom regions are crucial to drive the carbon export to the deep layers, in terms of total productivity they represent only a small fraction of the basin activity.

	Chl (mg/m^3)	PP ($gCm^{-2}yr^{-1}$)	TPP ($10^{12}gCyr^{-1}$)	TPP% sub basin	TPP% MED
EMED	0.12	105.37	170.71		
EMED Blooms			4.68	2.7	1.7
Calabrian	0.12	107.53	0.88	0.5	0.3
South Adriatic	0.17	114.49	3.15	1.8	1.2
Rhodes Gyre	0.10	104.39	0.65	0.4	0.2
WMED	0.21	122.78	100.68		
WMED Blooms			28.19	28.0	10.3
Alboran	0.38	157.96	9.11	9.0	3.3
NWMED	0.24	129.62	13.50	13.4	4.9
Ligurian	0.26	123.87	5.57	5.5	2.0
MED	0.16	112.37	272.83		
MED Blooms			32.87		12.0

Table 8-1. Average chlorophyll-*a* concentrations, PP and the TPP for the bloom areas considered. TPP percentages are relative to the main sub-basins.

8.3 ZONAL AND LATITUDINAL GRADIENTS

Chapter 4 and 5 were devoted to study the seasonal and climatological patterns of both chlorophyll and PP in the basin, evidenced by monthly and seasonally averaged maps. North-South and East-West gradients are detectable for most of the year and throughout the basin and, together with the cited relationship deep convection/blooms, can be considered a peculiar characteristic of the Mediterranean.

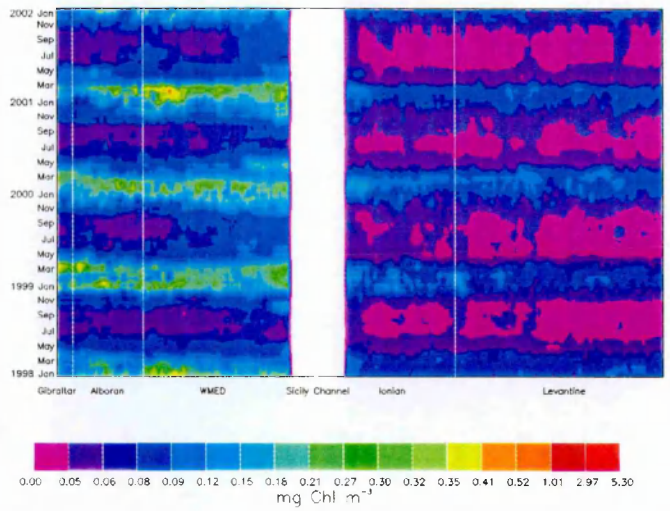

Figure 8-1. Chlorophyll concentration for the transect 1 (see Figure 8-2 for the location of the transect)

The East-West distribution of the Mediterranean surface biomass is evident in Figure 8-1, where a transect, derived from values extracted from the SeaWiFS chlorophyll-*a* imageries in the years 1998-2001, is shown (see Figure 8-2 for the definition of the transec3t). The strong oligotrophy of the EMED is clearly evident, as well as the enhanced biomass in January-February in the WMED, due to the Alboran and Algerian basin dynamics.

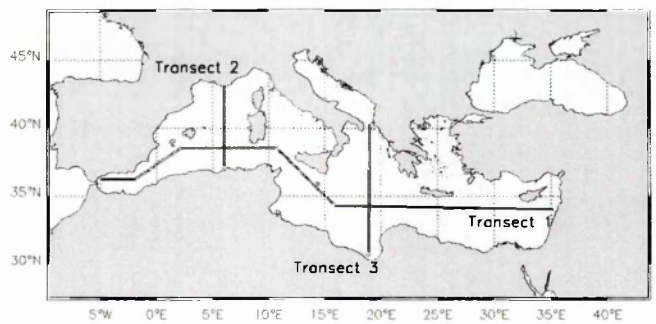

Figure 8-2. Definition of the transects.

However, excluding such regions, also the WMED displays large oligotrophic patterns, only slightly richer in biomass than the ones observed in the EMED. A similar plot derived by the PP maps (Figure 8-3) confirms the described picture, with the WMED regions similarly productive for most of the year and the EMED ones exhibiting a more pronounced seasonal variability.

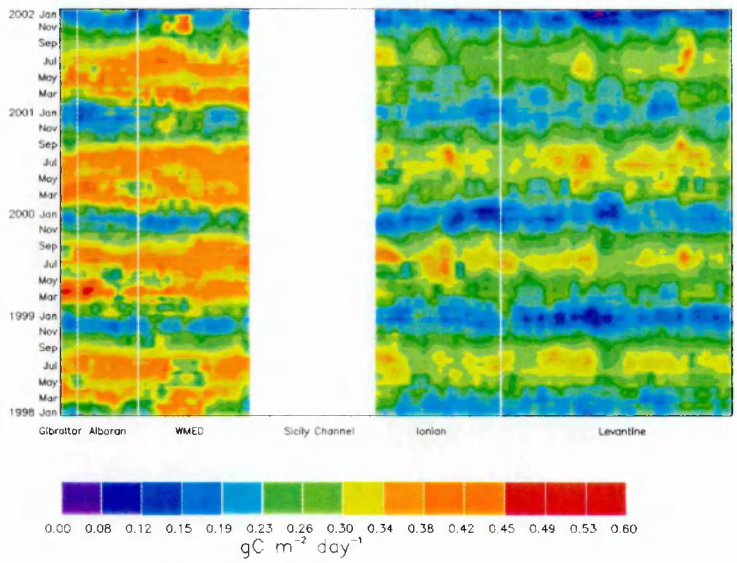

Figure 8-3. Primary production for the transect 1 (see Figure 8-2 for the location of the transect)

In terms of annual budgets, however, the gap appears less pronounced. Figure 8-4 displays the incremental chlorophyll-*a* concentration and PP in the period covered by my analysis (1998-2001) for the EMED and the WMED, respectively. Incremental values are calculated adding the chlorophyll-*a* concentration or the PP of the day *n* to the cumulative value up to day *n-1*, starting from October 1 of each year.

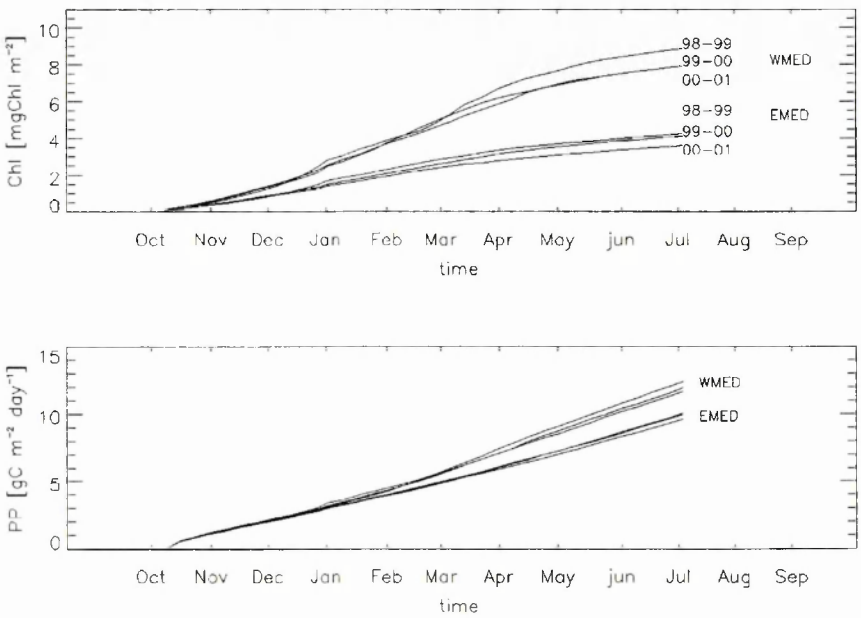

Figure 8-4. Incremental chlorophyll concentration (upper panel) and Primary production (lower panel) for the four years considered and for the two main Mediterranean sub-basins.

After a one-year cycle, the values obtained for PP in the two sub-basins do not differ significantly, whereas the correspondent total incremental chlorophyll-*a* concentrations are definitively different. Undoubtedly, the PP estimates are less accurate than the chlorophyll-*a* concentrations, because they include uncertainties due to the simplifications embedded in the model but, as we noted before, they are only slightly higher than recent assessments obtained with different methodologies (see Table 1-1 in the Introduction) and then can be considered realistic.

It is however important to note, that the incremental chlorophyll-*a* as defined above, does not reflect a rate of accumulation, rather it expresses the average value over the given time interval, multiplied by that interval. Therefore a constant slope indicates a constant chlorophyll concentration, and the slope itself is proportional to that concentration. Two features are evidenced by the analysis of the plots. From October to mid January the PP is almost identical in the two basins but in the EMED it is based on a lower biomass standing stock and in the WMED produces a higher accumulation rate of biomass. This, in turn, suggests more favorable conditions (mostly light) and faster recycling in the EMED than in the WMED. From January until early May there is a significant difference in the slope among the two subbasins. This again reflects the more intense phytoplankton accumulation in the WMED as compared to EMED, which in this case illustrates the different manifestation of the Winter-Spring bloom in the two subbasins.

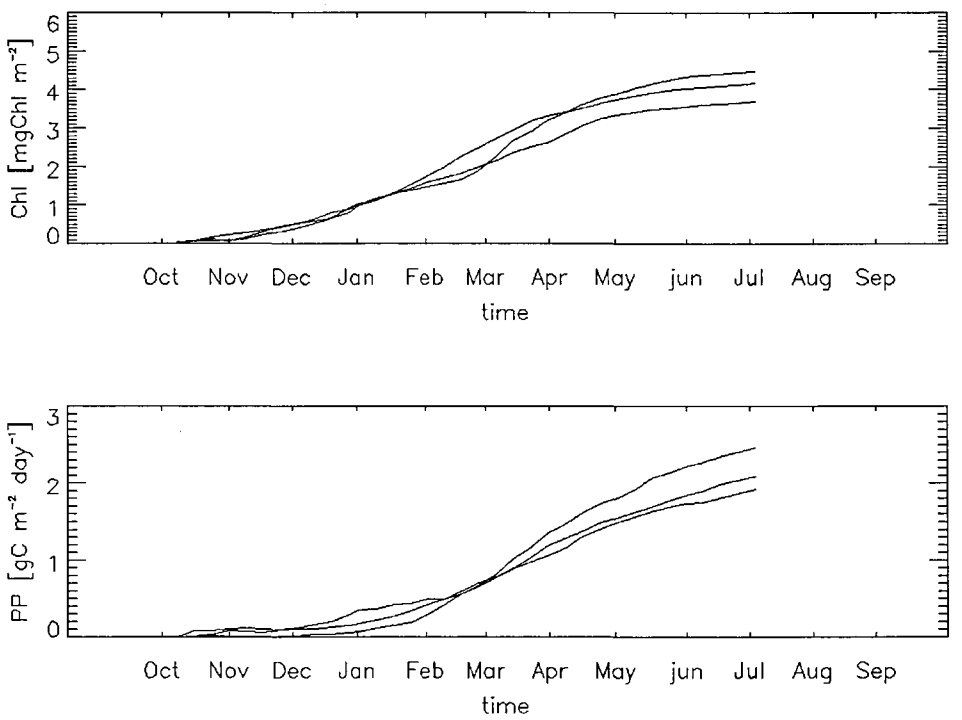

Figure 8-5. Difference between interannual average of incremental chlorophyll-*a* and PP of the WMED versus the EMED

All the above is even better evidenced by the difference among the interannual average of both chlorophyll-*a* and PP of the two subbasins (Figure 8-5).

During the winter months the PP of the EMED basin reaches higher values than in autumn and in some case equals the WMED values, which causes the east-west gradient to be very weak or almost non-existent in the November and December (see also the climatological maps).

In Chapter 4 the comparative analysis between the chlorophyll-*a* surface fields and the "good weather" maps derived from the ECMWF data were discussed. The number of days with favorable whether conditions in October and November was generally higher in the EMED (7-11) than in the WMED (4-7), and this fact was considered the main cause of the absence of bloom conditions (in terms of chlorophyll-*a* concentration) in the EMED region during the following months. The impact of the weather may be hypothesized as follows. A high number of days with "good weather" conditions

provoke a relatively weak winter mixing (also emphasized by the model outputs of the mixed layer depth discussed in paragraph 7.3.3). This fact should induce a less effective refueling of nutrients in the surface layers, which would result poor in nutrients at the end of the winter. In addition, the steady utilization of the nutrients also because of the 'good' whether precludes any significant accumulation and, therefore, depresses the fraction of the new production versus the total production. This is clearly summarized in Table 8-2. Even if chlorophyll-*a* values are substantially lower in the EMED, the high number of favorable days during the fall months enhances the PP in the region.

In October and November, the number of days with favorable conditions is almost twice in the EMED than in the WMED basin, which drives the EMED versus a steady, relatively low production, and creates the preconditioning for the spring subbasin differences. The steady production allowed by the increased solar radiation due to the low cloudiness and the different light availability in the WMED dampen, or even, invert the West-East gradient, making possible a 60% increase of chlorophyll-*a* concentration in the EMED from October to December.

	# of "good weather days"		**Mean Chlorophyll Concentration ($mg\ m^{-3}$)**		**Mean Primary Production ($gCm^{-2}yr^{-1}$)**	
	EMED	**WMED**	**EMED**	**WMED**	**EMED**	**WMED**
October	11	7	0.095	0.137	0.26	0.27
November	7	4	0.121	0.207	0.23	0.24
December	5	5	0.151	0.27	0.22	0.24
March	/	/	0.131	0.324	0.27	0.38

Table 8-2. Summary of the mean values of chlorophyll concentration, primary production and number of good weather days.

In other words, the environmental factors, which make the two sub-basins different, are not constant throughout the year and in late fall-early winter, the east-west gradients are strongly reduced (compare for example the data in Table 8-2 relative to March), to disappear in some cases.

What is then the impact of the east-west gradients on total budget of PP in the Mediterranean?

Due to its greater extension, the total quantity of fixed carbon in the EMED results 70% higher than in the WMED (see Table 8-1). That number is further increased if the mean contributions of the bloom areas are subtracted from the absolute values of TPP. The difference between the two sub-basins would then amount to approximately one third of the total production of the basin, which means that the EMED would double the production of the WMED.

Since the surface of the EMED is approximately two times that of the WMED, this suggests that if it were not for the blooms, the two subbasins would display a very similar trophic regime. In other words, even if the contribution of the blooms to the annual budget of the basin is weak, it is important in balancing the diverse regimes of the two sub-basins, and then in maintaining the observed gradient.

A last comment has to be added.

The reconstruction I made of the different seasonal patterns in the two basins was essentially based on the light regime and the time-course of the mixed layer depth. I did not refer to the other significant difference among the two subbasins, i.e., the value of the stream function (see Introduction). The prevalent anticyclonic vorticity in the EMED versus the prevalent cyclonic vorticity of the WMED certainly contribute to determine a different vertical transport of the nutrients and are a very important determinant in the formation of blooms. Being those features closely linked to the general circulation of the basin, which ultimately depends on the climate dynamics, drastic changes in the patterns of primary production might be expected as a consequence of climate change.

As for the north-south gradient, similar observations can be done. In the WMED, the strong activity of the NWMED area produces a constant gradient detectable throughout the year, only weakened during the winter months (see Figure 8-6).

Similarly, in the EMED the very low biomass concentrations and PP values in the areas southern of the 35°N parallel, keep for almost the year a strong latitudinal gradient (see Figure 8-7).

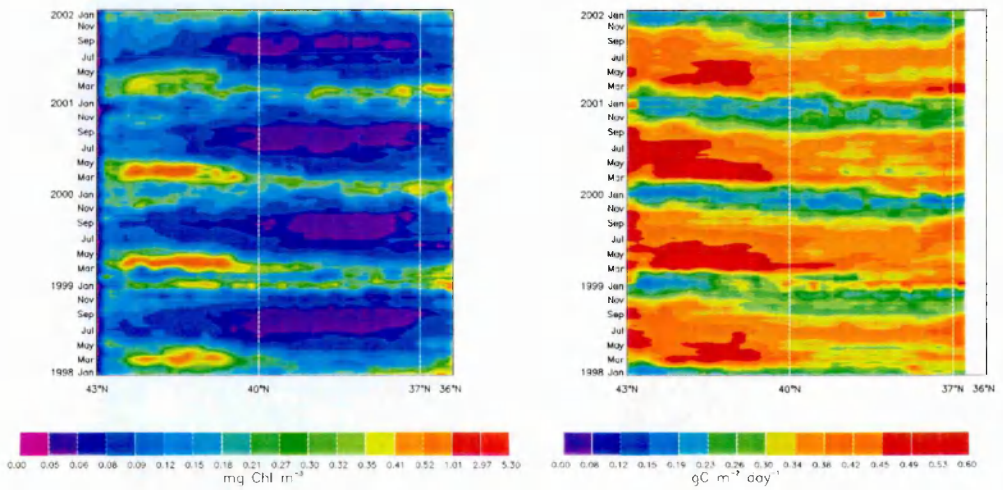

Figure 8-6. Chlorophyll concentration (left) and Primary Production (right) for the transect 2 (see Figure 8-2 for the location of the transect).

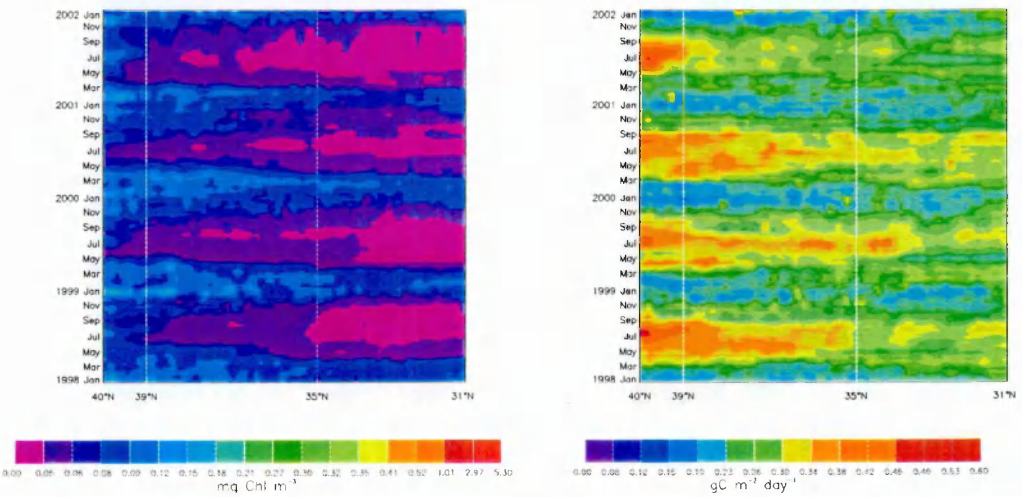

Figure 8-7. Chlorophyll concentration (left) and Primary Production (right) for the transect 3 (see Figure 8-2 for the location of the transect)

8.4 THE RELEVANCE OF THE INTERANNUAL VARIABILITY ON THE MEDITERRANEAN TROPHIC REGIME

The interannual variability was considered during the previous chapters mainly discussing the most relevant blooms of the basin. The results obtained demonstrated that the bloom areas experience a strong interannual variability, which can be partially explained in terms of external forcing (see later).

As already debated, the regions exhibiting strong and rapid biomass growth ("the blooms") are crucial for the carbon cycle of the basin and then require to be investigated in order to understand the key mechanisms of the processes associated.

Here, however, I will focus on the total budget of the Mediterranean, following a different approach, which was partially introduced before (see paragraph 8.2). Briefly, the Mediterranean was divided according to the trophic regimes, separating the bloom regions from the others. In this way the interannual variability of the Mediterranean was analyzed accounting also for the impacts of the bloom areas in determining it.

The mean TPP for the whole basin during the four years analyzed is 272.83 $*10^{12}$ gC $year^{-1}$ with interannual variations (Table 8-3) less then 4% (the highest difference is for 2001 -3.8%). Similarly, the interannual variability for the two main subbasins does not exceed 5%.

	MED		WMED		EMED	
	TPP	**%TPP bias**	**TPP**	**%TPP bias**	**TPP**	**%TPP bias**
1998	272.75	0.03	98	2.66	172.96	1.32
1999	279.24	2.35	104.63	3.93	173.39	1.57
2000	276.9	1.49	101.33	0.65	174.18	2.04
2001	262.43	3.81	98.74	1.92	162.29	4.93
Mean	272.83		100.675		170.705	

Table 8-3. Summary of the interannual TPP variability for the MED, WMED and EMED in the four analyzed years. The %TPP indicates the percentage bias of every year respect to the multi-years mean. TPP values are in 10^{12} gC yr^{-1}.

Table 8-4 displays the same statistics of Table 8-3, but determined subtracting to each TPP value the correspondent estimate relative to the bloom region (i.e. the TPP values for the EMED are derived subtracting to the EMED values in Table 8-3 the sum of the TPP values for the South Adriatic, the Calabrian and the Rhodes Gyre blooms).

	MED		WMED		EMED	
	TPP	**%TPP bias**	**TPP**	**%TPP bias**	**TPP**	**%TPP bias**
1998	243.95	0.73	70.52	2.72	168.13	1.27
1999	247.82	2.33	74.78	3.16	168.64	1.58
2000	246.85	1.93	73.32	1.14	169.37	2.01
2001	230.10	4.99	71.34	1.59	157.96	4.86
Mean	242.18		72.49		166.025	

Table 8-4. As for Table 8-3, but subtracting to each sub-basin the values correspondent to its blooms.

There is no significant difference among the two results, being the retrieved percent biases still under 5%. This result implies that the main interannual variability of the basin (and of its main subbasins) is not driven by the regions where the most intense biomass growth is observed. As demonstrated, the bloom regions experience a strong variability in terms of both biomass concentrations and size of the phenomena. This implies in turn that the "bloom" and the "no-bloom" areas follow different temporal evolutions and dynamics.

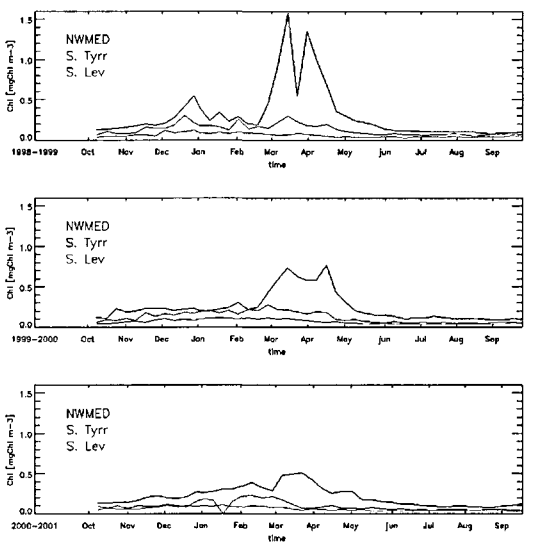

Figure 8-8. Time series of SeaWiFS chlorophyll concentration for the NWMED (black line), South Tyrrhenian (blue lines) and South Levantine (red lines) regions. Upper, central and lower panels refer to 1998-1999, 1999-2000 and 2000-2001 time series, respectively.

To verify the above results, a more detailed analysis was carried out, focusing on three different zones, supposed to be representatives of the two different trophic regimes ("bloom" and "no-bloom"). As example of a "bloom" area the NWMED region was selected, while for the "no-bloom" conditions the South Levantine and the South-Tyrrhenian were chosen. The first two are in turn the most and the less productive areas of the MED. The latter was selected because in the climatological and monthly maps displays a seasonal variability, but no intense phytoplankton growth.

From the SeaWiFS derived maps of chlorophyll-*a* concentrations and PP, the pixels comprised in the selected regions were extracted and averaged over the area, for the four years considered. To better follow the natural phytoplankton cycle, the time interval goes from October to the next October.

Figure 8-8 and Figure 8-9 show the temporal evolution in the three selected regions of the chlorophyll-*a* concentration and PP, respectively.

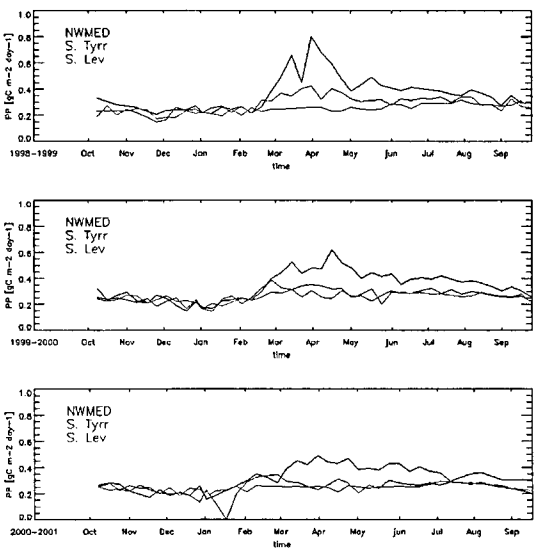

Figure 8-9. Time series of SeaWiFS derived Primary Production for the NWMED (black line), South Tyrrhenian (blue lines) and South Levantine (red lines) regions. Upper, central and lower panels refer to 1998-1999, 1999-2000 and 2000-2001 time series, respectively.

The "bloom" area (NWMED) enhances its activity during the spring months, to decrease afterwards in both chlorophyll-*a* concentration and PP (the latter slowly, the first very rapidly). Despite a large interannual variability, this trend is however kept

during all the years analyzed. By contrast, the "no-bloom" regions exhibit a weaker variability, in terms of both seasonal and interannual trends.

To verify the differences, Figure 8-8 was re-plotted, dividing the chlorophyll-*a* concentrations by the absolute maximum for each area and for each time window (Figure 8-10).

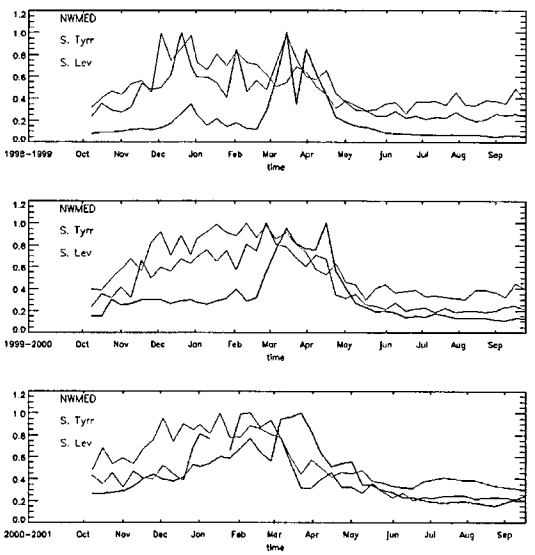

Figure 8-10. Time series of the relative chlorophyll for the three selected Mediterranean regions.

Several interesting features appear.

- As already noted, the NWMED region shows its extreme values in spring. The average pre-bloom concentrations are generally similar to the post-bloom ones. It is noteworthy, however, than when the bloom is weak (i.e. spring 2001) the relative concentrations (but also the absolute ones; compare upper and lower panels in Figure 8-8) start to increase in December, instead of March. In other words, the absence of a bloom event is compensated by a more diffuse chlorophyll increase, less intense but more spread over time. The net result is that the chlorophyll values temporally integrated over the year are not very different in the three years studied (i.e. 0.28 for the 1998-1999, 0.23 for the 1999-2000, 0.21 for the 2000-2001).

- Respect to the NWMED, the South Tyrrhenian area displays a temporal pattern more smoothed, though displaying a peak. The position of the maximum is, however, more variable respect to the NWMED. In the 1998-1999, for example, the absolute maximum occurs during December-1998. More interesting, in all the years studied, the region exhibits a peak in chlorophyll concentration, which is anticipated of 1-2 months respect to the NWMED absolute maximum.
- Similarly to the South Tyrrhenian, the South Levantine patterns are less sharp, showing almost undetectable peaks and a general trend to increase from October to March, followed by a rapid decline afterwards.

Considering the two "no-bloom" areas together, the temporal patterns appear as a two states system, which experiences a switch between the two conditions in April-May and in October-November. Such regime seems to be permanent during the years analyzed, explaining the weak interannual variability of the two sub-basins. By contrast, the "bloom" areas exhibit a more marked interannual variability, which can lead, under particular conditions, even to the absence of an intense bloom. When this happens, (i.e. 2000-2001) the temporal patterns of the area resemble those of the "no-bloom" regions.

8.5 THE DIVERSE ROLES OF THE ATMOSPHERIC PROCESSES

The conditions leading to a phytoplankton bloom in the open ocean are a sufficient concentration of nutrients in the upper layer and a favorable light field. Both are related to the seasonal cycle of the atmospheric processes, which rule the intensity of the winter overturning and of the PAR. The timing also plays a crucial role because, to be effective, the two conditions must co-occur.

The results of the analysis on the role of atmosphere forcing on the phytoplankton dynamics in the Mediterranean can be summarized as follows:

- The bloom areas are located were patterns of enhanced atmospheric forcing, studied here in terms of air-sea fluxes and wind stress, are present. Figures 8-11 show the climatological maps of total heat flux and wind stress as obtained by Demirov and Pinardi, (2002). Undoubtedly, the correspondence between areas of bloom and regions with strong atmospheric anomalies is striking, and it is also confirmed by Figure 8-12, which displays the winter Mediterranean nutrient concentration at 10 and 100 meters depth, as derived by the climatological database MEDAR-MEDATLAS. In fact, only where the atmospheric forcing is sufficiently intense, surface nutrient are enough high to sustain a large bloom. It is however important to note that such condition is necessary but not sufficient. The interplay between atmospheric forcing, nutrient upwelling and phytoplankton response is modulated by several other factors (i.e. hydrodynamic patterns or grazing effect), which in turn control the phytoplankton dynamics but also are controlled by the environmental conditions.

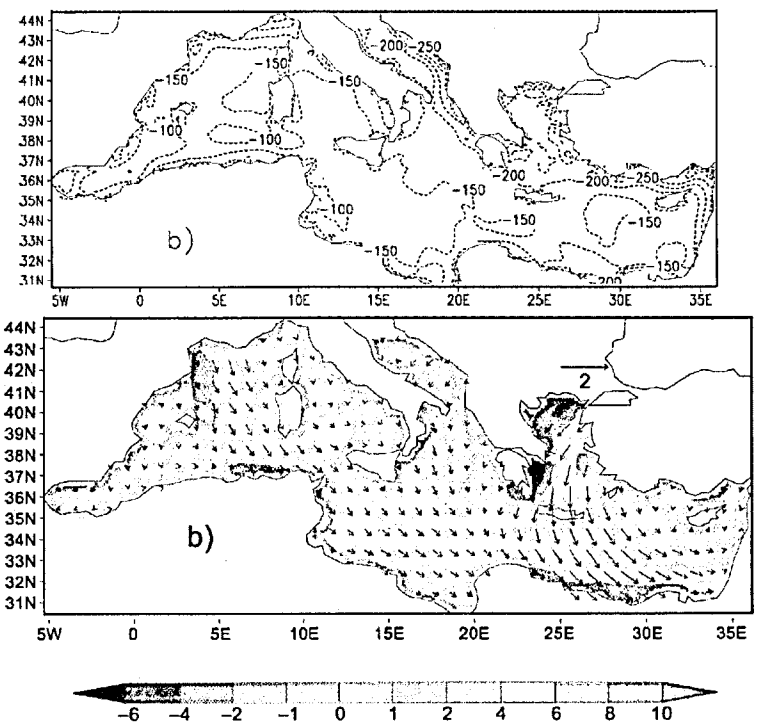

Figure 8-11. Winter (DJF) surface net heat flux (Upper panel in W/m^2), wind stress (arrows on lower panel in dyn/cm^2) and wind stress curl (lower panel 10^6 dyn/cm^3) averaged for years 1988–1993. (Redrawn by Demirov and Pinardi, 2002).

- As consequence, the phytoplankton response is not linear (see Adriatic), and to fully explain the observed interannual variability, the other factors must be considered. Notwithstanding, the match between anomalies in the atmospheric forcing and bloom areas is a striking feature of the Mediterranean Sea.

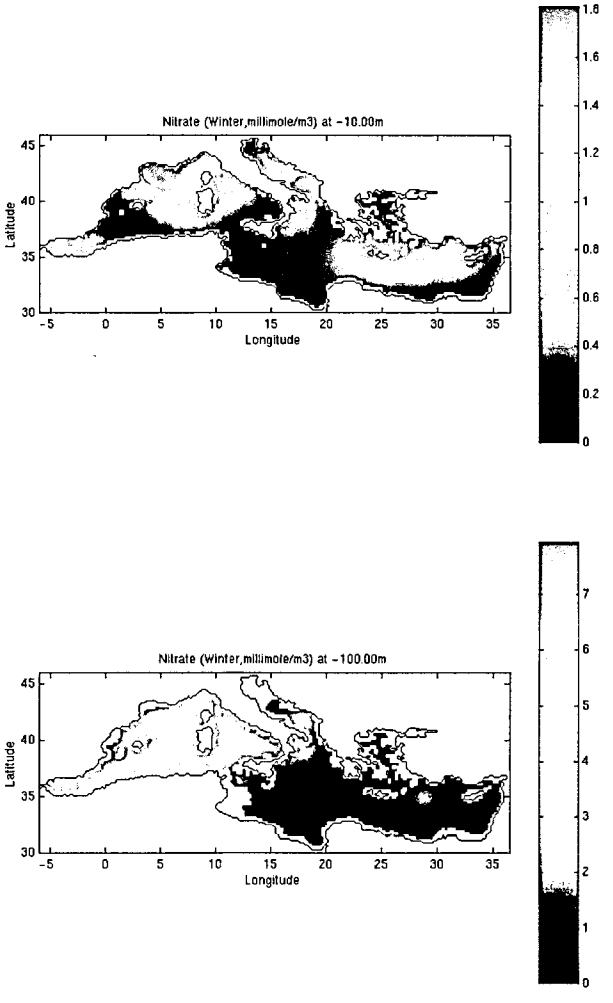

Figure 8-12. Winter Climatological Nutrients Concentration as derived by MEDAR-MEDATLAS data base. Upper panel shows the 10 m concentrations, while the lower the 100 m. Note that the scales on the palette are different and the units are millimole/m^3.

- As for the wind effect on the bloom area, an intense study was carried out in the NWMED region, exploiting the ECMWF and SeaWinds-derived surface wind fields. Confirming the results obtained by various authors, my analysis highlighted the role of wind as modulator of the phytoplankton growth, mainly when the bloom event was already set-on. The mechanism invoked here and

confirmed by other authors (i.e. Anderson and Prieur, 2000)) supposes that the hydrological cyclonic regime (permanent feature of the large scale dynamics of the area see Millot, 1999) maintains high the sub-surface nutrients concentrations during spring. Even if in spring the atmosphere starts to warm the surface layers and induces a water column stabilization, the intense wind regime of the area acts on the opposite way, remixing the upper layers. Figure 8-12 shows that the high surface (10 m) nutrients concentration extends to the whole area between the Balearic Islands and the Italian coast. This means that even short but intense winds burst (as the ones analyzed in the paragraph 6.2.4) are able to redistribute nutrients in the surface layers from the underneath standing-stocks. Only when the air-sea fluxes are definitively higher than zero (i.e. at the end of May), the process stops.

- The "no-bloom" area, which was demonstrated to dominate the biological activity of the basin, shows a more complex interaction with the atmospheric forcing. The results obtained from the analysis of MXL model outputs (see chapter Chapter 7) demonstrated that the winter overturning does not permit an efficient uplift of nutrient. Even in the case of strong modifications of the hydrodynamic regime, as for the EMT conditions, the effects on the "no-bloom" areas remain substantially weak. However, in the previous paragraph, I demonstrated that the temporal evolution of the "no-bloom" regions follows a well-defined trend, characterized by a small but rather constant chlorophyll concentrations from November to May. Such trend was mainly related to the particular atmospheric regime of the Mediterranean area during the so-called "enlarged winter" (see chapter 4.4). The analysis on the "good weather" days demonstrated that favorable conditions for phytoplankton growth (i.e. low cloudiness, no wind, high sea level pressure) occur in the basin also during late fall/early winter, then when the principal limitations to biomass growth is the

light rather than nutrients. In other words, the mild Mediterranean winters, on one side prevent the development of large and diffuse blooms, on the other mitigate partially the light limitations, permitting a weak but evident biomass enhancement.

To better highlight the relevance of the previous comment, it is useful to frame the Mediterranean basin in a more general view, which encompasses also the North Atlantic (NA) Ocean.

In the NA occurs the most intense (in terms of both temporal and spatial extension) phytoplanktonic bloom of the global ocean (Follows and Dutkiewicz, 2002; Siegel, et al., 2002a). The meridional limit of the NA bloom is generally located between 35° and 40° North, with the biomass concentrations increasing with the increasing latitudes. South of this limit the trophic regime is considered tropical or sub-tropical (Dutkiewicz, et al., 2001; Longhurst, 1995), then characterized by a strong oligotrophy and a weak seasonal variability. Following the analysis reported by Siegel et al. (2002a), the blooms in the regions located between the 35° N and the 45°N start in the first days of the year (January-February), whereas in the northern region (where the most intense concentrations are observed) the bloom onset occurs in spring (March-April).

The Mediterranean then is located on the boundary of these two regions and my research highlighted that it comprises both the NA trophic regimes. The mean situation (the "no-bloom" areas) exhibits a tropical or a sub-tropical regime, disturbed however by regions where, under particular conditions (both atmospheric and hydrographic), NA bloom-like events take place.

We can try then to answer to the classical, even though simplifying question, whether the basin is light limited or nutrient limited.

The Mediterranean picture obtained exploiting the SeaWiFS data coincides in most of the aspects with the classical description, widely accepted, of an oligotrophic basin with regions where local mesotrophic or eutrophic conditions occur (see chapter 1).

The constraints imposed by the two main straits (Sicily and Gibraltar) are supposed to explain mostly the basin oligotrophy and the west-east gradient. In addition, the general anti-cyclonic regime of the EMED and the strong vertical density gradient due to the characteristics of the surface and intermediate Mediterranean waters are supposed to prevent an efficient nutrients uptake and a "Sverdrup"-like spring bloom. Many authors addressed to the question in the recent past (among the others Bethoux, 1989; Bethoux, et al., 1998; Crise, et al., 1999; Crispi, et al., 2001).

However, our results suggest that, even if the final picture remains substantially similar, the mechanism that produces it, is slight different from the previous analyses.

It was discussed (paragraph 4.4) the possibility that, phytoplankton growth in mixing conditions could occur in Mediterranean. As already highlighted by Huisman et al. (1999), such circumstances do not contradict the Sverdrup paradigm, but simply extends it to a different environment.

Siegel et al. (2002a) applied the Sverdrup approach to estimate the temporal and spatial patterns of the North Atlantic spring bloom. They reviewed the available assessment of the Sverdrup critical irradiance I_c and developed a methodology to analyze the observed latitudinal variations in the timing of the NA bloom initiation. Here, we also focused on the I_c, though with a different aim. In fact, we were interested to verify the "strength" of the nutrient limitation in the basin, which permits at the same time to infer on the response of the phytoplankton to the characteristic Mediterranean light-conditions.

The Sverdrup conditions can be written as (Sverdrup, 1953):

Eq. (8-1)
$$I_c = \frac{I_0}{KZ_{CR}}\left(1 - e^{-KZ_{CR}}\right)$$

where I_0 is the flux of incident PAR, K is the diffuse attenuation coefficient for PAR, and Z_{CR} (the Sverdrup critical depth) is defined as the depth where the integrated total

production equals the integrated losses. Various values of I_c were then calculated using Eq. (8-1) for a series of Z_{CR} values ranging from 0 to 1000 meters in the three regions selected before (the NWMED, the South Tyrrhenian Sea, the South Levantine basin), which are supposed to represent the different conditions of the basin. PAR values were obtained from SeaWiFS measurements (see Chapter 5), as for the K's, they are the K_490 SeaWiFS products (see appendix II). An I_c of 1.3 einstein m^{-2} day^{-1}, as retrieved by Siegel et al. (2002a) as median of its data, was considered as the threshold value.

Figure 8-13 displays the results obtained for the three selected regions. As supposed, the depth of the I_c threshold (which indicates the light intensity at the depth where consumption equals production) is always deeper than the observed mixed layer depth in the South Tyrrhenian and South Levantine regions, as reported in the literature. This indicates that in such regions, but it is supposed in all the "no-bloom" areas of the Mediterranean, a light constraint is never at work.

It is however important to note that this does not mean that the areas are not biologically active. In fact, satellite data (see Figure 8-5 and Figure 8-10) demonstrated that slight and uniform biomass increases occur in the "no-bloom" areas throughout the late-fall and early winter periods. Furthermore, the critical depth analysis demonstrated that the absence of bloom events in such areas could be ascribed to the continuous utilization of nutrients in the surface layers during winter. The favorable light conditions detected in the Mediterranean during winter, do not limit the biomass growth, but prevent an accumulation of a nutrient stock in the upper layer, large enough to sustain an intense bloom in spring.

Very different is the situation in the NWMED area. The severe and intense winter atmospheric conditions of the region deepen the mixed layer depth below Zcr, and, continuously mixing the upper layers, prevent the utilization of nutrients. Such nutrient, "survived" to the winter, can be utilized by the phytoplankton in spring in intermittent pulses before and even after the water column stabilized.

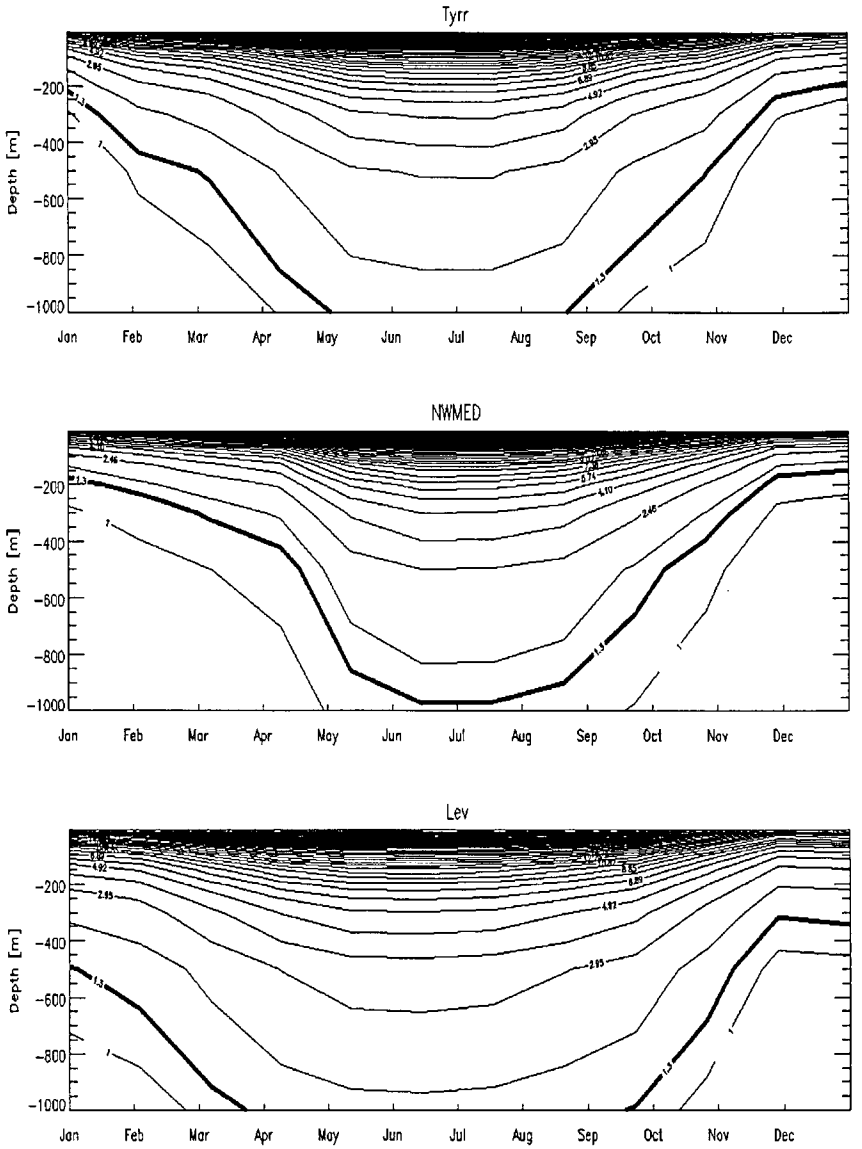

Figure 8-13. Estimates of the Sverdrup critical depth for various mixed layer depth (Y-axis) and in the three selected Mediterranean regions (South Tyrrhenian, NWMED, South Levantine in upper, central and lower panels, respectively). Units are in mol photons m^{-2} day^{-1}.Solid lines indicate the values 1.3 as reported by Siegel et al. (2003).

From these a re-appraise of the nutrient limitations in the Mediterranean basin. As known, the impossibility of part of the basin to make "Sverdrup" like bloom derives primarily by a nutrient deficiency in the upper layers in spring. However, our results suggest that this nutrients scarcity is also due to the favorable Mediterranean light conditions, which permit to the phytoplankton to consume nutrients during winter. Even if the deepening of the mixed layer extends quite uniformly throughout the winter

season, events of stabilization of the water column (associated to the "good weather" days) enhance the consumption of the nutrients up-welled up to that moment and then prevents the formation of a stock utilizable in spring. To confirm this picture it is sufficient to compare the MEDAR-MEDATLAS seasonal climatological surface maps of the Mediterranean in winter and in autumn (see Figure 8-14). Except for the "bloom" areas and disregarding the effect of the spatial extrapolation, the values showed are very close in the two periods, demonstrating that in the surface layer the nutrients do not accumulate.

We can therefore partially reconsider the dynamics of the phytoplankton in the Mediterranean. The effects of the atmospheric winter forcing (weak surface layers overturning and high irradiance) provoke a trophic regime, which is markedly tropical. Even if a weak seasonality in the no-bloom areas is observed, the autumn-winter conditions are not very far from the spring ones, and only in summer the dynamics changes substantially. Our results suggest that the definition of oligotrophic basin can be still adopted for the Mediterranean, but with a trophic dynamics, which differs from what was believed up to now. In fact, fall and winter, which are often considered period of "low" phytoplankton activities, contribute relevantly to the TPP of the basin.

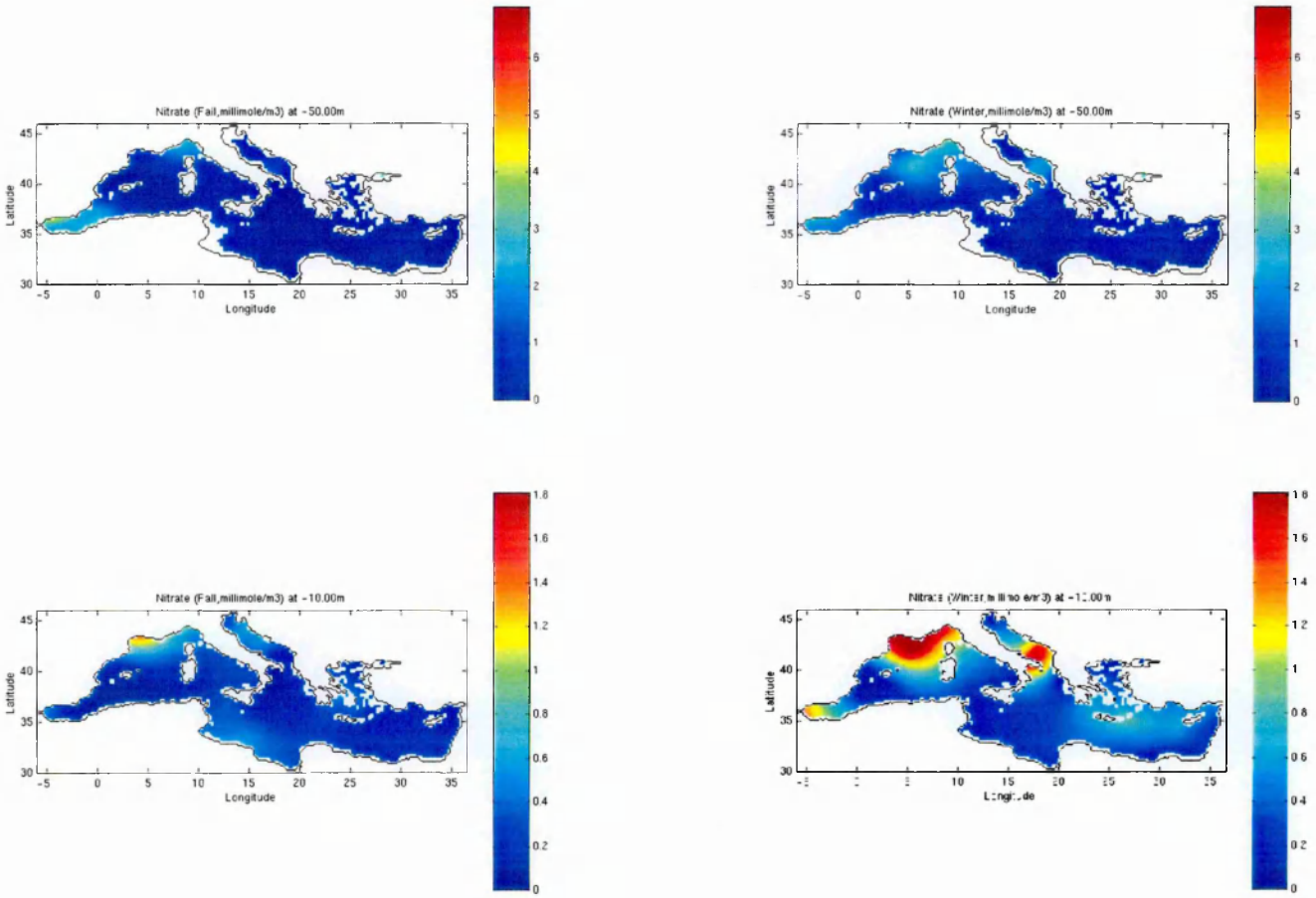

Figure 8-14. Autumn (left) and Winter (right) Climatological Nutrients Concentration as derived by MEDAR-MEDATLAS data base. Units are in millimole/m^3.

8.6 LONG TERM TRENDS

Two analyses were attempted to verify the long-term trends in the Mediterranean basin. Both were carried out exploiting the data and the results of the studies conducted by MA91 and AMA95, which obtained a picture of the Mediterranean trophic regime at the end of the seventies, using the CZCS satellite measurements.

In Chapter 7, the time series of CZCS and SeaWiFS data were analyzed and compared to verify the impact of the EMT on the trophic regime of the basin. The main result obtained was that the large change in the thermohaline circulation experienced by the EMED did not affect the surface biological dynamics of the basin, except for the Western Ionian Sea, where a novel feature was detected, and for the SA region, where the increased nutrient availability resulted in an enhancement of the bloom intensity (Santoleri, et al., 2003). A detailed discussion on the limits of the comparison was carried out, to be confident with the analysis and on the results obtained. Despite of the observed discrepancies between the two time series, the CZCS and the SeaWiFS data were considered comparable. The scope of the study was however essentially addressed to identify large and intense changes on the patterns of surface phytoplankton, rather than to compare the absolute values of the chlorophyll-*a* concentration. Furthermore, only the EMED basin was considered.

By contrast, the second analysis was focused on the comparison of the chlorophyll-*a* and PP estimates as obtained using SeaWiFS and CZCS data. The first were implemented with the DORMA algorithm, whereas for the second the AMA95 and MA91 assessments were adopted. The comparison was enlarged to the whole basin, and, in this case, the absolute values of chlorophyll-*a* and PP were undoubtedly relevant.

The comparison highlighted that the mean spatial patterns of the basin are generally consistent. Chlorophyll-*a* concentrations and PP values displayed similar ranges of

variability in the two time series, though the MA91 and AMA95 data were generally sharper and higher.

However, two principal discrepancies were found, and they will be firstly discussed separately, to later analyze whether any connections exist.

Before this, the CZCS data adopted for the comparison has to be reconsidered, through a tentative assessment of their absolute errors, which could permit to evaluate the consistence of the observed dissimilarities.

8.6.1 A re-appraisal of the MA91 and AMA95 CZCS data

Erratic CZCS chlorophyll-*a* estimates are the most obvious candidate to explain the discrepancies between the AMA95 and MA91 data and the SeaWiFS assessment.

It is well known that the main sources of error in the CZCS data derived from the atmospheric correction uncertainty and from the degradation of the sensor apparatus.

The first problem was addressed by MA91-AMA95 using a pixel-by-pixel method, which retrieved the L_{wn}'s, *via* an iterative procedure able also to distinguish between case I and case II waters (Bricaud and Morel, 1987) and accounting for the Ozone influence (André and Morel, 1991). The second problem was related to the degradation of the CZCS sensor after the 1981. It was solved by MA91 fixing the satellite winter chlorophyll-*a* concentration in the deep water convection area of the NWMED equal to 0.04 mg m^{-3} and then re-tuning the whole data set on a basis of this correction. In AMA95, in absence of similar information, the scenes collected after the 1981 were forced to reproduce the statistical distribution of the 1979 imageries collected in the same period of the year.

The scarce numbers of the available in situ observations did not permit to AMA95 and MA91 to perform a matchup analysis. However, in their paper, a validation of satellite chlorophyll-*a* concentration with some Mediterranean in situ measurements

was carried out, though the estimates were compared without the exact temporal and spatial matching between the two data.

Despite the crudeness of the analysis, the CZCS chlorophyll concentrations are not far from the in situ measurements, as displayed by AMA95 table 3, though the satellite data are generally higher. Therefore, a small error in the bio-optical CZCS algorithm could be one of causes of the discrepancies. Moreover, the algorithm was tuned to retrieve chlorophyll+pheopigments concentrations, which are higher than the purely chlorophyll-*a* ones. Another supposed cause could be the interannual variability of the basin that, modifying the mean values, could have induced the observed differences. Finally, in some regions and in the winter season, when the cloud-cover is highest, the number of observations used to compute the CZCS averages was quite small, affecting then the statistical relevance of the analysis.

In brief, all the above let suppose that CZCS chlorophyll data retrieved with the AMA91 and MA91 approach are generally higher than the actual values.

By contrast, the same authors reached different conclusions. An assessment of the error deriving from the Morel's CZCS data processing was shown by Bricaud and Morel (1987) on a basis of chlorophyll-*a* measurements carried out on the NWMED in March 1979 and in May 1982. A true matchup analysis was performed, even if satellite data were extracted from only two images (see figure 16 in Bricaud and Morel, 1987). The results obtained revealed that satellite and in situ data differed by ± 30-40% showing a generally good overall agreement. When discrepancies are considered, the general tendency of CZCS pigments concentration results in a systematic underestimation of the sea-truth data.

Finally, it is important to remember the conclusions of Gitelson et al. (1996), which demonstrated that the Gordon et al. (1983) standard bio-optical algorithm (but also Bricaud and Morel (1987) one, see Table 8-5) overestimated his data set of Levantine measurements.

Ratio	Chlorophyll concentration		
	(Bricaud and Morel, 1987)	(Gordon, et al., 1983)	(Gitelson, et al., 1996)
6.10	0.043	0.042	0.032
5.35	0.057	0.054	0.040
4.88	0.068	0.064	0.048
4.50	0.080	0.074	0.056
4.20	0.093	0.083	0.063
4.00	0.102	0.091	0.069
3.80	0.114	0.100	0.076
3.63	0.125	0.109	0.083
3.06	0.177	0.148	0.114

Table 8-5. Chlorophyll concentration below the 0.2 mg m^{-3} estimated using the three different CZCS bio-optical algorithms considered, for given values of the blue-green reflectance ratio (443 and 555 nm).

It is possible from all the above to determine an error bar for the AMA95 and MA91 chlorophyll-*a* concentrations? The Bricaud and Morel (1987) results are probably the only relevant in this discussion. At my knowledge, they represent the unique matchup analysis performed on the Mediterranean open ocean waters in the period of activity of CZCS. Furthermore and more importantly, they were obtained using satellite data computed with a procedure nearly identical to the one adopted by AMA95 and MA91. Therefore, in the following discussions the CZCS data will be considered with an average error of 40%. However, the uncertainty remains still large and must be considered in evaluating the results.

8.6.2 Decrease of chlorophyll in the WMED

During the CZCS years, the WMED chlorophyll-*a* concentrations, as computed by MA91, were substantially higher than during the SeaWiFS period. This is clearly highlighted in Table 4-1 in the chapter 4.

Applying a ±25% and ±40% errors bar to the SeaWiFS and CZCS data, respectively, the supposed bias results however embedded within the estimated errors (see Figure 8-15 upper panel).

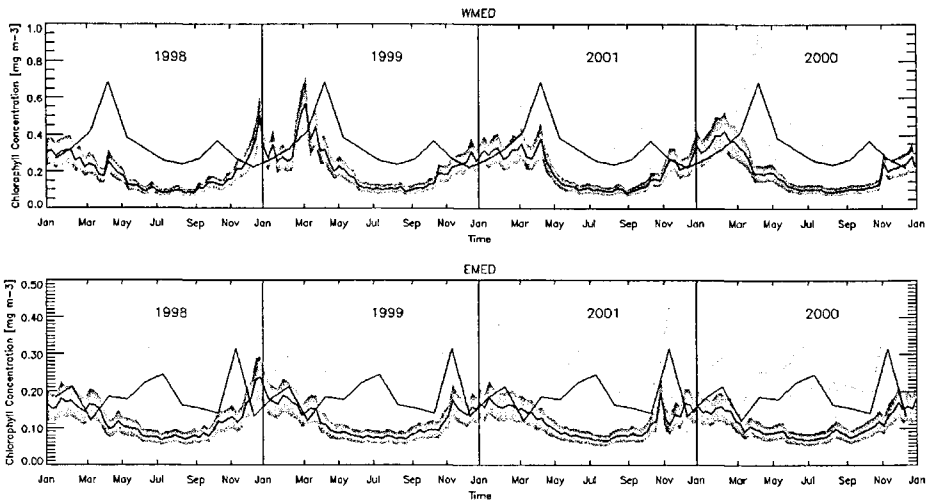

Figure 8-15. Time series of the spatially averaged chlorophyll concentration in the WMED (upper panel) and in the EMED (lower panel. Light gray contours indicate AMA95 and MA91 data ±40%; dark gray contours refer to SeaWiFS estimates ±25%.

However, let us suppose for a moment that the two chlorophyll-*a* estimates have comparable errors (i.e. the ±25% of the SeaWiFS data). It was demonstrated that this is a very strong assumption in the case of CZCS data, but it is adopted here only to speculate on the possible scenarios of the Mediterranean biological regime. On the other hand, even if the ±40% mean error bar on the CZCS chlorophyll is scientifically correct, however it is also reasonable to consider a minor mean error, though not evidences are available to corroborate this assertion.

When the ±25% error bar is applied to the CZCS data in the WMED (see Figure 8-16), the already observed discrepancies with the SeaWiFS chlorophyll-*a* are clearly highlighted. CZCS data are always higher than the SeaWiFS ones during spring and summer and in all the years analyzed.

The April peak of the MA91 chlorophyll contributes mostly to determine the greater values of the annual average, but in general the CZCS estimates are markedly higher. By contrast, during fall and winter the time series are very close and in some years (i.e. 2000), the SeaWiFS data exhibit the larger values of chlorophyll-*a* concentration.

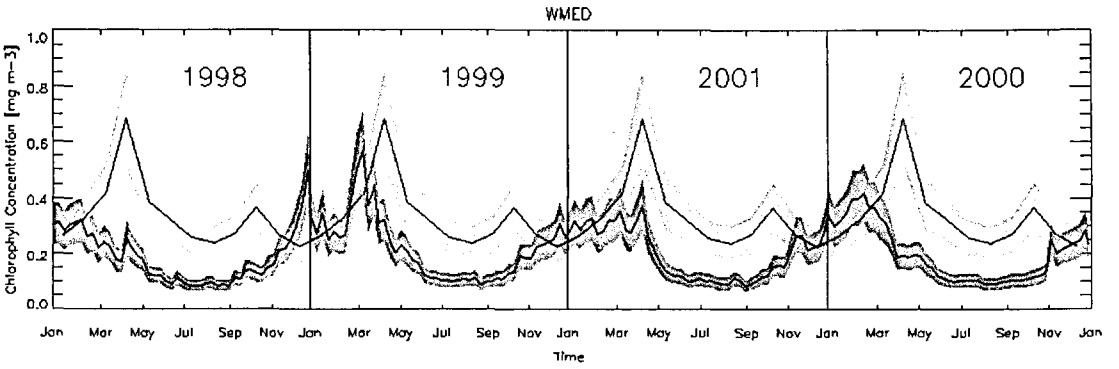

Figure 8-16. As Figure 8-15 but with error bars fixed at 25% fro both the sensors.

Due to the considerable uncertainty of the analysis, the results are necessarily affected by errors, but seem to indicate that, if any change occurred, it was mainly during the spring/summer period. In particular, the peaks of the time series seem to be most affected by the hypothesized change.

Very few time series of in situ data covering the analyzed period are available, and generally are located to coastal water or give only derived-information on the biomass concentration (i.e. the water transparency).

Marty et al. (2002) showed that chlorophyll-*a* concentrations at the only long-period WMED open ocean station i.e. DYFAMED, remain substantially unchanged between 1993-1999, with only a slight increase in the last years. If a change occurred, it should be then earlier then 1993. Coastal data from the Bay of Calvi, displays an evident decrease of the biomass concentration in the period between 1979 and 1998 (Goffart, et al., 2002). The authors hypothesize that the decrease of the phytoplankton concentration measured in the Bay of Calvi could be related to the change in the atmospheric conditions of the Mediterranean.

More interesting in this context, are the annual trends of the surface chlorophyll-*a* in the Bay of Calvi showed by the authors (see figure 2 in Goffart, et al., 2002). The post-1997 data are very low if compared with the pre-1997 estimates, but, in addition, they displays peaks in winter instead than in spring, as are observed in the 1988-1986 and

1979 time series. Thus, even if speculative, our results seem to be confirmed by the in-situ data, and then they will be discussed more accurately in the next paragraph.

8.6.3 The shift of the temporal pattern

The analysis of the seasonal and climatological maps, as well as the comparison of the time series and the results of the previous paragraph, highlighted that an evident temporal shift in the biomass pattern occurred between the CZCS period and the SeaWiFS years. To skip any problems due to the uncertainty of the data, Figure 8-17 and Figure 8-18 display the chlorophyll-*a* time series in the SeaWiFS and in the CZCS period divided by the absolute maximum in the considered period. Supposing that the general trends of CZCS are on average truthful, the problem due to the believed erratic values of MA91 and AMA95 chlorophyll-*a* concentration is overcome. Working only with relative values, it was supposed that the time series should be reasonably comparable.

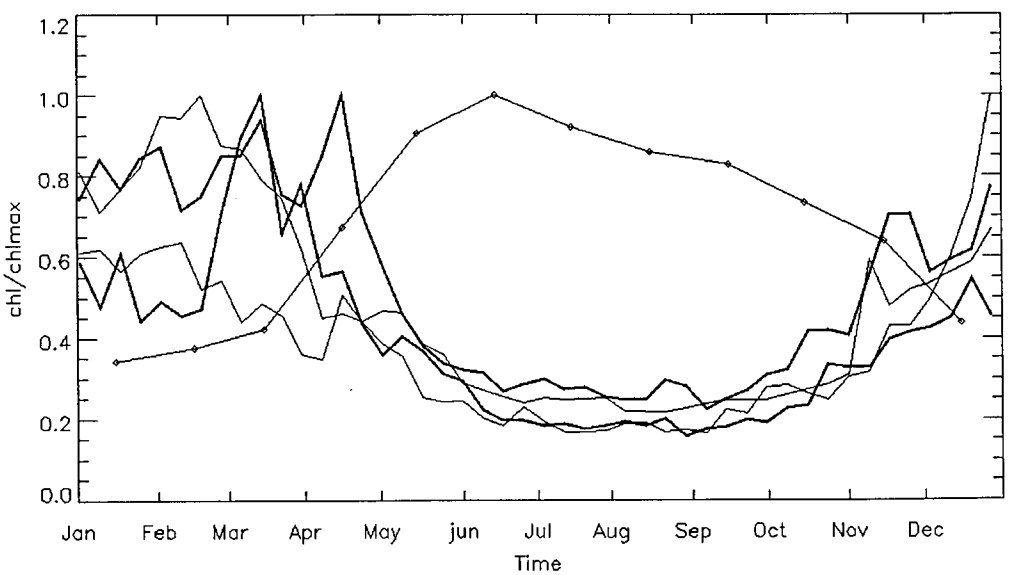

Figure 8-17. Time series of the relative chlorophyll averaged on the WMED. Lines indicate different SeaWiFS years, points MA91 data. Bold lines refer to the 1999 and 2000 SeaWiFS years.

Observing the two plots, the shift in the timing is clearly evident. WMED time series in SeaWiFS period display maximum values in the first months of the year, whereas the MA91 data, relative to CZCS 1979-1981 data, are peaked in May-June.

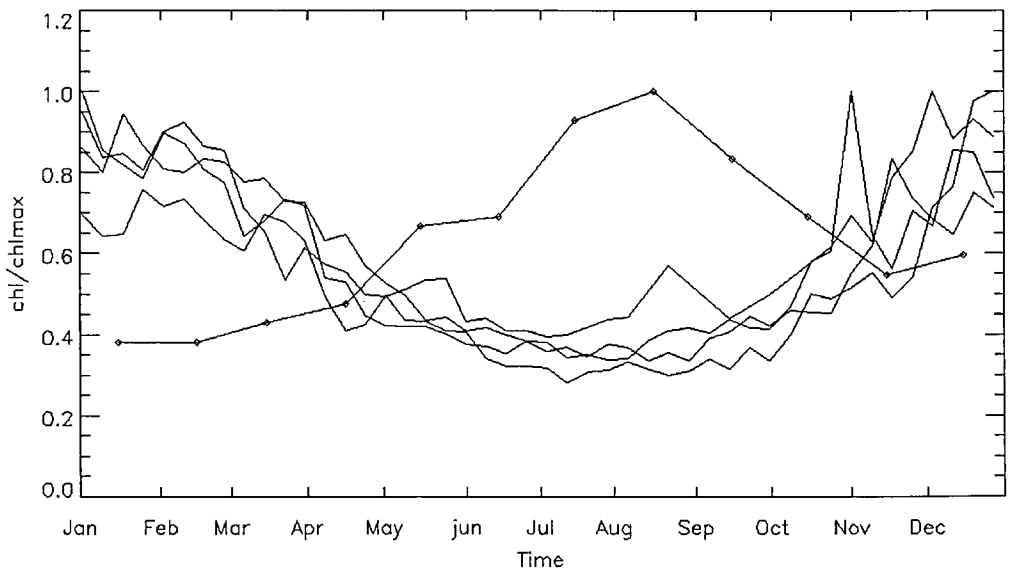

Figure 8-18. Time series of the relative chlorophyll averaged on the EMED. Lines indicate different SeaWiFS years, points AMA95 data.

It was discussed before the possible influence of SeaWiFS interannual variability on the comparison with CZCS estimates. The hypothesis was that the trophic situation observed by MA91 was similar to the ones observed in the 1999 and 2000 (i.e. large and intense NWMED bloom). If only these two years are considered, the shift between the time series is reduced to 1-2 months, but remains still evident. It is important to note that the general tendency of the CZCS data resembles closely the temporal trend of the "bloom" areas in the SeaWiFS era, differing only in the temporal extension of the blooms events, which is sharper in the SeaWiFS data (compare for example Figure 8-17 and Figure 8-10).

In the EMED, the differences in the temporal pattern are impressive. In the SeaWiFS time series the peaks are anticipated by quite six months respect to the CZCS, being concentrated in the late-fall/winter period. AMA95 data have an evident maximum in the summer months.

In the SeaWiFS period then the basin displays a marked increase of biomass during the winter months, and then shifted of 4-6 months respect to the years of CZCS activity. Even considering the uncertainty related to such analysis, the data suggest that an important change occurred in the Mediterranean between the periods of activity of the two considered ocean color data set. It is important to note, however, that the amplitude of such change is not easily quantifiable, using the available ocean color data only. The uncertainty related to the different processing of the two time-series, makes very difficult any comparison in terms the intensity of the change (see previous chapter). However, the success of the CZCS in reproducing the most important features of the basin, let us suppose that the gradients and the timing are reasonable retrieved, and then comparable with the most recent similar estimates, namely the SeaWiFS ones.

8.6.4 The observed changes in the ocean color and the climate change

In the paragraph 8.5, the role of the atmospheric forcing in driving the temporal and spatial patterns of marine phytoplankton was discussed. It was concluded that in both bloom and no-bloom areas the atmosphere plays a crucial role, which can be summarized in three key points:

- it drives the intensity of the growth in the bloom area, even if in a not-linear way;
- it rules the temporal trends of the no-bloom areas, which exhibit small to moderate increases of biomass during the winter "good weather" days;
- it controls the switch between the two trophic conditions, namely bloom and no-bloom;
- only in periods and regions characterized by intense atmospheric forcing, bloom condition were observed.

All the above let us to hypothesize, that the observed shift between the seventies and the present days could be related to some basin and regional scales atmospheric change in the Mediterranean areas.

As matter of fact, several evidences proved that such change occurred.

An intensification of the winds field over the Aegean Sea and a series of particularly severe winters on the North Levantine Sea in the years 1986-1989, are supposed to be the first cause the EMT (Stratford and Haines, 2002). In addition Samuel et al. (1999) emphasized that a weakening of the Mistral winds was observed, decreasing its intensity after the 1988.

Similar evidences were proposed by Trigo et al. (2000), which analyzing data in the period 1958 to 1996, introduced an index of the intensity of atmospheric cyclones on the Mediterranean, calculated on a basis of the air pressure fields. Their data highlighted that the number of occurrence of severe winter cyclones on the basin diminished in the period considered, resulting at the present days quite halved respect to the eighteens. Finally, Pirazzoli and Tomasin (2003) demonstrated that the winds intensity in the central Mediterranean (Tyrrhenian Sea, Sicily Channel and Western Ionian) was increased since the 1970's, showing an evident trend in most of the region studied. By contrast, in the Adriatic Sea no evident change was detected.

Summarizing the above results, in the WMED the wind field results less intense, with a weakened Mistral and an intensification in the Tyrrhenian Sea, whereas in EMED, the Rhodes region exhibits an amplification of the wind stress (see figure 4 in Samuel, et al., 1999). In the same period, the activity of the atmospheric cyclones on the Mediterranean decreased strongly during the Fall-Winter seasons (October to March).

Considering the results obtained before, an interpretation of these signals in terms of the impact on the biota can be attempted.

- Regarding the bloom areas, it was demonstrated that part of the variability could be explained in terms of wind intensity.

- This is particularly true for the NWMED bloom, but also, for example, for the RG. The reduced strength of the Mistral forcing should have induced a minor intensity of the phytoplankton spring growth, which in turn resulted in a limited extension of the bloom area. It was verified (see paragraph **6.2.4**) that when the winds stress is particularly low, the blooming area results strongly reduced (i.e. 1998), showing high chlorophyll-*a* values only in the mixed patch region. The supposed decrease of WMED averaged chlorophyll-*a* concentration could be then ascribed to the weakening of the winds stirring in the NWMED area, which produced blooms less intense than those detected in the CZCS years. Due to the relevant contribution of the NWMED bloom on the dynamics of the entire WMED basin, this fact could explain the observed discrepancies in the two data sets.

More interesting is the decrease of the number of active atmospheric cyclones in the area. Following Trigo et al. (2000), these atmospheric structures drive the winter weather conditions of the basin, and then control the cloud coverage and the winds intensity. As already discussed, the occurrence of mild conditions (the "good weather" days) was related to the seasonal variability of the "no-bloom" areas, which experience a slow but quite constant increase of biomass since October (in opposite tendency of the "bloom" regions where the increase of biomass was concentrated in the spring period). If the analysis of Trigo et al. (2000) is realistic, it is possible suppose that the number of "good weather" days in the CZCS years was very small. This in turn could have provoked a more intense winter mixing, which resulted in an increase of regions with "bloom" trophic regime, which a detriment of the "no-bloom" areas. The net results on the total dynamics of the basin, should be a shift of the temporal patterns as the one observed and showed in Figure 8-17 and Figure 8-18 and on net increase of the Mediterranean chlorophyll-*a*.

8.6.5 To what extent is the Mediterranean biota responding to climatic change?

The relationships between climatic conditions of the Mediterranean and the response of its autotrophic populations let suppose that the basin can be used as a good indicator to the hypothesized global climatic change.

The argument was already discussed in the recent past (Bethoux and Gentili, 1996; Bethoux and Gentili, 1999; Duarte, et al., 1999; Turley, 1999). The experience of the EMT, however, demonstrated that also severe changes in the physical dynamic of the basin, which are directly related to global climatic change (see Samuel, et al., 1999), only slightly affected the biological component of the Mediterranean.

On the other hand, it is important to distinguish between changes affecting the whole basin dynamics from those interesting only the air-sea boundary layers. Even though they are obviously related, in fact, only the latter could influence relevantly the phytoplankton populations of the Mediterranean. As matter of fact, while the links between global climate, Mediterranean atmospheric local dynamics and large scale circulation were intensively analyzed (Krahmann and Schott, 1998; Tsimplis and Josey, 2001; Vignudelli, et al., 1999) only few studies were focused on the effect of the climatic change on the surface layers of the basin. Korres et al. (2000), for example, demonstrated that the response of the Mediterranean SST to anomalous cooling atmospheric events resulted in an intensification of the subbasins scale gyres, which occur six months after the winter forcing anomaly events. The authors argued that the dynamics after a strong winter events could change the ocean response to the subsequent heating cycle, producing a delayed response to external forcing.

The results of Korres et al. (2000) could be relevant in the present discussion because implicitly admit that the surface layers of the Mediterranean (i.e. the mixed layer) respond rapidly to atmospheric change (i.e. less than one year).

Several evidences (Krahmann and Schott, 1998; Tsimplis and Josey, 2001; Vignudelli, et al., 1999) seem to prove that the variability of the Mediterranean climate is mainly driven by the North Atlantic Oscillation (NAO), which is one of the major modes of variability in the Northern Hemisphere. The NAO index, which is the difference between the normalized sea level pressure at Gibraltar and over the southwest Iceland, is often considered a useful indicator of the strength of the NAO (Hurrel and Van Loon, 1997).

The analysis of Trigo et al. (2000) demonstrated that the reduction of Mediterranean atmospheric cyclones can be positively correlated with high NAO index. Pushing to extreme conclusions the previous discussions could be then hypothesized that in the year of high NAO index, the Mediterranean biota are less facilitate to produce blooms, intensifying its tropical regimes. On the other hand, the inverse picture could be then applied in the years of low NAO index.

Though stimulating, the existence of such teleconnections are however, still an hypothesis. Even for the atmospheric studies, which are supported by a huge amount of observations and of numerical exercises, not at all comparable with the oceanic ones, the relationships between global and local events are still debated. We are however convinced, on a basis of the results obtained in the previous chapters, that the sensitivity of the biological Mediterranean marine compartment to the weather conditions is particularly high. More difficult is the definition of the relative contribution of the local and global influences.

8.7 NOTE ADDED IN PROOF

During the preparation of the final draft of the thesis, a paper focused on some of the issues discussed here was submitted to an international journal ("Seasonal and interannual variability in algal biomass and primary production in the Mediterranean Sea, as derived from four years of SeaWiFS observations", by Bosc, E., Bricaud A. and

D. Antoine, submitted to Global Biogeochemical Cycles, BOS03 hereafter). Thanks to the authors, I had the possibility to read the draft and to compare their results with the ones obtained during my study.

BOS03 utilized 8-days chlorophyll-a average maps derived from SeaWiFS GAC data on the Mediterranean to describe the spatial and temporal variability of the basin surface biomass. A regional chlorophyll-a algorithm was developed and applied on SeaWiFS data to reduce the observed bias in the satellite estimates. Finally, the BRI02 approach was used to derive PP maps, and an exhaustive description of the principal features of the basin was carried out. The BOS03 paper represents an excellent occasion to test the results obtained in my research, and then some preliminary comments, which discus and compare the two studies, follows.

The regional algorithm adopted by BOS03, used the radiance ratio 443/555 and a log-linear expression derived fitting a Mediterranean in situ bio-optical data-set. They compared the resulting estimates with the in situ data at DYFAMED, obtaining a good agreement in the ranges of medium and high chlorophyll-a concentration. However, only rarely their outputs retrieve values lower than 0.1 mg m^{-3}, overestimating then all the DYFAMED values in the range 0.0-0.1 mg m^{-3}.

The authors observed that the atmospheric correction still influences the performance of the satellite data, confirming the results obtained in my study. Furthermore:

- The log-linear expression of the BOS03 regional algorithm (as shown in BRI02) could induce an overestimation of the chlorophyll concentration when the radiance ratio increases. This effect, however, it is supposed to be weak (see the discussion on the different performances of L-DORMA and NL-DORMA).
- The BOS03 application of BRI02 regional algorithm was performed deriving the radiance ratios from the OC4v4 chlorophyll-a estimates (as obtained by SEADAS), and then using it in the log-linear expression of the BRI02 algorithm. As already highlighted by the authors, this approach could induce errors related

to the multiple ratio selection of the OC4v4 (i.e. it is not possible *a priori* to know the selected ratio) and to the Siegel dark pixel assumption (i.e. the atmospheric correction was based on the preliminary chlorophyll-a estimates with OC4v4). However, in both the cases, the derived error should affect the final chlorophyll estimates in the high ranges, and then are supposed to have week effect on the low values.

- The results of the section 3.3.2 demonstrated that the radiance ratio 443/555 is underestimated by SeaWiFS. Even though the number of total matchup points is still inadequate to retrieve definitive conclusions, the SeaWiFS inaccuracy was observed also by Pinkerton et al. (2002). Furthermore, they demonstrated that most of the error of the OC4v4 algorithm (and then of all the algorithms using such ratio) could be ascribed to the use of the 443/555 ratio, confirming then the results obtained here. The retrieved radiance ratio underestimation results directly in an overestimation of the chlorophyll-a concentration, which, due to the log-linear expression of the BRI02 algorithm, is mainly evident in the low ranges. This effect probably explains most of the observed bias.

The diverse performances of the BRI02 and DORMA algorithms have an effect on the following analysis, which are focused on the description of the Mediterranean biomass dynamics. The BOS03 regional and basin scale values are often higher than the estimates presented here, in terms of both chlorophyll-a concentrations and PP.

However, if the absolute values are not considered, the spatial and temporal patterns are almost identical. This fact, though expected, confirms the validity of the present study in all the issues that are in common with BOS03 (i.e. climatological analysis), but also reinforces the results obtained on the other topics (i.e. blooms discussion).

CHAPTER 9

Appendix

9.1 APPENDIX I - DEFINITIONS OF OPTICAL QUANTITIES

9.1.1 Primary Definition

Quantity	Definition	Symbol	SI Unit	Comments
Zenith angle		θ	Degree	It is the angle between a given light beam and the upward vertical
Azimuth angle		φ	Degree	It is the angle between the vertical plane including the light beam and some other plane.
Radiant energy		W	Joule	
Radiant flux	$\frac{dW}{dt}$	ϕ	Watt	It is the flux of all the radiant energy radiated from a source, in all directions
Radiant intensity	$\frac{d\Phi}{d\omega}$	I	Watt sr^{-1}	It is the radiant flux at that point in a specified direction of an infinitesimal cone, divided by the element of solid angle ω-
Radiance	$\frac{d^2\Phi}{dA \cdot d\omega}$	L	Watt sr^{-1} m^{-2}	In a given point, it is the radiant flux at that point in a given direction per unit solid angle per unit area at right angles to the direction of propagation.
Irradiance	$\frac{d\Phi}{dS}$	E	Watt m^{-2}	It is the total radiant flux incident on an infinitesimal element of a surface, divided by the area of that element.

In the sea, it is suitable to discuss the irradiance (radiance) passing through a horizontal plane at particular depth below the sea surface. Flux passing down (up) into

the lower (highest) part of the water column is described as downwelling irradiance E_d / radiance L_d (upwelling irradiance E_u /upwelling radiance L_u).

The ratio of the upward to downward irradiance at a given point is the *irradiance reflectance:*

$$R = \frac{E_u}{E_d}$$

9.1.2 Relationships between primary quantities

The difference between E_d and E_d is the *net downward irradiance*, which is related to the radiance by:

$$E = \int_{4\pi} L(\theta,\phi)\cdot\cos\theta\cdot d\omega$$

Similarly:

$$E_d = \int_{2\pi} L(\theta,\phi)\cdot\cos\theta\cdot d\omega$$

$$E_u = -\int_{2\pi} L(\theta,\phi)\cdot\cos\theta\cdot d\omega$$

The terms E_u and L_u are related each other by the Q factor defined as:

$$Q = \frac{L_u}{E_u}$$

In the case of a Lambertian source Q is assumed equal to π. A Lambertian source is one in which the radiance L is independent of the angle from which it is viewed; the radiation field is considered isotropic and its radiance distribution is totally diffused. Q

appears to be between 4 and 5 and somewhat dependent on wavelength for radiance distributions observed in nature (Austin, 1980).

9.1.3 Remote sensing parameters

The ratio between L_d and E_u is defined (Austin, 1980) as the Remote Sensing Reflectance

$$R_{rs} = \frac{L_u}{E_d} = \frac{R}{Q}$$

It is related to the L_w (as obtained from the atmospheric correction procedure) by (Gordon and Clarke, 1981))the following relationship:

$$L_w = \frac{[1-\rho(\theta_{sat})]RE_d}{n^2 Q} = \frac{[1-\rho(\theta_{sat})]R_{rs}E_d}{n^2}$$

where n is the index of refraction of sea water, ρ is the Fresnel reflectance for upwelling radiance at normal incidence and θ_{sat} is the satellite zenith angle.

To compare Lw values obtained from region and time different, it is appropriate for remote sensing applications to calculate the *Normalized Water Leaving Radiance* L_{wn}, which is that which would exit the sea surface if the Sun were at the zenith and if the atmosphere were absent (Gordon, et al., 1983):

$$L_{wn} = \frac{L_w}{t(\theta_0)\cos(\theta_0)}$$

where t is the diffuse transmittance of the atmosphere.

9.2 APPENDIX II – SEAWIFS DATA PROCESSING

(This section is derived by the "Summary of SeaWiFS operational data products" document, available on line at the web-address http://seawifs.gsfc.nasa.gov/sdps/ and by Sciarra et al., 2003).

9.2.1 SeaWiFS operational products

All the SeaWiFS data employed in this research are processed using the SeaDAS Software (SeaWiFS Data Analysis System), which is a comprehensive image analysis package for processing, displaying and analyzing all SeaWiFS data products and ancillary data. The source code is free and available via FTP. SeaDAS is supported by the NASA ocean biochemistry program in the framework of the SeaWiFS project, and it embeds all the theoretical and practical methods to process SeaWiFS (but also other sensors) data. Several updates are released, following the improvements of the protocols in retrieving and processing the ocean color data. To date (April 2003), the SEADAS version 4.4 is the current one, and it is adopted to produce all the data used in the present research.

SeaWiFS data, as well as other remote sensing data, are classified on a basis of the processing status. In the case of SeaWiFS, additional products (the ancillary information) are involved in the processing methodologies.

Here follows a brief list of the satellite and ancillary data involved in the SEADAS processing.

- Level 0 is the starting input, which is converted in the Level-1A data. Level-0 data contains raw radiance counts from all bands as well as spacecraft and instrument telemetry.
- Level-1A data contain all the Level-0 data, appended calibration and navigation data, and instrument and selected spacecraft telemetry that are reformatted and

also appended. There are Level-1A products for each of the following data types: global-area coverage (GAC), local-area coverage (LAC), lunar calibration, solar calibration, TDI/gain check, and HRPT (High Resolution Picture Transmission) for direct-readout data. The generic term LAC is also used to refer to all full-resolution, recorded data, including lunar, solar, and TDI data. HRPT data are collected at one of numerous HRPT ground stations, whereas all other data types are from recording dumps to the Wallops Flight Facility. GAC data are subsampled from full-resolution data with every fourth pixel of a scan line (from LAC pixels 147 to 1135) and every fourth scan line being recorded for each swath (the Earth data collection portion of an orbit). Thus, GAC data are comprised of 248 pixels per scan line, whereas all other types are comprised of 1,285 pixels per scan line. A GAC scene will also represent an entire swath, whereas LAC scenes are defined by the number of continuously recorded scans, and HRPT scenes are defined by the number of continuously received scans from one satellite pass.

- Level 2 (L2) data consists of derived geophysical parameters produced using the Level 1A radiances as input. Each Level-2 is generated from a corresponding Level-1A The main data contents of the product are the geophysical values for each pixel derived from the Level-1A raw radiance counts by applying the sensor calibration, atmospheric corrections, and bio-optical algorithms. Each Level-2 product corresponds exactly in geographical coverage (scan-line and pixel extent) to that of its parent Level-1A product and is stored in one physical HDF file. For the GAC data the products available are (SeaDAS version 4.4): six water-leaving radiances for bands at 412, 443, 490, 510, 555, 670 nm, the chlorophyll-*a* concentration, the diffuse attenuation coefficient at band at 490 nm, the ratio of chlorophyll-*a* concentration to the diffuse attenuation coefficient, the epsilon value for the aerosol correction of bands 765 and 865

nm, the angstrom coefficient for bands 490 and 865 nm, and the aerosol optical thickness at band at 865 nm. For LAC data the products are summarized in tables Table 9-1 and Table 9-2.

PRODUCT NAME	DESCRIPTION
nLw_nnn	Normalized water-leaving radiance
Lw_nnn	Water-leaving radiance
Lr_nnn	Rayleigh radiance
La_nnn	Aerosol radiance
TLg_nnn	Top-of-atmosphere (TOA) glint radiance
tLf_nnn	Foam (white-cap) radiance
Lt_nnn	Calibrated TOA radiance
T_sol_nnn	Rayleigh-aerosol transmittance, sun to ground
t_sen_nnn	Rayleigh-aerosol transmittance, ground to sensor
t_oz_sol_nnn	Ozone transmittance, sun to ground
t_oz_sen_nnn	Ozone transmittance, ground to sensor
taua_nnn	Aerosol optical depth
tau_nnn	Aerosol optical depth (alternate name for taua_nnn)
angstrom_nnn	Aerosol angstrom coefficient, alpha(nnn,865)
Es_nnn	Extraterrestrial solar irradiance
rhos_nnn	Surface reflectance
t_o2_nnn	Total oxygen transmittance
rhot_nnn	Top of atmosphere reflectance
Rrs_nnn	Remote sensing reflectance
t_f_nnn	Fresnel transmittance correction factor. (same for all bands except where view geometry is band dependent)
foq_nnn	Bi-directional reflectance correction factor.

Table 9-1. List of the 21 radiance products, where *nnn* denotes the band number.

- Ancillary data include Wind, Pressure, Precipitable H_20 and Ozone. Meteorological data are obtained by the National Center Environmental Prediction (NCEP). The source of the ozone data is the NOAA's TIROS Operational Vertical Sounder (TOVS).
- Mask and flags: the SeaDAS processing system permits to evaluate the quality of the data by the use of masks and flags, which are obtained during the production of the Level-2 file (see Table 9-3 and McClain et al., 1995).

PRODUCT NAME	DESCRIPTION
chl_oc2	Chlorophyll a concentration (OC2 algorithm)
chl_oc4	Chlorophyll a concentration (OC4 algorithm)
chl_octsc	Chlorophyll a concentration (OCTS-C algorithm)
chl_nn	Chlorophyll a concentration (derived from Neural Net Pigment algorithm)
chl_ndpi	Chlorophyll a concentration (derived from Normalized Difference Pigment algorithm)
chlor_a	Alternate name for chl_oc4
pig_oc2	Pigment concentration (derived from chl_oc2)
pig_oc4	Pigment concentration (derived from chl_oc4)
pig_octsc	Pigment concentration (derived from chl_octsc)
pig_nn	Pigment concentration (Neural Net Pigment algorithm)
pig_ndpi	Pigment concentration (Normalized Difference Pigment algorithm)
L2_flags	Level 2 processing flags
aer_model_min	Minimum bounding aerosol model #
aer_model_max	Maximum bounding aerosol model #
aer_model_ratio	Model mixing ratio
aer_num_iter	Number of aerosol iterations, NIR correction
Epsilon	Retrieved epsilon used for model selection
eps_78	Alternate name for epsilon (scaled to byte)
Solz	Solar zenith angle
Sola	Solar azimuth angle
Senz	Sensor zenith angle
Sena	Sensor azimuth angle
K_490	Diffuse attenuation coefficient at 490 nm
Par	Photosynthetically active radiation
glint_coeff	Glint radiance normalized by solar irradiance
aerindex	Aerosol index (for identification of absorbing aerosols)
Ozone	Ozone concentration (from input ancillary data)
windspeed	Magnitude of wind (m/s)
windangle	Wind direction (deg) N=0, E=90
Zwind	Zonal wind speed (m/s)
mwind	Meridional wind speed (m/s)
Water_vapor	Precipitable water concentration
pressure	Barometric Pressure
humidity	Relative Humidity
Cloud_albedo	Reflectance used for cloud/ice thresholding (historical name)
Fsol	Solar distance correction factor per scan
Sst	Sea Surface Temperature (interpolated from climatology to pixel location)
chl_gsm01	Chlorophyll-a concentration (Garver-Siegel-Maritorena 2001 model)
Acdm_gsm01	Absorption Coefficient for dissolved detrital material (Garver-Siegel-Maritorena Model)
bbp_gsm01	Particulate Backscatter Coefficient (Garver-Siegel-Maritorena 2001 Model)
Calcite	Calcite Concentration (Gordon, et al.)
evi	Enhanced Vegetation Index
ndvi	Normalized Difference Vegetation Index

Table 9-2. List and description of the SeaDAS SeaWiFS products.

- The mask and the flags contribute to a Quality Control (QC) check on the SeaWiFS data. Even if the algorithms related to flags and masks are the same, they act on a different way on the data stream. During the pixel by pixel

processing, SEADAS checks the occurrence of the conditions for a questionable pixel, storing this information on the L2_flags product. However, if masks are active, the processed pixel is considered erratic and the procedure starts to process the next one. Then, it is possible to process all the pixels in a scene, maintaining however the information on the QC in the L2_flags product. On the other hand, to gain CPU time, all the questionable pixels (as derived by the QC) can be discarded, and no geophysical information are calculated.

1	Atmospheric correction algorithm failure
2	Land (MASKLAND)
3	Missing ancillary data
4	High sun glint (MASKGLINT)
5	High TOA radiance (MASKHILT)
6	Large sensor zenith angle (MASKSATZEN)
7	Shallow water (MASKBATH)
8	Negative water-leaving radiance
9	Stray light (MASKSTLIGHT)
10	Cloud or ice (MASKCLOUD)
11	Coccolithophores
12	Turbid water
13	Large solar zenith angle (MASKSUNZEN)
14	High aerosol concentration
15	Cloud shadow
16	Chlorophyll algorithm failure
17	Questionable navigation
18	Absorbing aerosol
19	Tricodesmium
20	NIR algorithm exceeded maximum iteration
21	Moderate sun glint
22	Questionable chlorophyll
23	Questionable atmospheric correction
24	Dark pixel
25	Sea ice expected
26	Navigation failure
27	Filter rejection

Table 9-3. List of the SeaDAS masks and flags.

9.2.2 The acquisition and processing system

The Satellite Oceanography Group (GOS) of Rome developed a system (FD) that provides satellite ocean colour images and data on the web. The system has been developed to produce: 1) fast delivery images for monitoring applications and operational support on oceanographic cruises; 2) accurate ocean colour products for geophysical studies. Real Time Images of SeaWiFS chlorophyll-*a* concentration,

clouds/case I/case II water flags and true color images are obtained by processing the satellite passes using climatological ancillary data. These images are provided daily through an *ad hoc* automatic procedure that processes the raw satellite data and makes it available on the web within an hour after the acquisition. All the images are stored in a gallery archive organized in a calendar chart for the selection of the images to display. In addition, accurate maps of the most relevant products (see later) are produced in near real time (typically after 4 days) as soon as daily meteorological ancillary data are made available on the NASA website.

All the data are stored on disk up to level 2. This permits an easy and rapid reprocessing of data if necessary (i.e. for a new version of SEADAS, for creation of specific non-standard products, for testing new algorithms or data processing).

9.2.2.1 SeaWiFS raw data

SeaWiFS sensor acquires approximately 15 pole-to-pole orbital swaths of data per day, and approximately 90% of the ocean surface is scanned every two days. SeaWiFS acquires data at a nadir resolution of 1 km per pixel (Local Area Coverage resolution). This data is broadcast continuously and can be recorded by any High Resolution Picture Transmission (HRPT) ground station within range. Each HRPT pass will be kept as one image. So HRPT scenes can range from very short (if the satellite is at the horizon of the station) to very long (several minutes). The Satellite Oceanography Group (GOS) operates an HRPT receiving station located in Rome (41.84°N, 12.65°E) since 1998. Data from NOAA/AVHRR and Orbview-2/SeaWiFS images are acquired and processed daily. Through an agreement with NASA and Orbimage, the Rome section of the Institute of Atmospheric Sciences and Climate (ISAC) of the National Council of Research of Italy (CNR) is operating the only SeaWiFS real-time direct readout station (HROM) with complete coverage of the Mediterranean Sea. The SeaWiFS mission is a public-private partnership between NASA and Orbital Sciences Corporation. For that

reason, access to the data during the mission is restricted to Authorized Users who will use the data for scientific purposes. HROM is a NASA authorized station along with 102 other stations worldwide. Two or three swaths per day are necessary for a complete coverage of the Mediterranean basin. The SeaWiFS scan has a width of 58.3 deg and a coverage of 2500 km. The scan period is of 0.167 seconds. This means that a usual swath of about 2900 scanned lines takes about eight minutes for being acquired by the HROM ground station.

9.2.2.2 Operational environment

The FD system performs the following three main functions: data acquisition, data processing and data distribution.

The *acquisition function* is performed by the Quorum HRPT Data Capture Engine. It is a system that consists of a 1.2 m parabolic antenna equipped with a Tracking Antenna Controller, a GPS receiver, a MetCom DSP receiver and a set of electronics that interact with the QtrackNTDB program, operating under Windows 2000, which has controlling and data capture functions, decryption included.

The input for the acquisition function is the encrypted HRPT data, broadcasted continuously by the satellite for reception by the HRPT stations. In general HRPT data are lost unless received by a ground station or recorded. Each HRPT scene is kept as one image, so it can range from very short (if the satellite is at the horizon of the station) to very long (several minutes). LAC (Local Area Coverage) data is actually Recorded HRPT data. LACs are output up to three times per day according to the Orbview-2 direct broadcast schedule, and are de-crypted by the Data Capture Facility prior to being frame formatted. The so reconstructed files are called Level 0 file (L0).

The *processing function* basically consists of a Level 0 to 1 processor, a Level 1 to 2 processor and a Level 2 to needed products processor. Processors are simply related by sequential input-outputs: the output of a processor is the input of the following one.

Two softwares are involved in performing the processing steps: SeaDAS version 4.4 and DSP.

DSP (Display Software Package) is a software system supporting oceanographic satellite data and image processing. It has been developed by the remote sensing group of the University of Miami /RSMAS. It runs under Unix operative system.

SeaDAS is used for the first two processing steps and for part of the third one. DSP is used exclusively for the third processing step.

9.2.3 The processing

9.2.3.1 L0 to L1

The L0 to L1 conversion is conducted in the SeaDAS environment. The program reads in SeaWiFS Level 0, 10-bit Data Capture Facility (DCF) frame-formatter files and creates a Level-1A file in Hierarchical Data Format (HDF) for each scene. Level 1A image data are raw, and all spacecraft and instrument telemetry are retained in raw form as in the Level 0 data. In addition, geolocation data, instrument telemetry and selected spacecraft telemetry are converted and appended. The program needs a file called elements.dat to calculate the navigation information that is included in the L1A output. The data in the file are orbit position and velocity elements produced by the program, using onboard GPS data and a high order orbit propagation model. They are accurate and are used to meet navigation accuracy (goal is 1 pixel). The elements.dat file is needed as input to navigation algorithms in order to initialize the GPS filtering methods in the program. To obtain the best navigation, the most recent version of elements.dat from the SeaWiFS Project (from a NASA ftp site) is downloaded every day automatically. The downloaded file is derived using a larger number of GPS data and may incorporate occasional navigation corrections. The L1 file produced is temporary stored on disk (a month) for further processing. An e-mail to send to the SeaWiFS

project is automatically generated in order to advise for ftp data ready to the Goddard DAAC NASA archive.

As the L1 file is produced it is immediately involved in the next processor: L1 to L2

9.2.3.2 L1 to L2 processing with climatological ancillary data

This SeaDAS program performs Level-2 processing on SeaWiFS data and generates Level-2 geophysical products by applying atmospheric corrections and bio-optical algorithms to the SeaWiFS data. There are 211 Level-2 products available for output. Any combination of these 211 products may be selected for output and written to up to 4 different output files. At this step of the processing chain, GOS has defined its output products by choosing the chlorophyll a concentration retrieved with the OC4 algorithm and the L2_flags for indicating if any algorithm failures or warning conditions occurred. The processor has a single L2 file as output in which are stored the appended data of the products selected.

The SeaWiFS Level-2 processing program requires both meteorological and ozone ancillary inputs. These two ancillary input files derive from either neal-real time (NRT) or climatology sources. The Near Real Time source takes about four days before be available. For this reason, climatological ancillary data are used in this processing step.

9.2.3.3 L1 to L2 processing with Near Real-Time Ancillary Data Products

The L1A files remain archived in the temporary GOS disk, waiting for the availability of the correspondent NRT ancillary data. The NRT ancillary data are meteorological (meridional wind, zonal wind, pressure, and relative humidity) and total ozone, used during the Level-2 operational processing. They are usually available after 4 days. The current source for meteorological data is the NCEP, while the current source for ozone data is TOVS.

In the NRT L2 processing a larger number of products is selected for being retrieved by the L1 file. Nineteen products are divided up into two outputting L2 files: an atmospheric file containing ten products related to atmosphere (i.e optical thickness, aerosol index) and an oceanic file containing 9 products related to water parameters (i.e. water leaving radiances for different bands, chlorophyll-a concentration). Using NRT ancillary data for L2 processing gives more accurate data values then using the climatological one especially in days in which the meteorological values differ from the long-term monthly means. For this reason GOS has chosen to process more products in NRT then in RT. Researchers need the most accurate data set for conducting their scientific studies.

9.2.3.4 Extraction and mapping

The NRT L2 output is a file of large dimensions. It can reach a size of 120 MByte and even more, depending on the number of scan lines of the passage and on the number of products processed. In order to have a mapped data image file for each product, a DSP procedure has been developed for performing the product extraction from the L2 file and its mapping on mercatore map. Products are mapped both in high resolution (1 km^2 per pixel) and in low resolution (4 km^2 per pixel) along with flags data. The twenty outputted product files are then archived both on disk and on DAT magnetic tapes. These products are classified as standard because of the normal use which GOS does of them.

1.1 APPENDIX III - IMAGES

1.1.1 NWMED REGION – Figures 6-1 and 6-3

Figure 6-1. SeaWiFS chlorophyll imagery time series in the NWMED region for the 1998

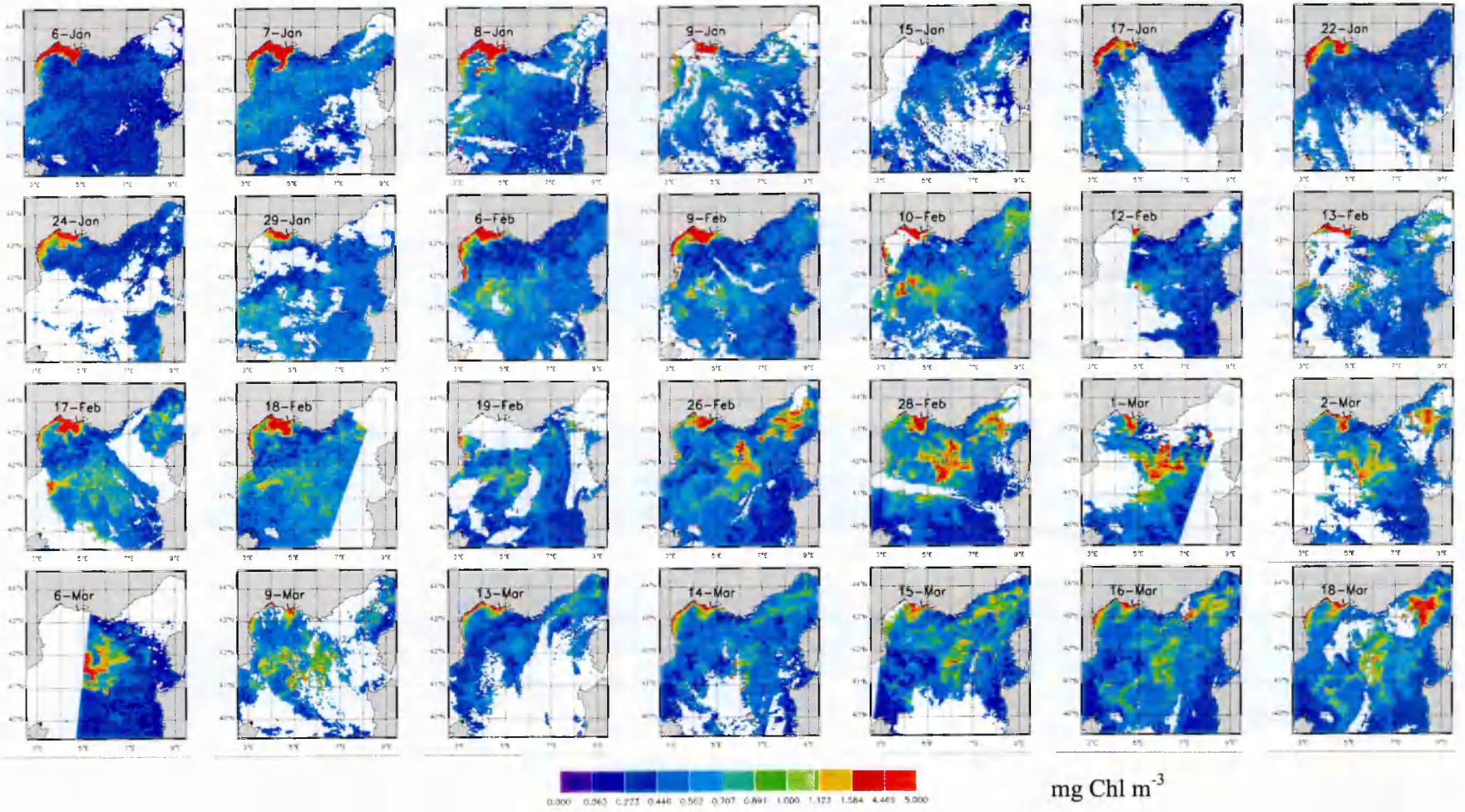

Figure 6-1 (cont). SeaWiFS chlorophyll imagery time series in the NWMED region for the 1998.

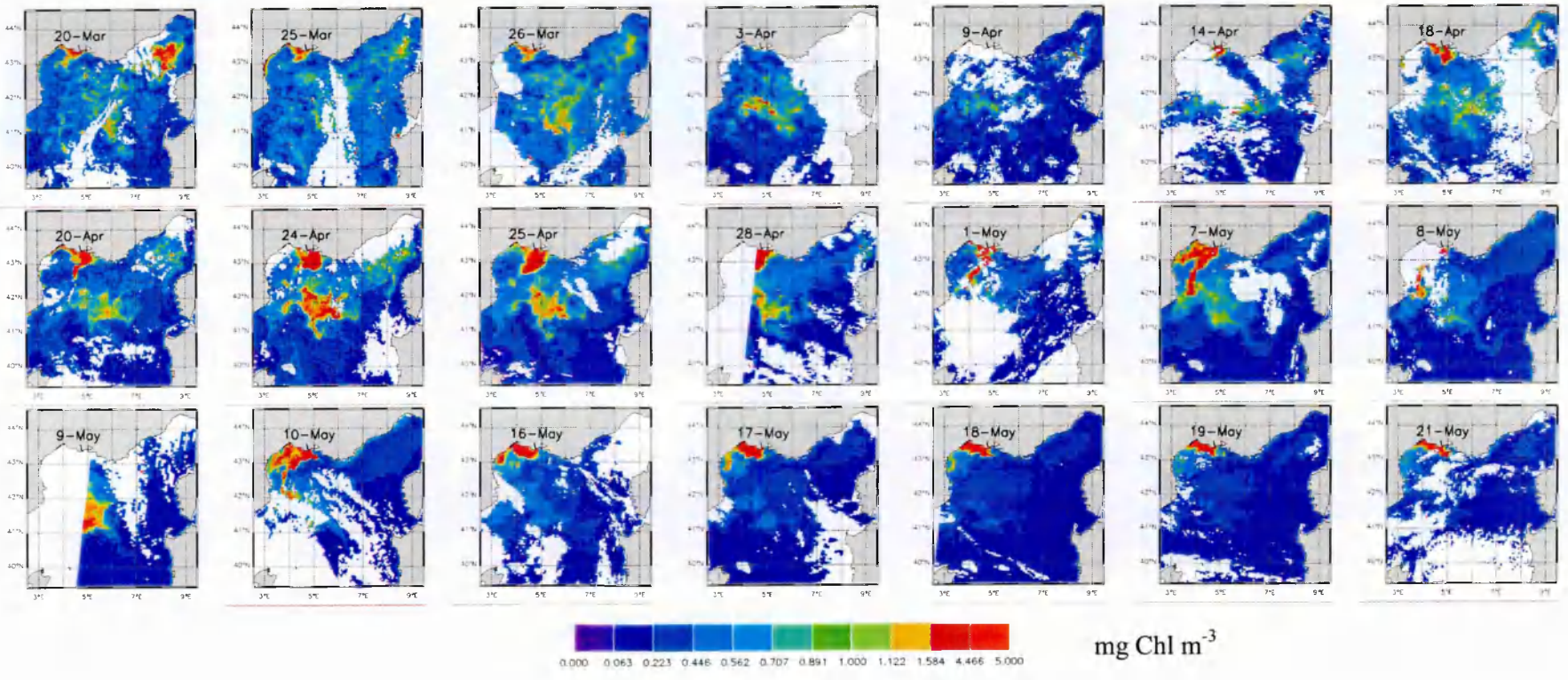

Figure 6-1 (cont). SeaWiFS chlorophyll imagery time series in the NWMED region for the 1999.

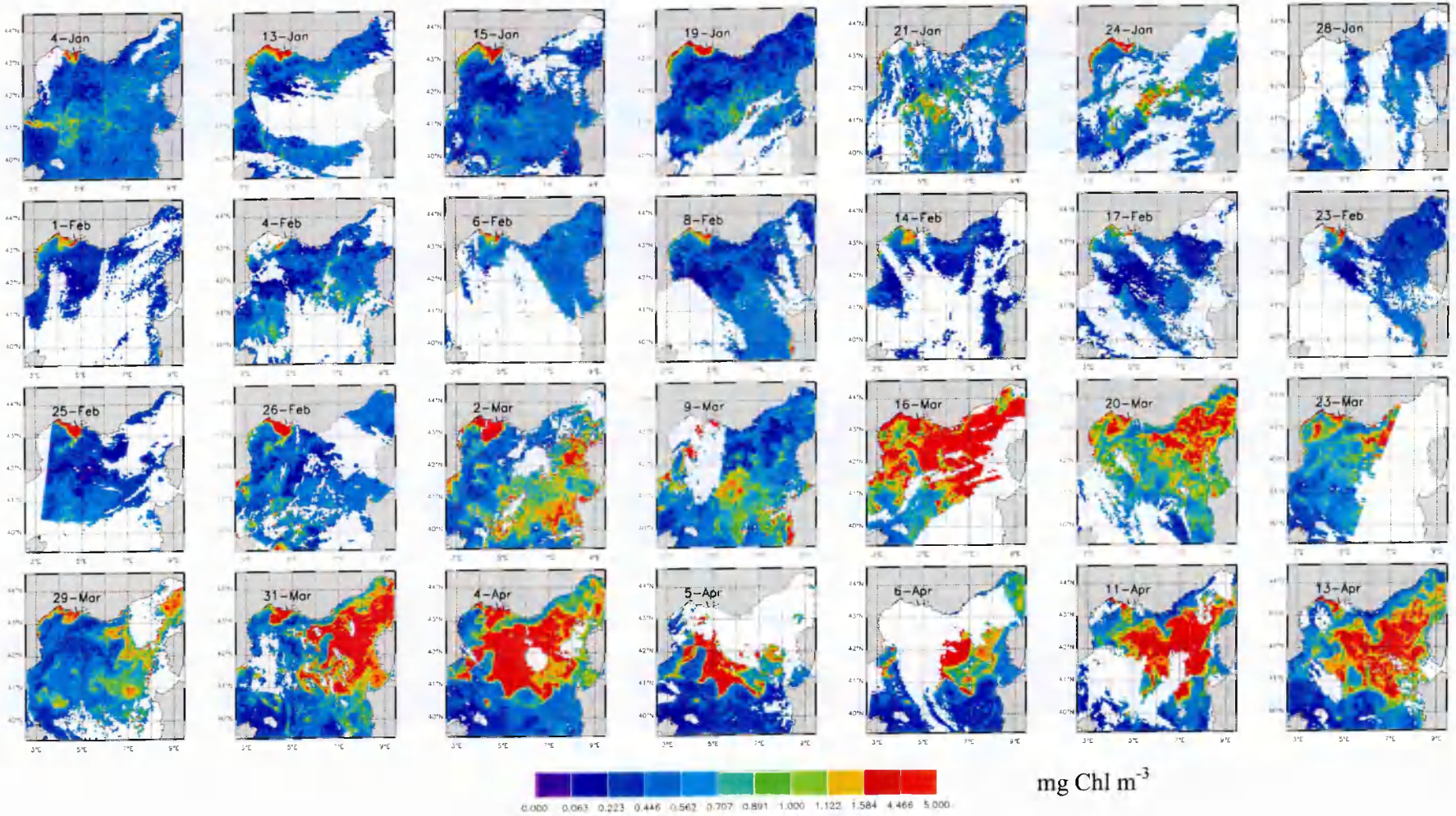

Figure 6-1 (cont). SeaWiFS chlorophyll imagery time series in the NWMED region for the 1999.

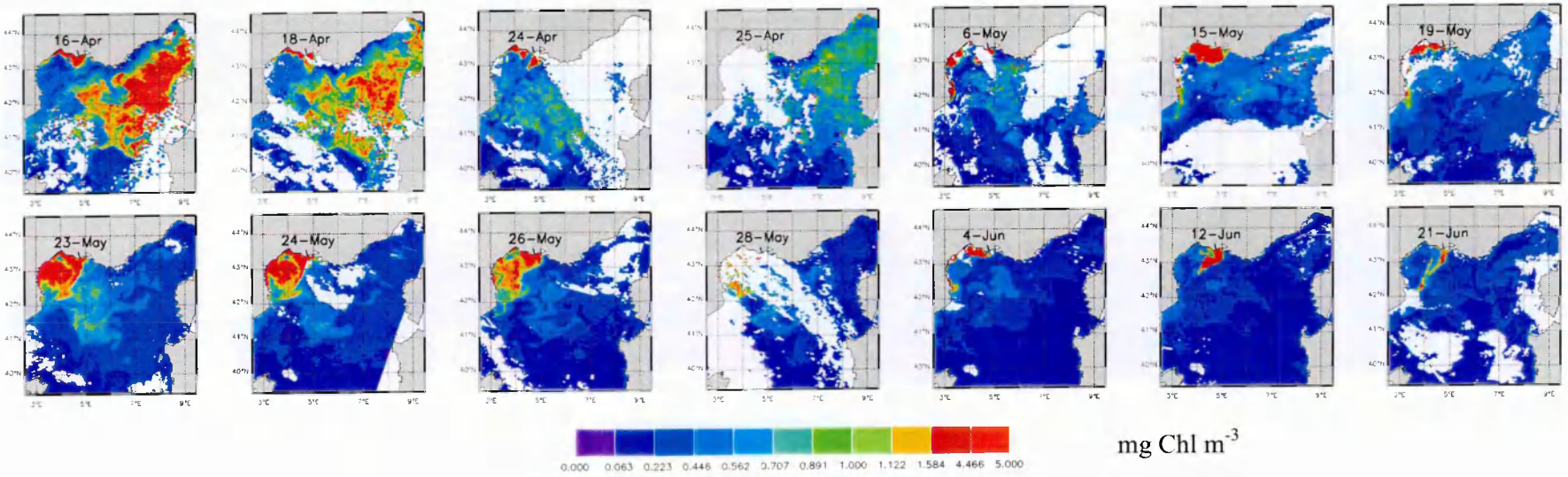

Figure 6-1 (cont). SeaWiFS chlorophyll imagery time series in the NWMED region for the 2000.

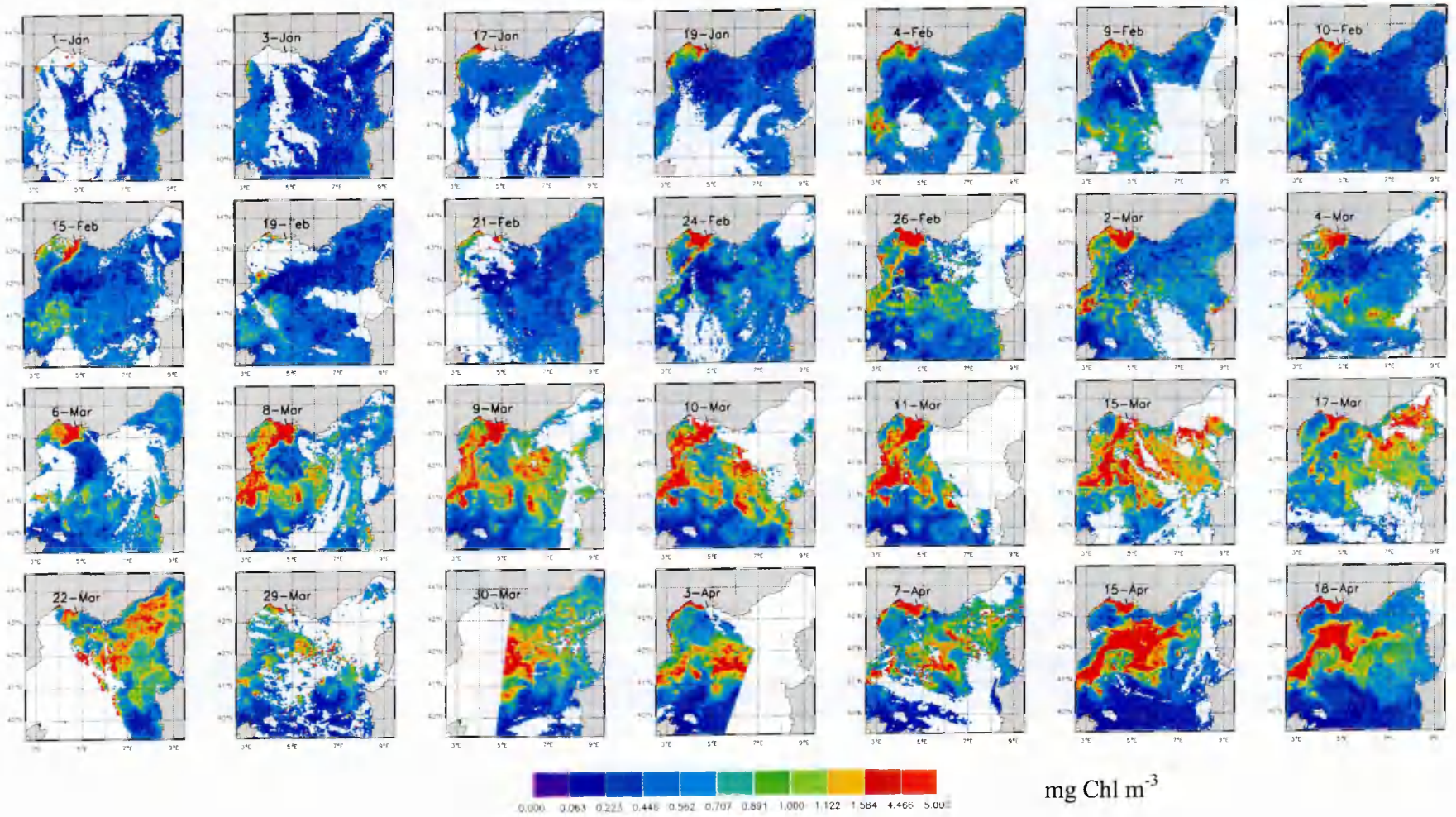

Figure 6-1 (cont). SeaWiFS chlorophyll imagery time series in the NWMED region for the 2000.

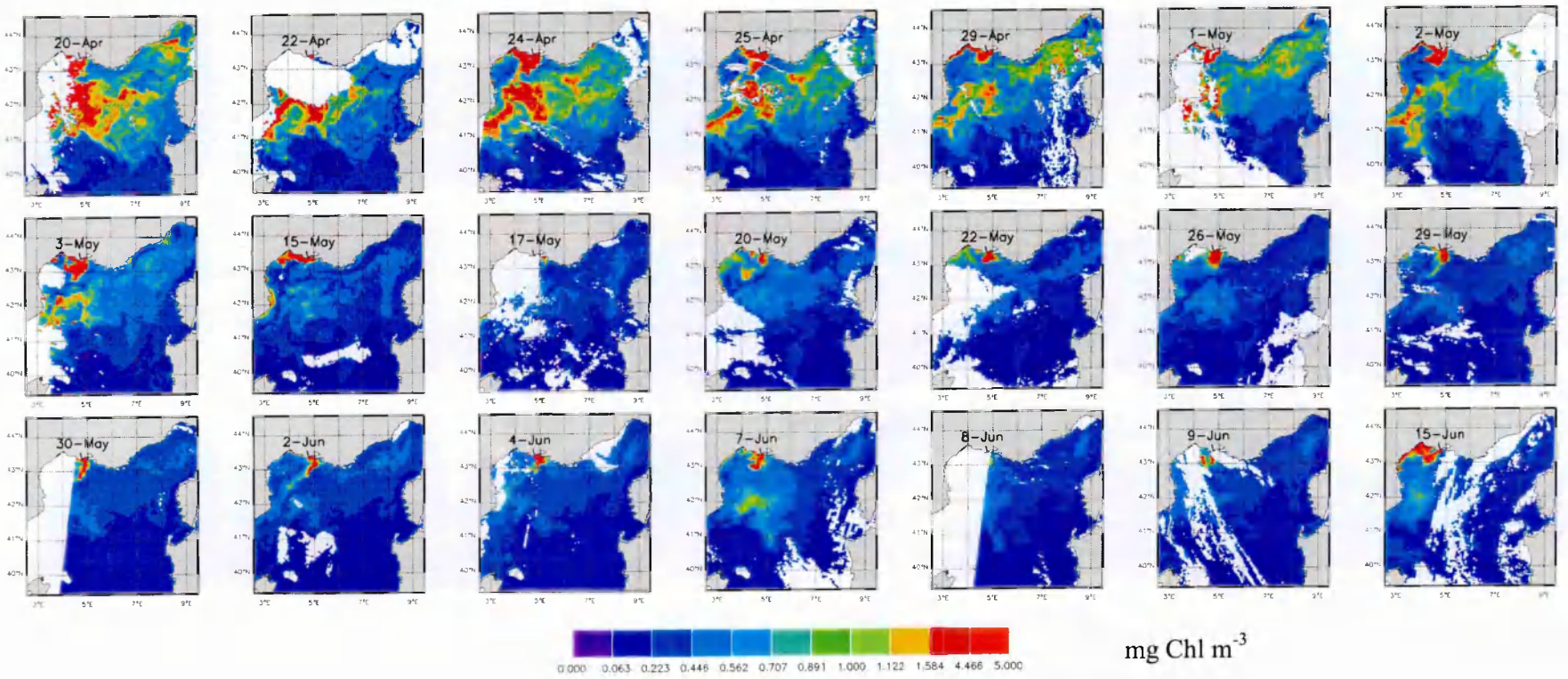

Figure 6-1 (cont). SeaWiFS chlorophyll imagery time series in the NWMED region for the 2001.

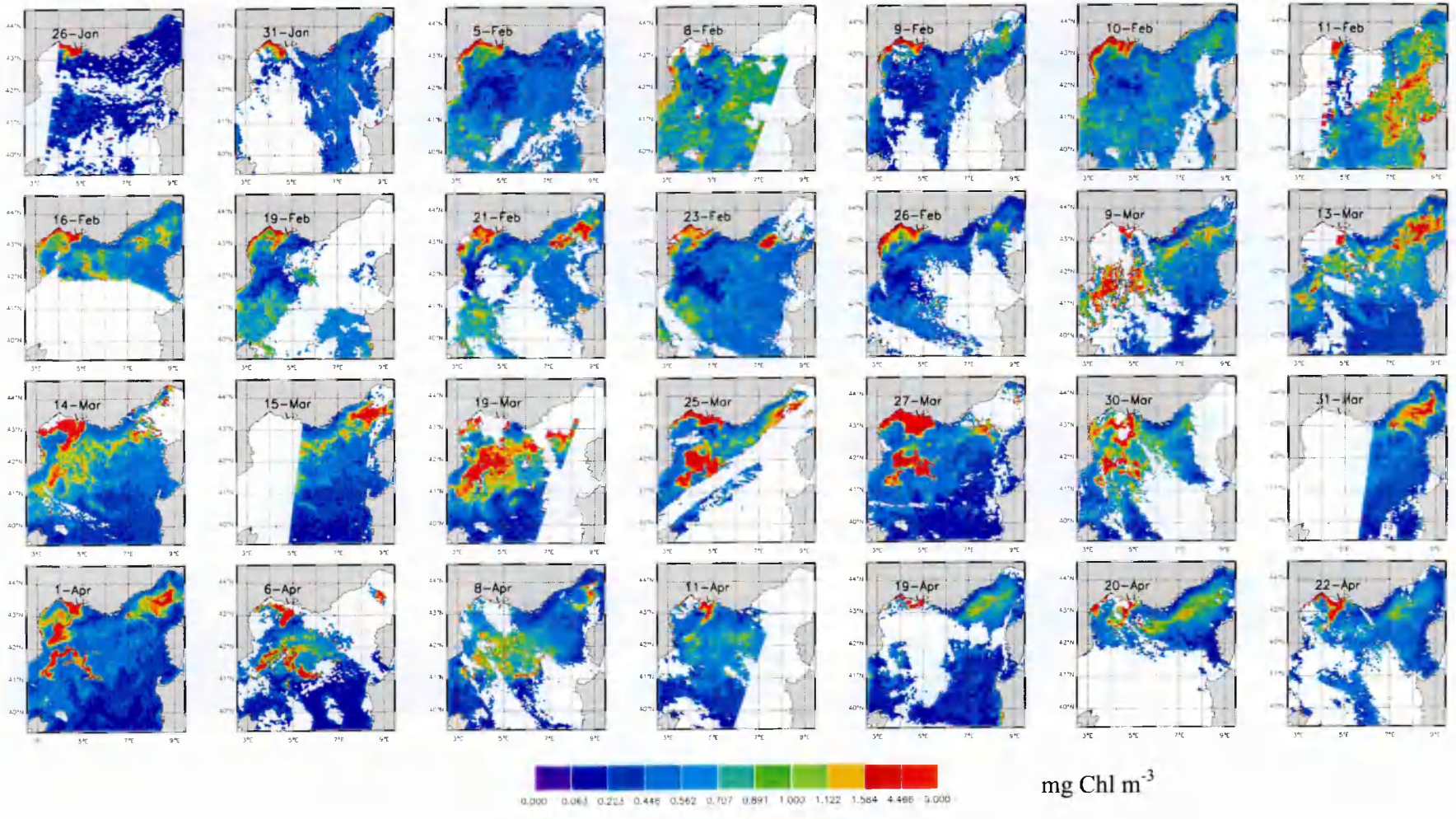

Figure 6-1 (cont). SeaWiFS chlorophyll imagery time series in the NWMED region for the 2001.

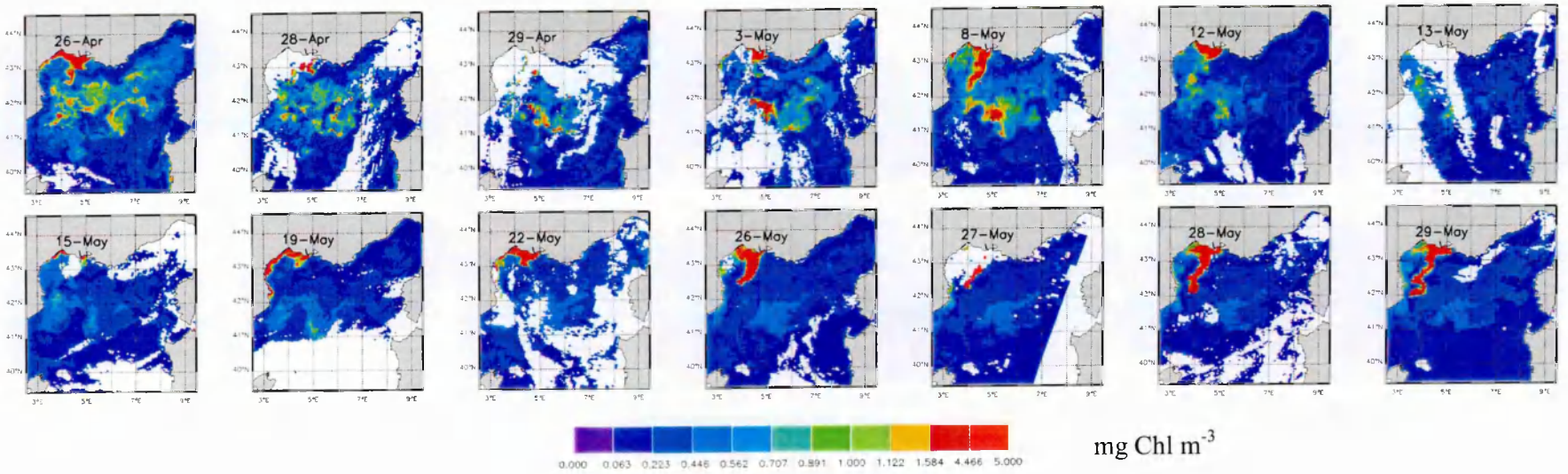

Figure 6-3. Chlorophyll concentrations and winds field stress (1998). Note that chlorophyll palette is different than figure 6-1.

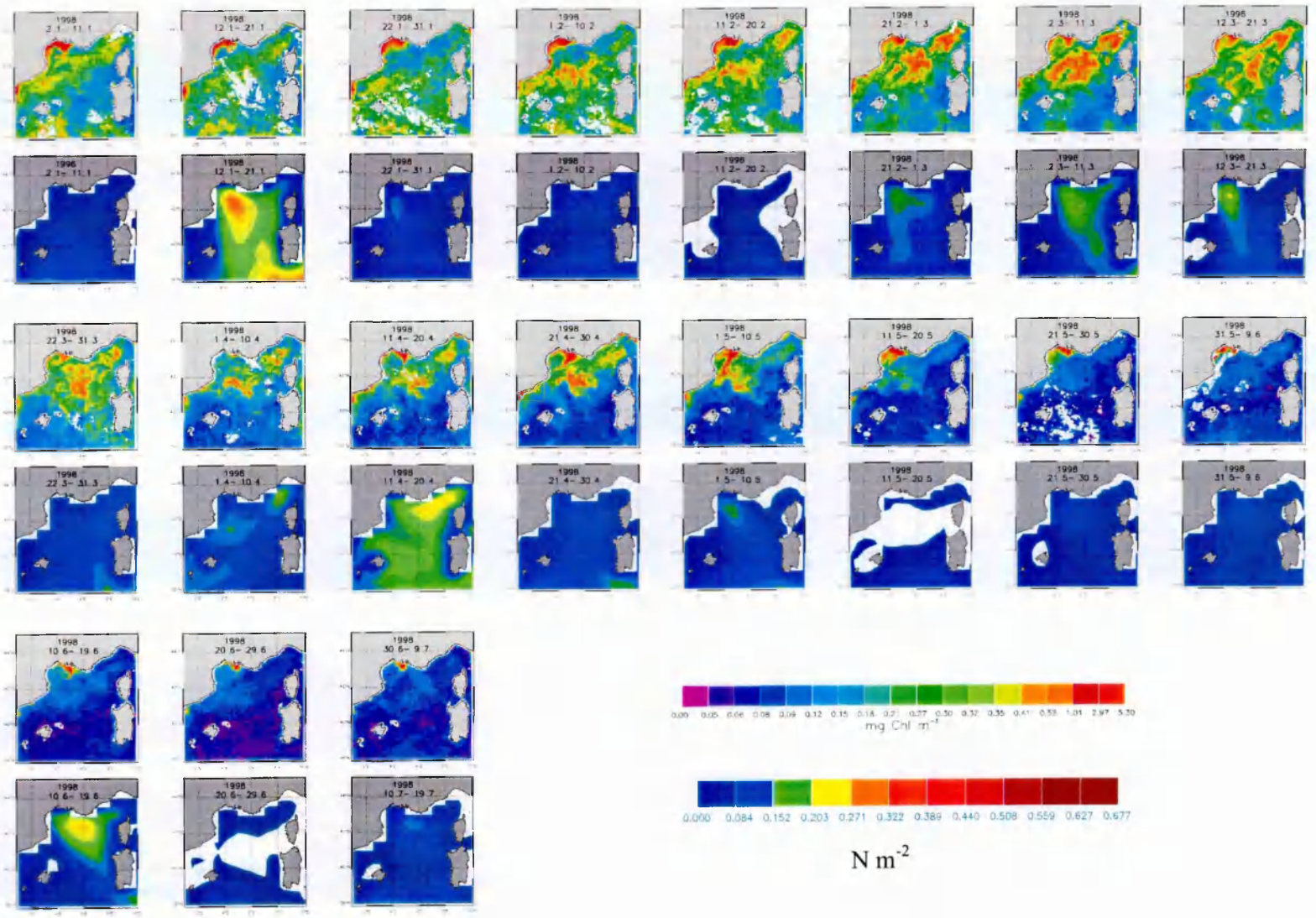

Figure 6-3. Chlorophyll concentrations and winds field stress (1999).

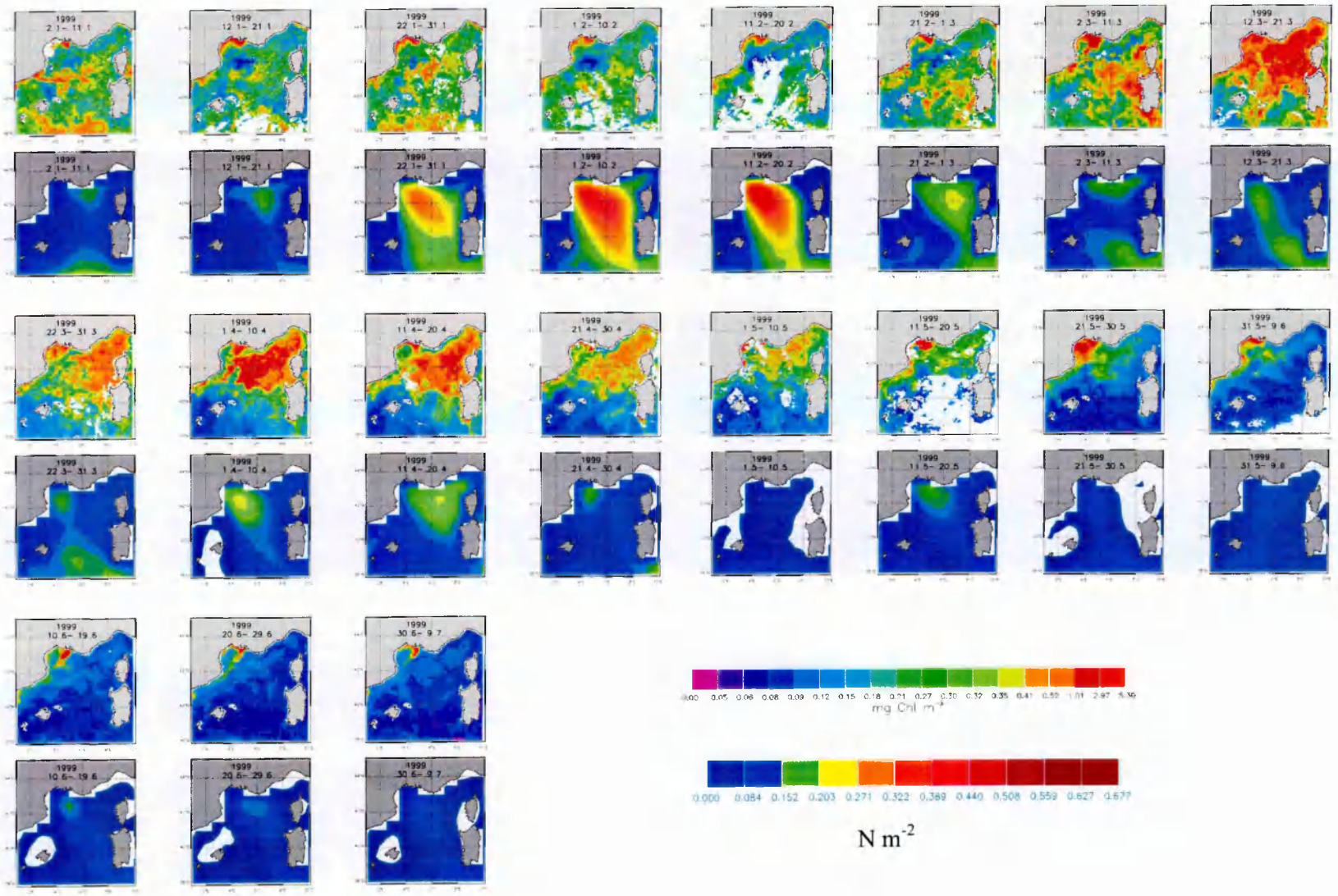

Figure 6-3. Chlorophyll concentrations and winds field stress (2000).

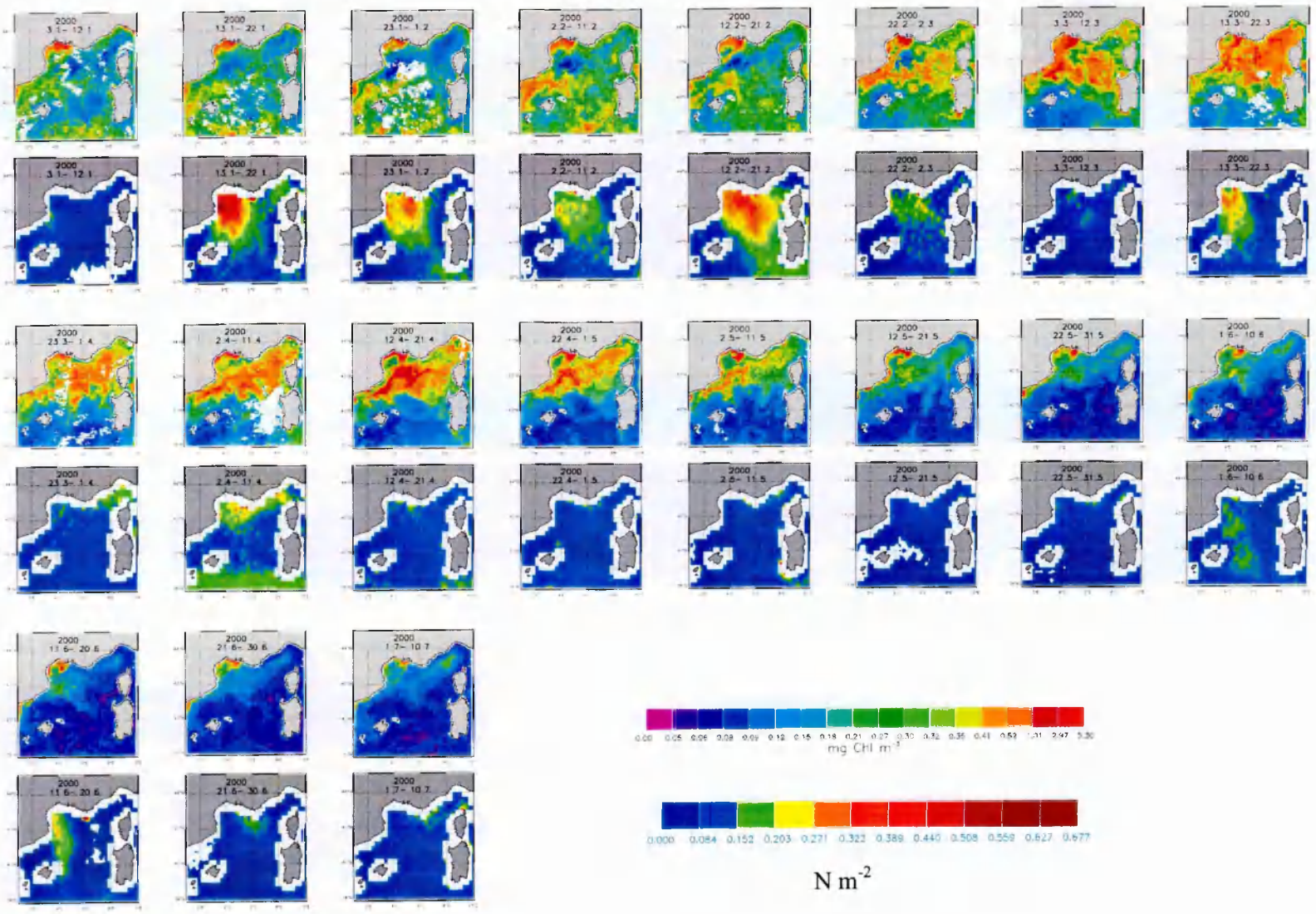

Figure 6-3. Chlorophyll concentrations and winds field stress (2001).

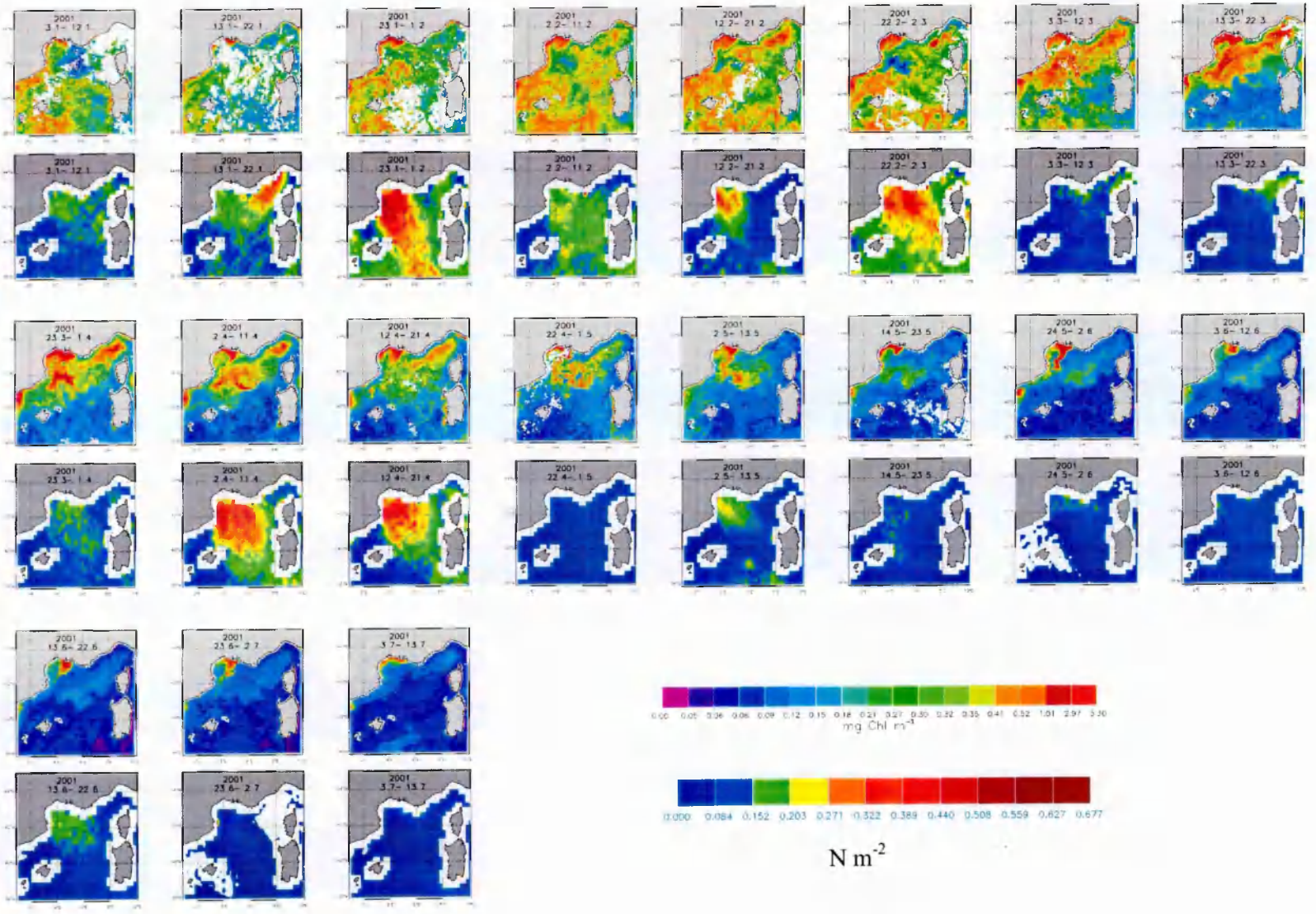

Figure 6-3. Chlorophyll concentrations and winds field stress (2002).

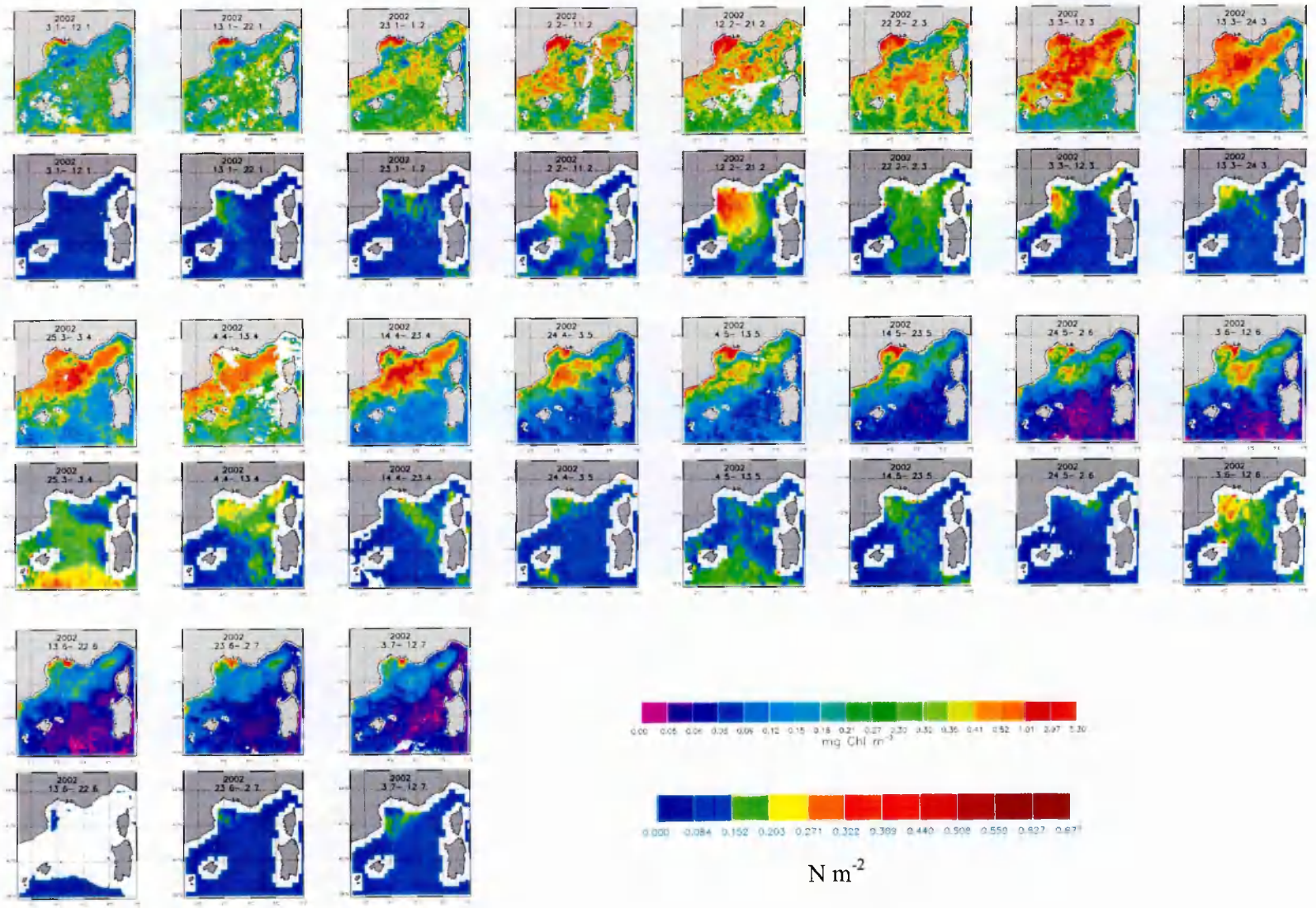

1.1.2 SOUTH ADRIATIC- Figures 6-4, 6-5, 6-6

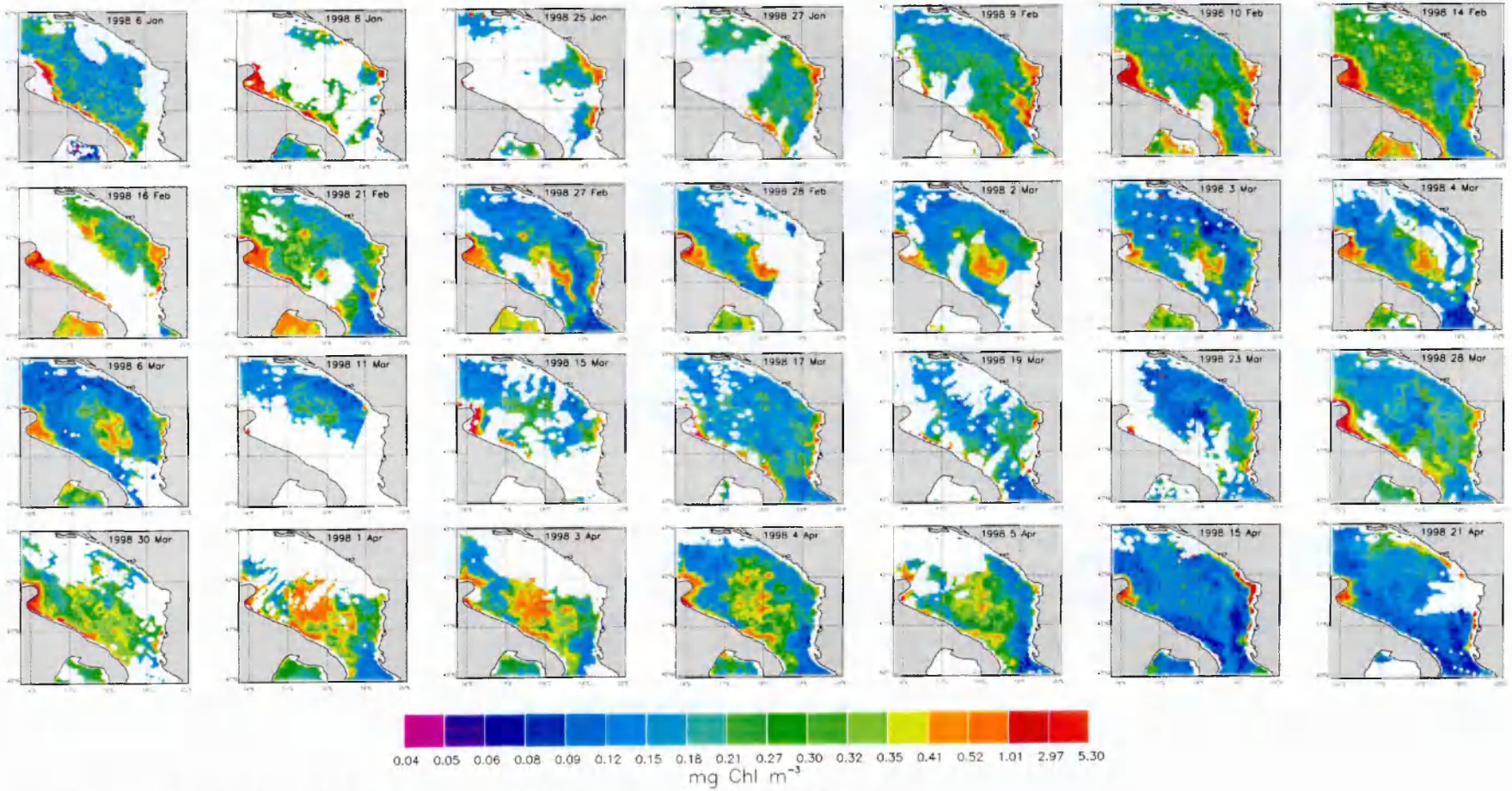

Figure 6-4. Year 1998: SeaWiFS chlorophyll imagery time series of the SA region

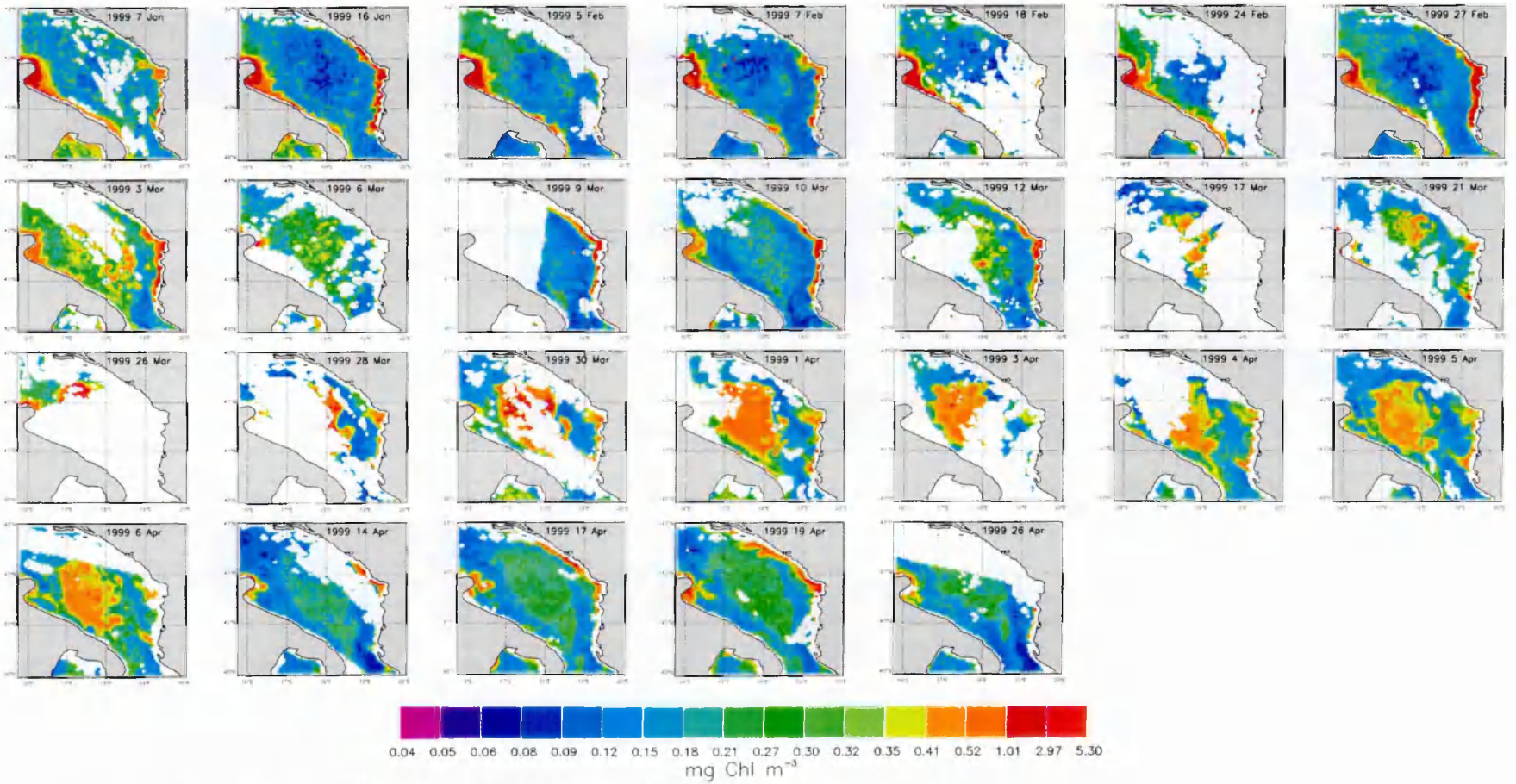

Figure 6-5. Year 1999: SeaWiFS chlorophyll-*a* imagery time series of the SA region.

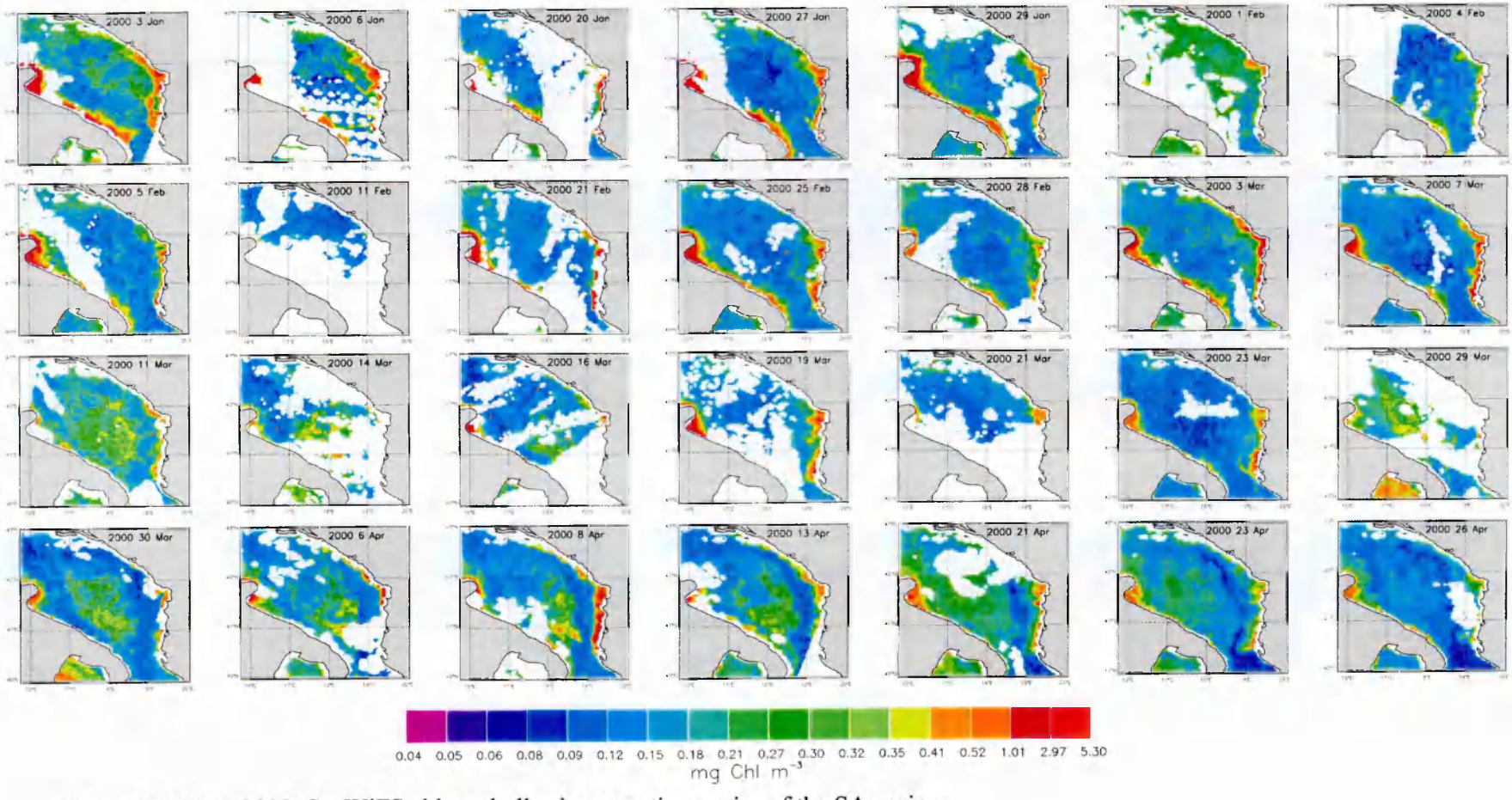

Figure 6-6. Year 2000: SeaWiFS chlorophyll-*a* imagery time series of the SA region

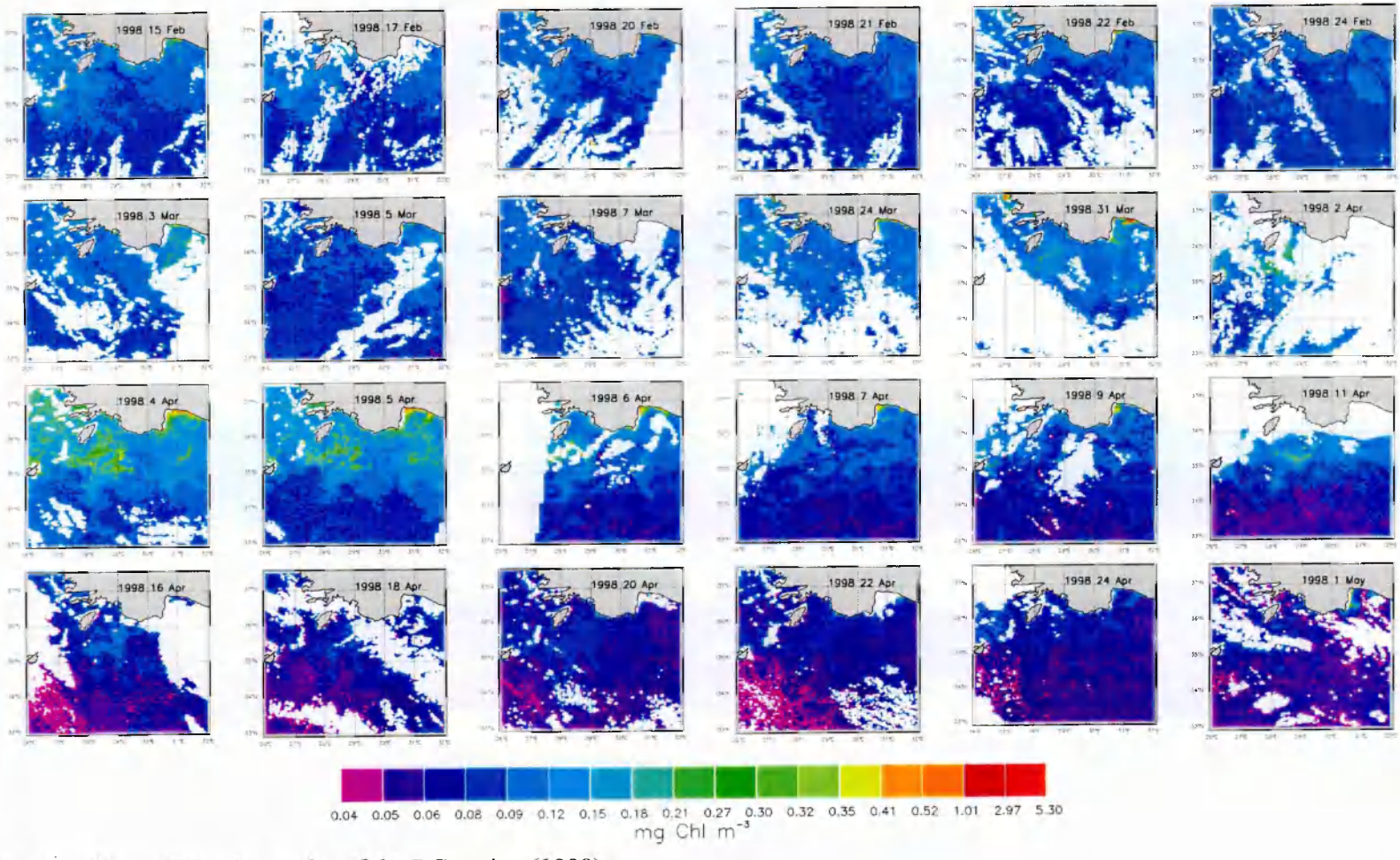

Figure 6-13. SeaWiFS imageries of the RG region (1998).

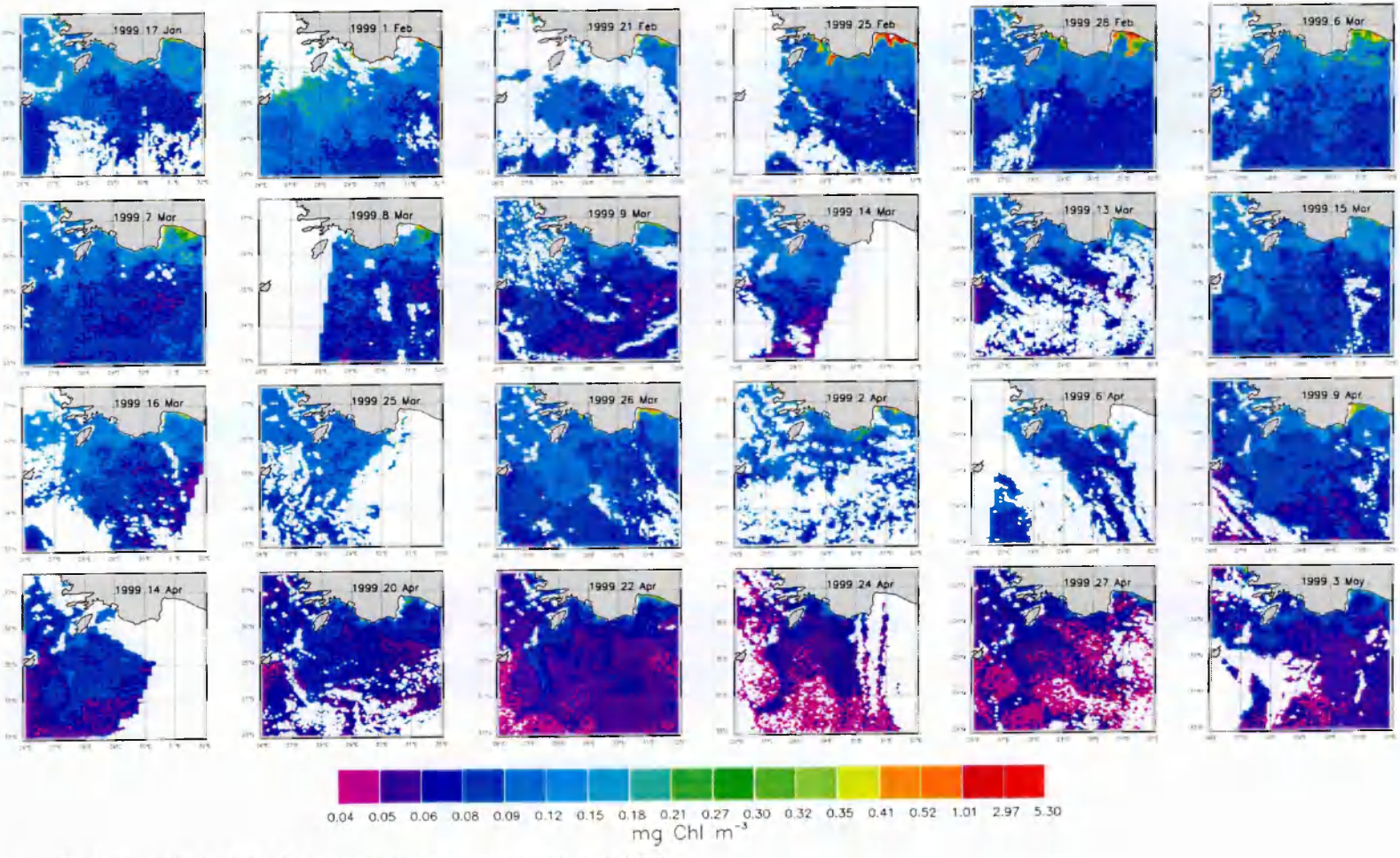

Figure 6-13 (cont). SeaWiFS imageries of the RG region (1999).

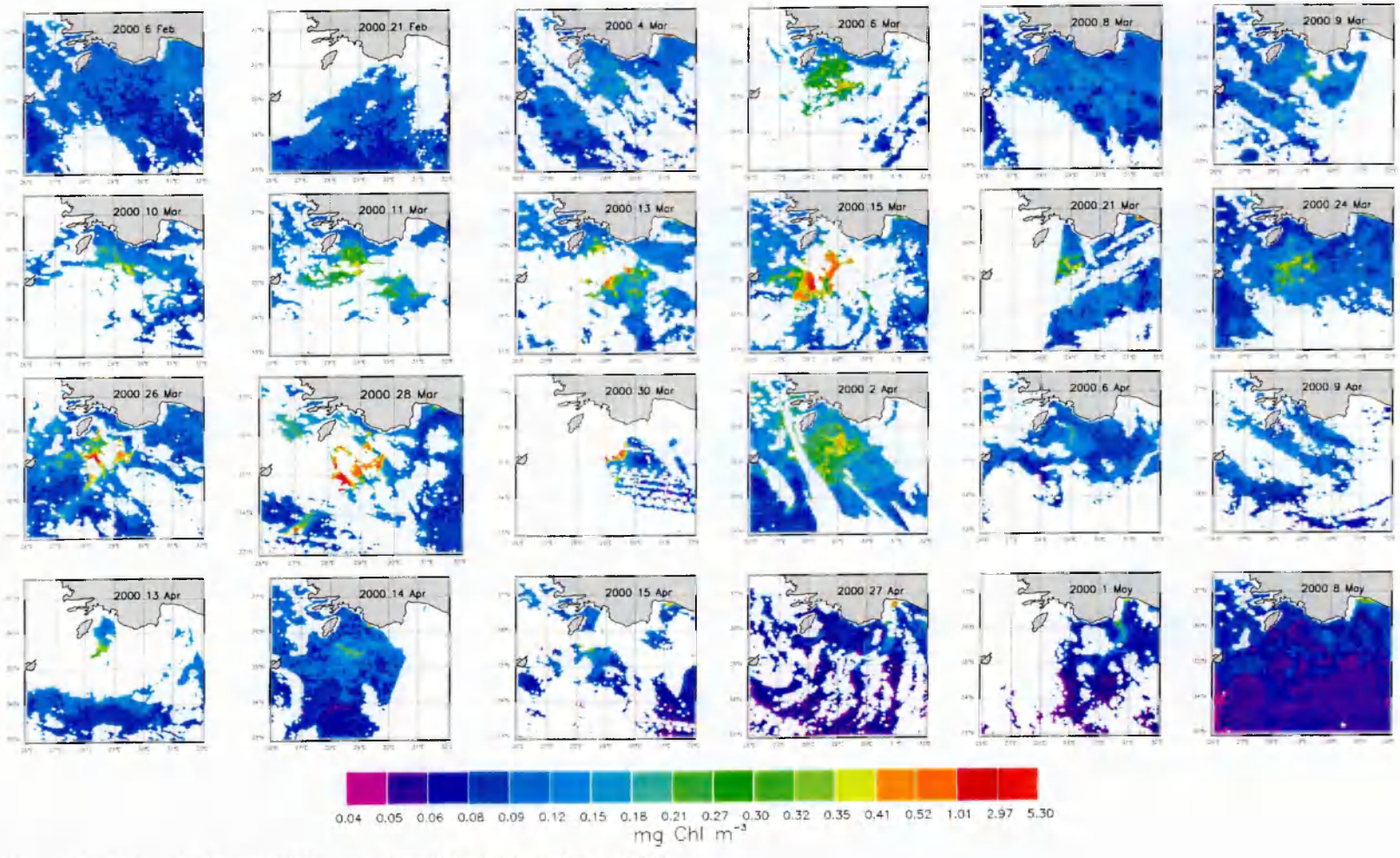

Figure 6-13 (cont). SeaWiFS imageries of the RG region (2000).

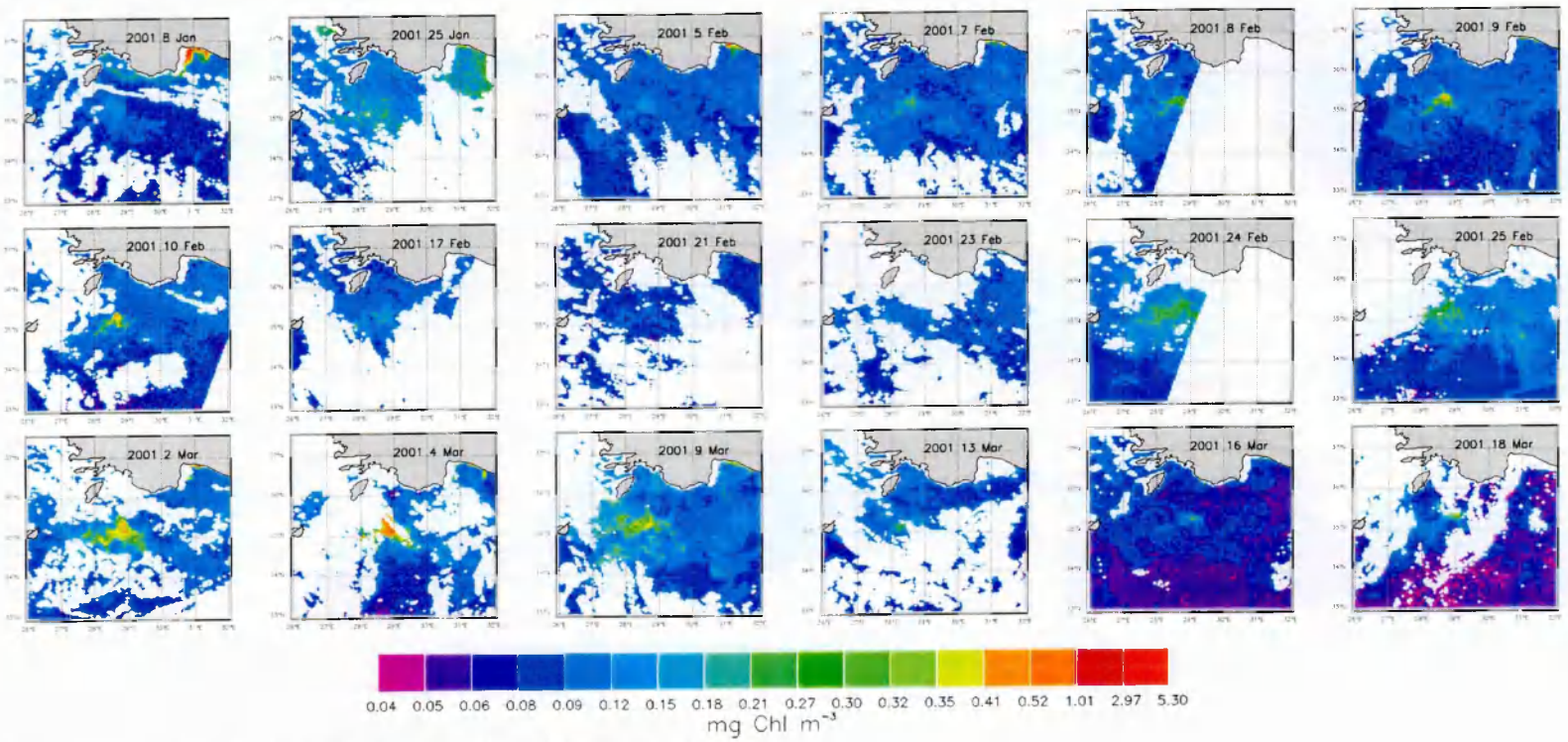

Figure 6-13 (cont). SeaWiFS imageries of the RG region (2001a).

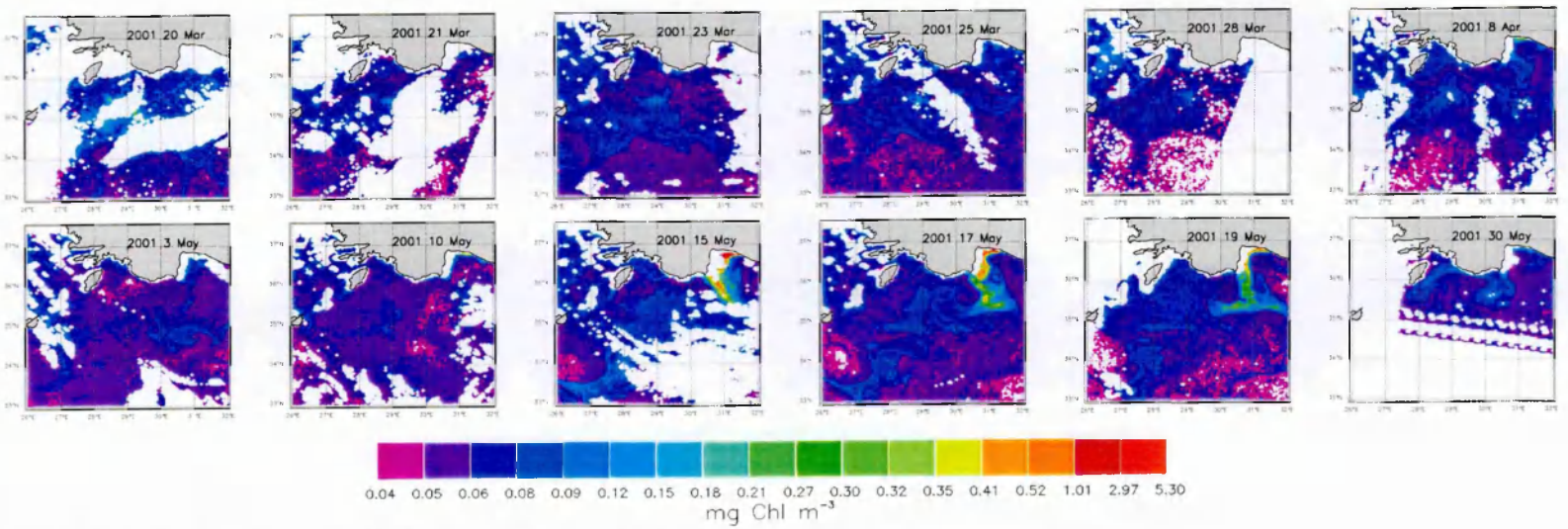

Figure 6-13 (cont). SeaWiFS imageries of the RG region (2001b).

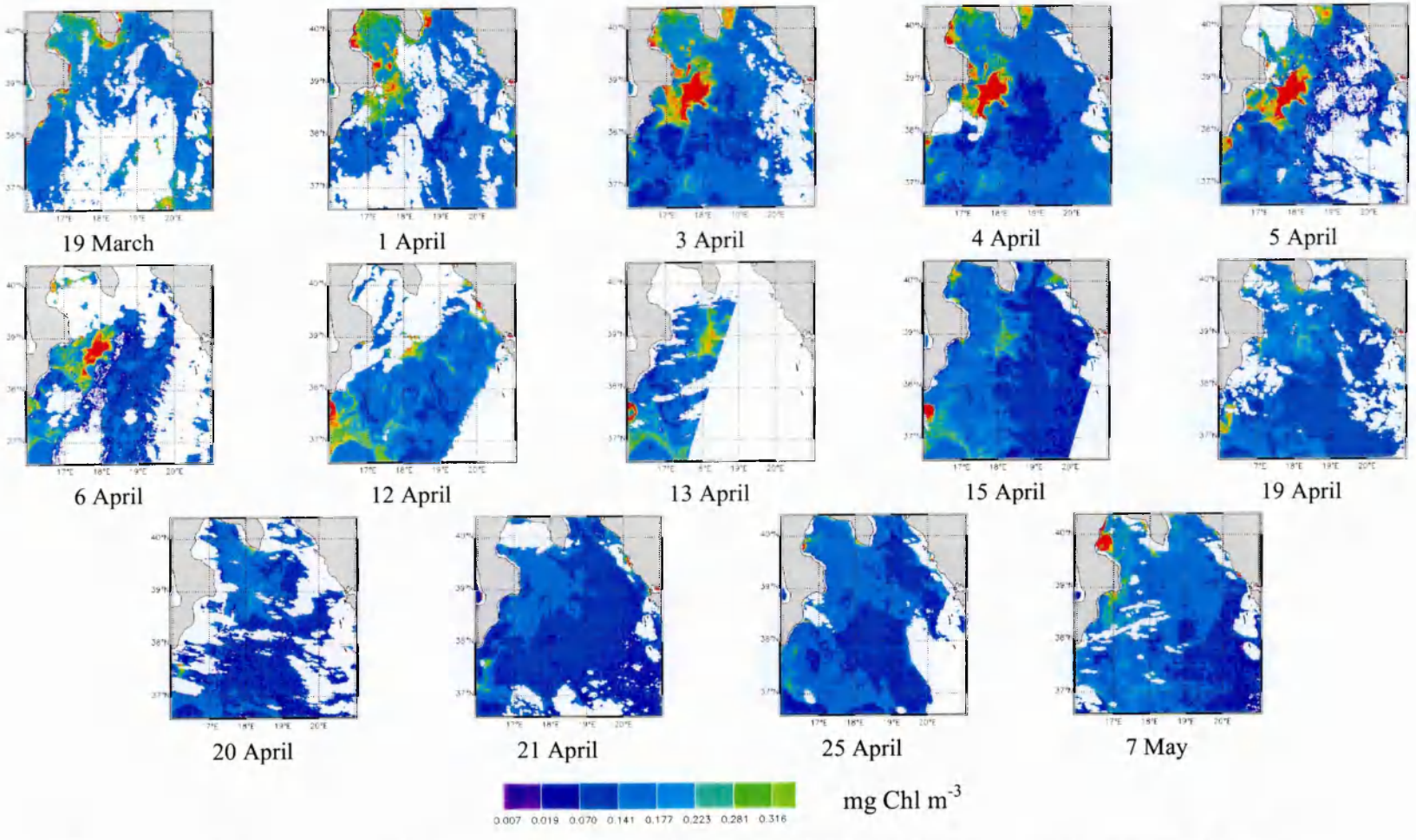

Figure7-1. Selected images of the SeaWiFS derived chlorophyll-*a* concentration over the Calabrian Bloom region (1998).

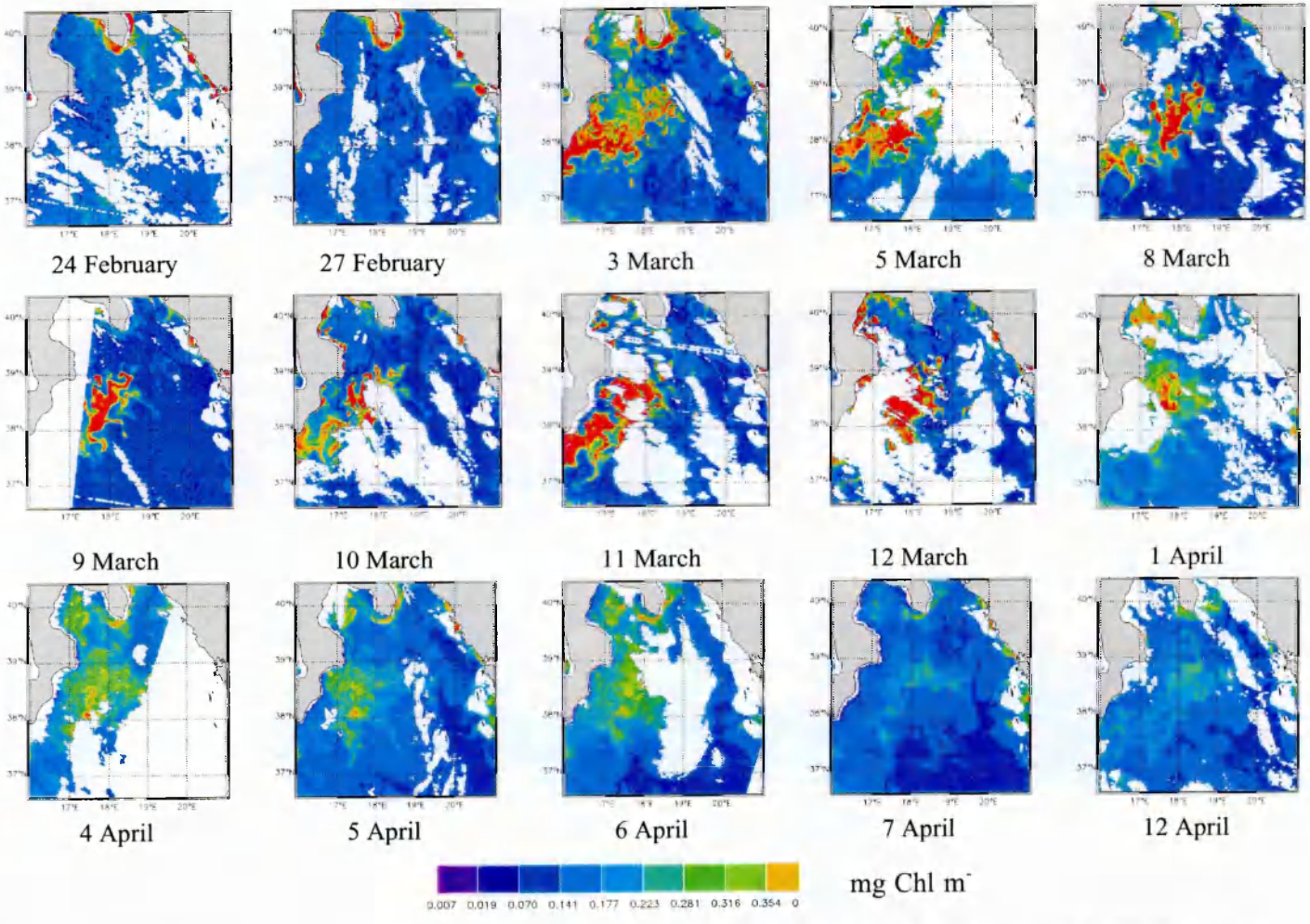

Figure7-1. Selected images of the SeaWiFS derived chlorophyll-*a* concentration over the Calabrian Bloom region (1999).

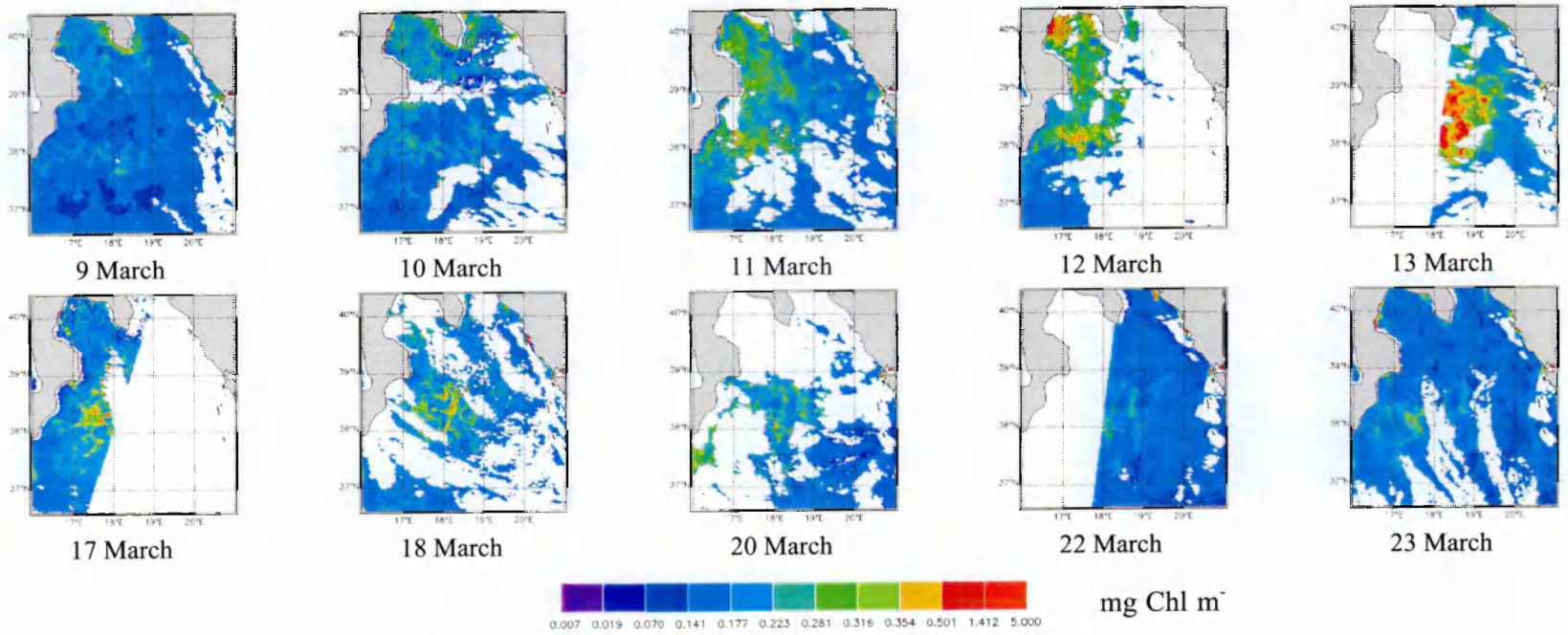

Figure7-1. Selected images of the SeaWiFS derived chlorophyll-*a* concentration over the Calabrian Bloom region (2000a).

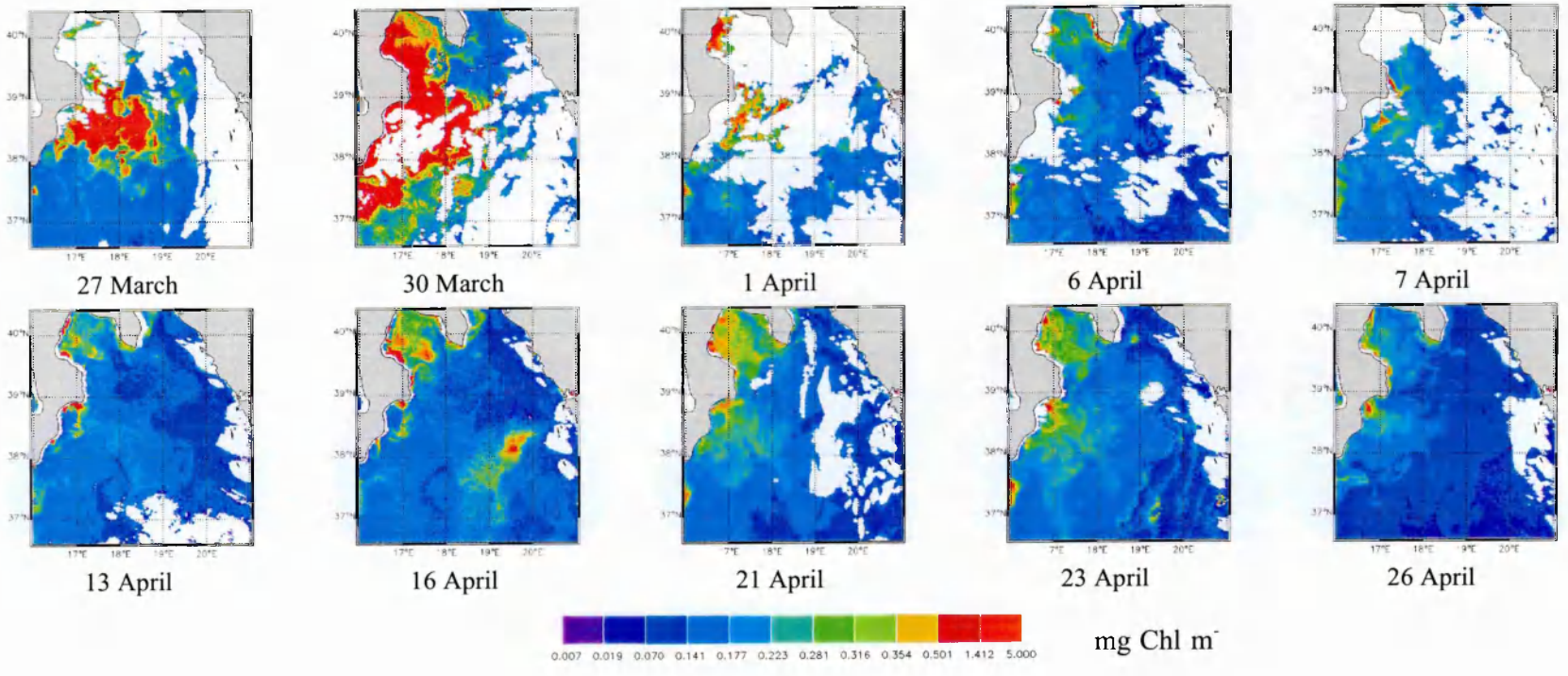

Figure7-1. Selected images of the SeaWiFS derived chlorophyll-*a* concentration over the Calabrian Bloom region (2000b).

CHAPTER 11

Bibliography

Acker, J. G., (1994). "The heritage of SeaWiFS: a retrospective on the CZCS Nimbus Experiment Team (NET) Program.", NASA Goddard Space Flight Center., Grenbelt, Maryland.

Afanasyev, Y. D., N. P. Nezlin and A. G. Kostianoy, (2001). "Patterns of seasonal dynamics of remotely sensed chlorophyll and physical environment in the Newfoundland region". *Remote sensing of environment*, 76: 268-282.

Aiken, J., G. Moore, C. C. Trees, S. B. Hooker and D. K. Clark, (1995). "The SeaWiFS CZCS-type pigment algorithm", NASA, Greenbelt, MD, 20771, USA.

Aiken, J., G. F. Moore and P. M. Hooligan, (1992). "Remote sensing of oceanic biology in relation of global climate change". *Journal of Phycology*, 28: 579-590.

Ainsworth, E. J., C. Pietras and S. Bailey, (2001). "Analyses of Match-up results". In: G. Fargion, R. A. Barnes and C. R. McClain (Editors), In situ aerosol optical thickness collected by the SIMBIOS program (1997-2000): protocols and data QC and analysis. NASA, Greenbelt, Maryland.

Allen, J. T., D. A. Smeed, J. Tintore and S. Ruiz, ′, (2001). "Mesoscale subduction at the Almeria–Oran front: Part 1. Ageostrophic flows". *Journal of Marine Systems*, 30: 263-285.

Alvarez-Salgado, A. X., F. G. Figueiras, F. F. Perez, S. B. Groom, E. Nogueira, A. V. Borges, L. Chou, C. G. Castro, M. G., A. F. Rios, A. E. J. Miller, M. Frankignoulle, G. Savidge and R. Wollast, (2003). "The Portugal coastal counter current off NW Spain: new insights on its biogeochemical variability". *Progress in Oceanography*, 56: 281-231.

Anderson, V. and L. Prieur, (2000). "One month study in the open NW Mediterranean Sea (DYNAPROC experiment, May 1995): overview of the hydrobiogeochemical structures and effects of wind events". *Deep Sea Research*, 47: 397-422.

André, J. M. and A. Morel, (1991). "Atmospheric corrections and interpretation of marine radiances in CZCS imagery, revisited". *Oceanologica Acta*, 14: 3-22.

Antoine, D. and A. Morel, (1996). "Oceanic primary production 1. Adaptation of a spectral light-photosynthesis model in view of application to satellite chlorophyll observations". *Global Biogeochemical Cycles*, 10(1): 43-55.

Antoine, D., A. Morel and J. M. André, (1995). "Algal pigment distribution and primary production in the eastern Mediterranean as derived from CZCS observations". *Journal of Geophysical Research*, 100(C8): 16193-16210.

Arrigo, K. R. and C. R. McClain, (1994). "Spring phytoplankton production in the Western Ross Sea". *Science*, 266: 261-263.

Artale, V., D. Iudicone, R. Santoleri, V. Rupolo, S. Marullo and D'Ortenzio, (2002). "The role of surface fluxes in OGCM using satellite SST. Validation of and sensitivity to the forcing frequency of the Mediterranean thermohaline circulation". *Journal of Geophysical Research*: doi:10.1029/2000JC000452.

Artegiani, A., D. Bregant, E. Paschini, N. Pinardi, F. Raicich and A. Raicich, (1997a). "The Adriatic Sea general circulation: Part I: Air-Sea Interactions and water mass structure". *Journal of Physical Oceanography*, 27: 1492,1514.

Artegiani, A., D. Bregant, E. Paschini, N. Pinardi, F. Raicich and A. Raicich, (1997b). "The Adriatic Sea general circulation: Part II: Baroclinic circulation structure". *Journal of Physical Oceanography*, 27: 1515,1532.

Astraldi, M. and G. P. Gasparini, (1992). "The seasonal characteristics of the circulation in the North Mediterranean Basin and their relationship with the atmospheric-climatic conditions". *Journal of Geophysical Research*, 97(6): 9531-9540.

Astraldi, M., G. P. Gasparini, L. Gervasio and E. Salusti, (2001). "Dense water dynamics along the Strait of Sicily". *Journal of Physical Oceanography*, 31: 3457-3475.

Austin, R. W., (1974). "The remote sensing of spectral radiance from below the ocean surface". In: N. G. Jerlov and E. Steemann-Nielsen (Editors), Optical Aspects of Oceanography. Academic Press, London, UK, pp. 317-344.

Austin, R. W., (1980). "Gulf of Mexico ocean-color surface-truth measurements". *Boundary Layer Metereology*, 18: 269-285.

Azov, Y., (1991). *Eastern Mediterranean - a Marine Desert ?*, EMECS '90, pp. 225-232.

Baith, K. R., R. Lindsay, F. G. and C. R. McClain, (2001). "SeaDAS: Data Analysis System Developed for Ocean Color Satellite Sensors". *EOS, Trans AGU*, 82(18): 1-4.

Balch, W. M., R. H. Evans, J. W. Brown, G. C. Feldman, C. R. McClain and W. Esaias, (1992). "The remote sensing of ocean primary productivity: use of a new data compilation to test satellite algorithms". *Journal of Geophysical Research*, 97: 2279-2293.

Banzon, P. V., E. Bohm, F. D'Ortenzio, R. Santoleri, E. D'Acunzo and L. Lamorgese, (1999). *Spatial and temporal variability in the Adriatic Sea ; combined use of SeaWiFS and AVHRR data.* In: G. Cecchi, E. T. Engman and E. Zilioli (Editors), Remote Sensing for Earth Science, Ocean and Sea Ice Applications. SPIE, pp. 558-566.

Barale, V., P. Malanotte-Rizzoli and M. C. Hendershott, (1984). "Remotely sensing the surface dynamics of the Adriatic Sea". *Deep Sea Research*, 31: 1433-1459.

Barale, V., C. R. McClain and P. Malanotte-Rizzoli, (1986). "Space and time variability of the surface color field in the Northern Adriatic Sea". *Journal of Geophysical Research*, 91: 12957-12974.

Barnes, R. A., J. Eplee, R.E., F. S. Patt and C. R. McClain, (1999). "Changes in the radiometric sensitivity of SeaWiFS determined from lunar and solar-based measurements.". *Applied Optics*, 25: 4640-4664.

Behrenfeld, M. J. and P. G. Falkowski, (1997). "Photosynthetic rates derived from satellite-based chlorophyll concentration". *Limnology and oceanography*, 42(1): 1-20.

Bethoux, J. P., (1979). "Budgets of the Mediterranean Sea. Their dependence on local climate and on characteristics of the Atlantic water". *Oceanologica Acta*, 2(2): 157-163.

Bethoux, J. P., (1981). "Le phosphore et l'azote en Mer Mediterranee, bilans et fertilité potentielle". *Marine Chemistry*, 10: 141-158.

Bethoux, J. P., (1989). "Oxygen consumption, new production, vertical advection and environmental evolution in the Mediterranean Sea". *Deep Sea Research*, 36(5): 769-780.

Bethoux, J. P. and G. Copin-Montégut, (1986). "Biological fixation of the atmospheric nitrogen in the Mediterranean Sea". *Limnology and oceanography*, 31(6): 1353-1358.

Bethoux, J. P. and B. Gentili, (1996). "The Mediterranean Sea, coastal and deep-sea signatures of climatic and environmental changes". *Journal of Marine Systems*, 7: 383-394.

Bethoux, J. P. and B. Gentili, (1999). "Functioning of the Mediterranean Sea: past and present changes related to freshwater input and climate changes". *Journal of Marine Systems*, 20: 33-47.

Bethoux, J. P., P. Morin, C. Chaumery, O. Connan, B. Gentili and D. Ruiz-Pino, (1998). "Nutrients in the Mediterranean Sea, mass balance and statistical analysis of concentrations with respect to environmental change.". *Marine Chemistry*, 63: 155-169.

Bethoux, J. P., P. Morin, C. Madec and B. Gentili, (1992). "Phosphorus and nitrogen behaviour in Mediterranean Sea.". *Deep Sea Research*, 39(9A): 1641-1654.

Bignami, F., S. Marullo, R. Santoleri and M. E. Schiano, (1995). "Longwave radiation budget in the Mediterranean Sea". *Journal of Geophysical Research*, 100: 2501-2514.

Bishop, J. K. B. and W. B. Rossow, (1991). "Spatial and temporal variability of global surface solar irradiance". *Journal of Geophysical Research*, 96: 16839-16858.

Boldrin, A., S. Miserocchi, S. Rabitti, M. M. Turchetto, V. Balboni and G. Socal, (2002). "Particulate matter in the southern Adriatic and Ionian Sea: characterisation and downward fluxes". *Journal of Marine Systems*, 33-34: 389-410.

Brankart, J. M. and N. Pinardi, (2001). "Abrupt cooling of the Mediterranean levantine intermediate water at the beginning of the 1980s: observational evidence and model simulation.". *Journal of Physical Oceanography*, 31(8 part 2): 2307-2320.

Bricaud, A., M. Babin, A. Morel and H. Claustre, (1995). "Variability in the chlorophyll specific absorption coefficients of natural phytoplankton: analysis and parameterisation". *Journal of Geophysical Research*, 100(C7): 13321.

Bricaud, A., E. Bosc and D. Antoine, (2002). "Algal biomass and sea surface temperature in the Mediterranean Basin. Intercomparison of data from various satellite sensors, and implications for primary production estimates.". *Remote sensing of environment*, 81: 163-178.

Bricaud, A. and A. Morel, (1987). "Atmopsheric corrections and interpretation of marine radiances in CZCS imagery: use of reflectance model.". *Oceanologica Acta*, 7: 33-50.

Bricaud, A., A. Morel and L. Prieur, (1981). "Absorption by dissolved organic matter of the sea (yellow substance) in the UV and visible domains". *Limnology and oceanography*, 26(1): 43.

Bryden, H. L. and T. H. Kinder, (1991). "Steady two-layer exchange through the Strait of Gibraltar.". *Deep-Sea Research*, 38(S1): 445-463.

Buongiorno Nardelli, B. and E. Salusti, (2000). "On dense water formation criteria and their application to the Mediterranean Sea". *Deep Sea Research*, 47: 193-221.

Campbell, J., D. Antoine, R. Armstrong, K. R. Arrigo, W. M. Balch, R. Barber, M. J. Behrenfeld, R. R. Bidigare, J. K. B. Bishop, M. E. Carr, W. Esaias, P. G. Falkowski, N. Hoepffner, R. Iverson, D. Kiefer, S. E. Lohrenz, J. Marra, A. Morel, J. P. Ryan, V. Vedernikov, K. Waters, C. Yentsch and J. A. Yoder, (2001). "Comparison of algorithms for estimating ocean primary production from surface chlorophyll, temperature, and irradiance". *Global Biogeochemical Cycles*, 16(3): 10129-10138.

Carder, K. L., F. R. Chen, Z. P. Lee, S. K. Hawes and D. Kamykowski, (1999). "Semianalytic MODIS algorithms for chlorophyll a and absorption with bio-optical domains based on nitrate-depletion temperatures.". *Journal of Geophysical Research*, 104(C3): 5403-5421.

Chaturvedi, N. and A. Narain, (2003). "Chlorophyll distribution pattern in the Arabian Sea: seasonal and regional variability, as observed from SeaWiFS data". *International Journal of Remote Sensing*, 24(3): 511-518.

Civitarese, G., A. Crise, G. Crispi and R. Mosetti, (1996). "Circulation effects on nitrogen dynamics in the Ionian Sea". *Oceanologica Acta*, 19(6): 209-621.

Civitarese, G. and M. Gacic, (2001). "Had the Eastern Mediterranean Transient an Impact on the new production in the Southern Adriatic?". *Geophysical Research Letters*, 28(8): 1627-1639.

Clark, D. K., (1997). "Bio-optical algorithms - Case 1 waters", NASA, MODIS Team, Documentation Report - ATDB 19, Greenbelt, Maryland.

Clark, D. K., H. R. Gordon, K. J. Voss, Y. Ge, W. W. Broenkow and C. C. Trees, (1997). "Validation of atmospheric correction over the oceans.". *Journal of Geophysical Research*, 102: 17209-17217.

Clarke, G. L., G. C. Ewing and C. J. Lorenzen, (1970). "Spectra of backscattered light from the sea obtained ftom aircraft as a measure of chlorophyll concentration". *Science*, 167: 1119-1121.

Claustre, H., A. Morel, S. B. Hooker, M. Babin, D. Antoine, K. Oubelkheir, A. Bricaud, K. Leblanc, B. Quéguiner and S. Maritorena, (2002). "Is desert dust making oligotrophic waters greener?". *Geophysical Research Letters*, 29(10): 107-111.

Conan, P. and C. Millot, (1995). "Variability of the northern current off Marseilles, Western Mediterranean Sea, from February to June 1992". *Oceanologica Acta*, 18(2): 193-205.

Coste, B., P. LeCorre and H. J. Minas, (1988). "Re-evaluation of the nutrient exchanges in the Strait of Gibraltar". *Deep Sea Research*, 35(5): 767-775.

Crise, A., J. I. Allen, J. Baretta, G. Crispi, R. Mosetti and C. Solidoro, (1999). "The Mediterranean pelagic ecosystem response to physical forcing". *Progress in Oceanography*, 44: 219-243.

Crispi, G., A. Crise and E. Mauri, (1999). "A seasonal three-dimensional study of the nitrogen cycle in the Mediterranean Sea: Part II. Verification of the energy constrained trophic model". *Journal of Marine Systems*, 20: 357-379.

Crispi, G., R. Mosetti, C. Solidoro and A. Crise, (2001). "Nutrients cycling in Mediterranean basins: the role of the biological pump in the trophic regime". *Ecological Modelling*, 138: 101-114.

Cruzado, A., (1979). "Climatology and hydrology of the Mediterranean Region. Report on the state of pollution in the Mediterranean Sea.", UNESCO.

Demirov, E. and N. Pinardi, (2002). "Simulation of the Mediterranean Sea circulation from 1979 to 1993: Part I The interannual variability". *Journal of Marine System*, 33-34: 23-50.

Denman, K. L. and M. R. Abbott, (1988). "Time evolution of surface chlorophyll patterns from cross spectrum analysis of satellite color images". *Journal of Geophysical Research*, 93(C6): 6789-6805.

Dickson, R., J. Lazier, J. Meincke, P. Rhines and J. Swift, (1996). "Long-term coordinated changes in the convective activity of the North Atlantic.". *Progress in Oceanography*, 38: 241-296.

Ding, K. and H. R. Gordon, (1995). "Analysis of the influence of O2 A-band absorption on atmospheric correction of ocean-color imagery". *Applied Optics*, 34(12): 2068-2080.

Duarte, C. M., S. Agusti, H. Kennedt and D. Vaqué, (1999). "The Mediterranean climate as a template for Mediterranean marine ecosystems: the example of the northeast Spanish littoral". *Progress in Oceanography*, 44: 245-270.

Dugdale, R. C. and F. P. Wilkerson, (1988). "Nutrient sources and primary production in the Eastern Mediterranean.". *Oceanologica Acta*, 9(179-184).

Dutkiewicz, S., M. J. Follows, J. Marshall and W. W. Gregg, (2001). "Interannual variability of the phytoplankton abundances in the North Atlantic". *Deep Sea Research II*, 48: 2323-2344.

Ediger, D. and A. Yilmaz, (1996). "Characteristics of deep chlorophyll maximum in the northeastern Mediterranean with respect to environmental conditions". *Journal of Marine Systems*, 9: 291-303.

Emery, W. J. and W. J. Pickard, (1990). Descriptive physical oceanography. Pergamon Press, Oxford (UK), 244 pp.

ENVISAT, C.-V. T., (2000). "ENVISAT: calibration and validation plan.", European Space Agency.

Eppley, R. W. and B. J. Peterson, (1979). "Particulate organic matter flux and planktonic new production in the deep ocean". *Nature*, 282: 677-680.

EUROMODEL Group, (1995). "Progress from 1989 to 1992 in understanding the general circulation of the western Mediterranean sea". *Oceanologica Acta*, 18(255-271).

Evans, R. H. and H. R. Gordon, (1994). "CZCS "system calibration": a retrospective examination". *Journal of Geophysical Research*, 99(C4): 7293-7307.

Falkowski, P. G., (1988). "Ocean productivity from space". *Nature*, 335: 205.

Fargion, G., R. A. Barnes and C. R. McClain, (2001). "In Situ Aerosol Optical Thickness Collected by the SIMBIOS Program (1997-2000): Protocols, and Data QC and Analysis", NASA, Goddard Space Flight Center, NASA/TM-2001-209982, Greenbelt, Maryland.

Fargion, G. S. and C. R. McClain, (2000). "Three years of ocean color instrument intercomparisons and cross-calibrations by the SIMBIOS project (1997-2000)". In: C. R. Bostater and R. Santoleri (Editors), Remote sensing of the ocean and sea ice 2000. Proceedings of the SPIE, Barcelona, pp. 44-55.

Feldman, G. C. and e. al., (1989). "Availability of the global set". *EOS Trans. AGU*, 70: 634-635, 640-641.

Fielding, S., N. Crisp, J. T. Allen, M. C. Hartman, B. Rabe and H. S. J. Roe, (2001). "Mesoscale subduction at the Almeria–Oran front: Part 2. Biophysical interactions". *Journal of Marine System*, 30: 287-304.

Follows, M. J. and S. Dutkiewicz, (2002). "Meteorological modulation of the North Atlantic Spring Bloom". *Deep Sea Research II*, 49: 321-344.

Font, J., C. Millot, J. Salas, A. Julià and O. Chic, (1998). "The drift of modified Atlantic Water from the Alboran Sea to the Eastern Mediterranean". *Scientia Marina*, 62(3): 211-216.

Font, J., J. Salat and J. Tintore, (1988). "Permanent features of the circulation in the Catalan Sea". *Oceanologica Acta*, 9: 51-57.

Fougnie, B., P. Y. Deschamps, R. Frouin and B. G. Mitchell, (1998). "Measuring Water-Leaving Radiance with a Polarization Radiometer: Theory and Experimental Verification". *EOS Trans. AGU*, 79(1): 99.

Frouin, R., B. A. Franz and M. Wang, (2001). *Algorithm to estimate PAR from SeaWiFS data. Version 1.2 Documentation. Available at the address: http://seawifs.gsfc.nasa.gov/SEAWIFS/RECAL/Reprod4/par/docs/seawifs_par_wfigs.pdf.*

Gacic, M., G. Civitarese, S. Miserocchi, V. Cardin, A. Crise and E. Mauri, (2002). "The open-ocean convection in the Southern Adriatic: a controlling mechanism of the spring phytoplankton bloom". *Continental Shelf Research*, 22(14): 1897-1908.

Gacic, M., S. Marullo, R. Santoleri and A. Bergamasco, (1997). "Analysis of the seasonal and interannual variability of the sea surface temperature field in the Adriatic Sea from AVHRR data (1984-1992)". *Journal of Geophysical Research*, 102: 22937-22946.

Garcia-Gorriz, E. and M. E. Carr, (1999). "The climatological annual cycle of satellite-derived phytoplankton pigments in the Alboran Sea". *Geophysical Research Letters*, 26(19): 2985-2989.

Garcia-Gorriz, E. and M. E. Carr, (2001). "Physical control of phytoplankton distributions in the Alboran Sea: a numerical and satellite approach". *Journal of Geophysical Research*, 106(C8): 16795-16805.

Garçon, V. C., A. Oschlies, S. C. Doney, D. McGillicuddy and J. Waniek, (2001). "The role of mesoscale variability on plankton dynamics in the North Atlantic". *Deep Sea Research II*, 48: 2199-2256.

Gascard, J. C., (1978). "Mediterranean Deep Water Formation, Baroclinic Instability and Oceanic Eddies.". *Oceanologica Acta*, 1: 315-330.

Gill, A. E., (1982). Atmosphere-Ocean Dynamics. International Geophysics Series. Academic Press, New York, 662 pp.

Gilmann, C. and C. Garrett, (1994). "Heat flux parametrizations for the Mediterranean Sea: the role of atmospheric aerosols and constraints from water budget". *Journal of Geophysical Research*, 99(C3): 5119-5134.

Gitelson, A., A. Karnieli, N. Goldman, Y. Z. Yacobi and M. Mayo, (1996). "Chlorophyll estimation in the Southeastern Mediterranean using CZCS images: adaptation of an algorithm and its validation". *Journal of Marine Systems*, 9: 283-290.

Goffart, A., J.-H. Hecq and L. Legendre, (2002). "Changes in the development of the winter-spring phytoplankton bloom in the Bay of Calvi (NW Mediterranean) over the last two decades: a response to changing climate?". *Marine Ecology Progress Series*, 236: 45-60.

Gómez, F., N. González, F. Echevarría and C. M. García, (2000). "Distribution and fluxes of dissolved nutrients in the Strait of Gibraltar and its relationship to microphytoplankton biomass". *Estuarine, Coastal and Shelf Science*, 51: 439-449.

Gordon, H. R., (1978). "Removal of atmospheric effects from satellite imagery of the oceans.". *Applied Optics*, 17: 1631-1636.

Gordon, H. R., (1997). "Atmospheric correction of ocean color imagery in the Earth Observing System era.". *Journal of Geophysical Research*, 102(D14): 17081.

Gordon, H. R. and W. M. Balch, (1999). "MODIS detached coccolith concentration", NASA, Algorithm Theoretical Basis Document, Greenbelt, Maryland.

Gordon, H. R., G. C. Boynton, W. M. Balch, S. B. Groom, D. S. Harbour and T. J. Smyth, (2001). "Retrieval of Coccolithophore Calcite Concentration from SeaWiFS Imagery". *Geophysical Research Letters*, 28(8): 1587-590.

Gordon, H. R., J. W. Brown, R. H. Evans, O. B. Brown, Smith, Baker and D. K. Clark, (1988). "A semianalytic radiance model of ocean color". *Journal of Geophysical Research*, 93(D9): 10909-10924.

Gordon, H. R. and D. K. Clark, (1980). "Remote sensing optical properties of a stratified ocean: an improved interpretation". *Applied Optics*, 19: 3428-3430.

Gordon, H. R., D. K. Clark, J. W. Brown, O. B. Brown, R. H. Evans and W. W. Broenkow, (1983). "Phytoplankton pigment concentration in the Middle Atlantic Bight: comparison of ship determinations and CZCS estimates". *Applied Optics*, 22(1): 20-36.

Gordon, H. R., D. K. Clark, J. L. Mueller and W. A. Hovis, (1980). "Phytoplankton Pigments from the Nimbus- 7 Coastal Zone Color Scanner: Comparisons with Surface Measurements". *Science*, 210: 63-66.

Gordon, H. R. and D. K. Clarke, (1981). "Clear water radiances for atmospheric correction of coastal zone color scanner imagery". *Applied Optics*, 20: 4175-4180.

Gordon, H. R. and A. Morel, (1983). Remote Assessment of Ocean Color for Interpretation of Satellite Visible Imagery: A Review. Springer-Verlag, New York, 114 pp.

Gordon, H. R. and M. Wang, (1994). "Retrieval of water leaving radiance and aerosol optical thickness over the oceans with seawifs: a preliminary algorithm". *Applied optics*, 33(3): 443-458.

Gower, J. F. R., R. Doerffer and G. Bortsad, (1999). "Interpretation of the 685 nm peak in water leaving radiance spectra in terms of fluorescence, absorption and scattering, and its observation by MERIS". *International Journal of Remote Sensing*, 20(9): 1771-1785.

Gross, L., S. Thiria, R. Frouin and B. G. Mitchell, (2000). "Artificial neural networks for modelling the transfer function between marine reflectance and phytoplankton pigment concentration". *Journal of Geophysical Research*, 105(C2): 3483.

Guerzoni, S., E. Molinaroli and R. Chester, (1997). "Saharan dust inputs to western Mediterranean Sea: depositional patterns, geochemistry and sedimentology implications". *Deep Sea Research II*, 44(3-4): 631-644.

Hansen, J. E. and L. D. Tracid, (1977). "Light scattering in planetary atmospheres". *Space Science Reviews*, 16: 527-610.

Hecht, A., N. Pinardi and A. R. Robinson, (1988). "Currents, water masses, eddies and jets in the Mediterranean Levantine basin". *Journal of Physical Oceanography*, 18(10): 1320-1353.

Holben, B. N. and e. al., (1998). "AERONET-A Federated Instrument Network and Data Archive for Aerosol Characterization". *Remote sensing of environment*, 66: 1-16.

Hooker, S. B. and C. R. McClain, (2000). "The calibration and validation of Seawifs data". *Progress in Oceanography*, 45: 427-465.

Hooker, S. B., C. R. McClain, J. K. Firestone, T. L. Westphal, E.-N. Yeh and Y. Ge, (1994). "The SeaWiFS Bio-Optical Archive and Storage System (SeaBASS), Part 1.". NASA Tech. Memo. 104566, Vol. 20, S.B. Hooker and E.R. Firestone, Eds, NASA Goddard Space Flight Center, Greenbelt, Maryland.

Hooker, S. B., N. W. Rees and J. Aiken, (2000). "An objective methodology for identifying oceanic provinces". *Progress in Oceanography*, 45: 313-338.

Hopkins, T. S., (1999). "The thermohaline forcing of the Gibraltar exchange". *Journal of Marine Systems*, 20: 1-31.

Hovis, W. A., D. K. Clark, F. Anderson, R. W. Austin, W. H. Wilson, K. S. Baker, D. Ball, H. R. Gordon, J. L. Mueller, S. Z. El Sayed, B. Strurm, R. C. Wrigley and C. Yentsch, (1980). "Nimbus- 7 Coastal Zone Color Scanner:System Description and Initial Imagery". *Science*, 210(3): 60-63.

Huisman, J., P. Oostveen van and F. J. Weissing, (1999). "Critical depth and critical turbulence: Two different rnechanisms for the development of phytoplankton blooms". *Limnology and Oceanography*, 44(7): 1781-1878.

Hurrel, J. W. and H. Van Loon, (1997). "Decadal variations in climate associated with the North Atlantic Oscillation". *Climatic Change*, 36: 301-326.

Iida, T., S. I. Saitoh, T. Miyamura, M. Toratani, H. Fukushima and N. Shiga, (2002). "Temporal and spatial variability of coccolithophore blooms in the eastern Bering Sea, 1998-2001". *Progress in Oceanography*, 55: 165-175.

Iudicone, D. and NORBAL Team, (2002). *The vernal bloom in the NW Mediterranean: a unique combination of pysical and biological events*, Meeting of the European Geophysical Society. EGS, Nice, France, April, 2002.

Jerlov, N. G., (1976). Marine Optics. Elsevier, Amsterdam, 120 pp.

JGOFS, (1988). "Core measurements protocols: report of the core measurement working group". 6, Joint Global Ocean Flux Study.

Josey, S. A., E. C. Kent and P. K. Taylor, (1999). "New insights into the ocean heat budget closure problem from analysis of the SOC air-sea flux climatologic". *Journal of Climate*, 12(9): 2856-2880.

Kahru, M. and G. Mitchell, (1999). "Empirical chlorophyll algorithm and preliminary Seawifs validation for the California Current". *International Journal of Remote Sensing*, 20(17): 3423-3429.

Kilpatrick, K., R. G. Podesta and R. H. Evans, (2001). "Overview of the NOAA/NASA advanced very high resolution radiometer Pathfinder algorithm for sea surface temperature and associated matchup database". *Journal of Geophysical Research*, 106: 9179-9197.

Klein, B., W. Roether, G. Civitarese, M. Gacic, B. B. Manca and M. Ribera d'Alcalà, (2000). "Is the Adriatic returning to dominate the production of Eastern Mediterranean Deep Water?". *Geophysical Research Letters*, 27: 3377-3380.

Klein, B., W. Roether, B. B. Manca, D. Bregant, V. Beitzel, V. Kovaceivic and A. Lucchetta, (1999). "The large deep water transient in the eastern Mediterranean". *Deep Sea Research*, 46: 371-414.

Korres, G., N. Pinardi and A. Lascaratos, (2000). "The ocean response to low-frequency interannual atmospheric variability in the Mediterranean Sea. Part II: empirical orthogonal functions analysis". *Journal of Climate*, 13: 732-745.

Krahmann, G. and F. Schott, (1998). "Longterm increases in Western Mediterranean salinities and temperatures: anthropogenic and climatic sources". *Geophysical Research Letters*, 25(22): 4209-412.

Krom, M. D., S. Brenner, N. Kress, A. Neori and L. I. Gordon, (1992). "Nutrient dynamics and new production in a warm- core eddy from the Eastern Mediterranean Sea". *Deep Sea Research*, 39(3/4): 467.

Kudela, R. M. and F. P. Chavez, (2002). "Multi-platform remote sensing of new production in central California during the 1997–1998 El Nino". *Progress in Oceanography*, 54: 233-249.

Lacombe, H., J. C. Gascard, J. Gonella and J. P. Bethoux, (1981). "Response of the Mediterranean to the water and energy fluxes across its surface, on seasonal and interannual scales". *Oceanologica Acta*, 4(2): 120-130.

Larnicol, G., N. Ayoub and P. Y. Le Traon, (2002). "Major changes in Mediterranean Sea level variability from 7 years of TOPEX/Poseidon and ERS-1/2 data". *Journal of Marine System*, 33-34: 68-89.

Lascaratos, A., W. Roether, K. Nittis and B. Klein, (1999). "Recent changes in deep water formation and spreading in the eastern Mediterranean Sea: a review". *Progress in Oceanography*, 1(3): 5-36.

Lascaratos, A., R. G. Williams and E. Tragou, (1993). "A mixed layer study of the formation of levantine intermediate water". *Journal of Geophysics Research*, 98(C15): 14793-14749.

Legates, H. and C. Wilmott, (1990). "Mean seasonal and spatial variability in gauge corrected global precipitation". *International Journal of Climate*, 10: 11-127.

Levitus, S., (1982). "Climatological atlas of the world ocean". Prof. Paper 13, NOAA, U.S. Government Printing Office., Washington, DC.

Levy, M., L. Memery and J. Andre, (1998). "Simulation of primary production and export fluxes in the north-western Mediterranean Sea.". *Journal of Marine Research*, 56: 197-238.

Levy, M., L. Memery and G. Madec, (1999). "The onset of the spring bloom in the MEDOC area: mesoscale spatial variability". *Deep Sea Research*, 46: 1137.

Levy, M., L. Memery and G. Madec, (2000). "Combined effects of mesoscale processes and atmospheric high-frequency variability on the spring bloom in the MEDOC area". *Deep Sea Research*, 47: 27.

Lewis, M. R., (1995). "Coastal zone color scanner on Nimbus and sea-viewing wide field-of-view sensor on Seastar", Oceanographic applications of remote sensing. CRC Press Inc., Boca Raton, FL 332421 (USA), pp. 167-181.

Lohrenz, S. E., D. A. Wiesenburg, I. P. DePalma, K. S. Johnson and D. E. J. Gustafson, (1988). "Interrelationship among primary production, chlorophyll, and environmental conditions in frontal regions of the Western Mediterranean Sea". *Deep Sea Research*, 35(5): 793-810.

Longhurst, A., (1995). "Seasonal cycles of pelagic production and consumption". *Progress in Oceanography*, 36: 77-167.

Longhurst, A., (2001). "A major seasonal phytoplankton bloom in the Madagascar Basin". *Deep Sea Research*, 148: 2413-2422.

Macdonald, A., (1998). "The global ocean circulation: A hydrographic estimate and regional analysis,". *Progress in Oceanography*, 41: 281-382.

Macdonald, A. M. and C. Wunsch, (1996). "An estimate of global ocean circulation and heat fluxes". *Nature*, 382(6590): 436-439.

Malanotte-Rizzoli, P. and e. al., (1997). "A synthesis of the Ionian Sea hydrography, circulation and water mass pathways during POEM-Phase I". *Progress in Oceanography*, 39: 153-204.

Malanotte-Rizzoli, P., B. B. Manca, M. R. d'Alcalà, A. Theocharis, S. Brenner, G. Boudillon and E. Ozsoy, (1999). "The Eastern Mediterranean in the 80s and in the 90s: the big transition in the intermediate and deep circulations". *Dynamics of atmosphere and oceans*, 29: 365-395.

Manca, B. B., (2000). *Recent changes in dynamics of the eastern Mediterranean affecting the water characteristics of the adjacent basins*. In: CIESM (Editor), The Eastern Mediterranean climatic transient, Monaco, pp. 7-3.

Manca, B. B., B. Klein, N. Kress and M. Ribera d'Alcalà, (2002). *Low-Frequency changes of water mass structure, flow patterns and biochemical exchanges through the Eastern Mediterranean regions*. In: CIESM (Editor), Tracking long-term hydrological change in the Mediterranean Sea, pp. 61-70.

Manzella, G., G. Gasparini and M. Astraldi, (1988). "Water exchange between the eastern and western Mediterranean through the strait of Sicily". *Deep Sea Research*, 35(6).

Margat, J., (1992). "L'eau dans le bassin mediterranen", PNUE /CAR / PB.

Marshall, J. and F. Schott, (1999). "Open ocean deep convection: observations, models and theory". *Reviews of Geophysics*, 37(1): 1-64.

Martin, J. H. and e. al., (1994). "Testing the iron hypothesis in ecosystems of the equatorial pacific ocean". *Nature*, 371: 123-129.

Marty, J. C. and J. Chiaverini, (2002). "Seasonal and interannual variations in phytoplankton production at DYFAMED time-series station, Northwestern Mediterranean Sea". *Deep Sea Research II.*

Marty, J. C., J. Chiaverini, M. D. Pizay and B. Avril, (2002). "Seasonal and interannual dynamics of nutrients and phytoplankton pigments in the western Mediterranean Sea at the DYFAMED time-series station (1991 –1999)". *Deep Sea Research II*, 49: 1965 –1985.

Marullo, S., R. Santoleri, P. Malanotte-Rizzoli and A. Bergamasco, (1999). "The sea surface temperature field in the Eastern Mediterranean from advanced very high resolution radiometer (AVHRR) data Part I. Seasonal variability". *Journal of Marine System*, 20: 63-81.

McClain, C. R., K. R. Arrigo, W. Esaias, M. Darzi, F. S. Patt, R. H. Evans, C. W. Brown, J. W. Brown, R. A. Barnes and L. Kumar, (1995). "SeaWiFS Algorithms, Part 1". 104566, NASA Goddard Space Flight Center, Greenbelt, Maryland.

McClain, C. R., J. R. Christian, S. R. Signorini, M. R. Lewis, I. Asanuma, D. Turk and C. Dupouy-Douchement, (2002). "Satellite ocean-color observations of the tropical Pacific Ocean". *Deep Sea Research II*, 49: 2533-2560.

McGillicuddy, D., Kosneyrev, J. P. Ryan and J. A. Yoder, (2001). "Covariation of mesoscale ocean color and sea-surface temperature patterns in the Sargasso Sea". *Deep Sea Research II*, 48: 1823-1836.

MEDOC Group, (1970). "Observation of formation of deep water in the Mediterranean Sea". *Nature*, 227: 1037-1040.

Mellor, G., (1998). "User's guide for a three dimensional, primitive equation, numerical ocean model.", Princeton University.

Mertens, C. and F. Schott, (1998). "Interannual variability of deep water formation in the NW Mediterranean". *Journal of Physical Oceanography*, 28: 1410-1424.

Millot, C., (1987). "Circulation in the Western Mediterranean Sea". *Oceanologica Acta*, 10(2): 143-149.

Millot, C., (1999). "Circulation in the Western Mediterranean sea". *Journal of Marine Systems*, 20: 423-442.

Miquel, J. C., S. W. Fowler, J. LaRosa and P. Buat-Menard, (1994). "Dynamics of the downward flux of particles and carbon in the open NorthWestern Mediterranean Sea". *Deep Sea Research*, 41(2): 243-261.

Moore, K. D., K. J. Voss and H. R. Gordon, (2000). "Spectral reflectance of whitecaps: their contribution to water-leaving radiance". *Journal of Geophysical Research*, 105: 6493-6499.

Moran, X. A. G., I. Taupier-Letage, E. V. Vàszquez-Domìnguez, S. Ruiz, L. Arin, P. Raimbault and M. Estrada, (2001). "Physical-biological coupling in the Algerian Basin (SW Mediterranean): influence of mesoscale instabilities on the biomass and production of phytoplankton and bacterioplankton". *Deep Sea Research*, 48: 405-437.

Morel, A., (1980). "In water and remote measurements of ocean color". *Boundary Layer Meterology*, 18: 177-201.

Morel, A., (1988). "Optical modeling of the upper ocean in relation to its biogenous matter content (Case 1 water)". *Journal of Geophysical Research*, 93(C9): 10749-10768.

Morel, A., (1991). "Light and marine photosynthesis : a spectral model with geochemical and climatological implications". *Progress in Oceanography*, 26: 263-306.

Morel, A. and J. M. André, (1991). "Pigment distribution and primary production in the western Mediterranean as derived from CZCS observations". *Journal of Geophysical Research*, 96(C7): 12685-12691.

Morel, A., D. Antoine, M. Babin and Y. Dandonneau, (1996). "Measured and modeled primary production in the northeast Atlantic (EUMELI JGOFS program): the impact of natural variations in photosynthetic parameters on model predictive skill". *Deep Sea Research*, 43(8): 1273-1304.

Morel, A. and J. F. Berthon, (1989). "Surface pigments, algal biomass profiles, and potential production of the euphotic layer: relationship reinvestigated in view of remote-sensing applications". *Limnology and oceanography*, 34(8): 1545-1562.

Morel, A. and B. Gentili, (1996). "Diffuse reflectance of oceanic waters. III. Implication of bidirectionality for the remote-sensing problem". *Applied Optics*, 35(24): 4850-4861.

Morel, A. and L. Prieur, (1977). "Analysis of variations in ocean color". *Limnology and oceanography*, 22(4): 709-722.

Morel, A. and R. C. Smith, (1974). "Relation between total quanta and total energy for aquatic photosynthesis". *Limnology and oceanography*, 19(4): 591-600.

Moulin, C., F. Guillard, F. Dulac and C. E. Lambert, (1997). "Long-term daily monitoring on Saharan dust load over ocean using Meteosat ISCPP-B2 data.1. Methodology and preliminary results for 1983-1994 in the Mediterranean". *Journal of Geophysical Research*, 102(D14): 16.947-16.958.

Moutin, T. and P. Raimbault, (2002). "Primary production, carbon export and nutrients availability in western eastern Mediterranean Sea in early summer 1996 (MINOS cruise)". *Journal of Marine Systems*, 842: 273-288.

Mueller, J. L. and R. W. Austin, (1995). "Ocean Optics Protocols for SeaWiFS Validation, Revision 1, SeaWiFS Technical Report Series.", NASA Technical Memorandum 104566,S. B. Hooker, E. R. Firestone and J. G. Acker (eds.), Greenbelt, Maryland.

Myers, P. G., K. Haines and S. Josey, (1998). "On the importance of the choice of wind stress forcing to the modeling of the Mediterranean Sea circulation". *Journal of Geophysical Research*, 103(C8): 15729-15749.

Napolitano, E., T. Oguz, P. Malanotte-Rizzoli, A. Yilmaz and E. Sansone, (2000). "Simulations of biological production in the Rhodes and Ionian basins of the eastern Mediterranean". *Journal of Marine Systems*, 24: 277-298.

Neckel, H. and D. Labs, (1984). "The solar radiation between 3300 and 12500 A". *Solar Physics*, 90: 205.

Neveux, J. and M. Panouse, (1987). "Spectrofluorometric determination of chlorophylls and pheophytins". *Arch. Hydrobiol.*, 109(4): 567-581.

Nittis, K. and A. Lascaratos, (1998). "Diagnostic and prognostic numerical studies of LIW formation". *Journal of Marine Systems*, 18: 179-195.

O'Reilly, J. E., S. Maritorena, D. Siegel, M. C. O'Brien, D. Toole, B. G. Mitchell, M. Kahru, F. P. Chavez, P. Strutton, G. Cota, S. B. Hooker, C. R. McClain, K. L. Carder, F. Muller-Karger, L. Harding, A. Magnuson, D. Phinney, G. F. Moore, J. Aiken, K. R. Arrigo, R. Letelier and M. Culver, (2000). "Ocean color chlorophyll a algorithms for SeaWiFS, OC2, and OC4: version 4.". In: S. B. Hooker and E. R. Firestone (Editors), SeaWiFS Postlaunch Technical Report Series, vol.11. SeaWiFS postlaunch calibration and validation analyses: part 3. NASA Goddard Space Flight Center., Greenbelt, MD:, pp. 9-23.

O'Reilly, J. E., S. Maritorena, G. Mitchell, D. A. Siegel, K. L. Carder, D. L. Garver, M. Kahru and C. R. McClain, (1998). "Ocean color chlorophyll algorithms for Seawifs". *Journal of Geophysical Research*, 103(C11): 24937-24950.

Orlic, M., M. Gacic and P. E. LaViolette, (1992). "The currents and circulation in the Adriatic Sea". *Oceanologica Acta*, 15: 109-124.

Ozsoy, E., A. Hecht and e. al., (1993). "A synthesis of the Levantine Basin circulation and hydrography, 1985-1990". *Deep-Sea Research*.

Pinardi, N. and E. Masetti, (2000). "Variability of the large scale general circulation of the Mediterranean Sea from observations and modeling: a review". *Paleogeography, Paleoclimatology, Paleoecology*, 158(153-173).

Pinkerton, M. H., S. J. Lavender and J. Aiken, (2003). "Validation of SeaWiFS ocean color satellite data using a moored databuoy". *Journal of Geophysical Research*, 108(C5): 3133-3142.

Pirazzoli, P. A. and A. Tomasin, (2003). "Recent near-surface wind changes in the central Mediterranean and Adriatic areas". *International Journal of Climatology*, 23: 963-973.

Platt, T., (1985). *Phytoplankton production in oligotrophic marine ecosystem: The Mediterranean Sea.* In: N. C. Series (Editor), MEDITERRANEAN MARINE ECOSYSTEMS, pp. 231-246.

Platt, T. and S. Sathyendranath, (1988). "Oceanic primary production: estimation by remote sensing at local and regional scales". *Science*, 241: 1614.

Por, F. D., (1978). *Lessepsian migration.* The influx of the Red Sea biota into the Mediterranean by way of the Suez Canal. Springer, 234 pp.

Preisendorfer, R. W., (1961). "Application of radiative transfer theory to light measurements in the sea.". *Union Geodetic and Geophysical International*, 10: 11-29.

Prospero, J. M., (1996). "Saharan dust transport over the North Atlantic Ocean and Mediterranean: an overview.". In: S. Guerzoni and R. Chester (Editors), The impact of African dust across the Mediterranean. Kluwer Academic Publishers., Dordrecht, The Netherlands, pp. 133-152.

Rabitti, S., G. Civitarese and M. Ribera d'Alcalà, (1994). "Physical Oceanography of the Eastern Mediterranean (P.O.E.M.) data report: part 2 chemical and biological data.". Technical Report n. 13/94., Istituto di Biologia del Mare, CNR, Venice.

Reed, R. K., (1977). "On estimating insolation over the ocean". *Journal of Physical Oceanography*, 10: 482-484.

Reynolds, R. W. and T. M. Smith, (1995). "A high-resolution global sea surface temperature climatology". *Journal of Climate*, 8: 1571-1583.

Robarts, R. D., T. Zohary, M. J. Waiser and Y. Z. Yacobi, (1996). "Bacterial abundance, biomass, and production in relation to phytoplankton biomass in the Levantine Basin of the southeastern Mediterranean Sea.". *Marine Ecology Progress Series*, 137: 273-281.

Robinson, A. R. and M. Golnaraghi, (1995). "The Physical and dynamical oceanography of the Mediterranean sea". In: P. Malanotte-Rizzoli and A. R. Robinson (Editors), Ocean Processes in Climate Dynamics: Global and Mediterranean Examples. Proceedings of NATO-ASI. Kluwer Academic Publishers, Dordrecht, The Netherlands, pp. 255-306.

Robinson, A. R., M. Golnaraghi, W. G. Leslie, A. Artegiani, A. Hecht, E. Lazzoni, A. Michelato, E. Sansone, A. Theocharis and U. Uenlueata, (1991). "The eastern Mediterranean general circulation: Features, structure and variability". *Dynamics of Atmospheres and Oceans*, 15(3-5): 215-40.

Robinson, A. R., A. Hecht, N. Pinardi, J. Bishop, W. G. Leslie, Z. Rosentroub, A. J. Mariano and S. Brenner, (1987). "Small synoptic/mesoscale eddies and energetic variability of the eastern Levantine basin.". *Nature*, 327(6118): 131-133.

Robinson, I. S., (1985). Satellite Oceanography. Marine Science. Ellis Horwood, Wormley, 455 pp.

Roether, W. and e. al., (1996). "Recent changes in Eastern Mediterranean deep waters". *Science*, 271: 333-335.

Rossow, W. B., A. W. Walker, D. E. Beuschel and M. D. Roiter, (1996). "Documentation of new cloud datasets.", International Satellite Cloud Climatology Project.

Ruddick, K. G., F. Ovidio and M. Rijkeboer, (2000). "Atmospheric correction of SeaWiFS imagery for turbid coastal and inland waters". *Applied Optics*, 39: 897-912.

Ryan, J. P., J. A. Yoder, J. A. Barth and P. C. Cornillon, (1999). "Chlorophyll enhancement and mixing associated with meanders of the shelf break front in the Mid-Atlantic Bight". *Journal of Geophysical Research*, 104(C10): 23479-23493.

Sammari, C., C. Millot and L. Prieur, (1995). "Aspects of the seasonal and mesoscale varaiability of the Northern Current in the western Mediterranean Sea inferred from PROLIG-2 and PROS-6 experiments.". *Deep Sea Research II*, 42(6): 893-917.

Samuel, S., K. Haines, S. Josey and P. G. Myers, (1999). "Response of the Mediterranean Sea thermohaline circulation to observed changes in the winter wind stress field in the period 1980-1993". *Journal of Geophysical Research*, 104(C4): 7771-7784.

Santoleri, R., V. Banzon, S. Marullo, E. Napolitano, F. D'Ortenzio and R. H. Evans, (2003). "Year-to-year variability of the phytoplankton bloom in southern Adriatic Sea (1998-2000): SeaWiFS observations and modelling study". *Journal of Geophysical Research*, In press.

Sasaoka, K., S. I. Saitoh, I. Asanuma, K. Imai, M. Honda, Y. Nojiri and T. Saino, (2002). "Temporal and spatial variability of chlorophyll-a in the western subarctic Pacific determined from satellite and ship observations from 1997 to 1999". *Deep Sea Research II*, 49: 5557-5576.

Sathyendranath, S., S. Cota, V. Stuart, H. Maass and T. Platt, (2001). "Remote sensing of phytoplankton pigments: a comparison of empirical and theoretical approaches". *International Journal of Remote Sensing*, 22(2): 249-273.

Sathyendranath, S. and T. Platt, (1988). "The spectral irradiance field at the surface and in the interior of the ocean: a model for applications in oceanography and remote sensing". *Journal of Geophysical Research*, 93(C8): 9270-9280.

Send, U., J. Font, G. Krahmann, C. Millot, M. Rhein and J. Tintoré, (1999). "Recent advances in observing the physical oceanography of the western Mediterranean Sea". *Progress in Oceanography*, 44: 37-64.

Seritti, A., D. Russo, C. Santinelli, L. Nannicini, E. Murru and B. B. Manca, (2000). *Vertical distribution of DOC in the Ionian Sea.*, JGOFS Open Science Conference. Ocean Biogeochemistry: A New Paradigm., Bergen, Norway.

Shettle, E. P. and R. W. Fenn, (1979). "Models for the aerosols of the lower atmosphere and the effects of humidity variations on their optical properties", Air Force Geophysics Laboratory, Hanscomb Air Force Base, Mass.

Siegel, D. A., S. C. Doney and J. A. Yoder, (2002a). "The North Atlantic Spring Phytoplankton bloom and Sverdrup's critical depth hypothesis". *Science*, 296: 730-733.

Siegel, D. A., S. Maritorena, N. B. Nelson, D. A. Hansell and M. Lorenzi-Kayser, (2002b). "Global distribution and dynamics of colored dissolved and detrital organic materials". *Journal of Geophysical Research*, 107(C12): 3228-3249.

Siegel, D. A., M. Wang, S. Maritorena and W. Robinson, (2000). "Atmospheric correction of satellite ocean color imagery: the black pixel assumption". *Applied optics*, 39(21): 3582-3591.

Siegel, D. A., T. K. Westberry, M. C. O'Brian, N. B. Nelson, A. F. Michaels, J. R. Morrison, A. Scott, E. A. i. Caporell, J. C. Sorenson, S. Maritorena, S. A. Garver, E. A. Brody, J. Ubante and M. A. Hammer, (2001). "Bio-optical modelling of primary production on regional scales: the Bermuda BioOptics project". *Deep Sea Research II*, 48: 1865-1896.

Smetacek, V. and U. Passow, (1990). "Spring bloom initiation and Sverdrup's critical-depth model". *Limnology and oceanography*, 35(1): 228-234.

Smirnov, A., B. N. Holben, T. F. Eck, O. Dubovik and I. Slutsker, (2000). "Cloud screening and quality control algorithms for the AERONET data base". *Remote Sensing of the Environment*, 73: 337-349.

Smith, R. C. and K. S. Baker, (1978). "The bio-optical state of ocean waters and remote sensing". *Limnology and Oceanography*, 23: 247-259.

Smith, S. D., (1980). "Wind stress and heat flux over the ocean in gale force winds.". *Journal of Physical Oceanography*, 10: 709-726.

Smyth, T. J., P. I. Miller, S. B. Groom and S. J. Lavender, (2001). "Remote sensing of sea surface temperature and chlorophyll during Lagrangian experiments at the Iberian margin". *Progress in Oceanography*, 51: 269-281.

Sournia, A., (1973). "La production primaire planctonique en Mediterranee.". *Newsl. Coop. Invest. Mediterr.*(Spec. Issue 5): 128.

Spencer, M. W., C. Wu and D. G. Long, (1997). "Tradeoffs in the design of a spaceborne scanning pencil beam scatterometer: Application to Sea-Winds". *IEEE Trans. Geosci. Remote Sensing*, 35: 115-126.

Stramski, D., R. Reynolds, M. Kahru and G. Mitchell, (1999). "Estimation of particulate organic carbon in the ocean from satellite remote sensing". *Science*, 285: 239-242.

Stratford, K. and K. Haines, (2002). "Modelling nutrient cycling during the eastern Mediterranean transient event 1987-1995 and beyond". *Geophysical Research Letters*, 29(3): 10102-10106.

Sturm, B., V. Barale, D. Larkin, J. H. Andersen and M. Turner, (1999). "OCEAN code: the complete set of algorithms and models for the level_2 processing of European CZCS historical data". *International Journal of Remote Sensing*, 20(7): 1219-1248.

Subramaniam, A., C. W. Brown, R. R. Hood, E. J. Carpenter and D. G. Capone, (2002). "Detecting Trichodesmium blooms in SeaWiFS imagery". *Deep Sea Research II*, 49: 107-121.

Sullivan, Arrigo, McClain, Comiso and Firestone, (1993). "Distributions of phytoplankton blooms in the southern ocean". *science*, 262: 1832.

Sur, H. I., E. Ozsoy and U. Unluata, (1993). "Simultaneous deep and intermediate depth convection in the Northern Levantine Sea, winter 1992". *Oceanologica Acta*, 16: 33-43.

Sverdrup, H. U., (1953). "On conditions for the vernal blooming of phytoplankton.". *Journal du Conseil International de l' Exploration de la Mer*, 18: 287-295.

Taupier-Letage, I., I. Puillat, C. Millot and P. Raimbault, (2003). "Biological response to mesoscale eddies in the Algerian Basin". *Journal of Geophysical Research*, 108(C8): 3245-3261.

Thingstad, T. F. and F. Rassoulzadegan, (1999). "Conceptual models for the biogeochemical role of the photic zone microbial food web, with particular reference to the Mediterranean Sea". *Progress in Oceanography*, 44: 271–286.

Trigo, I. F., T. D. Davies and G. R. Bigg, (2000). "Decline in Mediterranean rainfall caused by weakening of Mediterranean cyclones". *Geophysical Research Letters*, 27(18): 2913-2916.

Tsimplis, M. N. and S. Josey, (2001). "Forcing of the Mediterranean Sea by atmospheric oscillations over the North Atlantic". *Geophysical Research Letters*, 28(5): 803-806.

Turley, C. M., (1999). "The changing Mediterranean Sea — a sensitive ecosystem?". *Progress in Oceanography*, 44: 387-400.

Tusseau-Vuillemin, M. E., L. Mortier and C. Herbaut, (1998). "Modelling nitrate fluxes in an open coastal environment (Gulf of Lions): transport versus biogeochemical processes". *Journal of Geophysical Research*, 103(C4): 7693-7708.

Tyrell, T., P. M. Hooligan and C. D. Mobley, (1999). "Optical impacts of oceanic coccolithophore blooms". *Journal of Geophysical Research*, 104(C2): 3223-3241.

Vidussi, F., J. C. Marty and J. Chiaverini, (2000). "Phytoplankton pigment variations during the transition from spring bloom to oligotrophy in the NW Mediterranean Sea". *Deep Sea Research*, 47: 423-445.

Vignudelli, S., G. Gasparini, M. Astraldi and M. E. Schiano, (1999). "A possible influence of the North Atlantic Oscillation on the circulation of the Western Mediterranean Sea". *Geophysical Research Letters*, 26(5): 623-626.

Visbeck, M., J. Fischer and F. Schott, (1995). "Preconditioning the Greenland Sea for deep convection: Ice formation and ice drift.". *Journal of Geophysics Research*, 100(C9): 18489-18501.

Wang, M., S. Bailey, C. Pietras, C. R. McClain and T. Riley, (2000). "SeaWiFS Aerosol optical thickness match-up analysis". In: C. R. McClain, R. A. Barnes, J. Eplee, R.E., B. A. Franz, C. H. Hsu, F. S. Patt, C. M. Pietras, W. D. Robinson, B. D. Schieber, G. M. Schmidt, M. Wang, S. Bailey and P. J. Werdell (Editors), SeaWiFS postlaunch calibration and validation analysis. NASA Goddard Space Flight Center, Greenbelt, Maryland.

Webb, A. R., A. F. Bais, M. Blumthaler, G. P. Gobbi, A. Kylling, R. Schmitt, S. Thiel, F. Barnaba, T. Danielsen, W. Junkermann, A. Kazantzidis, P. Kelly, R. Kift, G. L. Liberti, M. Misslbeck, B. Schallart, J. Schreder and C. Topaloglou, (2002). "Measuring Spectral Actinic Flux and Irradiance: Experimental Results. from the ADMIRA (Actinic Flux Determination from

Measurements of Irradiance)". *Journal of Atmospheric and Oceanic Technology*, 19(7): 1049-1062.

Werdell, T. and S. Bailey, (1999). "The SeaWiFS Bio-optical Archive and Storage System - SeaBASS.", NASA Goddard Space Flight Center, Greenbelt, Maryland.

Westbrook, A. G., M. H. Pinkerton, J. Aiken and D. A. Pilgrim, (2001). "Simulated performance of remote sensing ocean colour algorithms during the 1996 PRIME cruise". *Deep Sea Research II*, 48: 845-859.

Wiggert, J. D., B. H. Jones, T. D. Dickey, K. H. Brink, R. A. Weller, J. Marra and L. A. Codispoti, (2002). "The Northeast Monsoon's impact on mixing, phytoplankton biomass and nutrient cycling in the Arabian Sea". *Deep Sea Research II*, 47: 1353-1385.

Williams, N., (1998). "The Mediterranean Beckons to Europe's oceanographers". *Science*, 229: 463-464.

Williams, R. G. and M. J. Follows, (1998). "The Ekman transfer of nutrients and maintenance of new production over the North Atlantic". *Deep Sea Research*, 45: 461-489.

Williams, R. G., A. J. McLaren and M. J. Follows, (2000). "Estimating the convective supply of nitrate and implied variability in export production over the North Atlantic". *Global Biogeochemical Cycles*, 14(4): 1299-1313.

Yacobi, Y. Z., T. Zohary, N. Kress, A. Hecht, R. D. Robarts, M. Waiser and A. M. Wood, (1995). "Chlorophyll distribution throughout the Southeastern Mediterranean in relation to the physical structure of the water mass". *Journal of Marine Systems*, 6: 179-190.

Yilmaz, A., D. Ediger, O. Basturk and S. Tugrul, (1994). "Phytoplankton fluorescence and deep chlorophyll maxima in the Northeastern Mediterranean". *Oceanologica Acta*, 17(1): 66-77.

Yilmaz, A. and S. Tugrul, (1998). "The effect of cold- and warm-core eddies on the distribution and stoichiometry of dissolved nutrients in the Northeastern Mediterrane". *Journal of Marine Systems*, 16: 253-268.

Yoder, J. A., W. E. Esaias, G. C. Feldman and C. R. McClain, (1988). "Satellite Ocean color status report". *Oceanographic Magazine*, 1(35): 18-20.

Zaneveld, J. R. V., (1995). "A theoretical derivation of the dependence of the remotely sensed reflectance of the ocean on the inherent optical properties". *Journal of Geophysical Research*, 100(C/): 13135-13142.

Zavatarelli, M., J. W. Baretta, J. Baretta-Bekker and N. Pinardi, (2000). " The dynamics of the Adriatic Sea ecosystem. An idealized model study". *Deep Sea Research*, 5(937-970).

Zingone, A., R. Casotti, M. Ribera d'Alcalà, M. Scardi and D. Marino, (1995). "'St. Martin's summer': the case of an autumn phytoplankton bloom.". *Journal of Plankton Research*, 17: 575-593.

Zohary, T., S. Brenner, M. D. Krom, D. L. Angel, N. Kress, W. K. W. Li, A. Neori and Y. Z. Yacobi, (1998). "Buildup of microbial biomass during deep-winter mixing in a Mediterranean warm-core eddy.". *Marine Ecology Progress Series*, 167: 47-57.